Characterizing the Transport of the Stable Isotopes of Water in Unsaturated Soils

A Thesis Submitted to the College of
Graduate and Postdoctoral Studies
In Partial Fulfillment of the Requirements
For the Degree of Master of Science
In the Department of Civil, Geological, and Environmental Engineering
University of Saskatchewan
Saskatoon

By

Matthew Buchynski

PERMISSION TO USE

In presenting this thesis/dissertation in partial fulfillment of the requirements for a Postgraduate degree from the University of Saskatchewan, I agree that the Libraries of this University may make it freely available for inspection. I further agree that permission for copying of this thesis/dissertation in any manner, in whole or in part, for scholarly purposes may be granted by the professor or professors who supervised my thesis/dissertation work or, in their absence, by the Head of the Department or the Dean of the College in which my thesis work was done. It is understood that any copying or publication or use of this thesis/dissertation or parts thereof for financial gain shall not be allowed without my written permission. It is also understood that due recognition shall be given to me and to the University of Saskatchewan in any scholarly use which may be made of any material in my thesis/dissertation.

DISCLAIMER

The [name of company/corporation/brand name and website] were exclusively created to meet the thesis and/or exhibition requirements for the degree of Masters of Science at the University of Saskatchewan. Reference in this thesis/dissertation to any specific commercial products, process, or service by trade name, trademark, manufacturer, or otherwise, does not constitute or imply its endorsement, recommendation, or favoring by the University of Saskatchewan. The views and opinions of the author expressed herein do not state or reflect those of the University of Saskatchewan, and shall not be used for advertising or product endorsement purposes.

Requests for permission to copy or to make other uses of materials in this thesis/dissertation in whole or part should be addressed to:

Head of the Department of Civil, Geological, and Environmental Engineering

57 Campus Drive

University of Saskatchewan

Saskatoon, Saskatchewan S7N 5A9

Canada

OR

Dean

College of Graduate and Postdoctoral Studies

Room 116 Thorvaldson Building

110 Science Place

Saskatoon, Saskatchewan, S7N 5C9

Canada

ABSTRACT

High-resolution profiles of the stable isotopes of water in unsaturated soils are used to estimate infiltration. The peak shift method is used to calculate a net percolation rate by finding the location of isotope peaks. The literature applying the peak shift methods is plentiful. However, when extensive spreading occurs by diffusion and dispersion and a well-defined peak is no longer present the peak shift method is not applicable and another method of analysis is needed.

The goal of this work was to develop a better understanding of the diffusive and dispersive movement of isotopes within an unsaturated soil. Isotopes can be partitioned to the vapour phase where they can be stored and transported in addition to the aqueous phase. A dual phase relationship was derived to analyze isotope profiles where significant spreading has occurred.

A dual phase (i.e. vapour and liquid) diffusion – water content relationship was developed using water isotope, carbon dioxide, and oxygen gas diffusion literature including gaseous and aqueous phase tortuosities. This relationship was evaluated using the results from a set of double half-cell diffusion cells. Each cell allowed for a diffusion coefficient to be measured at specific volumetric water content. The experimental procedures proved to be challenging and required several iterations to collect quality data. Interpretation of the diffusion cell data resulted in a best fit dual phase model, using the gaseous phase tortuosity model of Penman (1940) and the aqueous phase tortuosity model recommended by Padilla et al. (1999) with the saturated tortuosity from Maxwell (1881).

The proposed diffusion model was also evaluated using the observations from a column test used to simulate infiltration under simple field conditions. Simulated rainfall was allowed to infiltrate and diffuse. Isotope values were measured over the column elevation at different times. These observations were used to verify the dual-phase diffusion model as well as several different dispersivity-water content relationships. The diffusion behavior observed in the column experiment was consistent with the combined dual-phase model selected from the diffusion cells.

ACKNOWLEDGEMENTS

This project would not be possible without a number of people. First I would like to first thank Lee Barbour for his extensive, guidance, support, encouragement, and patience. Adam Hammerlindl and Erin Schmeling for their helping the lab with experiment construction and analysis. My family for their understanding and support over the course of my studies. Jordan for always being there and supporting me over the years. And my fellow Grad students Sean and James for their help in writing, discussion and moral support.

Finally I would like to thank my committee members Jim Hendry, Grant Ferguson, and Charles Maule for providing guidance over the course of the program.

Funding for this program was graciously provided by the University of Saskatchewan, the National Sciences and Engineering Research Council (NSERC) and Syncrude Canada Ltd (SCL).

TABLE OF CONTENTS

LIST OF TABLES

LIST OF FIGURES

Chapter 1 - Introduction

Understanding of the rates of ground water recharge and contaminated water movement in unsaturated soils is of interest in many areas of hydrogeological research including ground water and surface water protection associated with industrial activities such as mining, site remediation and agriculture. For example, an understanding of rates of recharge, also known as net percolation, is foundational to understanding rates of effluent release from mine waste. There are many techniques available monitor the movement of water in unsaturated, coarse-textured soils. Scanlon et al. (2002) identified tracers, numerical modelling, and lysimeters as appropriate methods for estimating recharge in semi-arid unsaturated areas. Naturally occurring stable isotopes of water (deuterium, ^{2}H or D; and oxygen 18,^{18}O), are used as tracers in unsaturated soils (Dincer et al., 1974, Adomako et al., 2010, and Gazis and Feng, 2004), and are the primary focus of this work. The benefit of using the stable isotopes of water over other ions or compounds is that they provide a direct observation of water movement, as they are part of water molecules (HDO or $H_2{}^{18}O$). The origin of the isotopes can be naturally occuring seasonal variations in precipitation (Bath et al., 1982) or artificial (Zimmermann et al., 1967a).

The conventional method of estimating recharge with stable isotopes of water is to graphically find the depth of an isotope peak and determine how long it took for that peak to reach that depth. Studies that utilize peak shift methods include Dincer et al. (1974), Adomako et al. (2010), Bath et al. (1982), Cane and Clark (1999), and Gazis and Feng (2004). These methods are sufficient for near surface soil (less than 1 m depth) profiles, but break down when the profiles penetrate deeper (typically greater than 1 m) into soils where diffusive transport smooths the isotope profile (Cook et al., 1992). Rigorous interpretation of advection-dispersive transport is not utilized in peak shift methods because graphical interpretation provides for acceptable estimates of recharge.

Melayah et al. (1996a), Braud et al. (2005a), and Braud et al. (2009a) derived governing equations that describe the movement of isotopes through unsaturated soil profiles. Melayah et al. (1996b), Braud et al. (2005b), and Braud et al. (2009b) compared the governing equations to experimental results. These studies focus on near surface (less than 1 m depth) advectively dominated profiles. Dual-phase diffusive transport models are presented in these studies, but none compare the models to laboratory or field measurements of diffusion. The key components of the theoretical description

of isotopic transport are functional models for tortuosity (τ), free solution diffusion coefficient, and interphase partitioning and are typically not tested within these studies.

The current methods of analyzing isotope profiles fall short in two areas, which are to be addressed by the proposed study:

- The relationship between water content and the coefficient of diffusion for the aqueous and vapour phases for the stable isotopes of water;
- and evaluation of these functional relationships under laboratory observations of transport under conditions in which isotope diffusion is the main transport mechanism.

1.1 Objectives

The goal of this research project is to characterize the transport properties of the stable isotopes of water in unsaturated, coarse textured soils. To characterize transport the following objectives will be pursued.

1. Measure the relationship between the combined coefficient of molecular diffusion (i.e. through liquid and vapour phases) and water content for stable isotopes of water using laboratory diffusion cell testing, and compare this relationship to a theoretically derived relationship based on dual-phase diffusion (aqueous and vapour).
2. Develop a set of observations of stable isotope of water transport at a bench scale through the use of column testing for unsaturated coarse textured soil under advective, dispersive and diffusive transport.
3. Characterize advective, dispersive, and diffusive transport of stable isotopes of water by simulating laboratory results with a numerical model.

1.2 Scope

The scope of this project is limited to:

- Constructing, performing and analyzing laboratory tests (column test and diffusion cells);
- Formulating governing equations to describe transport in column test and diffusion cells;
- Creation/application of a numerical models to solve the transport equations for each laboratory test

- Comparison of different transport parameter functions for diffusion and mechanical dispersion.

This project does not include:

- Development of a vapour sampling protocol;
- Consideration of fractionation arising from water lost from system, ground freezing (i.e. fractionation due to ice formation), or geochemical reactions;
- Non-isothermal conditions or the influence of density dependent flow (vapour or liquid) on transport;

1.3 Outline of Thesis

This thesis contains the following six sections. First, a literature review (Chapter 2) will synthesize previous studies involving field-based measurements of recharge using isotope profiles in unsaturated surficial soils. Following the field-based measurements, a brief overview of the development of numerical transport models will be presented. Chapter 3 will present the theoretical development for the dual-phase diffusion coefficient that will be used in subsequent data interpretation. The methods chapter (Chapter 4) will outline the literature, design, construction, and experimental method associated with the two laboratory experiments. The collected data will be presented and the factors affecting the quality of this data will be discussed in Chapter 5. Numerical modeling and interpretation of the column data is presented in Chapter 6. Finally, the Conclusions and Recommendations (Chapter 7) will summarize the work, the key findings of the study, and present recommendations for further work that were discovered during the investigation.

Chapter 2 - Literature Review

Quantifying the rates of net percolation and water migration through mine waste, such as waste rock and tailings, is critical to assessing the migration of possible contaminants and the impact these contaminants may have on the environment following closure. Water movement in unsaturated soils, such as mine waste, can be investigated using a range of techniques (Scanlon et al., 2002, Flint et al., 2002), with a widely used method being isotope tracers. In this chapter, general background information as it pertains to the stable isotopes of water as a tracer is provided along with a description of how they have been used in hydrology and hydrogeology.

The general isotope background will be followed by a description of isotope peaks and the current application of the peak shift methods. Next will be a summary of the approaches that have been taken to numerically simulate the transport of isotopes in unsaturated, coarse textured soils. It is important to note that these approaches have not yet been widely used in research or practice. Since the stable isotopes of water are a dual-phase chemical species (i.e. they exist in both the aqueous and vapour phases), some background information on other dual-phase tracers such as oxygen gas (O_2) and carbon dioxide (CO_2), will be described as the theory is similar to that of the isotopes. This review section will conclude by highlighting some of limitations faced by the current methods of describing stable isotope transport in unsaturated soils.

2.1 Stable Isotopes of Water

There are many water isotopologues (water molecules containing different isotopes of hydrogen or oxygen) present in nature; of these, the three of primary interest in this study are $^{1}H^{1}H^{16}O$, $^{1}H^{2}H^{16}O$, and $^{1}H^{1}H^{18}O$. The most abundant of these is the isotopologue $^{1}H^{1}H^{16}O$, which will be referred to in this work as light or normal water. The other two isotopologues, referred to in this study as the stable isotopes of water or isotopes, contain either one deuterium ($HD^{16}O$), where D is a hydrogen atom of weight 2 ($D = {}^{2}H$), or one oxygen 18 ($HH^{18}O$). These stables isotopes of water are presented as δD or $\delta^{18}O$ in this work.

The most basic method of reporting the amount of the stable isotopes of water present within a water samples is using a concentration ratio, R (Equation 2.1, Clark and Fritz, 1997) where R is the ratio of the concentration of the stable isotope of interest to the concentration of the most abundant isotope of water in nature.

$$R = \frac{[Less\ Abundant\ Isotope]}{[Most\ Common\ Isotope]} \quad \text{.....(2.1)}$$

The R for deuterium and oxygen 18 is very small, generally having a value of approximately 10^{-6} (Criss, 1999). Because the value of R is difficult to measure and compare between different locations and laboratories (Clark and Fritz, 1997), international standards for the concentration ratios have been developed to normalize values for easier reporting, and comparison. The most commonly used standard ratio is the Vienna Standard Mean Ocean Water (VSMOW). The standards $D/^{1}H$ value is 155.76 ± 0.05 x 10^{-6} (Baertschi, 1976) and the $^{18}O/^{16}O$ value is 2005.2 ± 0.4 x 10^{-6} (Hagemann et al., 1970). To compare a measured R value to the standard ratios, the "delta" (δ) convention is used. The δ represents the deviation of the measured R value in thousandths, expressed as a per mille ‰, from the R value for a VSMOW as calculated by Equation 2.2 (Hoefs, 2009).

$$\delta = \left(\frac{R_{sample}}{R_{Standard}} - 1\right) 10^3 \text{ ‰ VSMOW} \quad \text{.....(2.2)}$$

The isotopic ratios will change whenever the isotopes are involved in a reaction. This process, referred to as isotopic fractionation, is "due to the differences in the rates of reaction for different molecular species" (Clark and Fritz, 1997). In the case of a closed system (no changes in total water mass) with liquid water and water vapour present, the ratio of isotopic ratios between each phase is referred to as equilibrium fractionation factor and is defined as follows:

$$\alpha_{equilibrium} = \frac{R_{water}}{R_{vapour}} = \frac{1000 + \delta_{water}}{1000 + \delta_{vapour}} \quad \text{.....(2.3)}$$

Equilibrium fractionation is a temperature dependent process; as the temperature increases the fractionation factor approaches 1, indicating that there is no difference in the isotopic ratios between the two phases (Clark and Fritz, 1997). Majoube (1971) found relationships experimentally that determine the $\alpha_{equilibrium}$ for δD and $\delta^{18}O$, as a function of temperature. The relationships of Majoube (1971) are almost exclusively used when calculating fractionation, with other experimental data sets tabulated in Clark and Fritz (1997).

2.2 Isotopes in the Hydrologic Cycle

To better understand naturally occurring isotope peaks in soils, a brief description of the variations in isotope values when water moves through the hydrological cycle is presented. The hydrologic cycle can be viewed conceptually as a series of evaporation and condensation events in which the stable isotopes of water undergo repeated fractionation. As a result of these fractionation events, Craig (1961) observed that the values of δD and $\delta^{18}O$ for precipitation water follow a linear relationship between warm and cold climates. The relationship is known as the global meteoric water line (GMWL) and is shown in Figure 2.1.

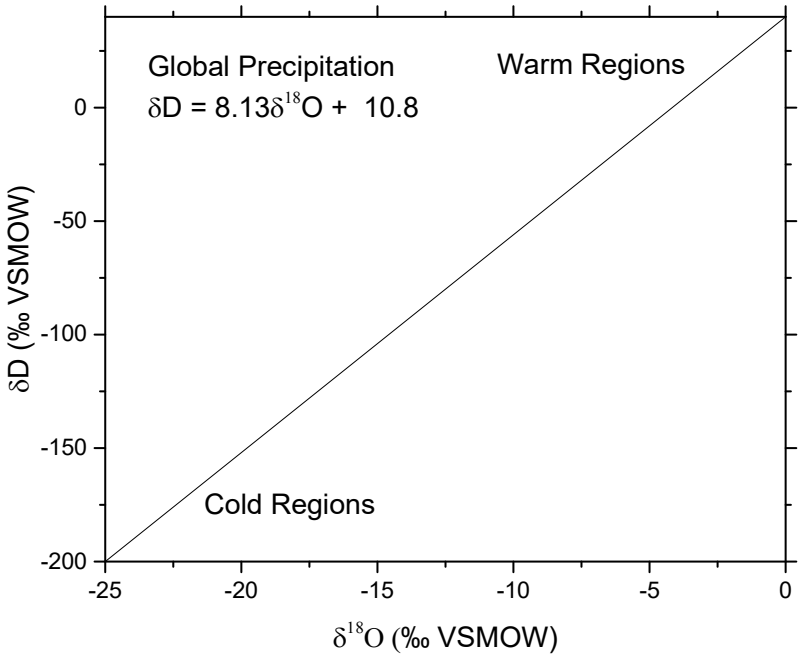

Figure 2.1 – Global Meteoric Water Line (GMWL) (after Clark and Fritz, 1997)

The GMWL has been shown, more recently by Clark and Fritz (1997), to be a result of the Rayleigh type fractionation process and atmospheric temperatures. The Rayleigh fractionation follows:

$$R = R_0 f^{(\alpha-1)} \quad \text{.....(2.4)}$$

Where R is the current isotope ratio (unitless), R_0 is the initial isotope ratio (unitless), f is the fraction of water left in a reservoir and α is the equilibrium fractionation factor (unitless). This equation shows, as a vapour reservoir (cloud) loses water and as temperature decreases, the amount

of isotope that can be exchanged to the liquid phase also goes down, resulting in a depleted rainwater signature. The effects of temperature are shown in Figure 2.2 (Clark and Fritz, 1997).

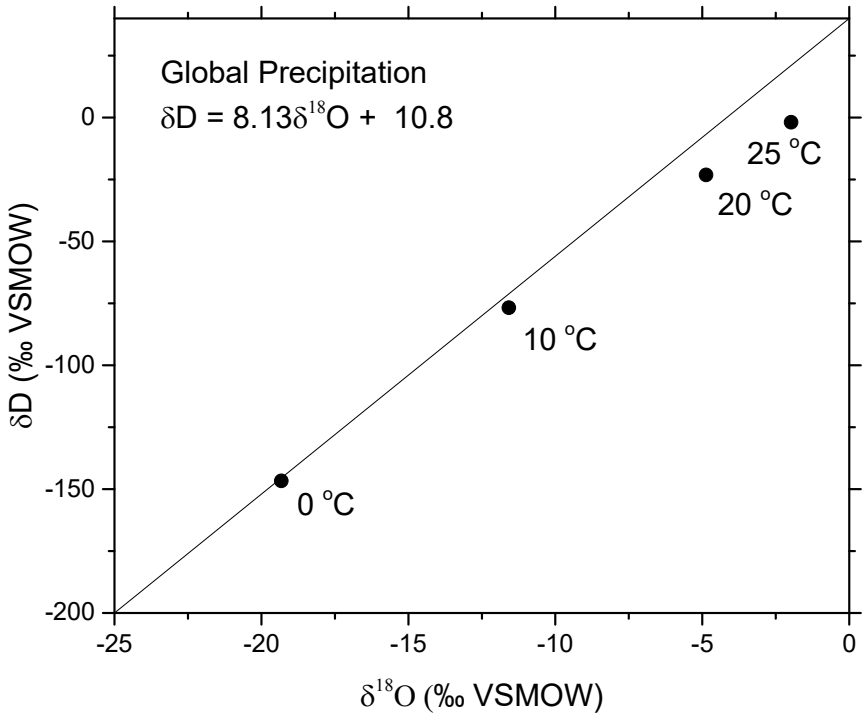

Figure 2.2 - δD and $\delta^{18}O$ relationship with temperature during rainout (after Clark and Fritz, 1997)

All collected precipitation water in a specific geographic region plots on a local meteoric water line (LMWL). The location of the precipitation isotope values varies seasonally with warmer precipitation having more enriched values. Fractionation processes such as evaporation can also be visualized as lines of progressive diversion from the LMWL. Mixing of different water sources can also be shown and found on a MWL. Figure 2.3 is an example of a MW highlighting, evaporation and mixing.

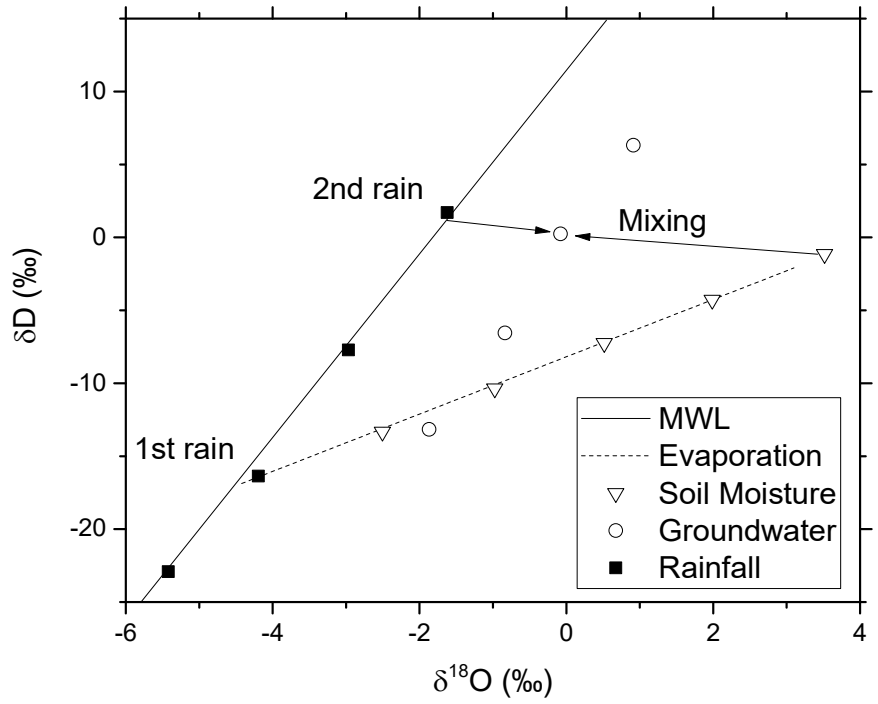

Figure 2.3 – Meteoric water line showing evaporation, mixing, process and rain waters (after Clark and Fritz, 1997)

2.3 Isotope Peaks in Soils

The widely used method of the stable isotopes of water to estimate net percolation is to use peaks found in the soil water. Artificial peaks can be created by applying an isotopically tagged water to an area. Artificial tracer methods have been used in early isotope studies (Zimmermann et al., 1967a) to distinguish between old and new water. Naturally occurring isotope profiles show seasonal oscillations between enriched and depleted peaks (Figure 2.4).

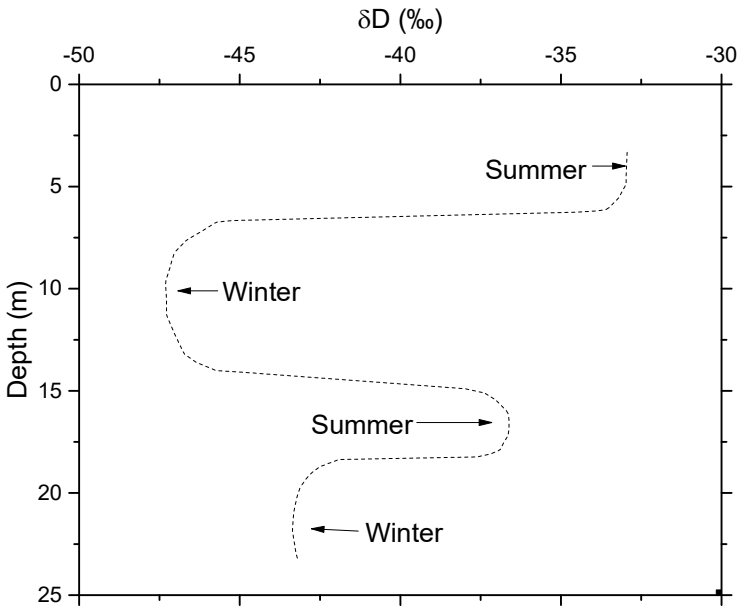

Figure 2.4 – Simplified typical unsaturated zone isotope profile, showing depleted snowmelt infiltration and enriched summer infiltration, Bordeaux, France. Isotope samples collected with suction probe (after Thoma et al., 1978).

The peak may be defined by either the enriched signal of warm recharge water or a depleted peak associated with the recharge of cold water such as snow melt waters. A peak can also be produced by displacement of near surface water that has been enriched as a result of evaporation (Figure 2.5). If the evaporated isotope peaks were to reach a quasi-steady state condition, Zimmermann et al. (1967b) theorized that the peaks will be moved deeper into the soil in a plug flow style when infiltration occurs.

Barnes and Allison (1983) extended the work of Zimmermann et al. (1967b) by creating an analytical solution to show what a quasi-steady state evaporative profile should look like under prolonged evaporation (Figure 2.6).

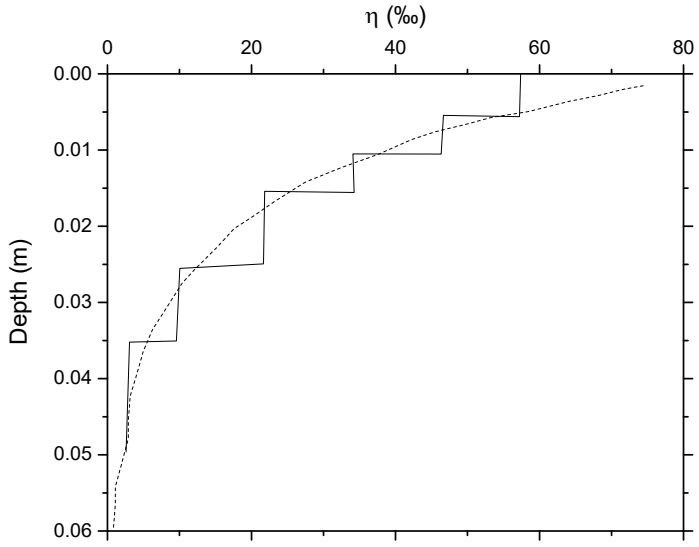

Figure 2.5 - Steady state isotope profile for a fine grained sandy soil. Dotted line shows the theoretical model and the solid line represents observed data for a saturated soil (after Zimmermann et al., 1967b).

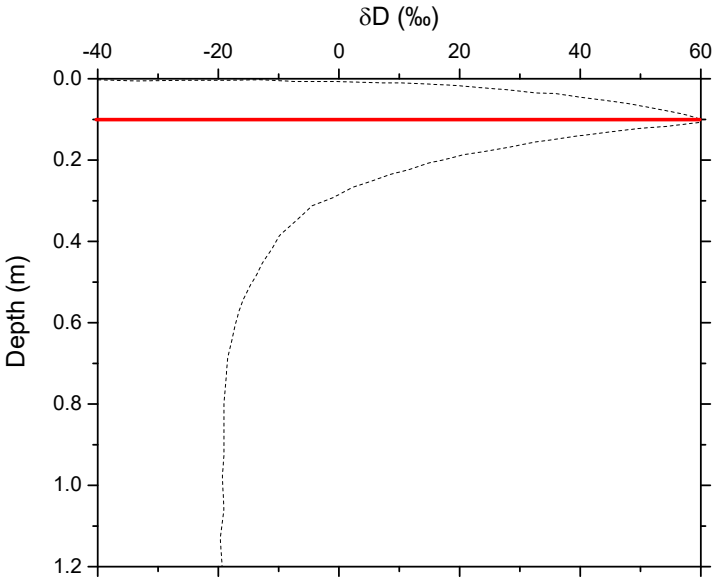

Figure 2.6 – Theoretical curve for evaporative peak in unsaturated soil column. The red line indicates the maximum isotope value from evaporation, and defines the boundary between the vapour transport region (above) and the liquid transport region (below). (after Barnes and Allison, 1983).

They surmised that monitoring of these profiles can be used to estimate evaporation. Several analytical methods are proposed and found to provide a good fit to observed isotope profiles under

evaporation in the laboratory (Figure 2.7, Allison et al., 1983) and under field conditions (Figure 2.8, Allison and Barnes, 1985).

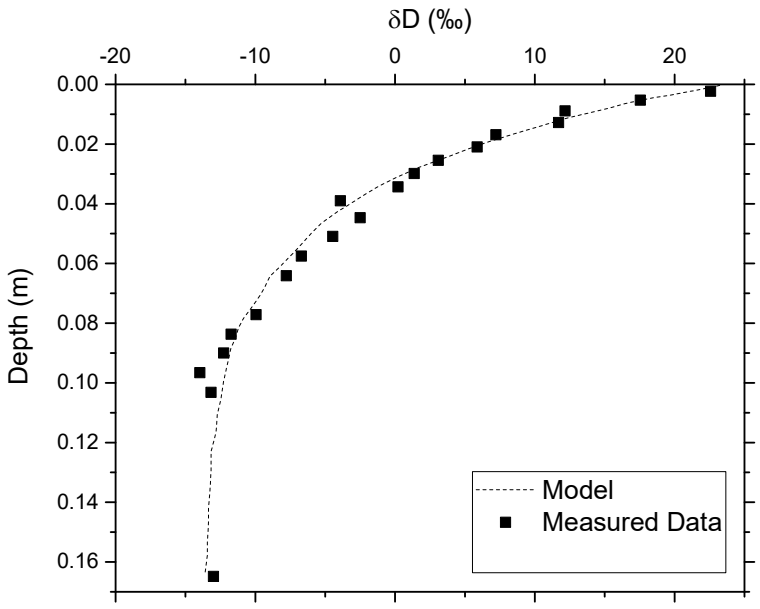

Figure 2.7 – Results of laboratory column evaporation study (after Allison et al., 1983).

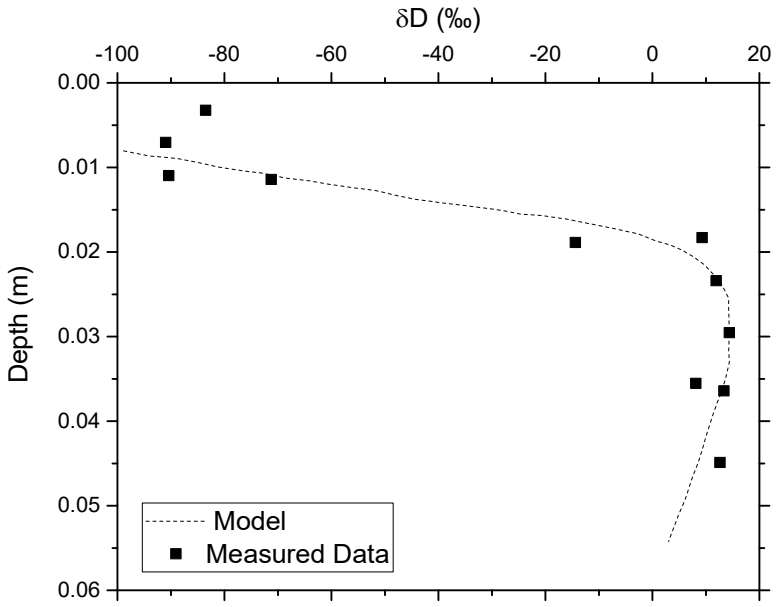

Figure 2.8 – Near surface isotope values collected from field site (after Allison and Barnes, 1985).

2.3.1 Estimating Recharge with Isotope Peaks

Zimmermann et al. (1967a) were the first authors to estimate net percolation from isotopic data (Braud et al., 2005a). They showed that the depth to the center of mass peak and an estimate of the water stored to that depth could be used to estimate recharge rates into the soil. Zimmermann et al. (1967a) also observed that the isotopic profile did undergo spreading as a result of molecular diffusion and mechanical dispersion; with more spreading within the deeper portions of the profile. However; they did not attempt to fit the observed spread in the isotopic values to a diffusion or mechanical dispersion model.

The observations and interpretations of Zimmermann et al. (1967a) led to the use of what is now referred to as the peak shift method (Zimmermann et al., 1967b). The peak shift method, in the simplest terms, estimates the average velocity of the water travelling through the soil based on the distance travelled by the isotopic peak divided by the time since it entered the soil profile, assuming piston flow. If the volume of water stored within the profile is known, the average infiltration rate can be determined.

Isotope peaks and the peak shift methods have been utilized in many studies to characterize recharge rates (Dincer et al., 1974, Bath et al., 1982, Cane and Clark, 1999, Gazis and Feng, 2004, Adomako et al., 2010). Deviation of isotope profiles from expected shapes has allowed researchers to identify different flow regimes in hill-slopes and around catchment edges (Asano et al., 2002, Garvelmann et al., 2012, Dusek et al., 2012, Klaus et al., 2013, Mueller et al., 2014). These studies highlight that there may be horizontal flows to a lower area that can be identified with isotope peaks.

The peak methods rely on the ability to define a distinct peak in the soil isotope profiles and consequently are most effectively applied over relatively shallow depths. The peak methods break down at greater depths because the location of peaks and troughs becomes less definitive with increased travel time as diffusive and dispersive processes occur. Compared to near surface (less than 1 m depth) studies of isotope profiles highlighted previously, studies of deeper profiles (greater than 1 m) are less common (Bath et al., 1982, Gaye and Edmunds, 1996, DePaolo et al., 2004, Cheng et al., 2014).

Cook et al. (1992) estimated the time for an isotope peak to be reduced to 20% of its original value based on recharge rates and the average time between distinct isotopic peaks (t_i). For example, annual cyclic peaks such as snowmelt, would have a t_i of 1 year. The persistence time then defines the length of time that tracer can be tracked (Figure 2.9).

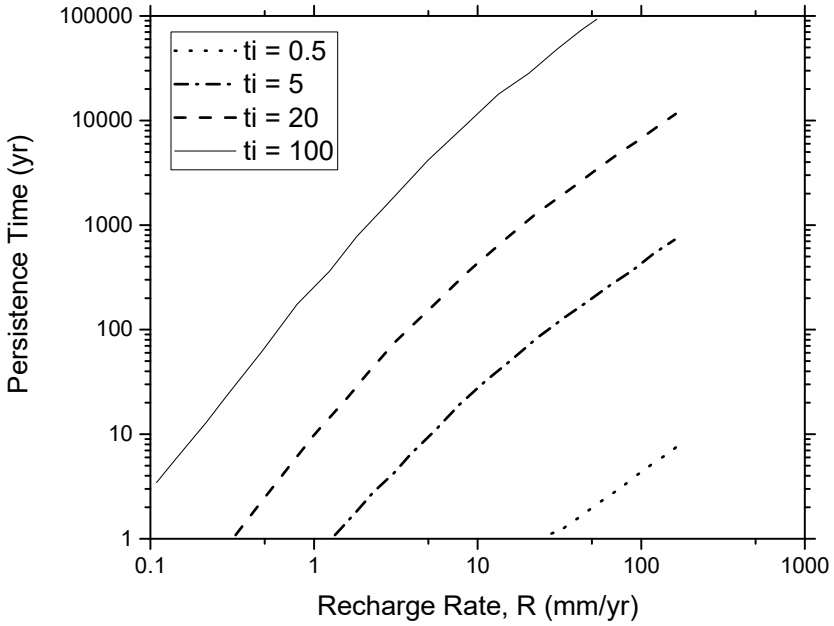

Figure 2.9 - Persistence time for tracer peaks in unsaturated soils (after Cook et al., 1992)

In Figure 2.10, an annual infiltration cycle (i.e. t_i = 1) is used to illustrate the observable depth of propagation of the isotopic tracer into a landform with different average annual volumetric water contents (θ_l).

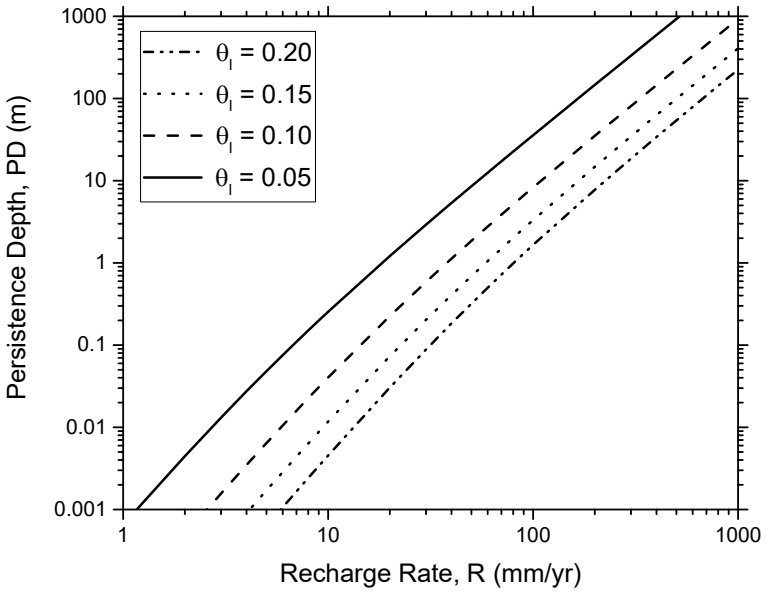

Figure 2.10 - Persistence depth of tracer peaks, constructed from Cook et al., 1992 figure with t_i = 1. Persistence depth = $\frac{\text{Recharge rate}}{1000\theta}$ (Persistence time)

This plot shows that lower θ_l and a higher recharge rate result in an isotope peak being visible at larger depths, compared to high θ_l and low recharge scenarios.

2.4 Transport of the Stable Isotopes of Water in Unsaturated Soils

The conventional methods of estimating recharge as outlined previously, do not incorporate a full description of the transport processes such as diffusion and mechanical dispersion. However, as isotope methods are increasingly applied to deeper profiles with more dynamic cycles of infiltration and evaporation, it has been recognized that a more rigorous description of transport processes is required to interpret field observations (Braud et al., 2005a). This section will highlight how more rigorous methods have been used to estimate isotope transport in unsaturated soils. A brief history of dual-phase model development will be presented, followed by a comparison to non-isotope studies and finally a presentation of the combined diffusion coefficient that is to be used.

2.4.1 Development of Dual-Phase Transport Models

The isotopes D and ^{18}O can be transported through an unsaturated soil via diffusion, mechanical dispersion, and advection in both the vapour and aqueous phases. Dual-phase transport models

assume all isotopes are transported in the liquid phase, but the storage and transport parameters are enhanced due to the presence of the vapour phase.

The first authors to develop a numerical dual-phase isotope transport model were Shurbaji and Phillips (1995). Their model was created to simulate the isotopic peaks created by surface evaporation in experimental studies from the literature. The numerical model was created in several blocks and each of the blocks (heat, water, and isotope) were compared to cases presented by other authors (Shurbaji and Phillips, 1995), but no comparison to measured data was made.

The next formulation of dual-phase isotope transport came from Mathieu and Bariac (1996a). Their work also focused on replicating the evaporative peak near the soil surface. Comparisons of the model were made to analytical solutions, but not to measured data. The depth of the investigation in this work was less than 0.3 m depth. An important observation made by Mathieu and Bariac (1996a) was: "The shape of the isotopic profiles, particularly the diffusion of the isotopic enrichment to depth, is actually quite sensitive to the porosity and tortuosity …" but minimal investigation into the tortuosity was done. A single value is calculated and used for tortuosity instead of a functional relationship depending on water content.

Melayah et al. (1996a) took the formulations of Mathieu and Bariac (1996a) and generalized them for use in "variable climactic conditions, as encountered under field situations" (Braud et al., 2005a). The focus of Melayah et al. (1996a) was to derive more rigorous descriptions of the interactions between the soil and the atmosphere, so the controls on the evaporative peaks could be better understood. A companion paper Melayah et al. (1996b) compared the mechanistic model to observed field conditions. A field was artificially irrigated with a sprinkler and the resulting infiltration and evaporation profiles were measured. The depth of the evaporative peak and infiltration has not proceeded deeper than 0.1 – 0.2 m. In these two works the tortuosity was set to a constant value of 0.4.

About 10 years later the numerical schemes of Melayah et al. (1996a) were improved upon by Braud et al. (2005a) in which: "some hypothesis were reconsidered and some inconsistencies corrected" (Braud et al., 2005a). The final derivation of the dual-phase isotope transport equation has a very similar form to those presented by the previous authors. These authors also "revisited the specification of the resistance to isotope transport between the soil surface and the atmosphere" (Braud et al., 2005a). The first paper, in a set of two, was to re-evaluate the soil atmosphere

interactions (Braud et al., 2005a).In the first paper a constant tortuosity value of 0.67 was used in initial testing. Braud et al. (2005b) applied new interaction formulae to observed laboratory conditions. For the two laboratory data sets compared to the model, three constant values of tortuosity and simple relationships scaling the volumetric air content with an exponent. A same tortuosity was used for the vapour and aqueous phases.

A second pair of papers was presented shortly after. Braud et al. (2009a) prepared another laboratory experiment where the surficial soil and atmospheric isotope concentrations could be easily measured, in order to better define the kinetic fractionation factor that dominates the isotope loss to the atmosphere. The second paper (Braud et al., 2009b), looks at applying the numerical models developed previously (Braud et al., 2005a) to the new laboratory experiments. From the work done in Braud et al. (2005b) the optimal value for tortuosity is a constant 0.4 (Braud et al., 2009b). The new observed data is reproduced by their numerical model, but similarly to the other numerical studies, the profiles are relatively shallow (~0.25 m).

2.4.2 Parallels to Gas Transport Literature

The diffusion portions of dual-phase isotope transport models have similar conceptual models and theoretical approaches to those used in soluble gas diffusion studies. Examples of these include the diffusion of O_2 in unsaturated cover soils (Aachib et al., 2004 and Aubertin et al., 2000) and diffusion of CO_2 in unsaturated soils (Šimůnek and Suarez, 1993).

The differences between gas transport literature and isotope transport literature are in the selection of the combined phase. In isotope studies, the aqueous phase is the primary transport phase due to the large storage available for the water isotopes. This is in contrast to gas studies were the larger storage is available in the gas phase. The gas diffusion studies use the gas phase as the primary transport phase, with enhanced diffusive transport and storage due to the aqueous phase. The focus of the two areas of study is different as well. Isotope literature focuses on advection dominated transport near the ground surface to explain recharge and evaporation. Gas transport literature tends to focus on diffusion through unsaturated soils, with less emphasis on surficial boundary conditions.

2.4.3 Diffusion Coefficients in Dual-Phase Studies

A full development of the dual-phase isotope transport model is detailed in Chapter 3. A simplified dual-phase diffusion coefficient is shown in Equation 2.5 with the actual dual-phase diffusion coefficient shown in Equation 2.6:

$$D_{com} = \ aqueous\ diffusion + \ vapour\ diffusion \quad \text{.....(2.5)}$$

$$D_{com} = \ \theta_l \tau_l D_0^{il} + \ \theta_v \tau_v H D_0^{iv} \quad \text{.....(2.6)}$$

where D_{com} is the dual-phase or combined diffusion coefficient (m^2/s), θ_l and θ_v are the volumetric water and air contents (m^3/m^3), respectively, τ_l and τ_v are the tortuosity of the aqueous and vapour phases (unitless), respectively, H is a Henry's Law equivalent that relates the aqueous and vapour phase concentrations (unitless), and D_0^{il} and D_0^{iv} are the free solution diffusion coefficients for isotopes in the aqueous and vapour phases (m^2/s), respectively. The parameters τ_l, τ_v, D_0^{il}, and D_0^{iv} are functions of temperature.

In this work D_0^{il}, D_0^{iv}, and H are known values from literature with the volumetric fluid contents (water and air) and liquid fluxes measurable for unsaturated soils. However, the parameters that describe isotope spreading, Λ and τ, are available in the literature but . Many models for these parameters as functions of θ_l are available for use, but will need to be tested against observational data, specifically for isotopes in unsaturated soils to see which is most appropriate.

2.5 Summary

The peak shift methods are widely used due to their ease of use, but do not account for spreading. Understanding the spreading of isotopes during infiltration requires a more robust method such as numerical modeling. Single-phase numerical modeling may be appropriate for most tracers, but for isotopes, a dual-phase approach is needed to account for the significant effects of the vapour phase.

Dual-phase models for isotopes evaporating at the soil surface are common. The theory that is derived for the evaporation studies is applicable for infiltration. Because the evaporation studies are not entirely focused on spreading, the numerical parameters that define spreading rates in unsaturated soils (τ and Λ) are not thoroughly characterized for isotopes. The spreading for dual-

phase isotope studies is derived in a similar manner to gas diffusion studies, but the gas diffusion studies focus on the τ models that best fit experimental data. Overall little focus on mechanical dispersion has been presented with the isotope and gas diffusion dual-phase studies. One isotope paper (Braud et al., 2009b) stated Λ to be important, but actual relationships were not investigated, and only typical, discrete values were used.

The current literature shows how isotopes can be used to estimate infiltration in unsaturated soils, but the transport parameters need to be better defined, analogous to the gas diffusion literature. The rest of this work will look at what transport parameters are needed to accurately model isotope spreading in unsaturated soils.

Chapter 3 - Theory

The conceptual and theoretical models for the dual-phase transport of the stable isotopes of water in unsaturated soils are presented in this chapter. The theoretical model is used to develop D_{com} and the form of D_{com} is discussed and compared to the forms of the single-phase aqueous diffusion and soluble gas diffusion models from literature. Finally this chapter will look at different forms of soil Λ and compare them.

3.1 Combined Dual-phase Transport Conceptual Model

The transport of a soluble gas or water isotope (in either an aqueous or vapour form) occurs in both the vapour and the aqueous phase in an unsaturated soil. This concept is illustrated in Figure 3.1. Since a soluble gas or water molecules are free to move between phases, some form of partitioning condition must be included in to models to describe the equilibrium condition for the species of interest between the two phases. This is noted by the partitioning arrows shown in the figure.

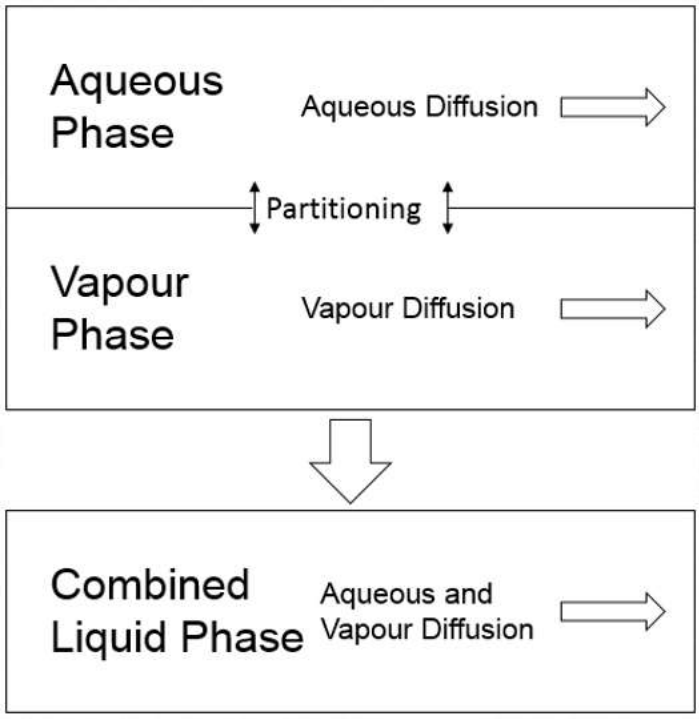

Figure 3.1 - Transport in two separate phases in an unsaturated soil including partitioning.

There are two governing equations required to describe the transport processes (one describing advective - diffusive/dispersive transport in each phase). The governing equations must be combined with an equation describing the partitioning of the tracer between the phases. In the case of soluble gases, equilibrium between the phases is described by Henry's Law (H), which states that the ratio of the concentration in the liquid phase relative to the vapour phase is constant and depends on temperature. A similar constant can be derived for the stable isotopes of water using equilibrium fractionation theory.

A combined phase modeling approach reduces the number of equations from two to one by assuming that the transported constituent in each (gas or isotope) phase is always in equilibrium with the same constituent in the other phase. If the partitioning relationship is linear and instantaneous then it follows that the concentration gradients in each phase are the same. This then allows the use of a combined liquid phase, where the impact of diffusive transport in the vapour phase can be incorporated simply as an enhanced rate of diffusion in the aqueous phase. A similar enhancement occurs in terms of changes in mass (i.e. storage term) in each phase. The mass stored within a total volume of soil, in a combined phase, can be tracked by using the concentration in the aqueous phase and accounting for the extra mass stored in the vapour phase.

3.2 Derivation of the Combined Dual-phase Transport Equation

The derivation of dual-phase isotope transport follows that of Braud et al. (2005a) and Melayah et al. (1996a) using notations similar to Braud et al. (2005a). A representative elementary volume (REV) will be used as a starting point. The change in isotopic mass of a REV is determined by the mass conservation equation. The mass conservation equation can be written as follows:

$$\frac{\partial m_i}{\partial t} = -\frac{\partial q_i}{\partial z} \quad \text{.....(3.1)}$$

where m_i is the mass of isotopes (kg/m^3), t is time (s), q_i is the isotope mass flux (kg/m^2/s) and z is the vertical distance (m). The total mass of isotopes contained within a unit volume of soil in both the liquid and vapour phases is defined as follows:

$$m_i = \theta_l C_i^l + \theta_v C_i^v \quad \text{.....(3.2)}$$

where θ_l and θ_v are the volumetric water content and air (vapour) content of the soil (m^3/m^3), respectively, and C_i^l and C_i^v are the concentrations of the isotopes in the aqueous and vapour phases (kg/m^3), respectively. The relationship between θ_l and θ_v is defined as follows:

$$\theta_v = n - \theta_l \quad \text{.....(3.3)}$$

where n is the soil porosity (m^3/m^3).

The total isotope fluxes for each phase is,

$$q_i^l = C_i^l q_l - D_i^{l^*} \frac{\partial C_i^l}{\partial z} \quad \text{.....(3.4)}$$

$$q_i^v = C_i^v q_v - D_i^{v^*} \frac{\partial C_i^v}{\partial z} \quad \text{.....(3.5)}$$

where q_i^l and q_i^v are the aqueous and vapour phase isotope fluxes ($kg/s/m^2$), respectively, q_l and q_v are the water and vapour fluid fluxes ($m^3/s/m^2$), respectively, $D_i^{l^*}$ and $D_i^{v^*}$ are the hydrodynamic dispersion coefficients for the isotope in the aqueous and vapour phases (m^2/s), respectively. q_i is the total isotopic flux ($kg/m^2/s$) defined by Equation 3.6,

$$q_i = q_i^l + q_i^v \quad \text{.....(3.6)}$$

Combining Equations 3.2, 3.3, 3.4, and 3.5, with 3.1 yields,

$$\frac{\partial(\theta_l C_i^l + (n - \theta_l) C_i^v)}{\partial t} = -\frac{\partial}{\partial z}\left(C_i^l q_l - D_i^{l^*} \frac{\partial C_i^l}{\partial z} + C_i^v q_v - D_i^{v^*} \frac{\partial C_i^v}{\partial z}\right) \quad \text{.....(3.7)}$$

Henry's Law for soluble gas relates the concentration of the species in the aqueous phase to the vapour phase as follows:

$$H = \frac{C_i^v}{C_i^l} \quad \text{.....(3.8)}$$

where H is the Henry's Law constant (unitless). The values of H for gases are defined from empirical measurements and, in a similar manner, experimental measurements of equilibrium

fractionation for isotopes can be cast as a Henry's Law constant. Henry's Law for isotopes as presented by Braud et al. (2005a) is,

$$H = \frac{1}{\alpha_i^*}\frac{\rho_v}{\rho_w} \quad \text{.....(3.9)}$$

where α_i^* is the equilibrium fractionation factor temperature (unitless), ρ_v is the density of water vapour (kg/m^3), and ρ_w is the density of water (kg/m^3). Each of the parameters in Equation 3.9 are functions of temperature, but are presented as single values in this study based on the assumption of isothermal conditions.

Combining Equations 3.8 and 3.7 results in:

$$\frac{\partial(\theta_l C_i^l + \theta_v H C_i^l)}{\partial t} = -\frac{\partial}{\partial z}\left(C_i^l q_l - D_i^{l^*}\frac{\partial C_i^l}{\partial z} + C_i^v q_v - D_i^{v^*}\frac{\partial H C_i^l}{\partial z}\right) \quad \text{.....(3.10)}$$

Re-arranging Equation 3.10 and collecting like terms leads to the final equation,

$$\frac{\partial\left[\theta_{com} C_i^l\right]}{\partial t} = \frac{\partial}{\partial z}\left[D_{com}\frac{\partial C_i^l}{\partial z} - q_{com} C_i^l\right] \quad \text{.....(3.11)}$$

where;

$$\theta_{com} = \lfloor \theta_l + \theta_v H \rfloor \quad \text{.....(3.12)}$$

$$D_{com} = \left(D_i^{l^*} + D_i^{v^*} H\right) \quad \text{.....(3.13)}$$

$$q_{com} = \left(q_l + H q_v - D_i^{v^*}\frac{\partial H}{\partial z}\right) \quad \text{.....(3.14)}$$

From here on the parameters of the dual-phase models with will be referred to as combined parameters. Equation 3.11 has the same form as the advection-dispersion equation. θ_{com} is the combined storage in the water and vapour phase and D_{com} is the combined diffusive and dispersive effects between both phases. q_{com} is the total water flux advective terms between both phases. The combined parameters from the dual-phase equations combine the transport and storage properties of each phase into a single property that can be used to find concentration changes to the combined

liquid phase, as outlined in the previous chapter. In deriving the equations in this way, the effects of vapour phase storage and transport can be accounted for by solving a single transport equation in commercial software packages, which do not readily solve simultaneous phase transport with coupling.

In order to simplify the interpretation of the column tests, the model is reduced further by assuming that there is no free or forced convection of the vapour phase (i.e. q_v = 0). Isothermal conditions cause the H gradient to be 0 ($\partial H/\partial z$). In the case of the stable isotopes of water, the value of H is very small (~10^{-5}), and consequently θ_{com} can be simplified to θ_l. The storage and advective terms can be simplified to,

$$\theta_{com} = \theta_l \quad \text{.....(3.15)}$$

$$q_{com} = q_l \quad \text{.....(3.16)}$$

To finish deriving the hydrodynamic dispersion coefficients, Melayah et al. (1996a) express the hydrodynamic dispersion coefficient for water as,

$$D_l^{l^*} = \Lambda|q_l| + \theta_l \tau_l D_l^{i0} \quad \text{.....(3.17)}$$

where D_l^{i0} is the free solution diffusion coefficient (m^2/s) of the isotope in water, τ_l is the tortuosity factor for the aqueous phase (unitless), and Λ is the dispersivity (m).

The coefficient of diffusion in the vapour phase can be expressed as:

$$D_l^{v^*} = \theta_v \tau_v D_v^{i0} \quad \text{.....(3.18)}$$

where D_v^{i0} is the free solution diffusion coefficient (m^2/s) of the isotope in vapour and τ_v is the tortuosity factor for the vapour phase (unitless). For the vapour phase D_v^{i0} is found by,

$$D_v^{i0} = D_v \left(\frac{D_l^v}{D_v}\right) \quad \text{.....(3.19)}$$

where D_v is the coefficient of diffusion of water vapour in air (m^2/s), and D_l^v/D_v is the diffusivity ratio (Merlivat, 1978) of isotopes in air (unitless). Combining the diffusion equations with D_{com} the final hydrodynamic dispersion coefficient can be found.

$$D_{com} = \Lambda_l|q_l| + \theta_l\tau_l D_l^{i0} + \theta_v\tau_v D_v^{i0} H \quad \text{.....(3.20)}$$

For isotope transport the δ values can be used in place of concentration, as is done in most numerical studies (Shurbaji and Phillips, 1995, Mathieu and Bariac, 1996a, Melayah et al., 1996a, and Braud et al., 2005a). This is highlighted in Appendix A. From here on, isotope concentrations will refer to the isotope δ values normalized (Section 6.1.1.1) to initial and boundary conditions.

3.3 D_{com} in Analytical and Numerical Solutions

The derivation of D_{com} creates additional steps when using the combined phase formulations in analytical or numerical solutions. Due to the ability to include or occlude the volumetric fluid content from a diffusion coefficient, the direct impact of the combined transport equation parameters will be compared to the analytical and numerical modeling methods that will be used later in this study.

3.3.1 Analytical

Two analytical solutions will be used for data analysis in Chapter 6. The first is the Ogata and Banks (1961) analytical solution,

$$\frac{C}{C_0} = \frac{1}{2} erfc\left(\frac{x}{\sqrt{2D_{analytical}t}}\right) \quad \text{.....(3.21)}$$

where, $\frac{C}{C_0}$ is the normalized concentration (unitless), x is the position (m), $D_{analytical}$ is the diffusion coefficient (m^2/s), and t is the time (s). The solution is derived from the equation

$$\frac{\partial C}{\partial t} = D_{analytical}\frac{\partial^2 C}{\partial x^2} - u\frac{\partial C}{\partial x} \quad \text{.....(3.22)}$$

with

$$x = ut \quad \text{.....(3.23)}$$

While no Fick' First Law is presented in this paper Equations 3.22 and 3.23 suggest that the area term (either θ_l or n) is not included with the D value. This is evident in the use of a velocity (u)

instead of a flux ($u = q/n$). If the area was included in the D value it should be presented as D/n to fit with the velocity term.

The second is the Carslaw and Jaeger (1959) analytical solution,

$$\frac{C}{C_0} = \frac{x_0}{L} + \frac{2}{\pi}\sum_{m=1}^{\infty} \frac{exp\left(\frac{-D_{analytical} m^2 \pi^2 t}{L^2}\right)}{m} cos\left(\frac{m\pi x}{L}\right) sin\left(\frac{m\pi x_0}{L}\right) \quad \text{.....(3.24)}$$

where, L is the length of the profile (m) and x_0 is halfway between the beginning of the profile and L (m). Shackelford and Daniel (1991) presents the form of Fick's Second Law in which Equation 3.24 is derived from and is

$$\frac{\partial C}{\partial t} = D_{analytical} \frac{\partial^2 C}{\partial x^2} \quad \text{.....(3.25)}$$

where

$$D_{analytical} = D_0 \tau \quad \text{.....(3.26)}$$

Equation 3.26 does not include the area term. Since both solutions do not include the area term in the evaluation of $D_{analytical}$, Equation 3.27 will be used to determine D_{co} from the analytical solutions.

$$D_{analytical} = \frac{D_{com}}{\theta_{com}} \quad \text{.....(3.27)}$$

3.3.2 Numerical

For numerical modeling of the combined transport equation, the software package CTRAN/W from GEO-SLOPE International was used. From the CTRAN/W product manual, Fick's First Law is presented as (page 73, Equation 10-3, February 2012 edition),

$$J = -\theta_l \frac{\partial C}{\partial x} \quad \text{.....(3.28)}$$

And the governing equation that is used to simulate transport is (page 73, Equation 10-3, February 2012 edition)

$$\theta_l \frac{\partial C}{\partial t} = \theta_l \left(\Lambda \frac{q_l}{\theta_l} + D_{numerical} \right) \frac{\partial^2 C}{\partial x^2} - q_l \frac{\partial C}{\partial t} \quad \text{.....(3.29)}$$

where $D_{numerical}$ is the molecular diffusion coefficient (m^2/s). Assuming only diffusion is occurring ($q_l = 0$) the equation can be simplified to,

$$\theta_l \frac{\partial C}{\partial t} = \theta_l (D_{numerical}) \frac{\partial^2 C}{\partial x^2} \quad \text{.....(3.30)}$$

This equation contains the molecular diffusion coefficient with the θ_l removed. For the combined phase diffusion, the fluid contents are contained within D_{com}. To use D_{com} in the commercial software, the following relationship needs to be used,

$$D_{numerical} = \frac{D_{com}}{\theta_{com}} \quad \text{.....(3.31)}$$

Both $D_{analytical}$ and $D_{numerical}$ are equated to D_{com}, by removal of the water storage term.

3.4 Comparison of the Combined Coefficient of Diffusion

The functional form of D_{com} for the stable isotopes of water can be compared to those forms used for non-volatile aqueous tracers to highlight the importance of incorporating a dual-phase model for the stable isotopes of water in unsaturated soils. This comparison assumes that no advective transport will be occurring ($q_l = q_v = 0$) and all spreading is purely molecular diffusion. Figure 3.2 shows the dual-phase model, with the water contents removed (D_{com}/θ_{com}), compared to other functional relationships for diffusion of a solute within the aqueous phase alone. The other functional relationships are a reduction in diffusion with desaturation (Lim et al., 1998) and a constant saturated value (Shackelford, 1991).

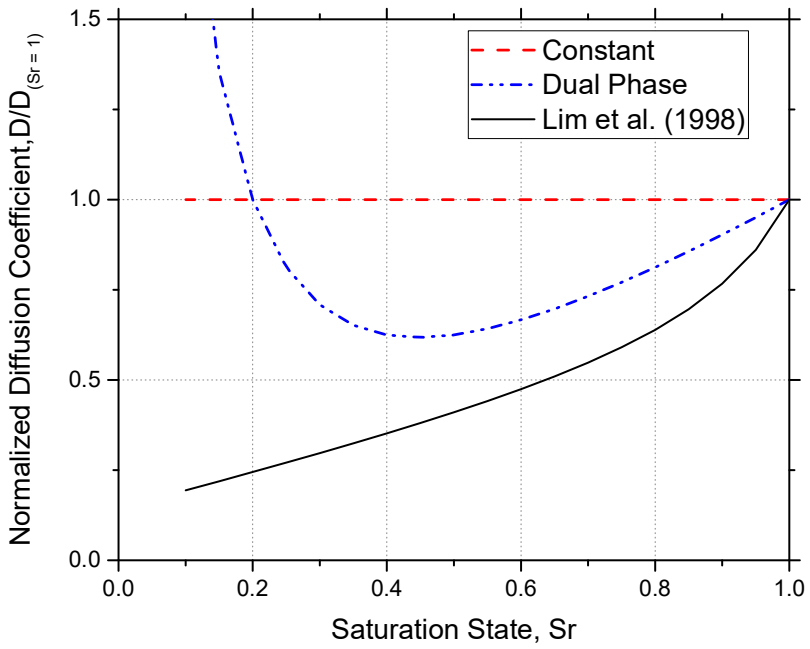

Figure 3.2 - Diffusion model for comparison. Parameters used for D_{com}, D_l^{i0} = 2E-9, D_v^{i0} = 2.5E-5, H = 2E-5, porosity = 0.4, $\tau_l = \theta_l/n$, $\tau_v = \theta_v/n$, with Sr = θ_l/n).

In the case of D_{com}/θ_{com} for the stable isotopes of water, the notable elements of the functional relationship are the minimum that develops at a saturation value of approximately 0.4 and the exceptionally high diffusion value at and below residual saturation. This is in contrast to the Lim et al. (1998) diffusion function for non-volatile solutes where the coefficient of diffusion continues to drop with θ_l. The diffusion coefficient tends towards zero once there is liquid phase discontinuity (i.e. θ_{res}) or to small lower limit reflecting diffusion through interconnected water films on the soil particles. Given that these low values of saturation are commonly encountered in field situations it is of interest to evaluate what effect this functional form might have on the transport of the stable isotopes when dual-phase transport is considered over a single-phase solution.

Gas diffusion studies use a similar combined phase approach to that utilized in this study. These studies have included evaluations of O_2 diffusion through soil covers and mine waste or CO_2 transport through a rooting zone. The functional relationship for the gas diffusion coefficient in unsaturated soils has been estimated using various models of τ as a function of θ_l.

The primary difference between dual-phase transport of soluble gases and isotopes are the differences in the value of H and the relative volumes of the primary transport phase (water in the

case of isotopes and vapour in the case of gas transport). The stable isotopes of water have high rates of diffusive transport in the vapour phase, but this phase has negligible storage. In gas diffusion studies, the gas phase has both a high rate of diffusive transport and tends to be the larger phase for gas storage due to the low solubility of most gases. These differences can be illustrated by comparing the combined diffusion coefficients (θ_{com} included in D_{com}) for the two types of studies as shown in Figure 3.3. The normalized D_{com} profile is not shown for CO_2 as it is indistinguishable from the O_2 profile until a saturation greater than approximately 0.975.

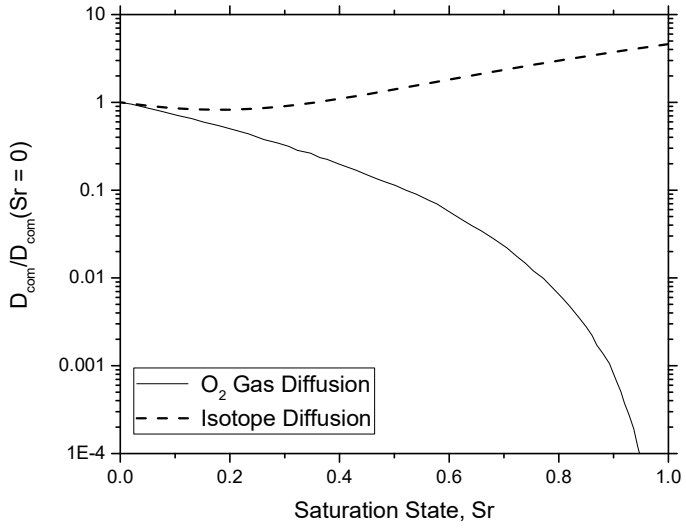

Figure 3.3 - Comparison of the combined isotope and combined O_2 diffusion relationships. Both functions are plotted using the vapour/gas phase as the combined phase (Sr = θ /n).

By using the vapour phase as the combined phase for the isotopes, the shape of the function, when normalized, is the same as using a combined aqueous phase. The non-normalized values for a combined vapour phase, are $1/H$ higher than aqueous. The combined vapour phase would result in a different mass flux being calculated, depending on the concentration gradient, but only the shape of the D_{com} function is being shown here.

3.5 Comparison of the Dispersivity (Λ_l)

Traditionally, mechanical dispersion is considered a constant value for a saturated soil (Kamp et al., 1994) and the value of Λ is dependent on problem scale. The larger the problem scale, typically the larger the Λ (Gelhar et al., 1992). Only a few studies have looked at the changes to soil Λ in an unsaturated soil. Some have attempted to create an empirical functional relationship for a soil,

based on soil texture properties and fitting to observed data (Sato et al., 1995 and Sato et al., 2003). Others have observed the Λ changes with decreasing saturation but have made no attempts at creating a functional relationship to describe the observations (Hutchison et al., 2003, Toride et al., 2003, and Torkzaban et al., 2006). Figure 3.4 shows some available relationships for Λ as a function of θ_l (Derived in Appendix A).

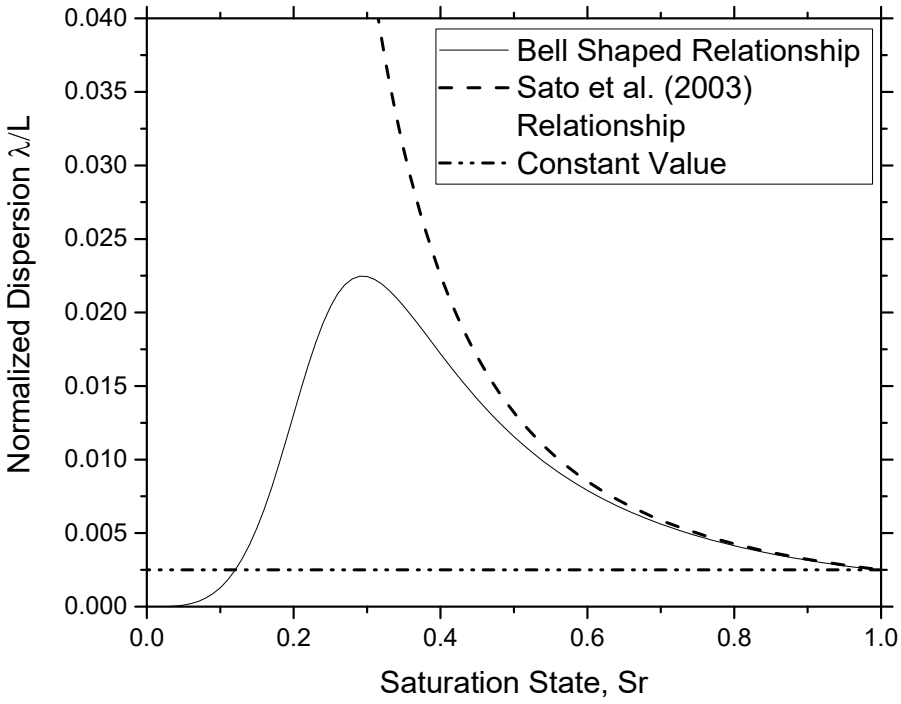

Figure 3.4 - Mechanical dispersion relationships (Sr = θ /porosity).

The increasing Λ with decreasing saturation function of Sato et al. (2003) suggests that as the degree of saturation decreases, the velocity variations become greater. A possible "bell" shaped relationship suggested by data from Toride et al. (2003) and Padilla et al. (1999) suggest a similar behavior to that reported by Sato et al. (2003) at higher saturations but appears to decrease again at lower saturations, possibly when capillary filled pores are replaced by water present only as residual water films. The third relationship compared is a constant value. The constant value is assumed to be the same as the saturated value for the other two relationships.

3.7 Summary

The combined dual-phase transport equations as derived are amenable to simulation using commercial single-phase transport codes as will be shown later in Chapter 6. In D_{com}, several

properties are well defined. These are q_l, H, θ_l and θ_v and the free solution diffusion coefficients D_v^{i0} and D_l^{i0} (Appendix A). The parameters τ_l and τ_v (Appendix A) will be drawn from literature sources and tested for their applicability to this study through modeling exercises completed in Chapter 6. The Λ models presented will be included in the final numerical modelling exercises to see which provides the best description of mechanical dispersion.

Chapter 4 - Experimental Methods and Materials

Two separate laboratory programs were undertaken as part of this research. In the first program, D_{com} will be measured using a double half-cell diffusion test at constant θ_l values. Two column tests were utilized in the second program to re-create a pulse input of water with a stable isotope tracer simulating rainfall or snowmelt. This allowed initial transport by advective-dispersive mechanisms followed by a prolonged period of negligible water flow in which the stable isotope is allowed to move primarily by diffusion. All the experiments were completed in a laboratory where the average temperature is 22.5 °C (no long term data available, personal communication with Adam Hammerlindl).

4.1 Diffusion Cell Experiment

The first laboratory experiment will attempt to determine the θ_l - D_{com} relationship. To do this a double half-cell diffusion test will be used. This section will provide relevant literature, characterization of the geologic media used, design considerations, details of the cells to be constructed, the apparatus and construction methods, and finally the deconstruction and sampling.

4.1.1 Background Literature on Double Half-Cell Diffusion Test

Diffusion testing of unsaturated soils has been done previously in the literature (Shackelford, 1991 and Lim et al., 1998), but only the double half-cell methods has been widely applied (Patil et al., 1963 and Hamamoto et al., 2009). Other diffusion testing methods have been proposed over the years (Barbour et al., 1996, Mbonimpa et al., 2003, and Sreedeep and Singh, 2008) but these methods do not allow for easy collection of soil in the volumes required for this isotopic analysis. The isotope analysis that will be used requires approximately 0.060 kg of soil at a minimum of 5% gravimetric water content (ω) (Wassenaar et al., 2008). The double half-cell method was selected for use as it can be scaled up to the soil volumes needed without a significant increase in cost and complexity.

There are two main experimental issues associated with double half-cell diffusion testing. The first is the need to ensure a constant suction over the entire cell. The suction profiles in the soil are dependent on the cell packing procedure and the cell orientation. Variations in suctions can lead to advective movement of a tracer within the cell. The second issue is the establishment of

connectivity in the fluid phase across the interface between the two half-cells. This is required to ensure proper liquid phase diffusion across the interface where the two half-cells are connected (Van Rees et al., 1991 and Gillham et al., 1984).

The general procedure for a double half-cell diffusion test is:

1. Pack two half-cells with soil and water, one with an elevated tracer concentration.
2. Join the cells together, and
3. Allow diffusion to occur over a set period.

Figure 4.1 shows the conceptual schematic for a typical experiment, with typical results shown in Figure 4.2 (Shackelford, 1991).

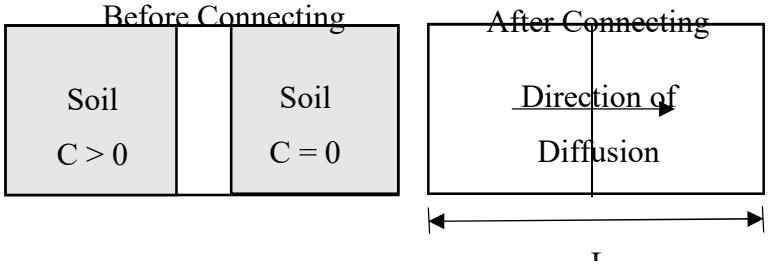

Figure 4.1 - Schematic of double half-cell diffusion test. Showing cells before connection and after connection (after Shackelford, 1991).

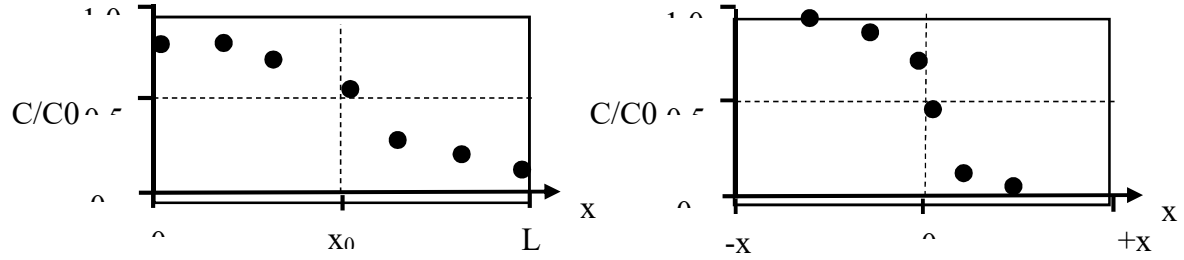

Figure 4.2 - Typical cell results. The left plot shows the conditions where the ends of the cell are no longer at a normalized concentration of 1 and 0, causing the cell to become finite. In the right plot the end values are at a normalized concentration of 1and 0. The right figure can be analyzed as if it were an infinite cell (after Shackelford, 1991).

The final distribution of tracer within the two half-cells can be interpreted using analytical solutions for diffusion. If solute diffusion has not advanced to the ends of the cell then the analytical solution for an infinite half-cell (Ogata and Banks, 1961) can be used. If the solute

diffusion has reached the end of the cell then the analytical solution for a finite cell (Carslaw and Jaeger, 1959) is used.

4.1.2 Diffusion Cell Experimental and Apparatus Design

The diffusion testing was done in four different experimental trials with five cells being constructed in each trial. Details of each trial can be found in Table 4.1 and Table 4.2. The additional trials of testing were used to overcome identified shortcomings in previous trials and to create a complete data set.

Table 4.1 – Overview of experimental trials created

Experimental Round	Shorthand	Soil Suction Control Method	Tracers	Reason for Experimental Round
1	R1	Mixed	Isotope	Initial experiment to find diffusion coefficients
2	R2	Mixed	Isotope	Improved upon R1 with a more efficient construction procedure
3	R3	Hanging Column	Isotope	Used to create natural drained channels versus the well distributed water of packed methods and explain variability in packed methods
4	R4	Axis Translation	Isotope and chloride	Improved upon the R3 experiments with a more robust drainage system and suction control

Table 4.2 – Personnel responsible for the construction and analysis of each experimental trial

Cell round	Personnel	Notes
R1	Author, Terryn Kuzyk, Mengna Lu	Class project
R2	Author	Data collection for thesis
R3	Author	Data collection for thesis
R4	Author, Shelby DeMars, Shahabul Alam	Class project, and Data collection for thesis

The diffusion cell construction material and sizes were based on the requirements for the isotope analysis. Home plumbing PVC pipe was selected because it is readily available, inexpensive, has couplers and caps prefabricated, has commercially available glues, and can will be easy to cut for the destructive sampling method required. The pipe is available in many sizes ranging from 1 inch (0.0254 m) to 6 inch (0.1524 m). The diameter of the pipe was selected to give the smallest sample thickness, while still meeting the mass requirements for isotopic analysis. A sample thickness of between 0.01 – 0.03 m was selected to capture the diffusive spreading of the isotopes. The 4 inch (0.1016 m) and 6 inch (0.1524 m) pipes were selected to provide sufficient soil for analyses at the desired sample thickness. The 6 inch (0.1524 m) pipe was discarded because of significantly increased costs, fewer coupling collars and caps available, and the increased mass of sand required. Only a limited amount of sand was available for the diffusion cells.

Based on Wassenaar et al. (2008), 0.060 kg of soil at a minimum of 5% ω are needed for an accurate isotope analysis in a 1L Ziploc® bag. This requires approximately 0.003 kg of water per liter of bag headspace. Using the larger 4L Ziploc ® bags, 0.1016 m diameter pipe, and a sample thickness of 0.02 m a total of 0.0033 kg of water per liter of bag space is available (ρ_{dry} = 1590 kg/m^3, porosity = 0.4, ω = 5%). For the final experiment (R4), the length of each sample slice was increased to 0.03 m to provide an additional 0.100 kg of soil sample for chloride analysis.

The total length of each half-cell was selected based on modeling of the transport of the isotopes. The diffusion rate used to model the isotope progression was the estimated value at saturation ($D_{com}/\theta_l = 1.5E-9$ m^2/s). The extent of the diffusive spreading after 30 days was found to be approximately 0.20 m. Each half-cell was constructed at a length of 0.20 m for all trials except for

R4 where it was increased to 0.27 m. The cells were allowed to diffuse for 11 to 35 days depending on when sampling equipment was available.

Five cells were created for each trial with target ω's selected to cover the entire saturation range. The ω for R1 were selected in 2.5% ω increments beginning with the minimum 5% ω as defined by Wassenaar et al. (2008). The ω for R2 were selected to be close to the R1 values, but adjusted to fill in the gaps from the R1. Trial R3 had a set of target ω's, but the failure of the drainage layer resulted in gravity drained conditions for each cell constructed. The ω for experiment R4 was selected to cover the data gap at lower ω.

The soil water placed in one of the half-cells had an elevated concentration of δD or chloride. In the experiments where no chloride was used, laboratory tap water was used to prepare the soil. When a chloride spike was used, distilled water was used to ensure that the chloride concentration in the non-spiked soil was below detection limits. The tracer spike concentrations used in each experiment is summarized in Table 4.3. The lack of a $\delta^{18}O$ spike was used as a check to ensure that there were no evaporative losses from the cells.

Table 4.3 – Initial conditions and source of spike concentration

Experiment	Non-Spiked Cell Isotope	Spiked Cell Isotope (‰)	Non-Spiked Cell Chloride	Spiked Cell Chloride (mg/L)
R1	Tap water	Spiked with D2O to ~-50	Not Used	Not Used
R2	Tap water	Spiked with D2O to ~-50	Not Used	Not Used
R3	Tap water	Spiked with D2O to ~-50	Not Used	Not Used
R4	Distilled water	Spiked with D2O to ~-50	Background distilled water	Spiked with NaCl to 100

4.1.3 Characterization and Preparation of Geologic Media

Two soils were used for the experiments. The first was a fine sand obtained from storage in the laboratory (sourced previously from Beaver Creek southeast of Saskatoon, Saskatchewan). The sand was composed of 96.5% sand, 3.5% silt and clay, and a grain density of 2670 kg/m^3 (Bruch, 1993). A second coarser sand was collected by the author from the Beaver Creek site. The sands were prepared by rinsing with tap water followed by air drying. In R1-R3, the sand was sieved

through a 425 µm sieve to remove large rocks, cemented soil, and organic matter. In R4, the fine sand was mixed with the coarse sand in a 2:1 mass ratio and then sieved through an 800 µm sieve.

The hanging column elevations for R3 were based on the soil water characteristic curve for the sand (a = 8.17 kPa, n = 3.2, m = 1-1/n, Van Genuchten, 1980). The SWRC properties were found by fitting the Van Genuchten (1980) SWRC relationship to a Modified Kovac's (Aubertin et al., 2003) SWRC. The Modified Kovacs SWRC was found from the particle size distribution (PSD) of the fine Beaver Creek Sand (d_{10} = 0.029 mm, d_{50} = 0.129 mm, d_{60} = 0.149 mm, found on a Malvern Mastersizer 2000 equipped with Hydro MU). The SWRC for the 2:1 mixed Beaver Creek Sand was estimated with the Modified Kovac's estimate, but no fit with the Van Genuchten (1980) SWRC was done (d_{10} = 0.090 mm, d_{50} = 0.216 mm, d_{60} = 0.244 mm found on a Malvern Mastersizer 2000 equipped with Hydro MU). A description of the coarse Beaver Creek Sand will be presented with the column experiment.

4.1.4 Diffusion Cell Experiment Methodology

The apparatus and construction procedure for experiments R1-2, R3 and R4 were all unique. The experiments were updated after each round of experimentation to create a more reliable and complete data set. The basic parts to each cell are the cell, cap and joining collar (Figure 4.3). The apparatus and procedures for R1-2, R3, and R4 follow.

Figure 4.3 – Parts of half-cell. Left: joint repair collar to join two half-cells. Middle: 0.1016 m diameter PVC pipe for the half-cell body. Right: PVC end cap for containing soil and water.

4.1.4.1 Diffusion Cell Experiments 1 and 2

Experiments R1 and R2 were filled with soil and water with a packing method. A PVC cap was glued on one end of the half-cell with the other left open. The mass of sand required obtain a porosity of 0.4 (ρ_{dry} = 1590 kg/m^3) and the mass of tap water required to achieve the target ω for each half-cell were collected. The water for the spiked half-cell was either prepared for each cell individually (R1) or drawn from a large reservoir prepared in advanced (R2). The masses of sand and water were placed in a metal bowl, thoroughly mixed and packed into a half-cell. The mixing and packing was done rapidly to minimize water loss and fractionation from evaporation.

All of the sand required for the cell was placed in lifts (approximately 50 mm thick) and compacted until a small amount of the sand was protruding just above the top of the cell (1-2 mm). The half-cells were placed together and sealed with a PVC collar that was glued into place. The total cell mass was recorded repeatedly to check for water loss over the experiment duration. A completed cell for trials R1 and R2 is shown in Figure 4.4.

Figure 4.4 – Assembled double half-cell. The cell in the picture is assembled at 0.40 m in length.

4.1.4.2 Diffusion Cell Experiment 3

Drainage of the sand was attempted in the R3 tests to minimize some of the limitations associated with the packing methods. The drainage system created had failed thus each of the cells had gravity drained conditions. The R3 cells were constructed with a drain tapped into the PVC cap (Figure 4.5) and a compacted silt was placed in the bottom of the cell (air entry value unknown), to provide a high air entry layer. On top of the silt a porous plastic plate (air entry value of ~15kPa, unknown origin) was used to keep the experimental sand and the silt from mixing (Figure 4.6).

Figure 4.5 – Drain on the bottom of a half-cell with a hose for a hanging column to be used to set the soil suction.

Figure 4.6 – Packing schematic for experiment R3.

The total mass of sand required to fill the cell was placed loose in the cell with an extra piece of pipe attached to extend the length of the cell. The sand was compacted by tapping the side of the cell with a rubber mallet, until the sand had densified to the top of the cell. The extra pipe was then removed. Before filling with water, the sand was saturated with CO_2 from the bottom up, to displace air and ensure full saturation when subsequently filled with water. After the CO_2 flood, the cell was filled with water in the same manner. Once the cell was fully saturated a Ziploc® bag

was taped over the exposed top to allow for a collapsible headspace, which would stop evaporative fractionation and not create back suction during drainage.

The cells were place near the hanging column apparatus (Figure 4.7) and the output hose attached to the collection bottles. When there was sufficient suction to retain the soil, the cells were placed on their side to reduce the effects of gravity on the suction profile. Once the drainage had stopped, the cells were joined together, weighed, and allowed to diffuse for a set amount of time. A completed cell can be seen in Figure 4.8.

Figure 4.7 – Cells under hanging column.

Figure 4.8 – Complete double half-cell for experiment R3, with drain hoses removed

4.1.4.3 Diffusion Cell Experiment 4

The R4 cells were constructed to resolve issues encountered in the R3 tests. The silt and porous plastic layer was replaced with high air entry porous ceramic plate (air entry value ~50kPa, diameter of 0.0762 m, thickness of 0.007 m, from Soil Moisture Equipment Corp.) that was siliconed (Dow Corning® 1199 Silicone Glazing Sealant) into a machined recess (Figure 4.9). The sealing was used to ensure that water could only leave the cell through the ceramic plate. The drainage method was changed from a hanging column to axis translation. Axis translation is a process of controlling matric suction, defined as air pressure minus water pressure, and is achieved by controlling the air pressure within a cell relative to a fixed water pressure set at the base of the high air-entry disk.

Figure 4.9 - PVC cap with ceramic plate siliconed in recess.

The construction of the R4 cells was more complex than the previous tests due to the use of a saturated ceramic plate. The caps with the ceramic were placed in a vacuum chamber to fully saturate the disks with water and remove any trapped air. Once the ceramic was saturated (~24 hours under vacuum), the caps were removed from the vacuum chamber, keeping enough water in the cap to submerge the ceramic plate and prevent drying. The PVC pipe was then glued on and the glue was allowed to dry (~3 hours). A wet packing method was used to fill the cells with sand. This method was used in place of the CO_2 flood to avoid desaturating the porous ceramic. The wet sand packing method was as follows:

1. A small amount of sand was placed in the water covering the ceramic plate (~0.030 kg),
2. This process was repeated until the sand reached near to the level of the free water,
3. Additional water was gently added to extend the depth of water approximately 0.02 m above the sand. The water was added by spraying it along the side of the cell, as to not disturb the already placed sand,
4. The cell was then tapped several times with a rubber mallet to compact the placed sand,
5. Steps 2-4 were then repeated ensuring equal amounts of sand are placed and a consistent compaction technique followed until the cell was full of saturated sand.

The cells were then sealed and compressed air was applied to drain the cells through the ceramic until the targeted θ_l was reached. A special cap was constructed to temporarily seal the top of the cells so they could be pressurized (Figure 4.10). The cap was attached by placing vacuum grease on the contact area and using a large metal hose clamp to hold the cap on tightly. Air pressure was increased incrementally until the desired amount of water had drained from the cell to achieve the target θ_l. The sealing cap was removed and the half-cells were joined together, weighed, and then allowed to diffuse.

Figure 4.10 - Top cap for axis translation drainage.

4.1.4.4 Cell Deconstruction and Analysis

When the cells were ready to be analyzed (time selected based on modelling), each cell was cut in half and each half was cut again into 0.02 m (0.03 m for R4) slices for analysis. The cells were cut using a band saw. Each slice, including sand water and PVC, was placed into its own 4L Ziploc® bag and identified with a unique name describing the positions of the cell that the sample came from. The mass of the entire slice and the bag were taken before the isotope analysis. In the R4 tests, 0.100 kg of soil and water were removed from the Ziploc® bag and prepared for chloride analysis.

The isotope analysis was done in The NSERC Aquitard Geochemistry Lab (University of Saskatchewan, Saskatoon, Saskatchewan) using several water isotope analyzers (analyzer used for

each cell in Appendix B). The error for all the analyzers used was the same (1σ for δD is ± 2.1‰, and for $\delta^{18}O$, 1σ is ± 0.4‰). Measurement of the stable isotopes of water composition of the sample pore-water followed the methods proposed by Wassenaar et al. (2008). The analysis had the following procedure:

1. Inflate the Ziploc bag with dry air
2. Place inflated bag inside a second Ziploc bag
3. Allow water to equilibrate with headspace for 12 hours.
4. Analyze soil vapour for approximately 5 minutes
5. Allow apparatus to return to initial conditions
6. Steps 4 and 5 were repeated until all collected samples were analyzed

After the isotope analysis was complete, the second bag was removed and the single bag and its contents were weighed again. The mass of the soil in each slice was measured using set of aluminum pans with a measured tare weight. A brush was used to get all the sand off of the PVC ring. The dry weight of the sand and pan was obtained after 24 hours of oven drying (100°C).

The thickness of the PVC ring for each sample slice was measured. For slices that were clearly of non – uniform thickness, measurements were averaged from the thickest portion, the thinnest portion, and one in the middle. On slices that looked uniform, the three measurements were taken approximately 120° apart and then averaged. The average slice thickness was used to determine the density and θ_l of each slice.

The isotopic composition of the spiked and un-spiked pore water were measured at different times. First was the liquid water, with and without a D_2O spike, and second was the pore-water isotopic composition of the mixed water and sand. Finally, in the case of the R4 tests, samples of water drained from each cell were measured. For Trial R4, the water samples were analyzed in the Cameco Aqueous Geochemistry Lab (University of Saskatchewan, Saskatoon, Saskatchewan) using Ion Chromatograph (IC). The IC analysis was performed using a Dionex ICS2100 coupled to a Dionex AS-AP Autosampler. The method that will be used is EPA method 300.1 (Price, 2009). The chloride detection limit was 0.05 mg/L with an error of 5%.

4.1.5 Data Collection

The data collected for each experimental round is highlighted in Table 4.4. The dry density (ρ_{dry}) will be used to calculate θ_l from ω.

Table 4.4 - Data Collection for each experimental round. Cell measurements were done on the complete cell and slice measurements were done on each cut slice.

Cell round	Isotope	Chloride	ρ_{bulk} and ρ_{dry}		ω	
			Cell	Slice	Cell	Slice
R1	Yes	No	Yes	No	Yes	No
R2	Yes	No	Yes	Yes	Yes	Yes
R3	Yes	No	Yes	Yes	Yes	Yes
R4	Yes	Yes	Yes	Yes	Yes	Yes

4.2 Column Experiment

This section describes the design and construction of the column tests. It will start with a brief review of relevant literature on the use of column tests for transport through unsaturated soils. Following will be a description of the column design, the experimental methodology, sampling procedures and a summary of the data was collected from each test.

4.2.1 Background Literature on Column Testing of Unsaturated Soils

Two key factors associated with the use of soil columns to study water flow and chemical transport are the creation of homogeneous soil packing and the need to limit or control preferential flow along the column sidewall. In a review paper on soil column design, Lewis and Sjöstrom (2010) suggest that the most effective packing method for an unsaturated soil column is through the use of a slurry packing method. In this study a dry packing method was selected and, based on the recommendation of Oliviera et al. (1996), the individual lifts were kept to 0.02 m in thickness to obtain a uniform density. The dry packing method was selected because the TDR probes that were placed into the column would have more support if the sand was already in place prior to insertion of the TDR. If the probes were inserted into the column before packing, placement of the sand could cause density variations or preferential flow paths near the TDR.

Lewis and Sjöstrom (2010) recommend that the size of a column should not exceed a 4:1 ratio of length to diameter in order to minimize the effects of preferential water flow along the sidewall. The length to diameter ratio for the constructed columns was 8.2:1, approximately twice as long as that recommended. Preferential side wall flow was limited by utilizing a sufficient low water application rate to ensure the column remained in an unsaturated condition and by applying water to the column away from the edges.

4.2.2 Characterization and Preparation of Geologic Media

The coarse Beaver Creek Sand (also used in the diffusion cell experiment) was collected from the field in several 20 L pails and then spread out to air dry in the laboratory. Following drying (< 1% ω) it was sieved through an 800 µm sieve to remove organic debris, large rocks, cobbles, and cemented sand. Any cemented sand found was gently ground with a mortar and pestle to free the sand grains then re-sieved. All of the collected sand was well mixed to make a homogeneous mixture of 75 kg of sand. The dry, mixed sand was placed in 20 L pails for storage until the columns were filled.

The PSD was found for the sand for initial estimates of the SWRC (d_{10} = 0.149 mm, d_{50} = 0.255 mm, d_{60} = 0.279 mm found on a Malvern Mastersizer 2000 equipped with Hydro MU). The full PSD for the coarse Beaver Creek Sand will be presented in Chapter 5.

For the coarse sand, the a and n hydraulic parameters (Van Genuchten, 1980) and saturated hydraulic conductivity (K_{sat}) of the soil will be estimated independent from the column experiment. The Van Genuchten, 1980 relationship was used because if its ease of application (compared to Fredlund et al. (1994)) while providing more freedom compared to a simpler model such as Brooks and Corey (1964). These values will be used for initial modeling of the column results. The Van Genuchten (1980) SWRC curve parameters were estimated by:

- fitting the SWRC curve to elevation - θ_l data collected from a Tempe Cell experiment and a bench scale column,
- modeling the drainage of the columns from saturation to field capacity, before the experiment was conducted, and
- by using the Modified Kovacs relationship of Aubertin et al. (2003) relating the SWRC to the soil PSD and fitting the SWRC with the Van Genuchten (1980) relationship.

The K_{sat} will be estimated by:

- conducting a falling head permeability test,
- modeling the drainage of the columns from saturation to field capacity, before the experiment was conducted, and
- by estimating the value using Hazen's formula (Carrier III, 2003).

4.2.3 Column Experimental and Apparatus Design

The columns for the infiltration experiments were made of clear acrylic to allow direct observation of the soil during the test. The internal diameter for the column was 0.182 m with a wall thickness of 0.0106 m. The large wall thickness was selected so the sampling ports could be machined into the side of the column without overstressing the column. A length of 1.50 m was selected to maximize the size of unsaturated zone that would develop above the capillary fringe. An outside diameter of 8 inches (0.2032 m) was selected because equipment was available in the lab at that size. However, the equipment that was intended to be used was not easily salvaged from previous research work.

The sand used in the columns was the same coarser dune sand used in the diffusion cells (Beaver Creek SK, Bruch, 1993). A coarse sand drainage layer was placed at the base of the column to provide a filter for the gravity drainage lower boundary.

The diameter of the sampling ports was selected to yield approximately 0.060 kg of soil per sample. Sampling was to be done three times during the experiment. The maximum length of each sample across the column diameter could be approximately 0.06 m. The selected sample diameter was 0.03 m that resulted in a sample volume of 42.4E-5 m^3. Assuming a ρ_{dry} of 1 590 kg/m^3, this sample volume would provide approximately 0.068 kg of soil, sufficient for isotope analysis at a ω greater than 5%. The assumed density was later found to be lower than that obtained in the column testing.

A filler plug was used to fill the void left by the soil sampling. If the void was repacked with sand there would be questions about whether the density and θ_l were consistent with the surrounding sand and whether liquid phase continuity was re-established. The use of the filler plug ensured that the surrounding soil was left intact, and since it was removable, it also allowed access for additional depths of sampling at the sample location as described in Section 4.2.4.3. It is important

to note that the replacement of the void space for three samples with a solid filler resulted in blockage of approximately 5.4E-3 m^2 of the approximately 26.2E-3 m^2 of area available for flow. This means that between sample 1 and sample 2, approximately 7% of the flow area will be disturbed. Between samples 2 and 3, approximately 14% of the area will be disturbed and after sample 3 approximately 21%.

The use of two columns allowed for the use of two different infiltration durations; half an hour and one hour, at the same water application rate. The two different application times allowed for analysis of diffusion over different θ_l ranges. In the column with a shorter application the initial advective advance of the tracer was limited and consequently diffusion occurred over a depth interval in which the θ_l were near field capacity (θ_{res}). In the case of the column with the longer application time, the tracer advanced deeper into the column where the θ_l begins to rise within the capillary fringe.

The single infiltration pulse followed by prolonged drainage allowed for a series of transport conditions to be observed:

1. Advection-dispersion during initial infiltration and drainage,
2. an intermediate time when neither dispersive nor diffusive transport are dominant.
3. And diffusion dominated transport following the cessation of drainage,

The actual times for sampling were selected based on initial modeling of the columns with parameters selected from bench scale lab experiments.

Both D and ^{18}O were used as tracers for the column tests. D is a relatively inexpensive tracer but ^{18}O is expensive. A relatively inexpensive way to obtain both tracers was to utilize Saskatoon tap water ($\delta D \approx -132.1‰ \pm 2.1‰$ and $\delta^{18}O \approx -16.3‰ \pm 0.4‰$ from column analysis) as the initial pore-water in the column and then use bottled water from a different climate zone as the spiked water. After previous testing several commercial bottled waters it was found that Aquafina® bottled water had the desired isotope content for the experiment (personal communication, Erin Schmeling). The Aquafina® water was purchased in 0.5 L bottles which were subsequently mixed and stored in a sealed 18 L water jug to provide sufficient water for both column tests. The water had a δD of $-85.5‰ \pm 2.1‰$ and a $\delta^{18}O$ of $-11.8‰ \pm 0.4‰$ after three measurements.

4.2.3.1 Column Apparatus Construction

The apparatus for the column experiment was composed of four parts; the column, the soil (including the drainage layer), the rainfall simulator, and the sampling equipment. The construction procedure for each follows.

4.2.3.2 Column

The columns were machined with sampling ports (0.0381 m diameter) placed 0.10 m apart along the length of the column (13 total per column). The TDR access ports were offset 90° around the circumference of the column and 0.05 m vertically from the sampling ports. The TDR access ports were drilled at a spacing of 0.10 m (13 sets per column) and were 0.0032 m (1/8 inch) holes spaced 0.04 m apart along the column width.

The bottom of the column was fitted with a 3/4 inch (0.0191 m) thick, 9 inch (0.2286 m) square, PVC plate. The plate was recessed so that the column could be glued into the base. A drainage hole to fit a brass 3/4 inch NPT garden hose adapter was drilled in the center of the base plate. The adapter allowed a garden hose segment to be used to collect and divert outflow waters to a calibrated reservoir. Figure 4.11 shows the machined column, with the sampling ports, TDR ports, and base plate visible.

Figure 4.11 - Column with sampling ports and TDR probe ports visible (under masking tape) before sand packing.

The sampling ports were created for bulk sampling of the column. A flat recess was machined into the side of the column with threads inside. A PVC cap and O-ring were used to seal the port and allow for easy removal for sampling (Figure 4.12).

Figure 4.12 - Sampling cap with threads and O-ring visible. Vacuum grease was needed to keep the O-rings from falling out of the machined recess and keep a water tight seal against the column.

The TDR probes (0.153 m length) were placed after the sand packing (Figure 4.13 shows them in place without sand). The probes were inserted until only enough of the probe was outside of the column so the coaxial cables could be attached.

Figure 4.13 - TDR probes placed in empty column. Probes are 0.153 m in length and are 84% of the column diameter.

4.2.3.3 Soil Packing

A fine metal mesh was siliconed over the drain hole to retain the soil in the column. A graded drainage layer was created over the screen using four individual layers of poorly graded sands as shown in Figure 4.14. These layers were densified by tapping the base with a rubber mallet. Each layer was finer than the underlying layer so that the final lift had a PSD similar to the experimental sand. The entire drainage layer was vibrated with the mallet until the finest sand had penetrated about halfway through the coarser sands. This vibration penetration ensured that none of the finer sand or experimental sand would be piped into the coarser sands during infiltration and drainage (Figure 4.15).

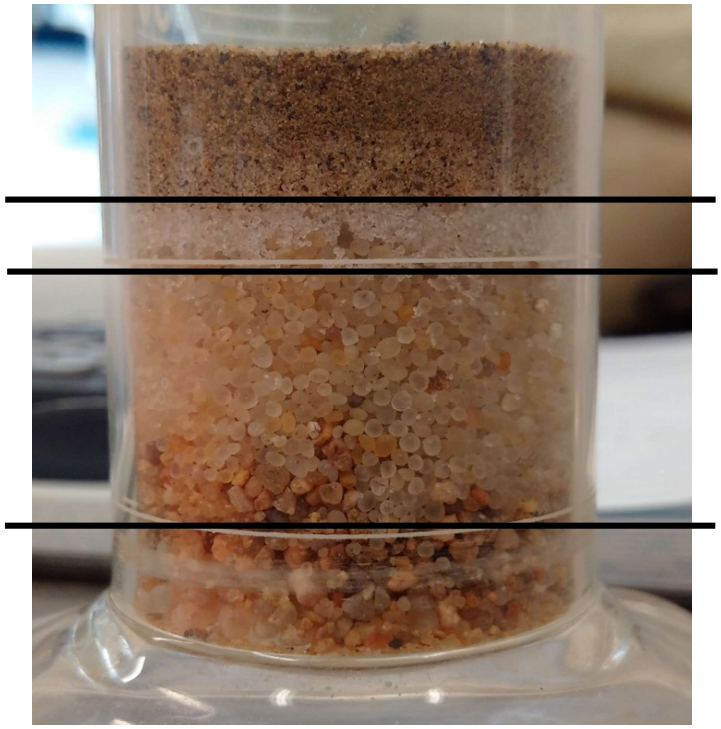

Figure 4.14 – Drainage layer sands with no densification. Proportions for the actual columns were different. The first (bottom) later is the coarsest followed by layers two, three (white sand), and four (dark fine sand). White lines on glass are 0.1 L gradations on a 1 L graduated cylinder.

Figure 4.15 –Bottom drainage layer for complete packed column. The third layer was much thicker under construction compared to Figure 4.14. The penetration of layer three can be seen into one and two from approximately 0.01 m to 0.025 m in column height. The fourth layer can be seen to have minimal penetration (~0.04 - 0.045 m elevation) into the third making a filter for the experimental sand above.

The sand was placed into the column by dropping the sand through extendable sections of PVC pipe (Figure 4.16) to funnel the sand to the bottom of the column with limited segregation. The pipe was placed on top of the drainage layer and filled with sand to the top. The pipe was then lifted 0.02 – 0.03 m and moved in a spiral pattern around the column. Once the sand in the pipe had gone down 0.04 – 0.05 m from the top of the pipe it was carefully refilled. This process was repeated until a section of the pipe was above the top of the column. The pipe section was removed and the column was tapped with a rubber mallet to densify the sand. The entire process was repeated until the column was filled to 0.05 m below the top edge of the acrylic column. During packing, the TDR probe ports were sealed with masking tape, and the sampling ports were sealed with their caps.

Figure 4.16 - Collapsible pipe sections for sand packing. Each section is 200 mm in length and 48 mm in diameter. The sections were slotted together and reinforced with a metal hose clamp so they did not come apart under the weight of the sand.

4.2.3.4 Rainfall Simulator

A rainfall simulator was used to apply the water pulse to the top of the column. The rainfall simulator consisted of a 9 inch (0.2286 m) square 3/16" thick (4.8 mm) PVC plate with a machined recess to fit on the top of a column. A grid of holes spaced 1 inch (25 mm) on center were machined through the plate for water application. Water was distributed to each of the holes in the plate from a PVC manifold. The manifold was 1 inch diameter pipe with a cap on each end. 1/8 inch (3.2 mm) airbrake line was siliconed into the manifold and the plate.

A rubber septum was placed on the end of each hose and a monoject250 (0.8 mm x 25.4 mm) needle was inserted through the septum. The plastic Luer-Lock side of the needle was cut off to remove the small reservoir at the end of the needle (Figure 4.17). The manifold was attached along the side of the plate at the approximate elevation of the outlet of each hose to ensure pressures remained as low as possible. A hose from a peristaltic pump was attached to the manifold to supply water at a controlled rate for the rain simulator. The complete rain cap can be seen in Figure 4.18.

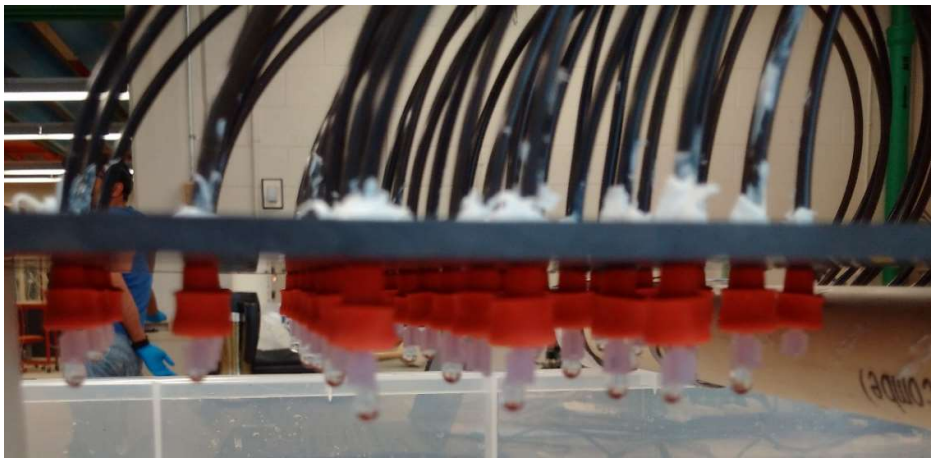

Figure 4.17 – Needles, septum and hoses in the top plate for the rainfall simulator.

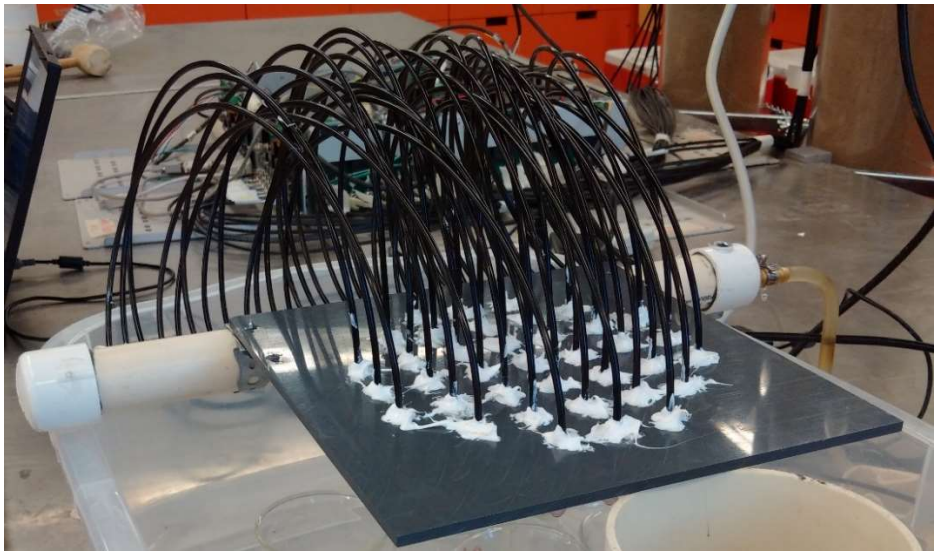

Figure 4.18 – Complete rainfall simulator.

4.2.3.5 Sampling Equipment

Three soil samples were taken from each sampling port over the course of the experiment and a final sample was taken just before column deconstruction. The soil was removed from the column using a miniature Shelby Tube (OD = 31.8 mm, ID = 30.1 mm), soil was retained using collars (OD = 35.1 mm, ID = 32.3 mm), and the voids were filled with PVC plugs (OD = 31.7 mm). The Shelby tube and collars were constructed out of stainless steel and the plugs were PVC. The collars and plugs were 59.3 mm long so three sections could be used in the column at the same time. A complete set of sampling equipment can be seen in Figure 4.19.

Figure 4.19 – Sampling equipment for bulk sampling of column soil. Top to bottom, Collar pushing tool, Shelby Tube, Plugs, and collars.

Outflow was collected from the columns using the hose attached to the base plate. A ball valve was plumbed inline before the end of the drain hose to stop water outflow as needed. The free draining end of the hose was placed in a 4 L bucket, with a 0.750 L beaker to monitor outflow volumes. The bucket had a small hole in the side and the lid was placed on to reduce the evaporative losses.

The TDR probes were attached to a multiplexor array (Campbell Scientific SDMX50) via coaxial cable. The multiplexor array was connected to a TDR unit (Campbell Scientific TDR100) and the entire system was controlled with a data collector (Campbell Scientific CR10X). The system was programed to take TDR measurements in 2 minute intervals, with each measurement taking one second. The TDR multiplexor system used can be seen in Figure 4.20.

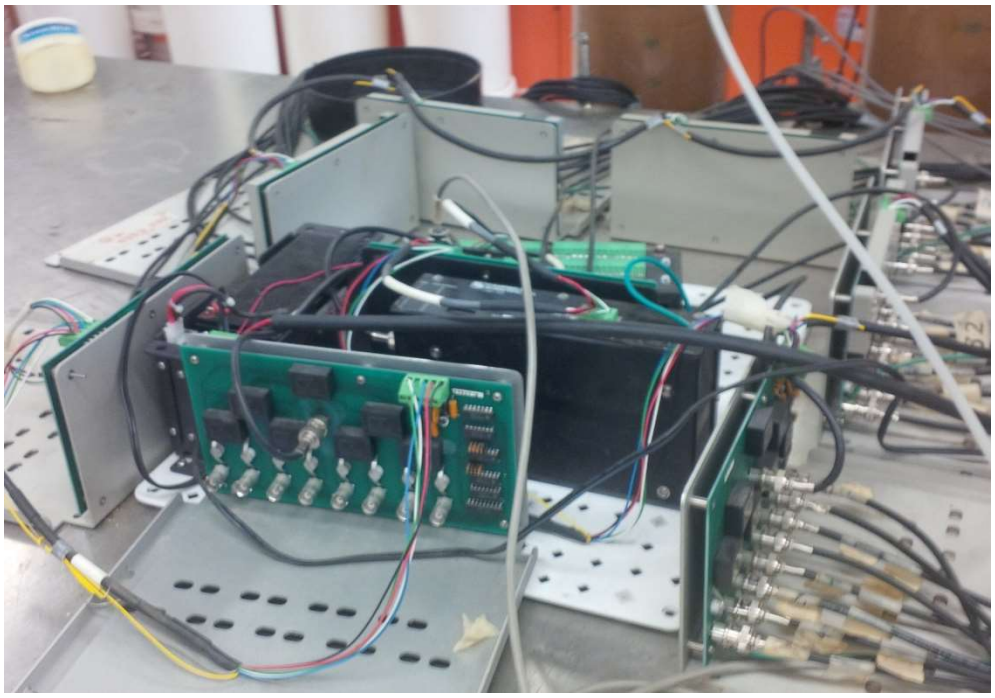

Figure 4.20 – TDR measurement system.

4.2.4 Column Experiment Methodology

The experimental procedure for each of the columns was the same, with differences noted where applicable. The experimental procedure will be described in three phases: column setup, column testing, and finally soil sampling.

4.2.4.1 Column Setup

Each column was prepared in the following manner. A CO_2 flood from the bottom up was used to displaced all of the air within the column and allow for complete saturation. For the CO_2 flood, a compressed gas cylinder was attached to the outflow tube and CO_2 was provided at the minimum flow rate at which the cylinder could be controlled. CO_2 saturation of the column was determined when a burning candle, placed on the top of the sand, was extinguished. The CO_2 flood was followed by saturation of the column with water from the bottom. Water was then pumped into the base of the column using a peristaltic pump that drew water from a 20 L pail of tap water. The pail was kept full to reduce the effects of evaporation on the isotope content of the water.

Once the column was saturated a separate drainage procedure was used for each of the columns. C1 was filled as above. After saturation the ball valve on the bottom was opened and the column

was allowed to drain for three days, then the experiment was started. C2 was saturated and allowed to drain, similar to C1, but, once the drainage had stopped, the column was re-saturated with water (no CO_2) and drained a second time, for three days, before the experiment was started.

During the final drainage for each column, the outflow volumes were recorded with time. Measurements of internal θ_l were made using the TDR system recording at 2 minute intervals. The drainage outflow and TDR data was used to estimate the hydraulic properties of the sand.

Following drainage of the column a piece of woven geotextile was placed on the top of the column and covered with a small layer of very coarse sand. The woven geotextile was used to protect the top of the sand from water droplets and to distribute the applied water. The coarse sand was used to hold down the geotextile and keep it in contact with the sand surface and ensure hydraulic connectivity.

The rainfall simulator was then prepared by filling the PVC manifold with water using the peristaltic pump. Air trapped in the manifold was vented out though the vent plug in the end caps. A high pumping rate was then used to push all the air out of the airbrake lines to the needles. The air free rainfall simulator was place on the top of the column.

4.2.4.2 Column Testing

Infiltration testing was initiated by applying a steady rate of water to the column using the rainfall simulator. The rate of rainfall application used was the lowest rate that the peristaltic pump used can provide. Spiked water was taken from the large sealed reservoir and placed in a 1 L graduated cylinder, and weighed. The peristaltic pump was attached to the rainfall simulator manifold and the free end of the hose was place into the spiked water source. The TDR system was started and the peristaltic pump was set at 0.010 kg/min. When the experiment was started not all the rain drop ports were supplying water to the column. To mitigate the reduced number of raindrops, the entire rainfall apparatus was rotated every 5 minutes to ensure even water coverage. Once application time had passed the peristaltic pump was turned off and the graduated cylinder was weighed again.

After the raining, the outflow was collected from the pail twice per day and the column was sampled at selected times. The TDR system was not run continuously, but at prescribed intervals, when the column was being sampled and during times of significant drainage.

4.2.4.3 Soil Sampling

The times at which soil sampling was undertaken were based on initial modeling of the columns, using parameters selected from initial laboratory testing. The times were selected to obtain samples at times when different transport processes were dominant. This included an early time when advective-dispersive transport was occurring, an intermediate time when the dominant transport mechanism was transitioning from advective-dispersive to diffusion, and a late time when diffusive transport was dominant. The sampling procedure for the first sample was as follows:

1. Sample port cap removed,
2. Collar placed over Shelby Tube,
3. Collar and Shelby tube advanced into the soil, stopping when the collar is just inside the column,
4. Shelby Tube twisted to break the sample free and the Shelby Tube was removed, leaving the collar in place.
5. Sample was placed into a 1 L Ziploc bag.
6. The plug was placed into the sample void,
7. The port cap is replaced.

For the second round of sampling the following procedure is used:

1. Sample port cap removed,
2. Plug removed
3. Soil was then sampled again by advancing a second collar with the first, over the Shelby Tube, deeper into the soil,
4. Shelby Tube twisted and removed, leaving collars in place.
5. Sample was placed in a 1 L Ziploc bag,
6. Plugs were placed in the sample voids,
7. The port cap is replaced.

The third sampling round was performed in the same method as the second. The fourth sampling round was done just before column deconstruction. For the final sample, the cap was removed, the first encountered plug and collar were removed and the soil sample was taken with the Shelby Tube at a 45° angle to the original samples (Figure 4.21)

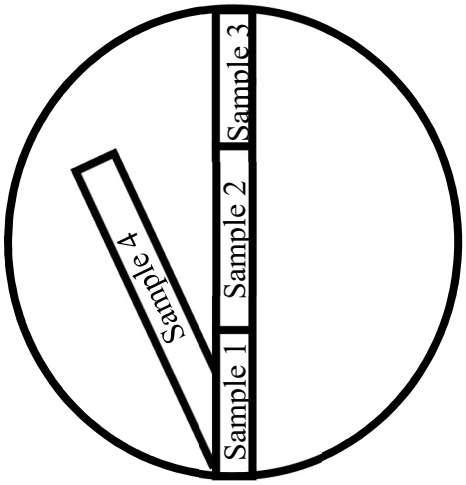

Figure 4.21 – Schematic of column sampling procedure.

The isotope analysis for the columns was done in the same lab, following the same procedure as the diffusion cells.

4.2.5 Data Collection

The isotope concentrations for the spiked water were measured before the experiments were conducted. The initial isotope concentrations for the column were calculated by averaging the isotope measurements in the lower portions of the column. This was done to account for isotopic interactions between the water and the sand, where the isotope content changes after mixing (discussed in Section 5.1.4).

From the columns the following data was collected:

- Isotope concentrations every 0.10 m of column height, for samples 1, 2, 3, and 4.
- Density measurements every 0.10 m for samples 1, 2, and 3.
- An overall column bulk density after packing,
- Water content (θ_l) profiles every 0.10 m, measured by oven drying and TDR, for samples 1, 2, and 3.
- Outflow volumes
- PSD every 0.10 m for samples 1, 2, and 3.

In total 13 samples are collected over the column's length. Each sample is applied to a column segment, which includes the column volume 0.05 m above and below the center of the sample port.

4.3 Summary

Both experiments were designed and completed to collect data for analysis. The design of the diffusion cells presented many challenges in the construction procedure, as can be seen in the four different methods that were needed to gain reliable results. The column experiments required significant pre-construction analysis (selection of sand) and preparation (collection of materials and column construction). The design of the columns did not fall within the guidelines set out by Lewis and Sjöstrom (2010), such as the ideal length to diameter ratio, but the shortcomings of the design were mitigated with changes to the construction and experimental procedures. The unfavorable length to diameter ratio was mitigated with a low infiltration rate to minimize fingering and preferential flow paths. The density and microstructure variations created during sand packing were minimized with the dry packing method used, contrary to the wet packing methods outlined. The experiments were constructed and completed and allowed for the collection of the desired data.

Chapter 5 - Presentation of Results

The results from the diffusion cell and column experiments are presented and discussed in this chapter. The interpretation of these results using numerical analyses is presented in the following chapter. Only typical sets of results are presented with all test results available in Appendices B and C.

5.1 Diffusion Cells

This section presents data on the variations in the measured ω and ρ_{dry} which are subsequently used to calculate θ_l distributions in each cell. The results highlight challenges associated with obtaining homogeneous conditions within the cell. The distributions of $\delta^{18}O$ are interpreted to see if water has been lost from the cells due to evaporation. Liquid phase connectivity between the cells is evaluated using the distribution of a chloride tracer. Together these observations will provide an understanding of the quality of the test data and the conclusions that can be drawn from these experiments.

Table 5.1 and Table 5.2 summarize test duration and achieved ω conditions, respectively. Cell R3-1 (experiment round 3, cell number 1) was not completed due to procedural failure. The liquid phase connectivity for the cell was lost near gravity drained conditions and the target ω could not be achieved. The cell was deconstructed to investigate the variations in ω throughout the cell during tilted drainage (approximately 1% change over half-cell height) and is not considered in the following analyses.

Table 5.1 – Experiment termination times for all four diffusion cell trials.

Experiment Round	Cell 1 time (days)	Cell 2 time (days)	Cell 3 time (days)	Cell 4 time (days)	Cell 5 time (days)
R1	11.9	21.8	28.8	33	35.7
R2	11.9	19.9	22.9	25.9	24.9
R3	N/A	38.1	36.0	35.2	36.1
R4	16.9	17.9	16.9	14.9	15.8

Table 5.2 – Average saturation ω for all four diffusion cell trials.

Experiment Round	Cell 1 average ω (%)	Cell 2 average ω (%)	Cell 3 average ω (%)	Cell 4 average ω (%)	Cell 5 average ω (%)
R1	7.3	9.8	12.4	14.9	17.4
R2	7.4	10.6	15.4	21.6	18.4
R3	N/A	20.8	20.5	18.6	19.1
R4	13.5	11.1	8.8	8.2	7.1

5.1.1 Variations in Cell Construction

Each cell constructed had a target ω and ρ_{dry} to create a specific θ_l. The target values as well as the average measured values following test completion are plotted in Figure 5.1 and Figure 5.2.

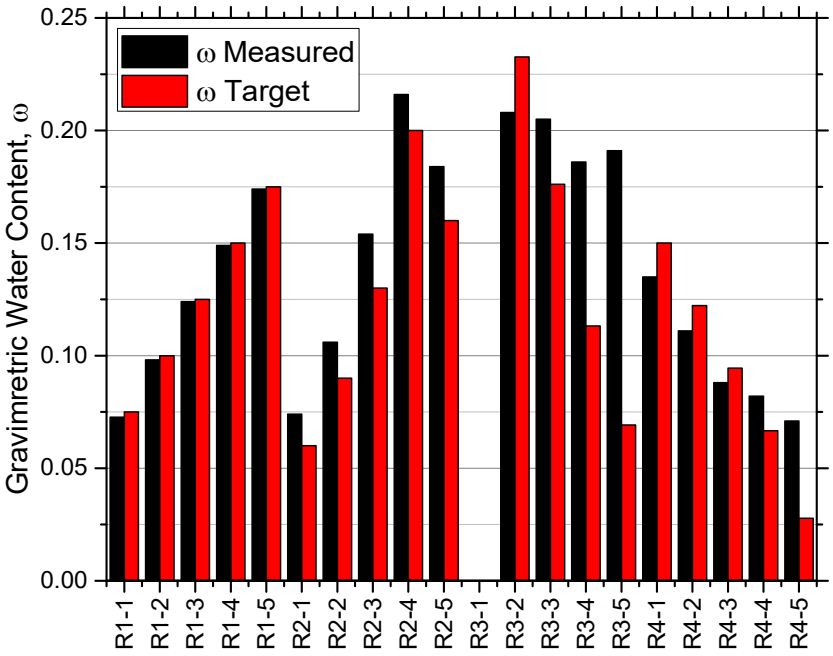

Figure 5.1 – Comparison of measured cell ω compared to target values. Measured values are averages of the measurements made on each of the cell slices.

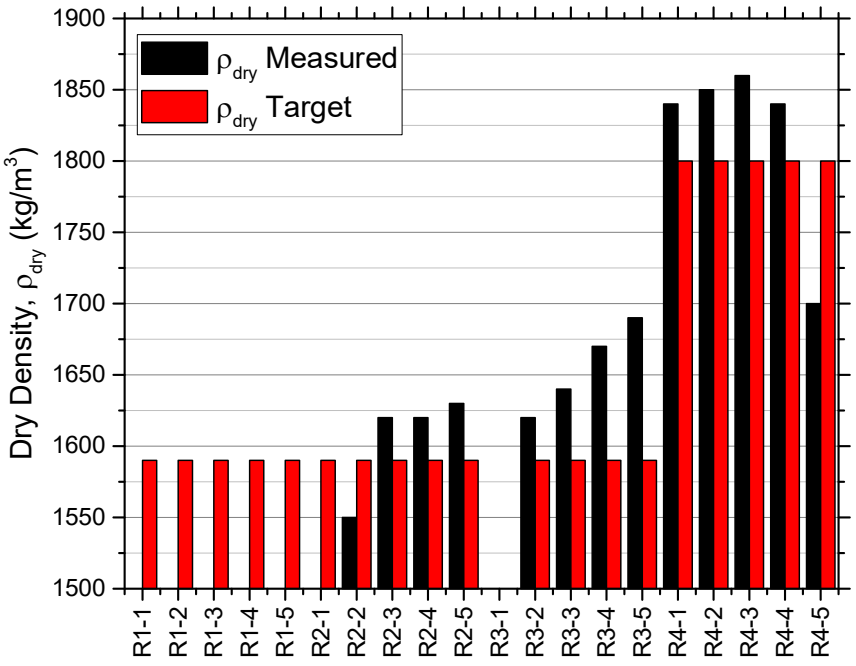

Figure 5.2 – Comparison of measured ρ_{dry} compared to target values. Measured values are averages of the measurements made on each of the cell slices. No measurements of density were made on the R1 experiments or on experiment R2-1.

The measured ω values for R1 are very close to the target. However, the lack of ρ_{dry} measurements, does not allow the targeted θ_l to be verified. The ω values for the R2 tests are all a few percent higher than the targeted value. The ρ_{dry} for R2 shows a small variation from the target with the second cell being less dense than targeted and the rest being higher.

The inability to drain the R3 cells past the limit of simple gravity drainage is evident in the data. All the measured values of ω for R3 were close to 20%. The density for the R3 experiments started close to the target, but appeared to increase in density with each cell constructed. This may have been due to densification of the samples under elevated applied suction and before the water connectivity failure occurred.

The target and measured ω values for R4 were in good agreement except for R4-5, where the soil did not drain sufficiently. This was attributed to the differences in the expected and actual water retention behavior. The density for the R4 cells was close to expected for the first four, but R4-5 had a very low measured density. It was not apparent why this cell had such a low density.

The variations within each cell also provide a qualitative index of the quality of cell sample preparation. The coefficient of variation (CV = (Standard Deviation)/(Average)*100)) for ω and ρ_{dry} was calculated for each cell. The CV (Figure 5.3) was used as it shows the variation as a percentage of the average, and allows the variation associated with the two variables controlling θ_l to be compared (ie, which value, the ω or ρ_{dry}, has more variability).

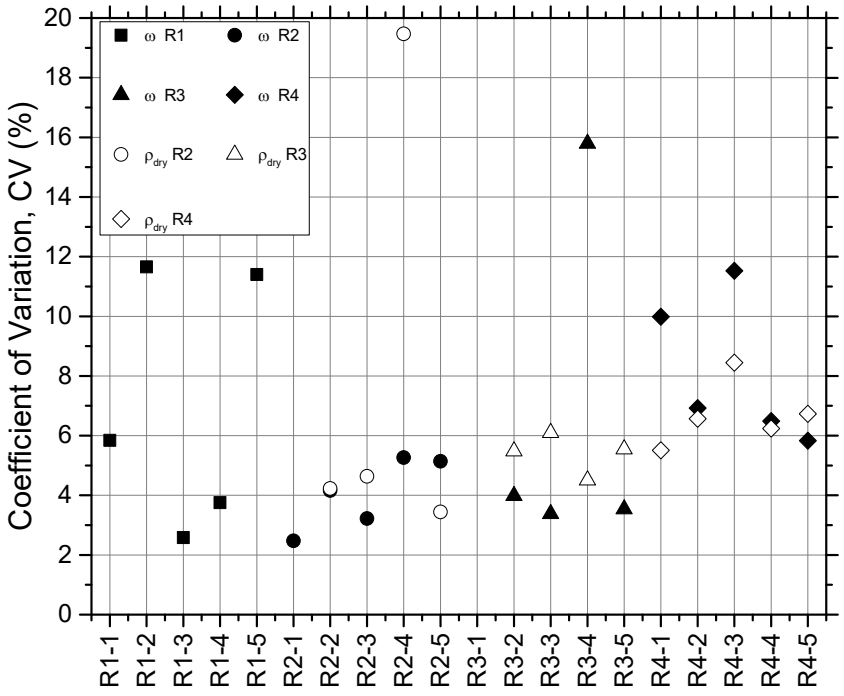

Figure 5.3 – Variation in the measurements made on each cell's slices, plotted to show the variation in ω (filled symbols) and ρ_{dry} (open symbols) for each cell. Different symbol shapes are used to distinguish the testing round from one another.

Excluding the two high variability data points (ρ_{dry} for R2-4 and ω for R3-4) the following observations can be made for ω between each trial. The CV for the R1 ω does not show high variability (CV from 2 to 12) and does not show any trends. The R2 ω has increasing variability with additional cell construction. This is different from expected, where more practice in the packing methods should yield lower variability. R3 shows consistent variability, indicating that the packing method does not create the most consistent profiles, but has a high degree of consistency between profiles themselves. The R4 cells show a decreasing trend in ω as the cells are constructed. This may indicate that the construction procedure was more efficient at creating low variability in ω, as more familiarity with the procedure was found.

It is interesting that the R4 CV values are higher than those for R2 in spite of the fact that the R4 cells were expected to have better control on soil packing and ω through suction control. The ρ_{dry} for each of the trials shows consistent variability within each procedure and between the different procedures.

R2-4 and R3-4 appear to have a particularly high CV's for ρ_{dry} and ω respectively. The high CV for ρ_{dry} for cell R2-4 is likely due to the observed loss of sand from the uncut cell into the center slices. The sand remained unconstrained due to the low soil suction applied (Figure 5.4).

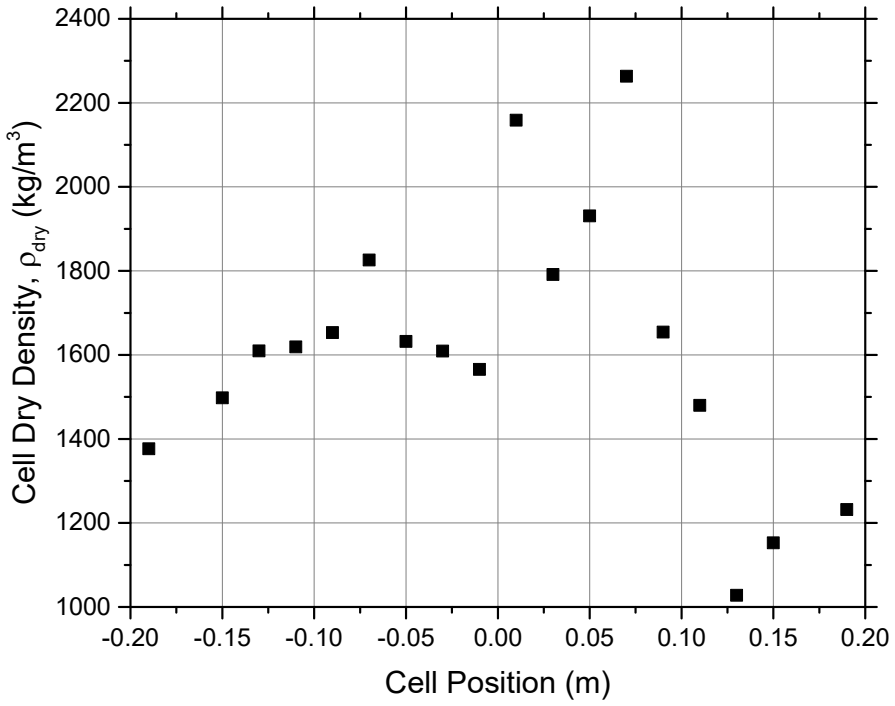

Figure 5.4 - ρ_{dry} profile for cell R2-4. High variation can be seen from 0 to 0.20 m.

For cell R3-4, a similarly high CV can be found in the ω (Figure 5.5). The two values around the -0.10 m cell position have a particularly low ω. This was assumed to be due to weighing errors of the wet soil. The data point at -0.11 m has a weighing error of approximately 0.03 kg while the data point at -0.09 m has a weighing error of approximately 0.015 kg.

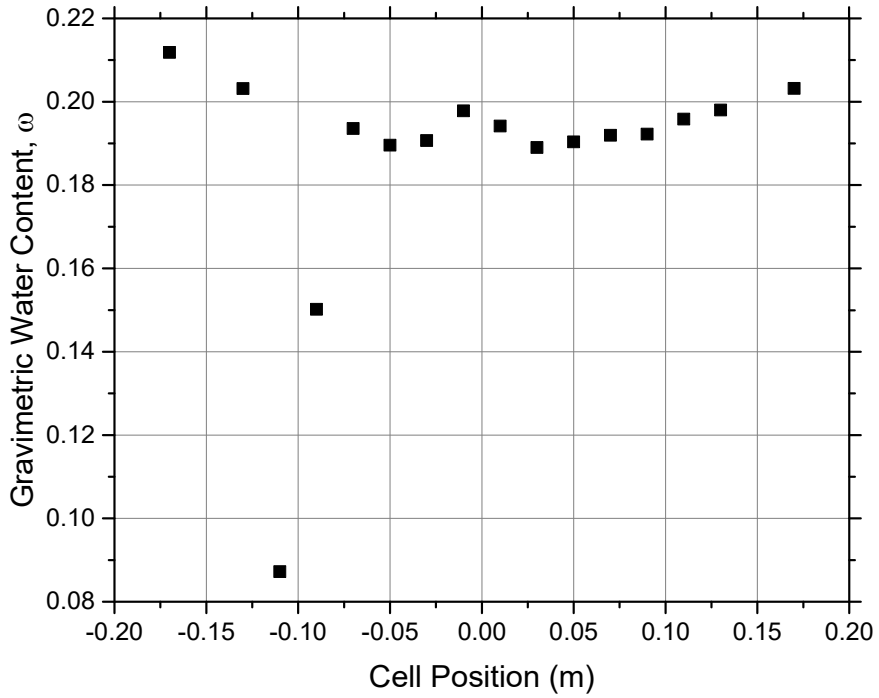

Figure 5.5 – ω profile for cell R3-4. Low ω found at a position of -0.10 m.

The average CV for each cell round is presented in Table 5.3. For experiment R1, no comparison between ω and ρ_{dry} can be made. For experiment R2 the CV values for ρ_{dry} and ω are similar. Experiment R3 has a lower CV in ω, while R4 had higher variability in ω. Overall R4 had the highest variability out of all the experiments.

Table 5.3 – Average CV values for ω and ρ_{dry} to determine which variable carries more variation for ω calculations. No average for ρ_{dry} for experiment R1 is calculated due to no density measurements taken. Outlier values for R2-4 and R3-4 are excluded from averages.

Experiment Round	Average CV, ω (%)	Average CV, ρ_{dry} (%)
R1	7.05	N/A
R2	4.05	4.10
R3	3.64	5.41
R4	8.15	6.70
Average of all CV	5.72	5.40

Large variations in θ_l can lead to water migration and consequently advective transport of the tracer would occur. The variations in θ_l are illustrated in Table 5.4 using the observed standard deviation in each cell.

Table 5.4 – Standard deviation of θ_l. Where no density was measured for each slice, an assumed "as packed" value of 1590 kg/m^3 was used.

Experiment Round	Cell 1 θ_l standard deviation (%)	Cell 2 θ_l standard deviation (%)	Cell 3 θ_l standard deviation (%)	Cell 4 θ_l standard deviation (%)	Cell 5 θ_l standard deviation (%)
R1	0.7	1.8	0.5	0.9	3.2
R2	0.3	0.8	1.3	7.3	1.9
R3	N/A	1.4	1.4	4.4	1.3
R4	2.8	2.2	2.7	1.6	1.1

An example of the highest variability θ_l profile and the lowest are shown in Figure 5.6.

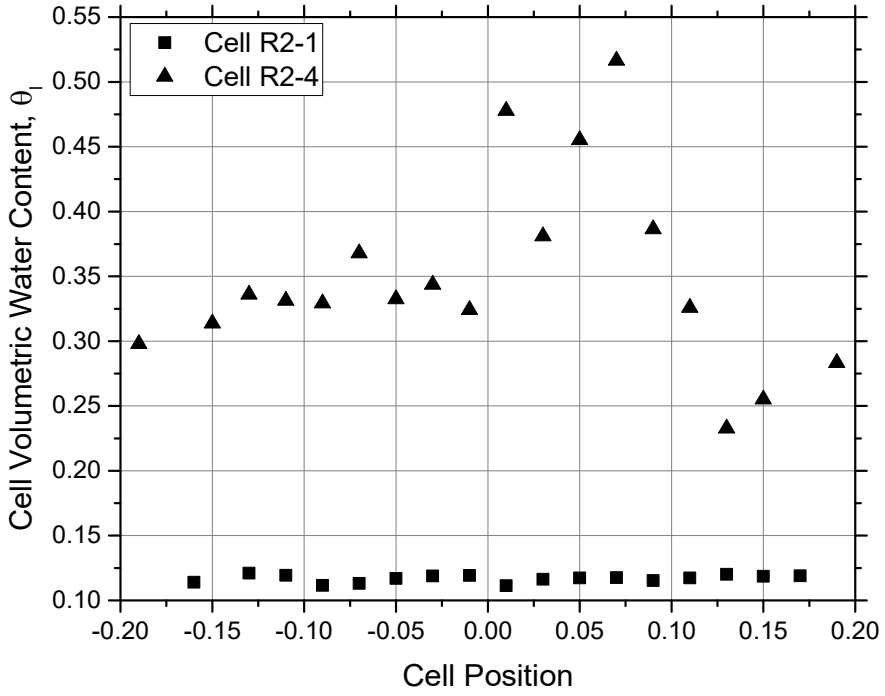

Figure 5.6 - θ_l profiles showing the highest variability (R2-4) and the lowest variability (R2-1) of all the experiments.

The largest changes in θ_l appears to occur at the end and in the middle of the cells. These variations may be due to either the redistribution of water or due to water loss through evaporation. Since the θ_l profiles are only known at the end of the experiment there is now way to verify this or quantify the amount of water movement.

The presence of evaporation could be indicated by changes in the $\delta^{18}O$ content of each sample cell slice. The standard deviation (σ) of the $\delta^{18}O$ measurements is presented in Table 5.5.

Table 5.5 – Standard deviation in $\delta^{18}O$ for each cell.

Experiment Round	Cell 1 $\delta^{18}O$ σ (‰)	Cell 2 $\delta^{18}O$ σ (‰)	Cell 3 $\delta^{18}O$ σ (‰)	Cell 4 $\delta^{18}O$ σ (‰)	Cell 5 $\delta^{18}O$ σ (‰)
R1	0.6	0.4	0.3	0.3	0.2
R2	0.4	0.4	0.2	0.3	0.4
R3	N/A	0.3	0.4	0.4	0.5
R4	1.3	0.7	1.6	1.9	0.8

If cells were not sealed properly during diffusion and evaporation had occurred, isotopic enrichment should be apparent in the cells. The $\delta^{18}O$ profiles with the highest and lowest standard deviation higher than the experimental error (1σ = 0.4 ‰) are shown in Figure 5.7.

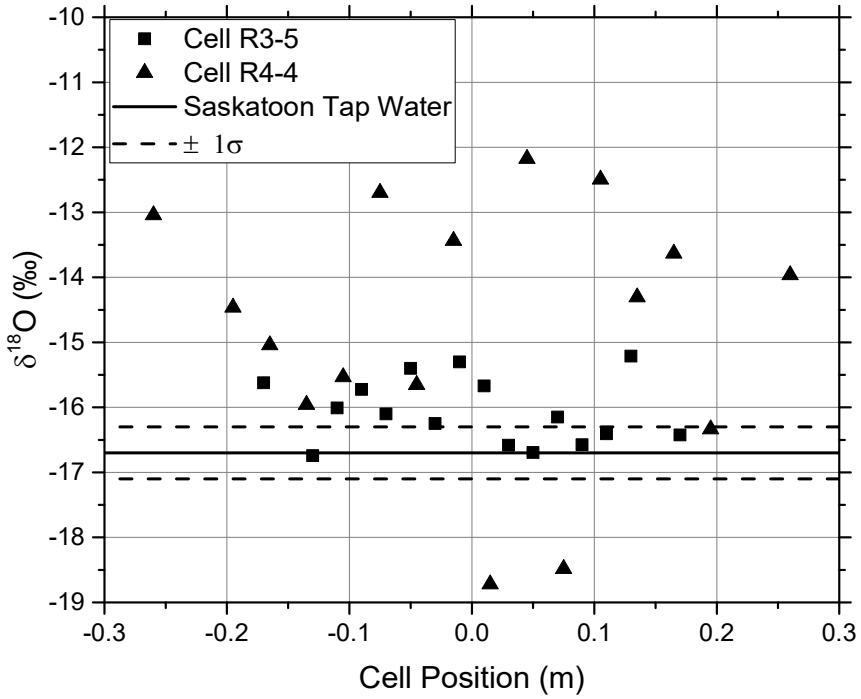

Figure 5.7 - $\delta^{18}O$ profiles for cells with the highest and lowest standard deviation higher than experimental error of 0.4 ‰.

The high variability $\delta^{18}O$ profiles do not show a consistent trend, with the exception of cell R4-1 and R4-2 (not shown). In these cells, the ends and the middle of the cell appear to be enriched in a pattern that suggests some evaporative enrichment. The other cells with high variability do not

show systematic changes in the $\delta^{18}O$ profiles, suggesting that evaporative enrichment did not occur.

5.1.2 Cell Liquid Phase Connectivity

One of the main concerns with double half-cell diffusion tests, outlined in the literature, is the inability to establish water phase connectivity when the cells are connected. This section will look at the δD and chloride profiles to investigate the success or failure of the connections in these experiments. An example of a δD profile is shown in Figure 5.8.

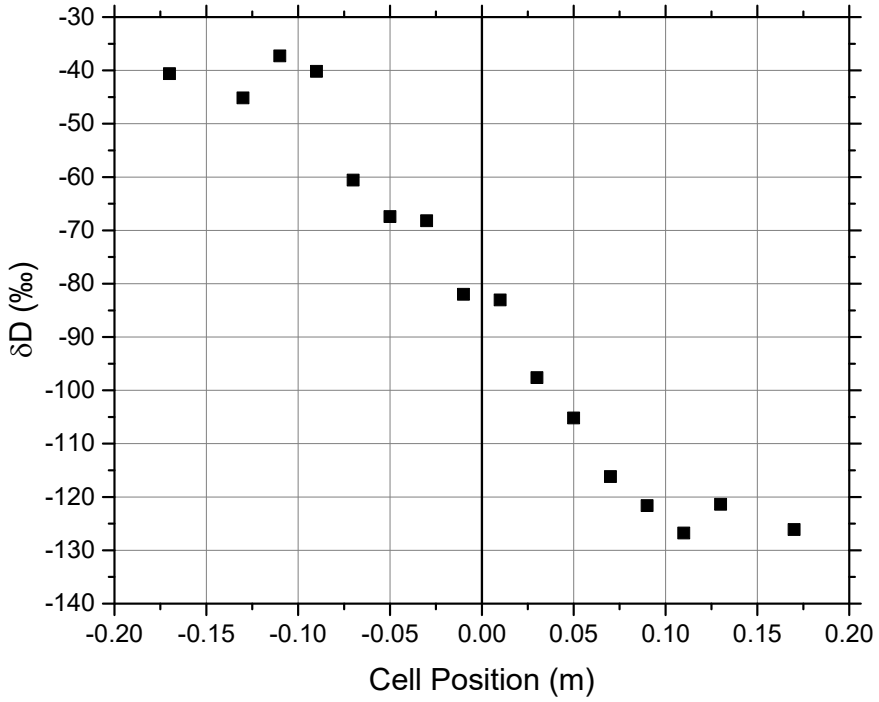

Figure 5.8 - Typical raw isotope data diffusion profile (R3-3).

The δD isotopes are able to move through both the vapour and liquid phases and consequently provide no clear indication of liquid phase connectivity between the two half-cells. The chloride tracer, which was used to obtain a single-phase diffusion coefficient, does provide a clear indication of liquid phase continuity. The results of the chloride analysis are shown in Figure 5.9.

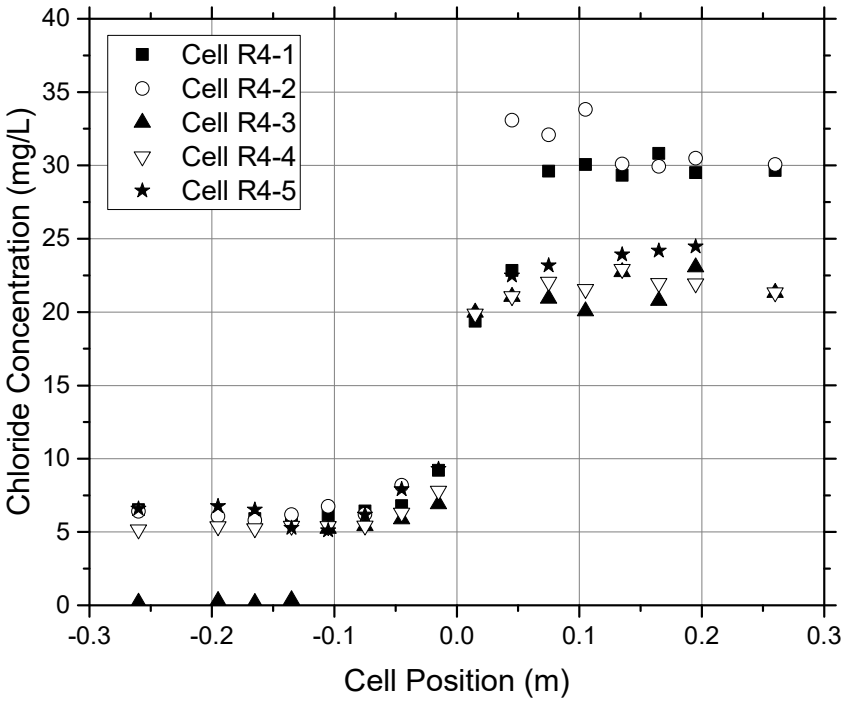

Figure 5.9 - Chloride profiles. R4-1 has the highest ω at 13.5% and R4-5 the driest with a ω of 7.1%.

The large break in Cl concentration at a cell position of 0 m indicates that the liquid phase was not fully connected. The lack of connection may impede dual-phase diffusion across the interface since the area available for liquid phase diffusion is reduced. Chloride diffusion was only measured for experimental round R4, but the effects of reduced liquid phase connectivity are assumed to be present in all previous experiments. The lack of proper liquid phase connectivity between the cells requires caution when analyzing the cell results and will be investigated in Section 6.1.1.2.

5.1.4 Cell Isotope Initial Conditions

High variability was encountered when measuring initial conditions. The isotope concentrations appeared to shift when water was mixed with sand. The non-spiked tap waters that were used were plotted on the Saskatoon meteoric water line ($\delta D = 7.72\ \delta^{18}O + 1.72$) to see if any enrichment or depletion was observed (Figure 5.10).

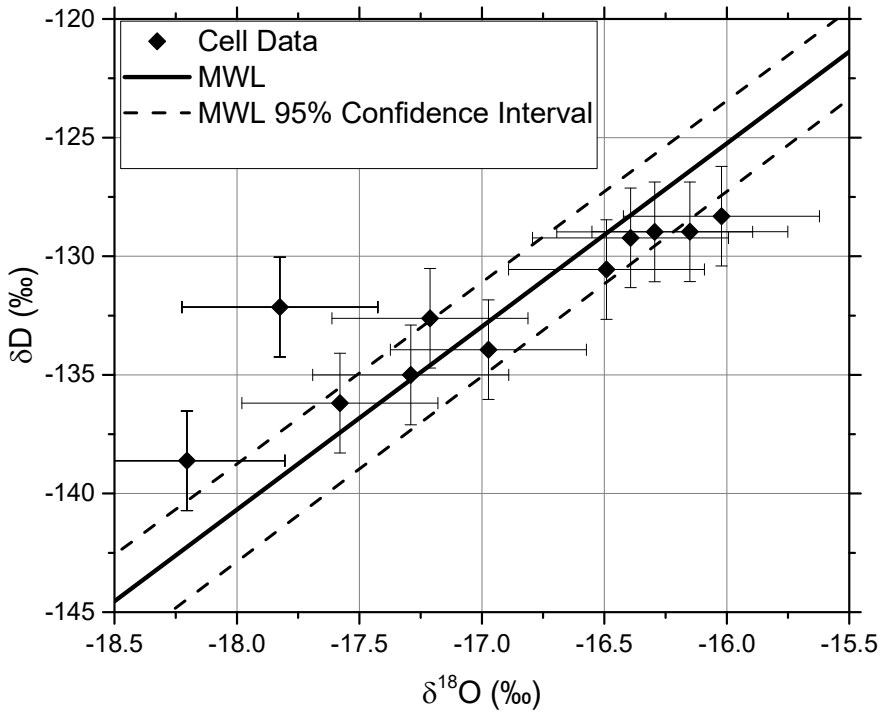

Figure 5.10 - Non-spiked water plotted against the Saskatoon meteoric water line to observe if evaporation had occurred.

Only one data point does not plot along the MWL. The anomalous point shows a possible fractionation associated with condensation of water. The condensed signature may have been due to temperature changes between the labs where the water samples were collected and analyzed. The source water for the experiments showed the expected δD and $\delta^{18}O$ values before spiking or mixing with soil.

Isotope analysis was done on spiked and non-spiked water before and after it had interacted with the sand (mixed or drained from cell). When the water is mixed with the soil, the resulting isotope concentration between the source water and water mixed with soil should ideally follow a 1:1 relationship, but this was not observed. Figure 5.11, Figure 5.12 and Figure 5.13 show the changes to isotope content after interaction with the soil.

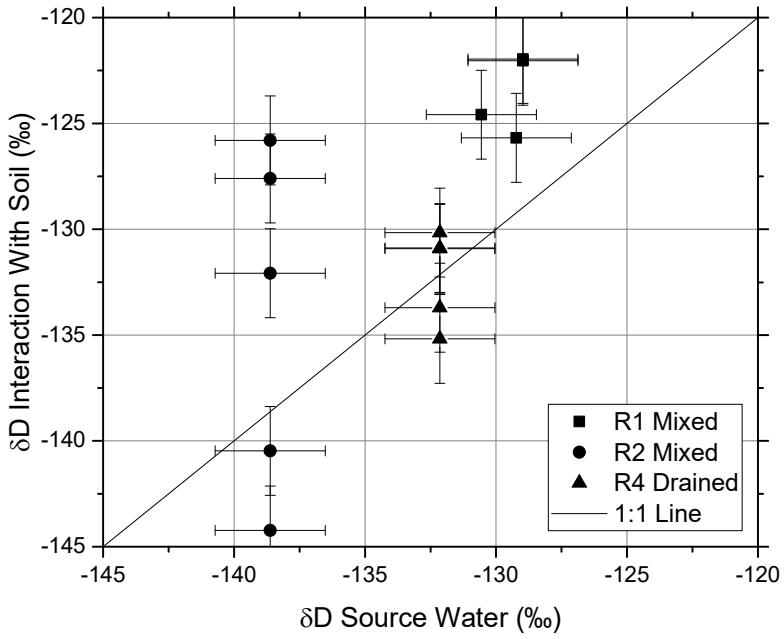

Figure 5.11 – Non - spiked δD water source compared to water isotopes after interaction with the soil. Black line shows a 1:1 relationship. The water/sand interaction has data points for R1-2 to R1-5 and R2-1 to R2-5. The drained values are all unique for R4.

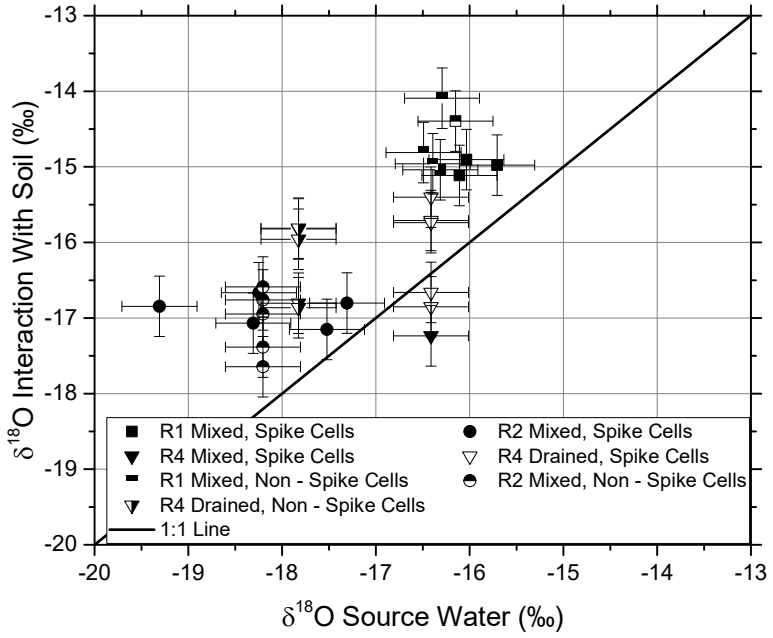

Figure 5.12– $\delta^{18}O$ water source compared to water isotopes after interaction with the soil. Black line shows a 1:1 relationship. The water – sand interaction of spiked water for experiments R1-2 to R1-5, R2-1 to R2-5 and a single value for R4. The non-spiked water – sand values are from R1-2 to R1-5 and R2-1 to R2-5. The drained values for both the spiked water and non-spiked water are from experiment R4.

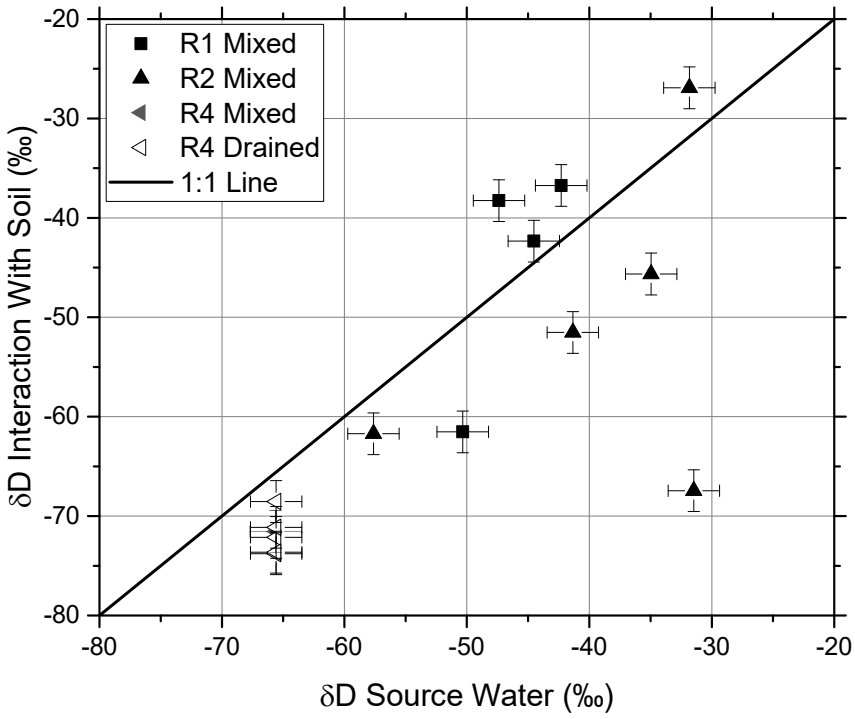

Figure 5.13 – Spiked δD water source compared to water isotopes after interaction with the soil. Black line shows a 1:1 relationship. The water/sand interaction has data points for R1-2 to R1-5, R2-1 to R2-5 and a single value for all of R4. The drained values are all unique for R4.

The enriched and depleted conditions were assumed to be due to the presence of residual water and isotopes in the sand after drying ($\omega \sim 0.7$ % before mixing). The residual water would have a highly enriched isotopic signature due to Rayleigh type distillation. Figure 5.14, developed in Appendix D, highlights the interactions between spiked and non-spiked water when mixed with the sands residual water. The theoretical mixing relationship is compared to the measured isotope data for R1 and R2 water samples. No data for R3 or R4 is plotted. The water and sand were mixed in a slurry where the effects of the residual water left in the dried soil would have little to no effect on the measured isotope value.

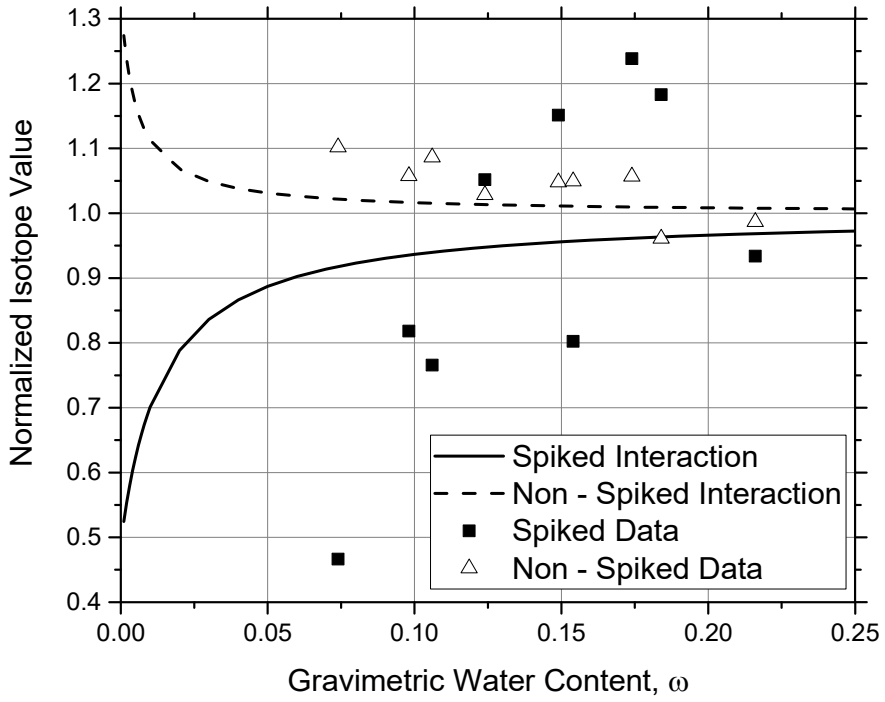

Figure 5.14 – Evolution of the normalized concentration of δD in the water that is added to soil for experimentation.

When highly enriched spiked water is added to the dry soil, the presence of the enriched residual water does not have a large impact on the final isotopic signature of the mixture. The presence of the residual water simply dilutes the final mixture relative to the targeted isotopic value. In the case of the non-spiked water the presence of the residual isotope concentration results in a systematic shift of the mixture to values that are higher than the source water added.

The data for the non-spiked cells seems to show an excellent fit to what is predicted. The spiked cells show more scatter in the data and do not appear to follow the trend expected. This may be due to the unknown amount of residual isotopes present in the dry soil. Not all the compared isotope values are explained by the mixing relationship provided. Some may have higher or lower deviations than expected.

5.2 Column Experiments

Data from the column experiments is presented in this section to evaluate the quality of the column preparation and the consistency of the monitoring data. The homogeneity of the soil within the columns is evaluated first to establish whether any observed concentration anomalies can be

explained by soil heterogeneity. A water and isotope mass balance are then used to assess if the water application, drainage, and spike application proceeded as expected.

The data that was collected, with the exception of the TDR data, was done at discrete time points. The soil sampling times for each column are presented in Table 5.6. Column experiment 1 and Column experiment 2 are hereafter referred to simply as C1 and C2, respectively. Similarly the sample times will be given a shorthand of SX, where X is the sample number as it was taken from the column.

Table 5.6 - Time for sample collection after rainfall was started.

Column	Time for Sample S1 (days)	Time for Sample S2 (days)	Time for Sample S3 (days)	Time for Sample S4 (days)
C1	0.5	27.2	97.1	191.1
C2	0.5	6.3	98.3	210.1

5.2.1 Column Soil Homogeneity

The quality of column packing was evaluated by comparing the measured ρ_{dry} profiles to the targeted densities. The θ_l profiles for each sample time will also be presented to provide an initial interpretation of the water migration within the column prior to modeling and analyses in Chapter 6.

5.2.1.1 Column Dry Density

The bulk column density was estimated based on the known mass of soil added and the column volume. Based on bench scale packing tests, the ρ_{dry} should have been approximately 1600 kg/m^3. Table 5.7 shows the column ρ_{dry} for each experiment.

Table 5.7 –Column ρ_{dry} data.

Column	Total Mass (kg)	Total Height Occupied (m)	Total Volume (m^3)	Column ρ_{dry} (kg/m^3)
C1	57.8	1.39	0.0361	1 600
C2	58.7	1.40	0.0364	1 610

Based on these results it appears that the initial packing of the columns produced a similar bulk density to the targeted value. The average column porosity would be 0.39 for both C1 and C2.

This porosity would be expected to decrease over the course of the experiments as filling and draining results in consolidation of the sand.

5.2.1.2 Column Density Profiles

The ρ_{dry} profile within the column was measured in two ways: by measurement of the mass collected in each Shelby Tube of known volume, and by back calculation using the measured ω and TDR θ_l. The average of the ρ_{dry} profiles for each column can be found in Table 5.8.

Table 5.8 – Column the average ρ_{dry} at S1-3, using both ρ_{dry} estimation techniques. Measured refers to measurements taken on Shelby tube samples. Calculated refers to values calculated from TDR θ_l and ω from the Shelby tube samples.

Column	Estimation Method	Average ρ_{dry} S1 (kg/m^3)	Average ρ_{dry} S2 (kg/m^3)	Average ρ_{dry} S3 (kg/m^3)
C1	Measured	1 540	1 840	1 780
C1	Calculated	1 370	1 480	1 260
C2	Measured	1 670	1 690	1 840
C2	Calculated	1 530	1 630	1 800

The two methods indicate there was an increase in the average column ρ_{dry} between samples S1 and S2. For C1 there is a decrease in density between samples S2 and S3. C2 shows an increase between S2 and S3. This may be due to sampling error for C1. No measurements of ρ_{dry} were made for the final sample round (S4). The back calculation led to some error when using the TDR measured θ_l data as measurements were taken at a 0.05 m offset vertically from the soil sampling locations. The θ_l that was used in the calculations was an average between the measurements above and below the sample elevation. Where no TDR value was recorded, a TDR measurement was made from averaging the measurements above and below.

The measurement of ρ_{dry} from the Shelby tube samples may have had errors due the tube not being completely full or due to compression of the soil during sampling. A constant volume (60 mm length by 30 mm diameter) was assumed for each samples volume. This may have introduced error into the density measurements if the collected sample volume was higher or lower than expected. A final estimate of ρ_{dry} was made by dividing the total dry soil mass collected from S1 to S3 by three constant volumes. Doing this removed the possible errors of the wrong mass being

applied to the constant volume. The ρ_{dry} profile for both columns, based on the total soil mass collected (herein called the ρ_{dry}), can be seen in Figure 5.15.

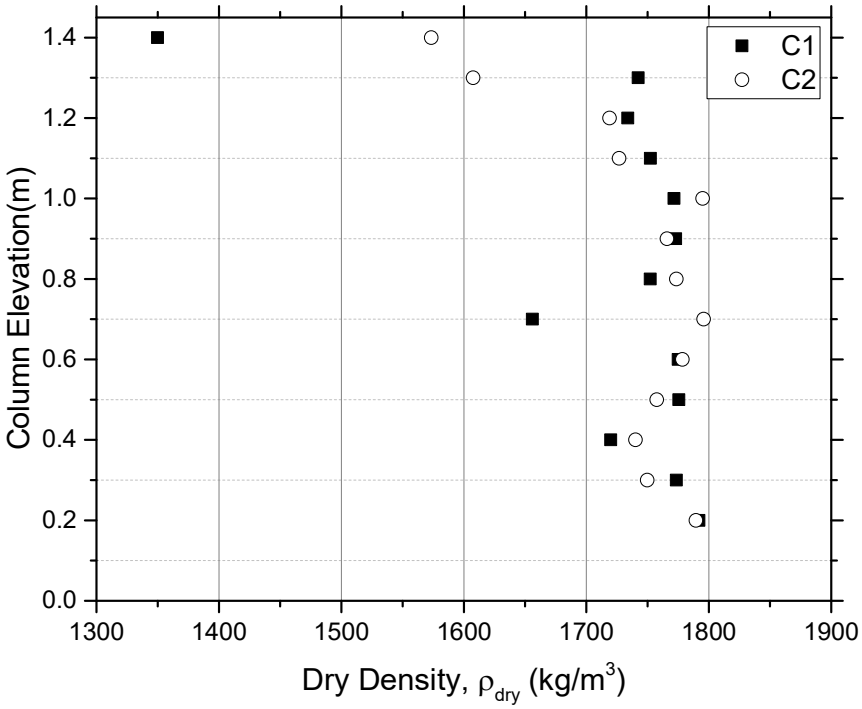

Figure 5.15 – ρ_{dry} profiles for C1 and C2.

A few irregularities can be observed in the ρ_{dry} profiles. The top portion of the column (1.4 m and above) has a lower ρ_{dry} than the rest of the column, likely due to the inability to compact this soil to the same ρ_{dry} as the soil below it. The overall trend observed in the column is increasing ρ_{dry} with depth as expected from to the placement of soil in non-uniform lifts with vibratory compaction. The average ρ_{dry} for C1 and C2 after S3 are 1 720 (kg/m^3) and 1 740 (kg/m3) respectively with a porosity of approximately 0.35 and 0.34, respectively.

5.2.1.3 Column Particle Size Distribution

Another measurement used to evaluate the homogeneity of the column packing was the PSD of the sampled sand. The sand was analyzed on a Malvern Mastersizer 2000 (equipped with Hydro MU) and the percent passing was found. Data was collected for C2, samples S1 and S2. The PSD's for S1 can be found in Figure 5.16.

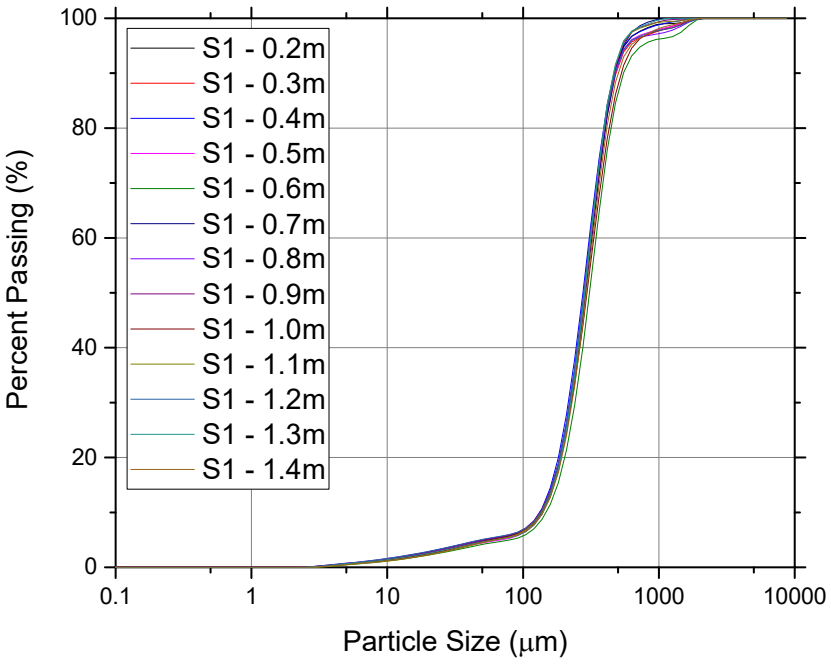

Figure 5.16 - C2 S1 particle size distribution for all sample locations.

The particle size results for S1 show deviations from one another near the coarse end of the grain sizes. This PSD shows that the column is relatively homogeneous throughout the elevation at S1. To gauge the quality of particle segregation during packing throughout the column radius, a PSD for S2 was found (Figure 5.17).

The PSD for S2 show similar deviations to S1. The deviation of the PSD's occurs at the coarse end. The two PSD's show homogeneity through the column elevation. The average of the S1 and S2 were used for comparison to see if the overall PSD is different between the radial positions within the column (Figure 5.18).

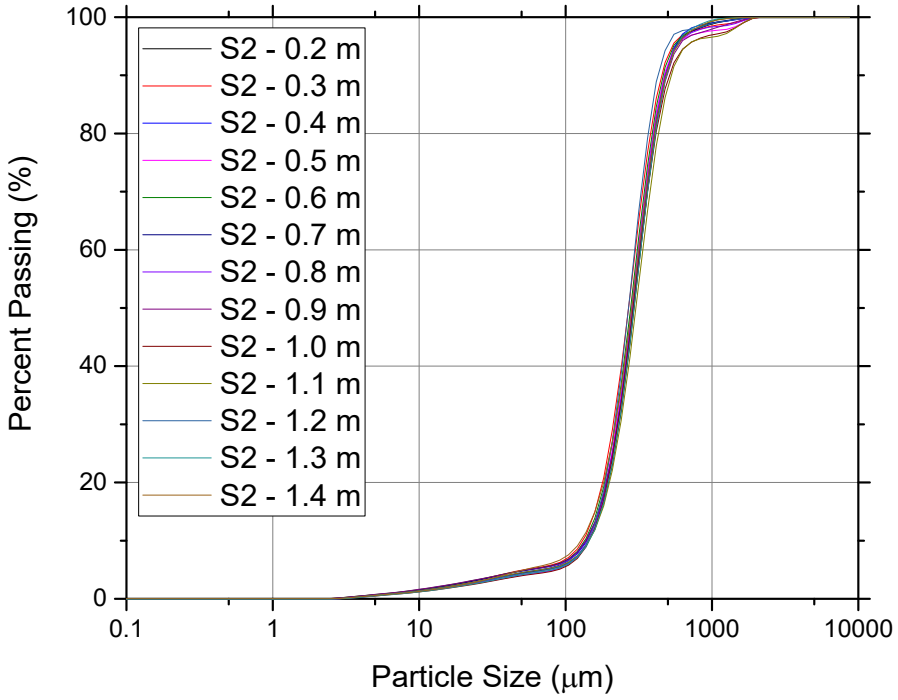

Figure 5.17 – C2 S2 particle size distribution for all sample ports.

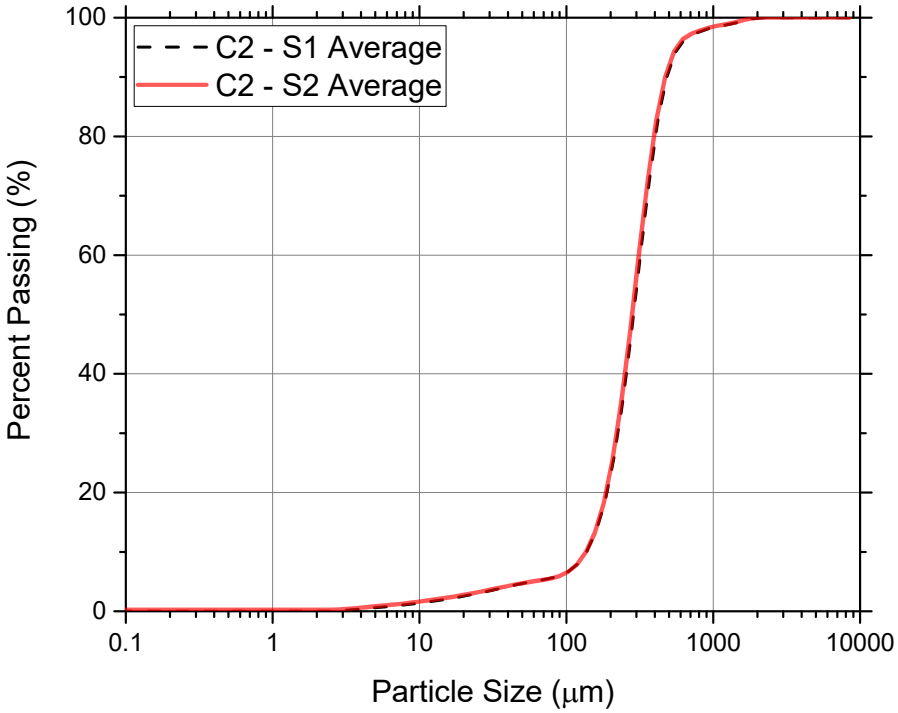

Figure 5.18 - Average particle size distribution for C2 S1 and C1 S2.

The averages do not show any significant deviations, indicating that the PSD does not significantly change radially within the column and that C2 is a homogeneous column. The packing procedure was deemed successful in minimizing particle size variations and C1 was assumed to have similar homogeneity.

The packing method, while not fully eliminating particle segregation, did provide a useful compromise between the time needed to pack (~6 hours) and the homogeneity of the column PSD and density. The main sources of particle segregation identified in this method are:

- The initial filling of the pipe,
- Placing segregated sand in the pipe,
- Segregation due to flow through the pipe while sand is being placed,
- Segregation due to pouring sand into the top pf the pipe from scoop,
- And segregation while the sand is flowing out of the pipe.

The main sources of density and structure variations identified in this method are:

- Non-uniform placement due to spiral placing method, potentially causing internal sand structure or layering,
- No tamping of sand, due to the placement of sand not being done in discrete layers,
- And densifying by vibration done every pipe segment, possibly causing an increase in density closer to the bottom of the column (increase in vertical stress with depth).

5.2.1.4 Other Observations

During initial column draining and during the first round of sampling, the sample ports were difficult to remove because of carbonate buildup in the threads. Precipitation of solids may have altered the available water and isotope transport pathways, however, there was no way to measure what effects it had on the experiments. Due to the use of a CO_2 flood, the increased CO_2 concentration in the soil allowed for dissolution of carbonate from the sand. When the added CO_2 was released, precipitation of the carbonates occurred.

After the experiments were complete observation of the columns in early February 2016 showed green colouration in several spots which appeared to be biofilms (Figure 5.19). The green

colouration was visible after experimentation but it is unclear if it had started during experimentation and caused changes in the soil structure and transport pathways.

Figure 5.19 - Green colouration in column.

5.2.2 Column Water Mass Balance

The water mass balance for the column is presented in two sections. In the first water balance, the observed outflow volumes are compared to the change in stored water volume estimated from the TDR measurements (drainage experiments). In the second water balance, the volume of added water during the infiltration phase is compared to the outflow volumes and the changes in the volume of water stored within the column (rainfall experiment). Where TDR θ_l measurements were missing due to TDR system errors, an average of the above and below measurements were made.

5.2.2.1 Drainage experiments

The preparation procedure for saturating the columns prior to experimentation will be presented here again, as it is important for analysis of the water balance during drainage. The preparation for column C1 is as follows: Soil packed > CO_2 flood > water flood > drainage > experiment start. The preparation for C2 contained an extra saturation and drainage step. The procedure was: Soil packed > CO_2 flood > water flood > drainage > water flood > drainage > experiment start.

During the final drainage stage the outflow was collected and the TDR system measured transient θ_l changes. Figure 5.20 and Figure 5.21 show the θ_l profiles for each column before and after drainage. The porosity is shown to highlight the saturated θ_l (ρ_{dry}) changes after drainage has occurred.

The outflow water was collected and the masses recorded. From the TDR profiles a total change in mass stored was found. The change in water storage estimated was smaller than the outflow masses. These masses are summarized in Table 5.9.

Table 5.9 – Water outflow collected compared to the change in storage by using TDR measurements

Column	Outflow Collected (kg)	Mass Change from TDR (kg)
C1	10.037	4.254
C2	8.033	7.073

This amount of collected water should be represented in the θ_l changes in the column over the time the water was collected. It is suspected that the initial TDR measurements were in error. An estimate of water storage at saturation was made from porosity and was compared to the drained TDR conditions (Table 5.10). Two porosity values were used. The first was the as packed porosity. This was the porosity of the columns after the initial packing, before any water-flooding was done. Second, the drained porosity, is the average column porosity based on the average density profiles presented in Section 5.2.1.2. This represents the porosity after densification occurred from water drainage.

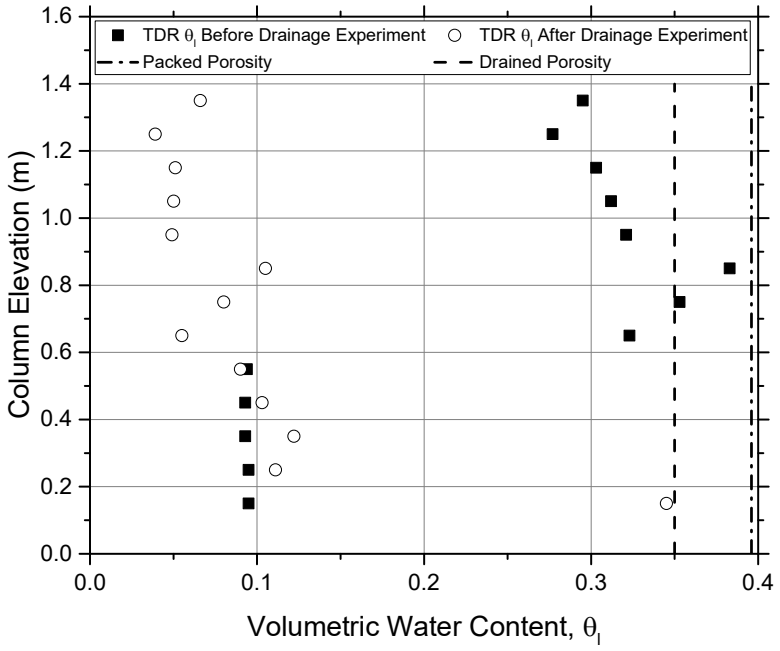

Figure 5.20 - TDR θ_l profiles for column C1. Initial is while the column is saturated and drained is taken to be the point in time where outflow had ceased.

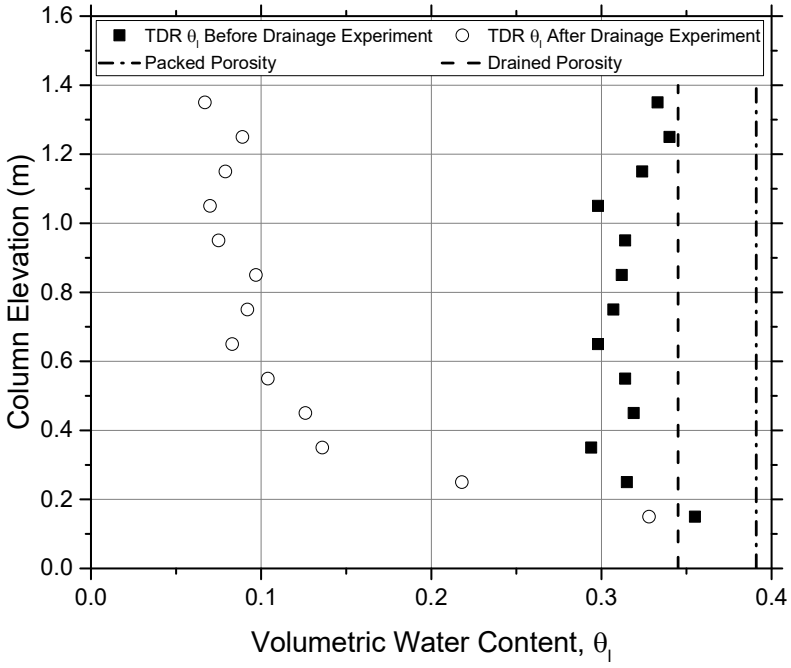

Figure 5.21 - TDR θ_l profiles for column C2. Initial is while the column is saturated and drained is taken to be the point in time where outflow had ceased.

Table 5.10 – Water outflow collected compared to the change in storage by using assumed saturated states.

Column	Outflow Collected (kg)	Packed Porosity (kg)	Drained Porosity (kg)
C1	10.037	10.661	8.925
C2	8.033	9.740	8.004

The water stored during the drainage tests should be based on the porosity of the dry packed material, for C1, before the soil has settled. C2 had an extra drainage step before the experiment was started. The second drainage event was the one used for the drainage test. It appears that compaction from water drainage was completed after the first drainage phase as the porosity of the column during the experimentation was correct for the initial storage conditions.

5.2.2.2 Rainfall Experiment and Water Content Profiles

The total mass of water added during the rainfall simulation and the total outflow collected after experimentation for C1 and C2 can be found in Table 5.11.

Table 5.11- Water mass balance for rain simulation experiment for both columns.

Column	Water Added (kg)	Water Collected (kg)
C1	0.591	0.551
C2	0.332	0.784

The mass balance for the first column was very close, with only a 0.040 kg difference. This column only had drainage collected four times. The second column, however, had twice as much mass collected as added. This may have been due to incomplete drainage prior to the start of the experiment, where the addition of water to the top mobilized water that would not be free during drainage due to hysteresis effects.

The measured θ_l results for each of the columns is presented in Figure 5.22 and Figure 5.23. The presented θ_l were calculated based on the ρ_{dry} and the measured ω.

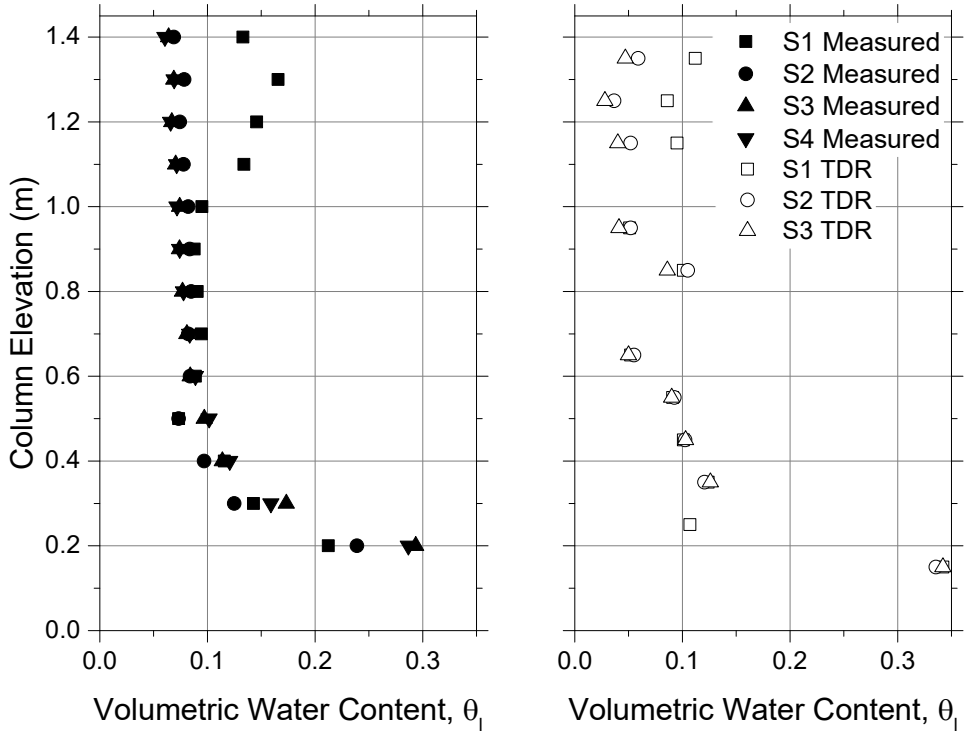

Figure 5.22 – C1 water content at each of the four sample times based on the ρ_{dry}.

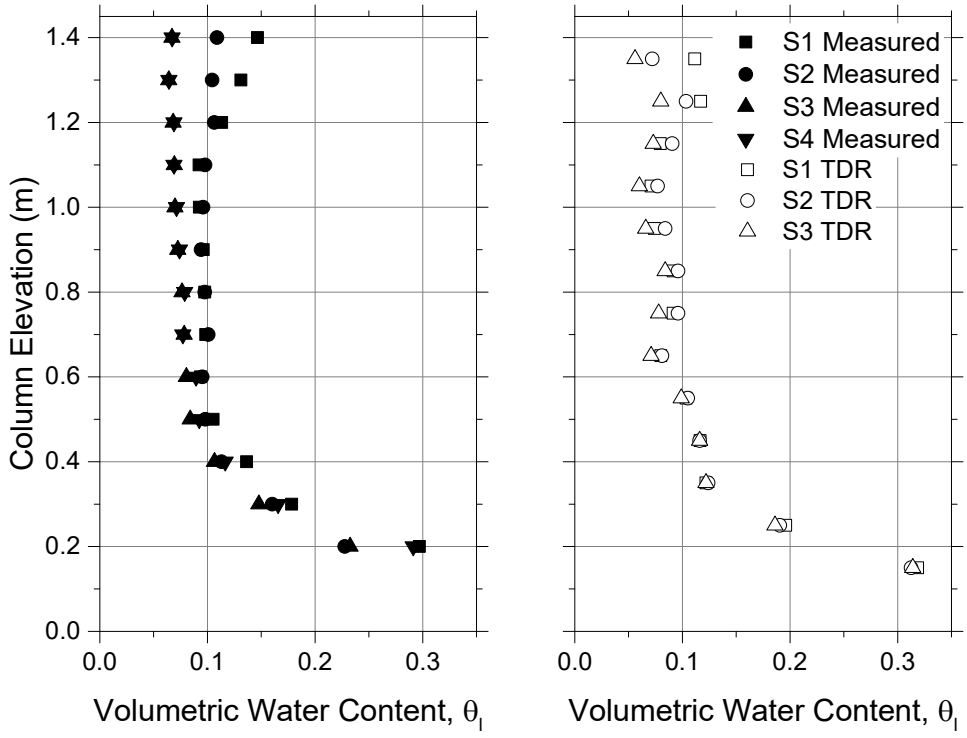

Figure 5.23 - C2 water content at each of the four sample times based on the ρ_{dry}.

The measured θ_l profiles were as expected. Most of the measurements in the lower portion of the columns matched well, showing a consistent measurement technique. Near the top of the column, at fully drained conditions, the θ_l profiles have a good fit to one another, showing a reliable value for the θ_{res}. Finally infiltration conditions are captured by the soil, for C1 S1 and C2 S1 and S2. The amount of water stored in the profile at each sample time is compared to the added mass in Table 5.12.

Table 5.12 – Water mass added to column and stored within column at sample times S1 and S2 compared to S4 over a selected elevation range. The final two sample times and C1 S2 were excluded as they were at full drained conditions.

Column	Added (kg)	S1 Measured (kg)	S1 TDR (kg)	S2 Measured (kg)	S2 TDR (kg)	Elevations used (m)
C1	0.591	0.811	0.548	N/A	N/A	1.1 – 1.4
C2	0.332	0.774	0.385	0.612	0.343	0.7 - 1.4

The TDR measurements for C1 S1 agrees with the mass added. C1 had elevations where the TDR system was not recording values. Where these missing data points were located, an average of the TDR value above and below was used. The amount of water added for C2 was captured in the TDR measurements. The oven dried θ_l for both columns show significantly more water stored than added. The better accuracy of the TDR values here is contradictory to the larger errors seen in the earlier drainage analysis. The error in the measured values is most likely due to an unstable wetting front, where the small samples did not collect a representative θ_l of the entire column segment. This indicates that preferential flow around the edges of the column may have also occurred.

5.2.3 Isotope Results

The isotope values were collected four times after the start of the experiment. All of the collected isotope data is plotted on a mixing line to see if any fractionation or other unforeseen isotopic interactions had occurred during the experiment. The measured concentration profiles are then presented along with an isotope mass balance of each column.

5.2.3.1 Isotope Mixing

The infiltration water for both C1 and C2 was drawn from the same reservoir. The average of three measurements on the source water was used for the top boundary (δD = -85.8 ‰ and $\delta^{18}O$ = -11.8 ‰). Isotopic analysis was not done on any outflow water as they were susceptible to evaporative enrichment. The column background isotope concentrations were averaged from the isotope measurements of S1 to S4, over the lower portion of the columns where the spiked water had not mixed with the background waters.

The background values for C1 were -131.9 ‰ for δD and a $\delta^{18}O$ of -16.3 ‰ for $\delta^{18}O$ while C2 had a δD of -132.2 ‰ and a $\delta^{18}O$ of -16.2 ‰. The elevation ranges used for calculating the background conditions are presented in Table 5.13.

Table 5.13 – Column samples used in column background average. The high sample changed depending on the rainfall volume and the relative penetration of the isotope front.

Column	S1		S2		S3		S4	
	Low (m)	High (m)	Low (m)	High (m)	Low (m)	High (m)	Low (m)	High (m)
C1	0.2	1.0	0.2	0.7	0.2	0.3	0.2	0.5
C2	0.2	1.0	0.2	0.9	0.2	0.9	0.2	0.7

The mixing of the spiked water and the tap water should have occurred along a mixing line between both end members. The data from each sample round, plotted against a mixing line, can be found in Figure 5.24 and Figure 5.25 for C1 and C2 respectively.

The significant deviations from the mixing line in C1 occur mostly below the mixing line suggesting evaporative enrichment (S1, S3, and S4). The few points that plot above the line show possible condensation (S2). In C2, deviations below the mixing line occur at all the sampling times. Only one data point (S4) plots above the line. Evaporative enrichment appears to be dominant in S2, where the lower portions show an evaporated signature.

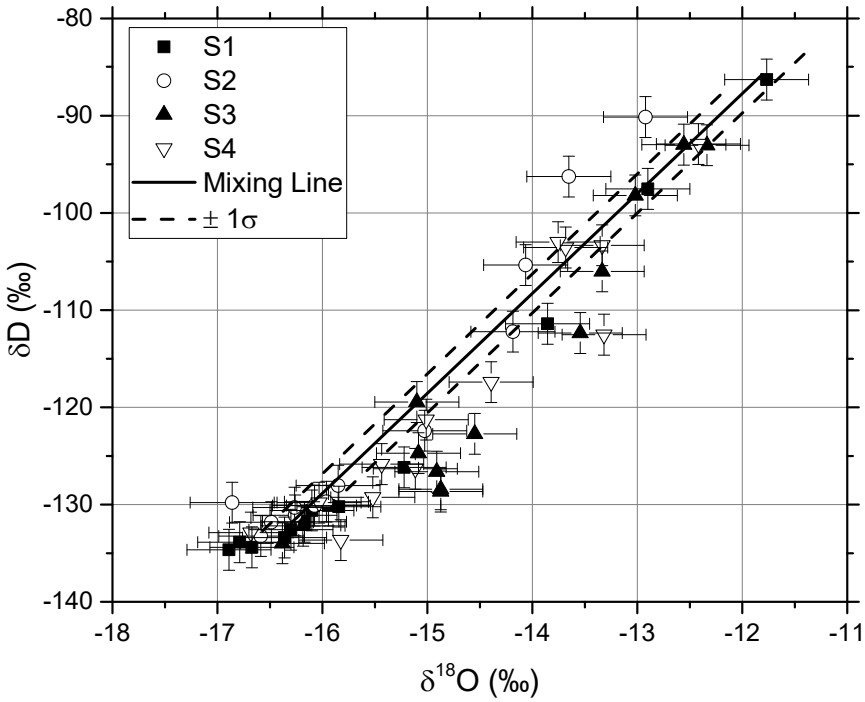

Figure 5.24 – Isotope mixing C1. No deviations at S1. S2 shows three deviations with condensed signature (0.4 m, 1.3 m, and 1.4 m column elevation). S3 shows 5 poitns with an evaporative signature (0.4 m, 0.5 m, 0.7 m, 0.8 m, and 1.0 m column elevation). Finally S4 shows 2 points with an evaporative signature (0.3 m and 1.0 m column elevation).

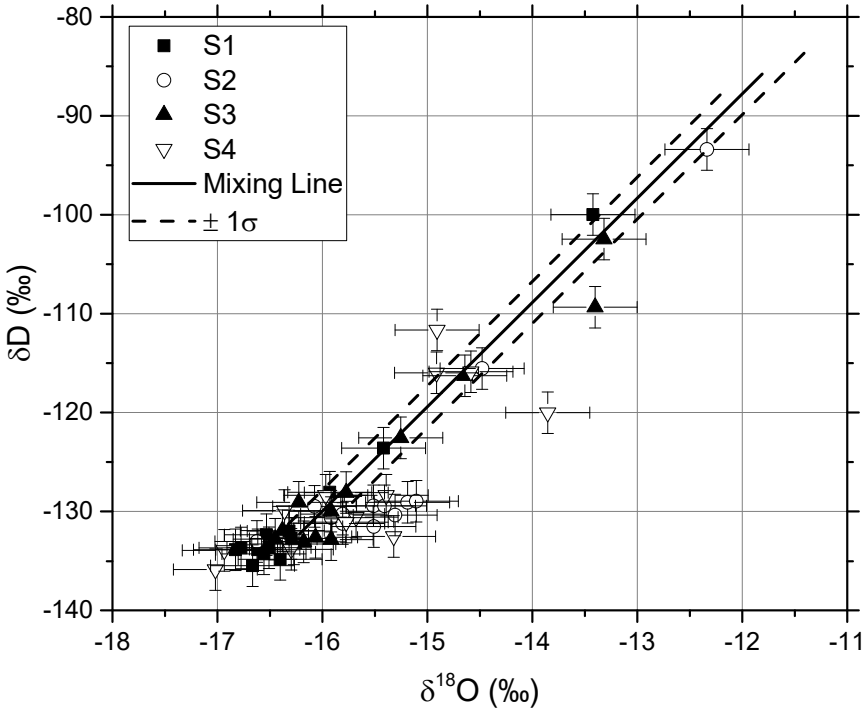

Figure 5.25 – Isotope mixing C2. S1 shows deviations in most of the data but these are attributed to the average used to create lower boundary and variations in Saskatoon tap water. S2 shows 5 points with an evaporative signature (0.2 m, 0.4 m, 1.0 m, 1.1 m, and 1.2 m column elevation). S3 shows 1 point with an evaporative signature at 1.3 m column elevation. Finally S4 shows 2 points with an evaporative signature (0.6 m and 0.8 m column elevation) and 1 point with a condensed signature (1.4 m column elevation).

The evaporative enrichment signature seen in the column does not appear to be systematic. Two possible locations of water loss are leakage are identified. One is through the sampling ports or diffusion of water vapour through the acrylic. The removal and replacing of the port caps could result in change in seal quality, depending on the cleanliness of the o-ring and contact area. The amount of evaporation, if present, was not measureable with the instrumentation used in the experiments. Water evaporation into the headspace between the soil and rain cap was another potential for evaporative water loss from the soil. However, the headspace was small (0.05 m height) and only 2E-5 kg of water could be stored at the lab temperature. This value is far too small to account for the amount of evaporative enrichment seen in the columns.

5.2.3.2 δD and $\delta^{18}O$ Profiles

The raw δ values that were measured were normalized prior to analysis, following the same method outlined for the diffusion cells in Chapter 6. The normalized results for the isotope measurements are shown in Figure 5.26 and Figure 5.27 for C1 and C2 respectively.

For both columns, the δD profiles show a shape that was closer to expected than the $\delta^{18}O$ profiles. The $\delta^{18}O$ data shows more scatter with a less defined center of mass. Table 5.14 shows the range of isotopes used in the experiment, the experimental error for each isotope, and the ratio of error to the range used.

Table 5.14 – Comparison of isotope concentration Δ added to the columns and the experimental error for each isotope. Δ calculated by comparing upper and lower boundary conditions.

Isotope	Isotope Δ added to column (‰)	Equipment Error (‰)	Error/Δ (%)
δD	46.5	2.1	4.5
$\delta^{18}O$	4.4	0.4	9.1

The increased error to Δ ratio for $\delta^{18}O$ may explain the increased variation seen in the isotope profiles. From this observation, the δD data will be used for analysis and modeling in the following chapter.

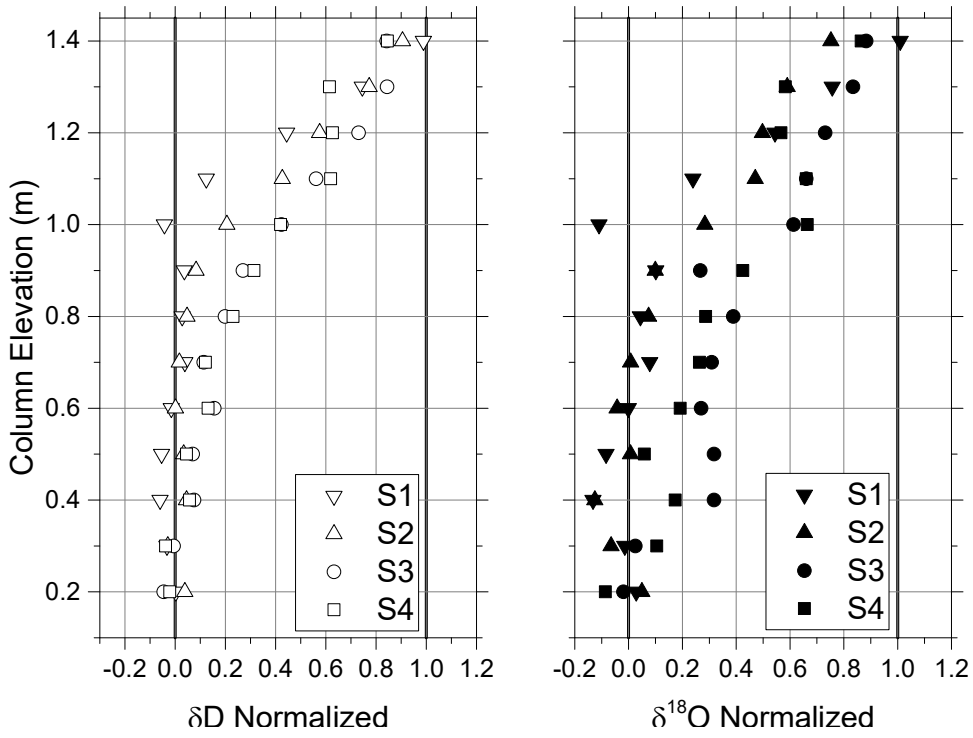

Figure 5.26 – δD and $\delta^{18}O$ isotope profiles for C1

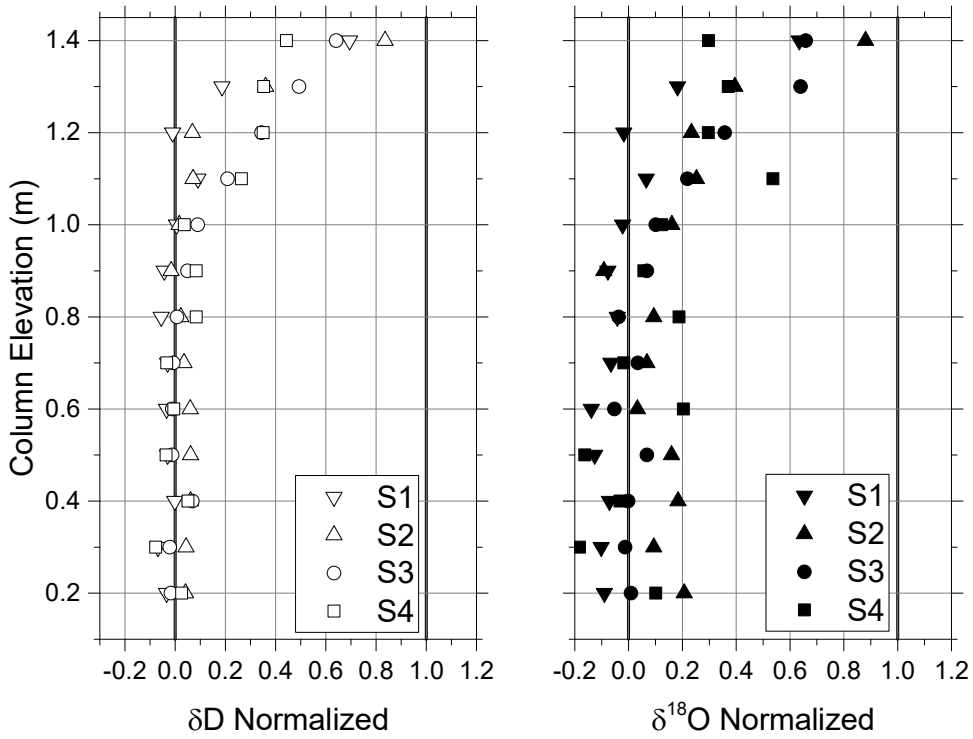

Figure 5.27 – δD and $\delta^{18}O$ isotope profiles for C2

5.2.3.3 Isotope Mass Balance

In order to better see the distribution of the δD added to the columns, a δ stored profile was created. The normalized mass of isotope stored for each column segment was found using Equation 5.1,

$$\delta \text{ stored} = \frac{C}{C_0}\theta_l(\text{Representative Sample Volume}) \quad \text{.....(5.1)}$$

where C/C_0 is the normalized isotope value , ranging from 0 to 1 (unitless), and the representative sample volume (0.0026 m^3) was found by calculating the column volume 0.05 m above and below the sample ports (m^3). The δ stored was then normalized by dividing the δ stored at each elevation by the total amount of isotope added to the column. The normalized cumulative δ stored profiles (Figure 5.28 and Figure 5.29) show expected isotope movement within the soil.

The isotope δ stored near the bottom of the column does not go to zero. By using the average of the background δ values the normalized concentration does not go to zero. Isotopic variations in the Saskatoon tap water may cause an increased or decreased in δ storage where no spike water is present. The variations in the tap water are more pronounced when a δ stored profile is created. The total δ stored can be found in Table 5.15.

Table 5.15 – δD added and measured for both columns

Column	Normalized δ Added	Total δ R1	Total δ R2	Total δ R	Total δ R4
C1	1	1.43	1.06	1.28	1.19
C2	1	0.73	1.44	0.95	0.82

For C1, the total δ stored is higher at every sample time. For C2, the δ stored lower than the isotope added, except at R2. The lower isotope stored compared to added may suggest that the amount of isotope added was less than expected.

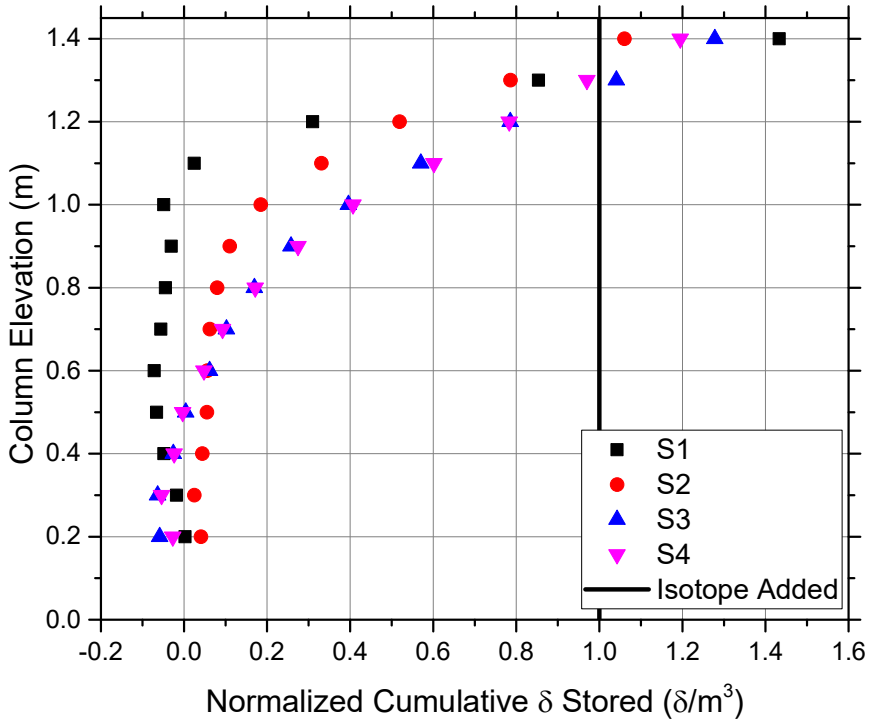

Figure 5.28 – Isotope δ stored for C1.

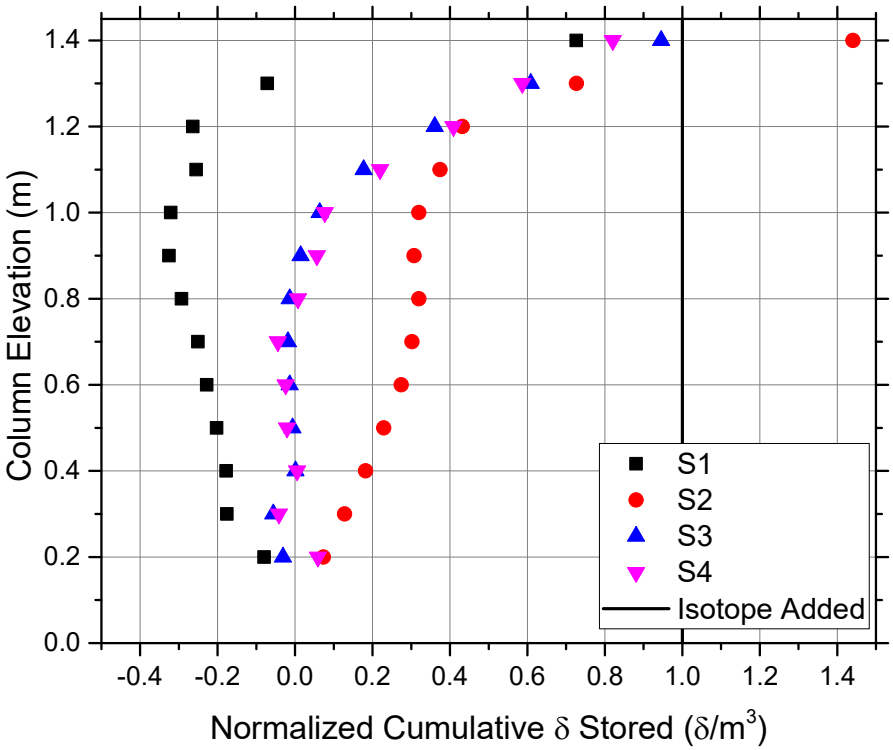

Figure 5.29 – Isotope δ stored for C2.

5.3 Summary

The results presented for the laboratory experiments show evidence that the experiments were completed successfully but were not without some concerns. The biggest concerns with the diffusion cell data was the variations in the constructed ρ_{dry} and ω, the liquid phase connectivity between the cell halves, and the actual isotopic value of the water added to the cells. These issues resulted in large error bars that lowered the confidence in the diffusion analysis.

The main concerns that were present in the column experiment were the homogeneity of the soil in the columns, and the water and isotope mass balances. The soil packing was completed successfully with most of the concerns with the collected data being present in the mass balances.

The masses of water added, collected as outflow, and stored within the column did not match, suggesting that soil structures may be present. These mismatched water balances may also be present due to hysteresis effects that were not investigated. The isotope data showed a poor fit between the amount of isotope added to the columns compared to what was measured.

Chapter 6 - Analysis and Discussion

The analysis of the data collected from the two experimental programs will be presented in this chapter. First the analysis of the diffusion cells will be presented and discussed, followed by the column experiments.

6.1 Diffusion Cells

The purpose of the diffusion cell testing was to measure the value of D_{com} at discrete θ_l and compare the measured data points to theoretical relationships. In this section, the values of D_{com} will be found for each diffusion cell. All the collected data will then be compared to theoretical predictions for D_{com} presented earlier in Chapter 3, by changing the τ models used. The discussion will highlight the key issues in the interpretation of the test data and discuss limitations such as cell construction and data quality.

6.1.1 Experimental D_{com} Measurements

The δD values within the diffusion cells were normalized to facilitate the comparison of the observed profiles to analytical models. The potential impact of aqueous phase discontinuity between the cells will be evaluated prior to a final estimation of the D_{com} values from each cell.

6.1.1.1 Normalized Isotope Concentrations

Normalized concentrations are calculated by dividing the difference between the observed concentration and a background concentration by the difference between the source concentration and the background concentration as represented by Equation 6.1,

$$\frac{C}{C_0} = \frac{\delta D - \delta D_{non-spike}}{\delta D_{spike} - \delta D_{non-spike}} \quad \text{.....(6.1)}$$

where C/C_0 is the normalized concentration, ranging from 0 to 1 (unitless), δD is the isotopic composition of the pore fluid for each cell slice (‰), $\delta D_{non-spike}$ is the isotope composition of the pore-fluid in the cell that represents then on-spiked conditions (‰), and δD_{spike} is the isotope composition of the pore-fluid in the cell that represents the initial spiked half-cell (‰). The δD

composition of the spiked and non-spiked sand was often different than the values of the spiked and non-spiked water used to prepare the sand samples.

Because of the mismatch in isotope values, the non-spike and spike δD values were selected so the values of C/C_0 at the ends of each cell were close to 0 or 1 with the midpoint of the profile close to 0.5. Table 6.1 shows the values that were used for each cell and how each was determined. Some of the cells required an assumed value of δD to create a symmetrical profile. This would suggest that the soil-water isotope interactions might have been greater than anticipated as described previously in Chapter 5 (Figure 5.14). Assumed values for δD were most common in R1 and R2.

Table 6.1 – Different boundary conditions selected for normalization of δD data for the diffusion cells. Prepared is within ± 1σ (± 2.1‰) from the measured water for each cell. Drained is within ± 1σ from the water collected from the cells after axis translation or hanging column drainage was complete. Mixed is within ± 1σ from the measured isotope value of prepared water mixed with the analysis sand. Values with two sources fall within ±σ from both measurements. Assumed refers to a value that was not based on any measurements but chosen so that the profile show a symmetrical shape.

Cell	Non-Spike δD (‰)	Value Source	Spike δD (‰)	Value Source
R1 – 1	-128	Prepared	-75	Assumed
R1 – 2	-129	Prepared	-75	Assumed
R1 – 3	-129	Prepared	-60	Assumed
R1 – 4	-131	Prepared	-55	Assumed
R1 – 5	-129	Prepared	-55	Assumed
R2 – 1	-127	Assumed	-32	Prepared
R2 – 2	-139	Prepared	-35	Prepared
R2 – 3	-139	Prepared	-32	Assumed
R2 – 4	-139	Prepared	-28	Assumed
R2 – 5	-139	Prepared	-32	Prepared
R3 – 2	-129	Prepared	-43	Prepared
R3 – 3	-125	Prepared	-40	Prepared
R3 – 4	-129	Prepared	-38	Prepared
R3 – 5	-128	Prepared	-37	Assumed
R4 – 1	-127	Prepared	-72	Drained
R4 – 2	-131	Drained/Prepared	-70	Mixed
R4 – 3	-134	Prepared	-70	Mixed
R4 – 4	-131	Drained/Prepared	-71	Drained/Mixed
R4 – 5	-134	Drained/Prepared	-74	Drained

6.1.1.2 Analysis of Aqueous Phase Discontinuity

The chloride profiles presented in Chapter 5 clearly highlight the presence of aqueous phase discontinuity between the two half-cells (Figure 5.9). To investigate the effects of reduced aqueous phase transport pathways on isotope transport, a sensitivity study was undertaken in which a small zone of $\theta_l = 0$ was assigned to the center of the cell. Cell R2-1 was selected for this evaluation

because the isotope data shows a classic diffusive profile with the expected shape and symmetry about the center of the cell. This cell has a single outlying data point but it does not significantly affect the results found from the profile. The normalized isotope profile can be found in Figure 6.1.

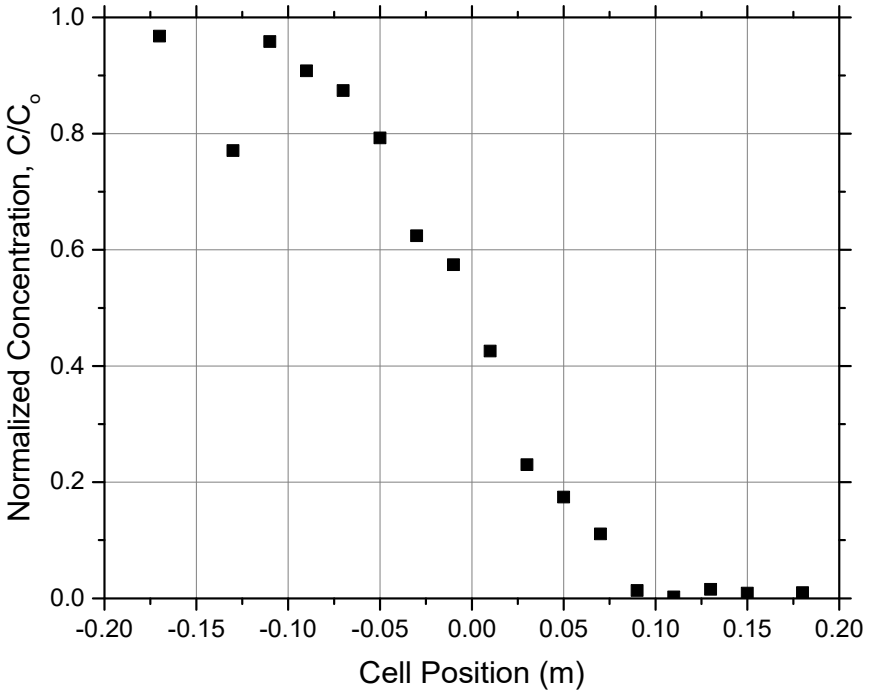

Figure 6.1 – Normalized Isotope profile for Cell R2-1, for aqueous phase discontinuity analysis.

A simulation was setup in GeoStudio's SEEP/W and CTRAN/W. The cell was created with a total length of 0.40 m, a height of 0.05 m and a thickness of 0.162 m. The model geometry was created with four separate areas, shown in Figure 6.2. The θ_l for sections 1 and 4 was set to 0.117 and the θ_l of sections 2 and 3 were set to 0. The porosity of the discontinuity was set to be the same as sections 1 and 4. The soil is assumed to be touching and the water phase is assumed not to be connected in the range close to the cell joint.

Variations in the size of aqueous phase disconnect were simulated by changing the combined thickness of sections 2 and 3. The combined thickness of these two sections were 0.00, 0.002, 0.006 and 0.010 m. The first simulation (thickness = 0.00 m) had the same D_{com}/θ_{com} for the entire domain (1.75E-9 m2/s), while the following three had a D_{com}/θ_{com} of 5E-5 m2/s (assumed value for diffusion of δD in air) set for sections 2 and 3, while the value for sections 1 and 4 was varied to find the best fit.

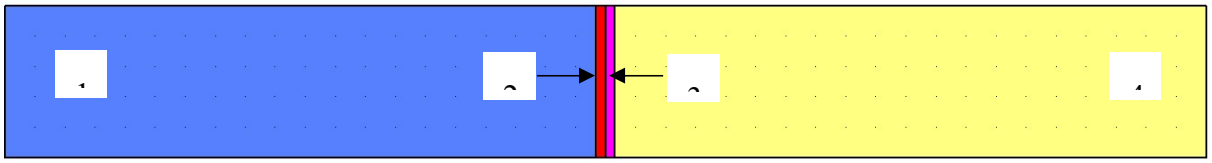

Figure 6.2 – Model geometry for diffusion cell analysis. The four different materials can be seen. In section 1 the concentration was set to 1 g/m^3 and the diffusion parameter was modified until the modeled profile fit the observed data. Section 2 had an initial concentration of 1, but for the cases where no aqueous phase connectivity was present, the diffusion value was set to 5E-5 m^2/s. Section 3 was the same size as 2 and had the same diffusion value set, but the initial concentration was set to 0. Finally section 4 is the same as 1 but with an initial concentration of 0.

The numerical model was used to find a diffusion value that best fit the measured cell data by minimizing the Residual Sum of Squares (RSS). A summary of the scenarios tested and the best fit diffusion values are found in Table 6.2.

Table 6.2 – Summary of discontinuity modeling scenarios.

Scenario	Discontinuity Thickness (m)	Diffusion for Model Sections 2 and 3 (m^2/s)	Best Fit Diffusion Value (E-9 m^2/s)	% error Compared to 0.00 m Thickness (%)
1	0.000	N/A	1.75	0
2	0.002	5E-5	1.69	4.0
3	0.006	5 E-5	1.55	11.7
4	0.010	5E-5	1.42	19.1

Plotting the thickness and the best fit diffusion values (Figure 6.3), a linear trend can be found.

Variations or specific values of D_{com}/θ_{com} for the discontinuity were not investigated because the fully unsaturated diffusion value is approximately 4 orders of magnitude larger than the observed diffusion values. Adjusting the vapour phase diffusion would not change the shape of the profiles or the best fit D_{com}/θ_{com} values measured.

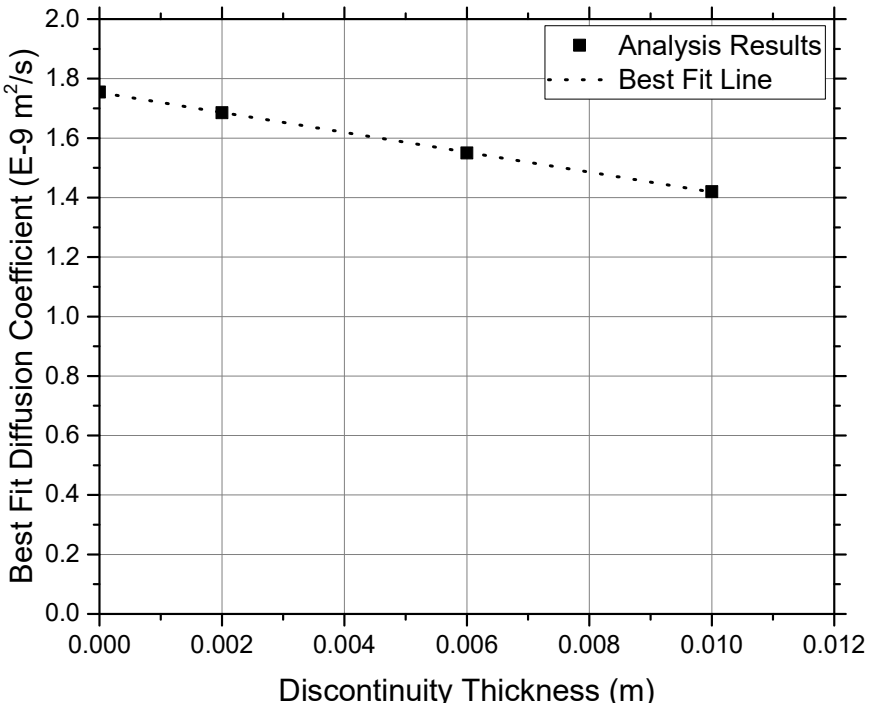

Figure 6.3 – Best fit diffusion values plotted against the discontinuity thickness showing a linear trend with an R^2 of 0.998. The best fit equation is y = -33.475x + 1.7531.

The d_{50} of the particle size distribution for the sand is 0.0005 m. Assuming the discontinuity is one particle diameter in thickness the error in D_{com} modeled should be approximately 1%. If the discontinuity is 10 particle diameters (0.005 m), the error is approximately 9.5%. It is highly unlikely that the discontinuity is larger than 10 particle diameters, and in this case a maximum 10 % error is deemed acceptable. This analysis was only done on one cell, but the remainder of the cells are assumed to show a similar trend. The results of this analysis indicate that the presence of the discontinuous aqueous phase should not introduce significant error if the cells are assumed to have a continuous liquid phase.

6.1.1.3 Observed Diffusion Values

The observed diffusion was found by varying the diffusion coefficient in the analytical solution until a best fit to the observed data was achieved. The method used to find the best fit was to minimize the RSS. The analytical solutions that were used are the Ogata and Banks (1961) for R1, R2, and R4 and Carslaw and Jaeger (1959) for R3.

The porosity values for each of the cells are different from one-another due to variations in packing. These differences will make analysis difficult because the diffusion models are sensitive to porosity. To remedy the variation, each of the cells were fit into a porosity category, and an assumed average porosity was used for analysis. The average porosities are 0.30, 0.35, and 0.40 with a range of ± 0.025. The exception here is cell R3-5, where the θ_l is higher than the porosity due to measurement errors and is moved from the 0.30 to 0.35 range. The values of RSS, the measured and assumed porosities are summarized in Table 6.3.

A value of D_{com} was calculated for the entire cell and each of the half-cells, giving three D_{co} measurements per cell. The entire cell gave the average D_{com} for that θ_l and each half-cell was used to find the upper and lower error bars to the average value. The observed D_{com} values are presented in Table 6.4.

Table 6.3 – Results of analytical analysis for observed diffusion coefficients. Cell test times, θ_l, and porosities are shown for discussion and comparison purposes.

Cell	Test Time (days)	Measured θ_l	Measured Porosity	Average Porosity for Analysis	RSS
R1 – 1	11.9	0.116	Unknown	0.40	0.1543
R1 – 2	21.8	0.156	Unknown	0.40	0.0135
R1 – 3	28.8	0.197	Unknown	0.40	0.0198
R1 – 4	33.0	0.238	Unknown	0.40	0.1091
R1 – 5	35.7	0.276	Unknown	0.40	0.0076
R2 – 1	11.9	0.117	0.42	0.40	0.0630
R2 – 2	19.9	0.165	0.39	0.40	0.0171
R2 – 3	22.9	0.249	0.39	0.40	0.0059
R2 – 4	25.9	0.350	0.38	0.40	0.0503
R2 – 5	24.9	0.301	0.39	0.40	0.0543
R3 – 2	38.1	0.336	0.38	0.40	0.0184
R3 – 3	36.0	0.335	0.37	0.35	0.0491
R3 – 4	35.2	0.310	0.36	0.35	0.0096
R3 – 5	36.1	0.322	0.31	0.35	0.0246
R4 – 1	16.9	0.249	0.30	0.30	0.0754
R4 – 2	17.9	0.210	0.30	0.30	0.0245
R4 – 3	16.9	0.164	0.31	0.30	0.0411
R4 – 4	14.9	0.152	0.36	0.35	0.0939
R4 – 5	15.8	0.120	0.42	0.40	0.0531

Table 6.4 – The lower, average, and upper D_com observed for each diffusion cell.

Cell	Lower D_{com} (E-10 m^2/s)	Average D_{com}(E-10 m^2/s)	Upper D_{com} (m^2/s)
R1 – 1	1.409	1.626	1.819
R1 – 2	1.748	1.880	2.046
R1 – 3	1.615	2.014	2.572
R1 – 4	1.743	3.915	6.742
R1 – 5	2.113	2.477	2.895
R2 – 1	1.389	2.046	3.228
R2 – 2	2.939	3.695	4.606
R2 – 3	3.034	3.313	3.627
R2 – 4	3.024	3.888	4.753
R2 – 5	4.866	5.342	6.104
R3 – 2	3.759	4.260	4.814
R3 – 3	3.671	3.913	4.197
R3 – 4	4.186	4.569	4.962
R3 – 5	2.718	3.347	4.125
R4 – 1	2.718	3.981	4.991
R4 – 2	2.995	3.655	4.345
R4 – 3	4.079	4.266	4.427
R4 – 4	3.535	4.088	4.538
R4 – 5	1.999	2.434	2.991

The cells with the lowest RSS and the highest RSS are highlighted in Figure 6.4 and Figure 6.5, respectively.

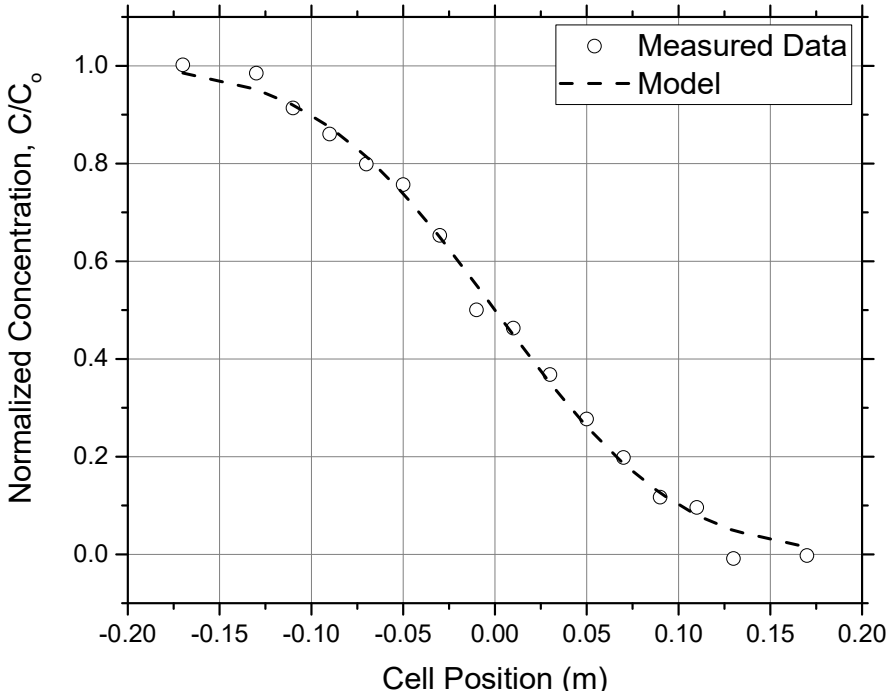

Figure 6.4 – Cell R2-3 profile showing fitted model to the observed data (RSS = 0.0059).

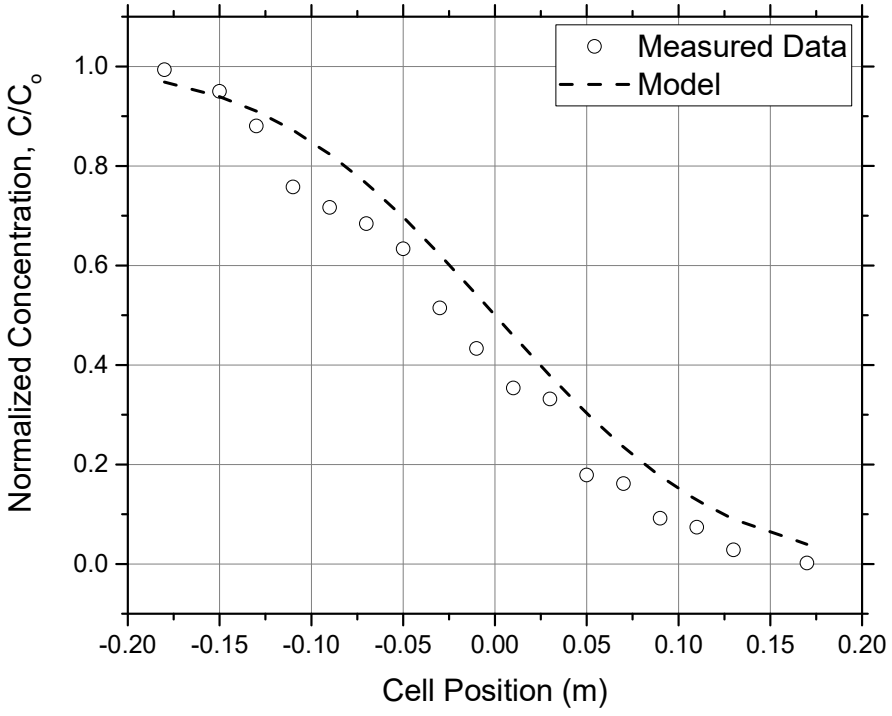

Figure 6.5 – Cell R1-1 profile showing fitted model to the observed data (RSS = 0.1543).

All the measured D_{com} data is plotted in Figure 6.6.

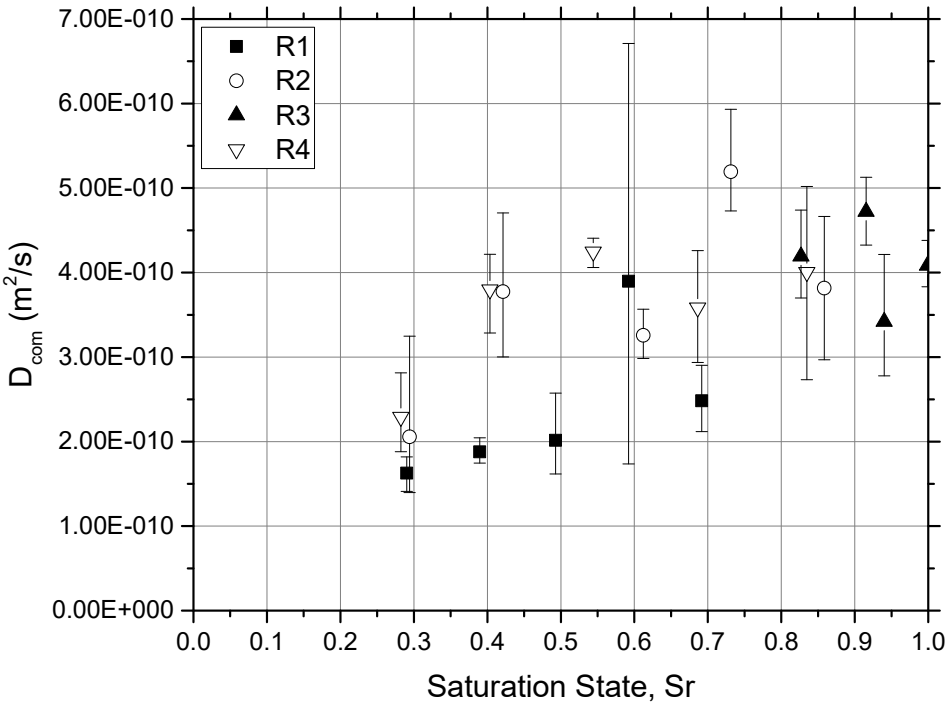

Figure 6.6 – Best fit data with error for each of the diffusion cells, where $S_r = \theta_{l\,measured}/\text{Average of Porosity Range}$.

The entire data set appears highly variable but with a generally decreasing value of D_{com} with decreasing saturation. A pattern in the D_{com} measurements is more apparent if these values are compared to theoretical models of D_{com} as is illustrated in the following section.

6.1.2 Diffusion – Water Content Relationship

In this section, τ models (Appendix A) for the aqueous and vapour phases are used along with the theoretical relationship for D_{com} (Equation 3.20, Section 3.2, $q_l = 0$) to create a series of functional relationships between D_{com} and saturation. These functional relationships were then compared to the observed data to find which combination of τ models best represents the measured D_{com}. The best fit models were selected based on RSS by calculating the D_{com} model at the saturation states of each cell. The models have hyphenated names which refer the source of the τ models used to represent vapour and aqueous phase diffusion. A summary of the best fit D_{com} models for each of the porosity ranges described previously are presented in Table 6.5.

Table 6.5 – Best fit D_{com} model for each of the analysis porosities used.

Porosity Range Average	Number of Cells	Best Fit D_{com} Model
0.40	12	PN – PD1
0.35	4	PN – PD2
0.30	3	PN – PD1

Each of the best fit models use Penman (1940) for the vapour phase, and a variation on Padilla et al. (1999) for the aqueous phase model. The best fit model for the porosity range average of 0.40, the constant model, and the linear model are plotted with the observed data in Figure 6.7a. A sensitivity analysis was done by scaling the free solution diffusion coefficients D_l^{i0} and D_v^{i0} by a factor of 0.5 and 1.5 each (Figure 6.7b). The porosity averages of 0.30 and 0.35 did not contain enough observed data points to cover the saturation range and as a result there was low confidence in the best fit models and thus the models are not presented with the observed data.

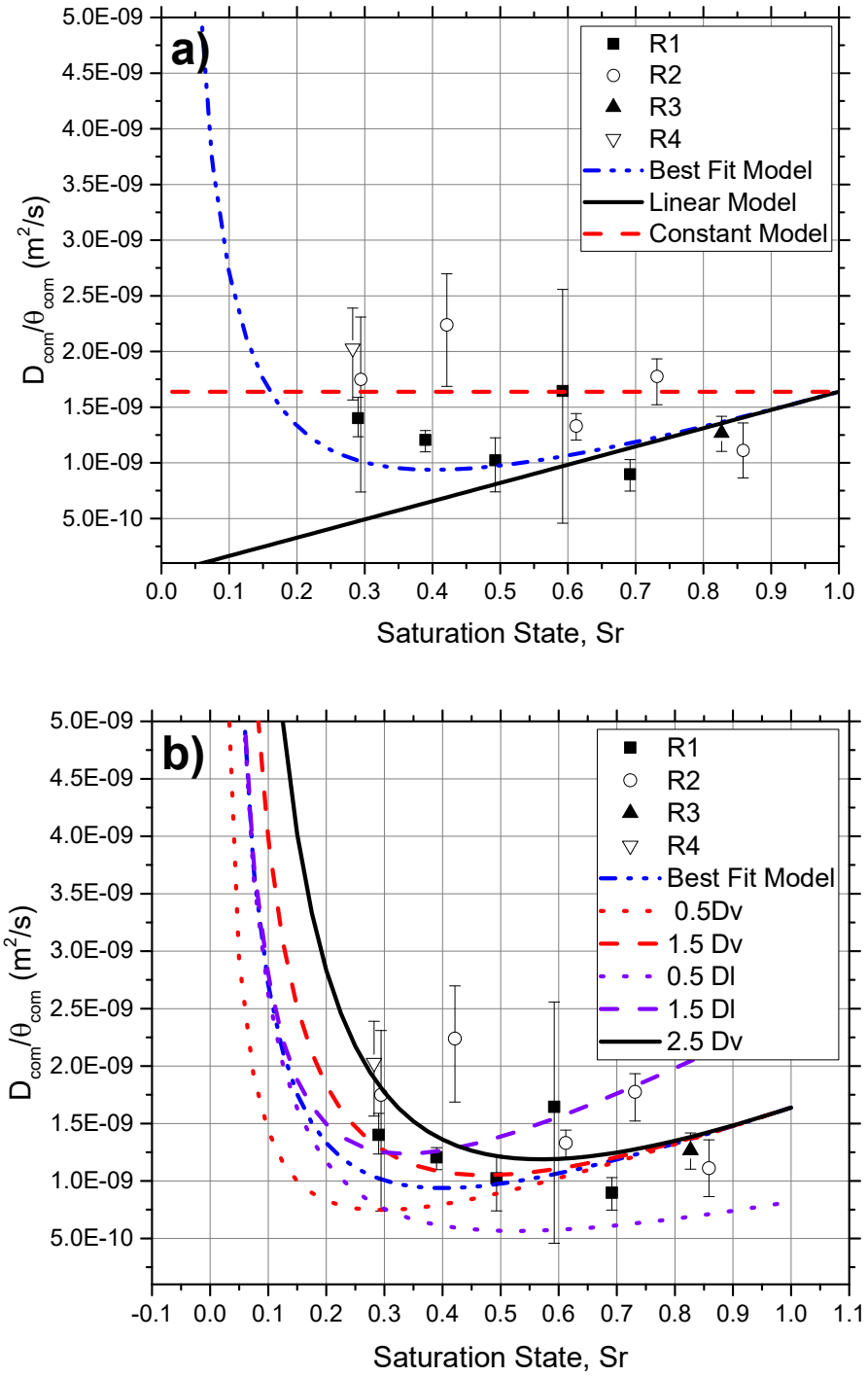

Figure 6.7 – a) Best fit model based on minimum RSS compared to observed data and other theoretical diffusion relationships. b) Sensitivity analysis highlighting the changes to the best fit dual phase relationship with varied free solution diffusion coefficients. The porosity used was 0.4, with $S_r = \theta_{l\,measured}/\text{Average of Porosity Range}$.

6.1.3 Discussion of Diffusion Cell Analysis

Chapter 5 highlighted some of the limitations of the D_{com} measurements. The variations in ρ_{dry} and ω will both result in variations in aqueous and vapour phase diffusion as well as potential advective transport. Comparison of the measurements with the theoretical functional relationships highlights that there is more scatter at mid-range θ_l. This may be due to the greater potential for vapour migration to occur at these θ_l due to gradients of temperature or soil suction.

The variations in the initial spike and non-spiked isotope values create more variation in the observed D_{com} compared to ω and ρ_{dry}. Small changes in the initial values can change the shape of the resulting profile and value of D_{com} measured. The actual values of the initial conditions, as shown in the Chapter 5, can have a large variation in isotope content depending on when they are measured.

Given the uncertainty associated with variations in ω, ρ_{dry}, and the initial isotope values, it is difficult to quantify a best fit D_{com} that accurately represents observed data. From Figure 6.7a it can be seen that that the best fit dual phase model describes the data from a saturation of 1 to approximately 0.5. In that range the linear model appears to describe the data as well. In the saturation range of 0.5 to 0 both the dual phase and the constant models describe the measured data. To fully understand which model would be most appropriate, more data points below residual saturation are needed.

What the data does show, is that the dual phase model is more appropriate than a single phase model for isotopes in unsaturated soils, but if the soil is not expected to dry below it's θ_{res} (here θ_{res} is approximately a saturation of 0.2), a constant model may be an appropriate simplification to the dual phase relationship. If the soil dries below the θ_{res} or the soil has a very coarse texture with a very low θ_{res}, the use of a constant model would break down as the transport in the vapour phase becomes highly significant.

The sensitivity analysis showed that the models are sensitive to changes in D_l^{i0} where the shape of the profile over most of the saturation range is different. When D_v^{i0} is varied the shape of the profile changes less and the effects are mostly seen below a saturation of 0.3. Modifying the D_l^{i0} and D_v^{i0} shows a better fit to the observed data as D_v^{i0} gets larger. The best fit to the observed data is found at approximately $2.5D_v^{i0}$.

6.2 Column Experiment

Analysis of the column experiment will involve four parts. The water migration through the columns will first be simulated which will allow calculation of the temporal and spatial variation of the Peclet numbers, in order to define the dominant transport mechanisms within the column. This understanding will then be used to guide the numerical simulation of diffusion and mechanical dispersion dominated phases of the tracer test.

6.2.1 Water Content Modeling

Modeling of the column θ_l was initiated by manually varying the SWRC and K_{sat} until the simulation provided a best visual match to the measured θ_l data. Following the initial fit, a compilation of all laboratory SWRC results is presented. Finally, the modeling and laboratory results are compared. A description of the water transport model used can be found in Appendix E.

6.2.1.1 Water Transport Model Optimization

The measured column ρ_{dry} was used as the starting column porosity. The Van Genuchten (1980) a and n parameters were adjusted by trial and error in attempt to fit the model to the lower portion of the column (< 0.7 m). After the lower elevations were fit, the θ_{res} and K_{sat}were adjusted until the top of the column had an acceptable fit to both the drained residual conditions and the increased θ_l that developed during infiltration. The measured profiles with the best fit models are shown in Figure 6.8 and Figure 6.9.

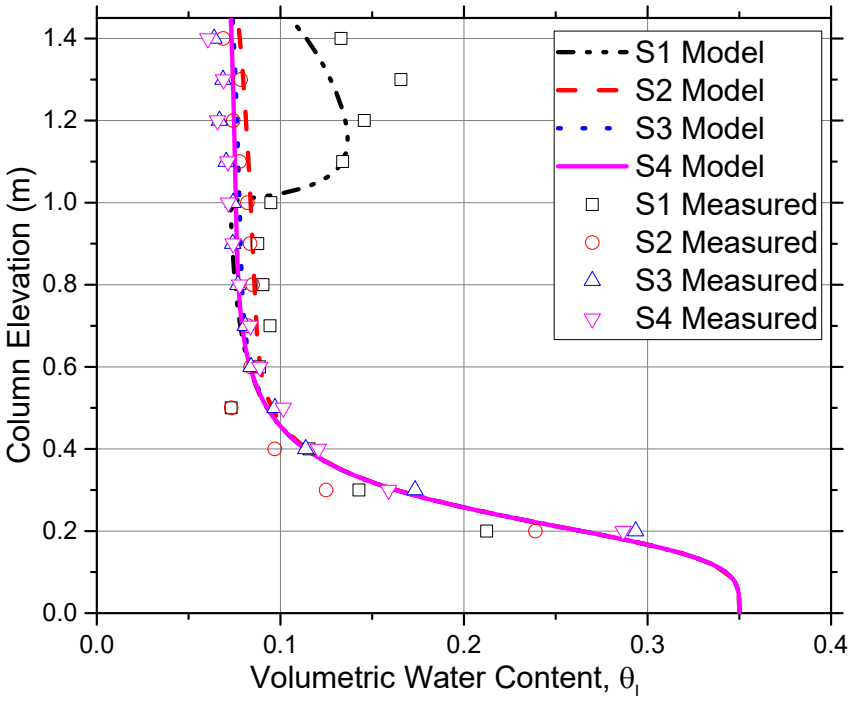

Figure 6.8 - C1 best fit model and measured water content data

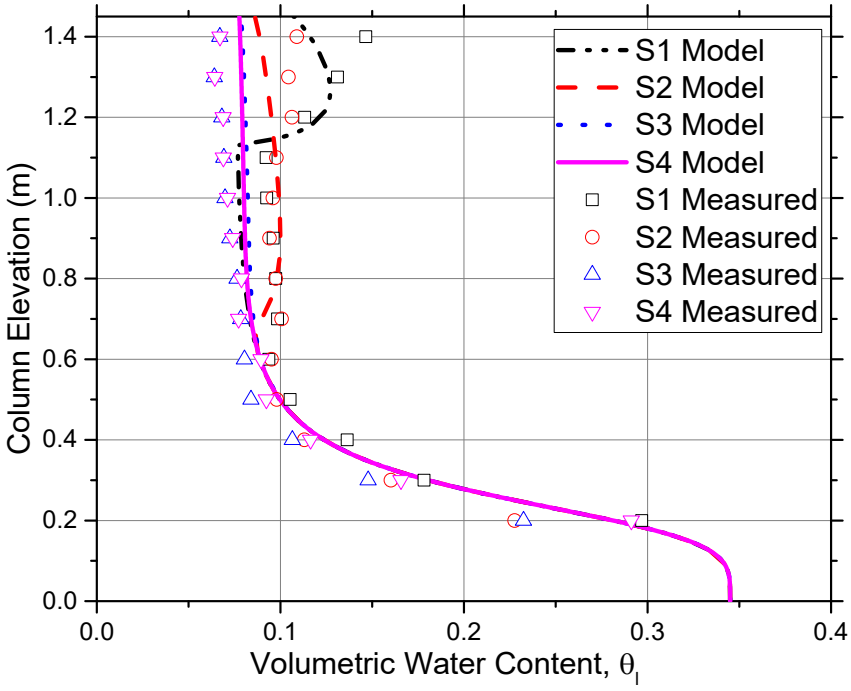

Figure 6.9 – C2 best fit model and measured water content data

In the middle of both columns (C1 1.0 m – 0.6 m and C2 1.1 m – 0.6 m), the first set of measured θ_l (S1) were higher than expected. This may have been due to displacement of water during

infiltration, increasing the θ_l just below the infiltration zone. The model captures the shape of the infiltration but does not replicate the specific values well. The variations at the top of the column are most likely due to the lack of proper densification of the soil, causing different hydraulic properties compared to the bulk of the column.

The best fit numerical models are compared to the TDR measurements at S1, S2, and S3 in Figure 6.10 and Figure 6.11.

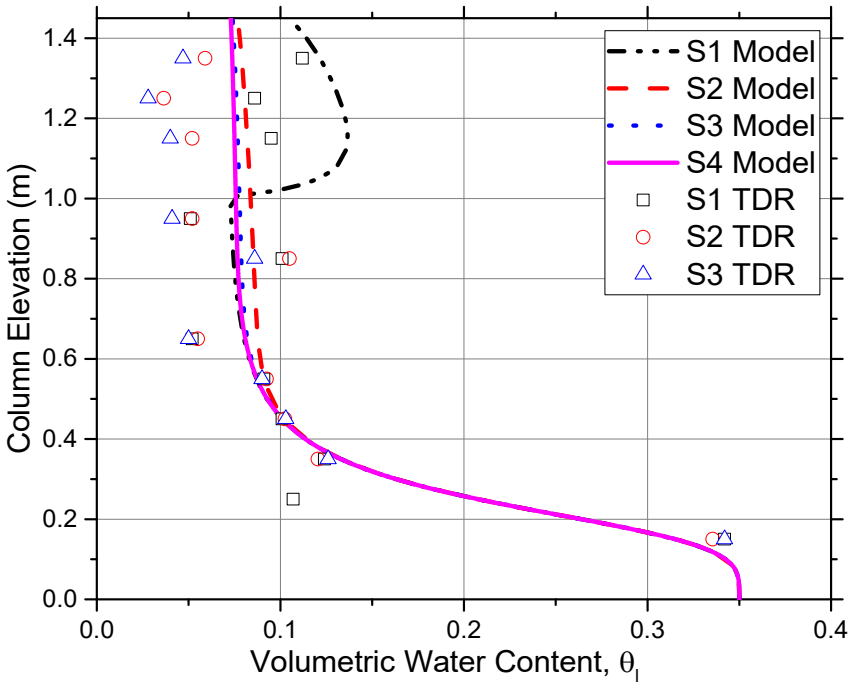

Figure 6.10 - C1 best fit model and TDR water content data

With the negative and incorrect data points removed for C1, the TDR measurements match the best fit model from the base of the column to 0.55 m. Above 0.55 m, the TDR measurements have a consistent pattern, but are shifted between each of the sample times. The top TDR measurements do not capture the shape observed in the oven dried θ_l data or the model.

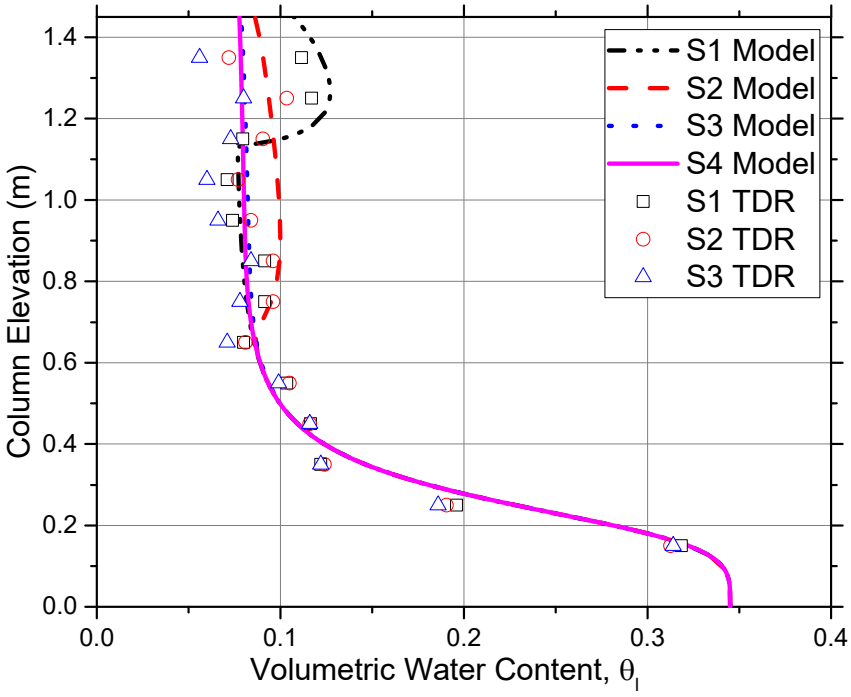

Figure 6.11 - C2 best fit model and TDR water content data

When comparing the column C2 data to the best fit model, the fit is acceptable over the column. Some oscillation in the TDR data from 0.65 m to 1.15 m can be seen. This oscillation was not captured in the measured data and it is not clear if it is a systematic change in θ_l or error within the TDR measurements. The top of the column at the first sample time fits with the model, but compared to the measured data, the water storage is lower. S2 shows a good fit in two locations (0.65 m to 0.85 m and 1.15 m to 1.125 m). The SWRC parameters of the best fit models are presented in Section 6.2.1.3.

6.2.1.2 Estimation of Transport Properties

Several laboratory experiments were conducted to estimate K_{sat} (Table 6.6) and the Van Genuchten (1980) SWRC parameters (Table 6.7). The modeling of the columns initial saturation and drainage step was completed before the rainfall experiment was conducted and is considered a laboratory experiment. The columns were saturated and allowed to drain while the TDR system was recording θ_l and the mass of the outflow was collected and measured.

The numerical model (Appendix E) was started at saturation and allowed to drain until steady state. The Van Genuchten (1980) SWRC parameters and the K_{sat} were adjusted until the TDR

measurements and the model θ_l showed an acceptable fit, while ensuring that the mass leaving the model over time matched the outflow measurements (Appendix E).

Table 6.6 – Results of hydraulic conductivity estimates for initial modeling guesses

Method	K_{sat} (m/s)	Notes
Falling head permeability test	1.65E-5	Average of 3 test on the same soil in apparatus
Drainage modeling C1	2.00E-4	Involved modeling all water parameters for soil
Drainage modeling C2	1.10E-4	Involved modeling all water parameters for soil
Hazen's Formula(Carrier III, 2003)	2.22E-4	$K = (D_{10})^2$ (D_{10} = 0.0149 cm)

The K_{sat} measurements all had good agreement except the falling head permeability test, which was an order of magnitude lower than the others. This may have been due to denser soil packed for the experiment or densification of the soil during the experiment.

Table 6.7 – Results of SWRC parameter estimation for initial column porosity (parameters for Van Genuchten, 1980 SWRC model)

Method	a (kPa)	n	Porosity	θ_{res}	Notes
Bench Scale Testing (Tempe cell and bench scale column)	2.5	3.3	0.41	0.066	Average of 2 lab tests, found in Figure 6.12. θ_{res} was an average of each experiments highest suction values.
Drainage modeling C1	1.6	3.0	0.40	0.080	Possible errors in outflow data collection and TDR measurements.
Drainage modeling C2	2.2	3.1	0.35	0.060	Possible errors in outflow data collection and TDR measurements.
Particle Size Distribution	3.4	3.9	0.40	0.020	The porosity was estimated from the results of independent packing experiment. θ_{res} was selected from the Modified Kovacs SWRC at 1000 kPa.

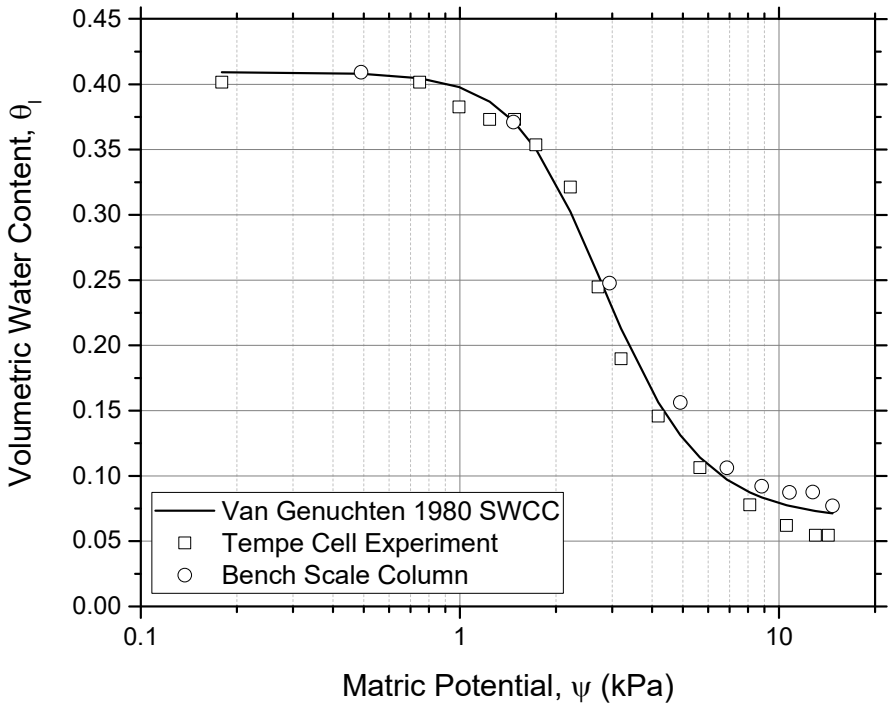

Figure 6.12 - Van Genuchten (1980) fit to the Tempe Cell and bench scale column θ_l - suction data.

The porosity found was expected for dry packing of coarse Beaver Creek Sand. The estimates of θ_{res} showed significant variation. Modeling of C2 and the bench scale experiments resulted in a similar θ_{res}, while modeling of C1 showed a higher value and the Modified Kovacs estimate resulted in an unrealistically low value for a coarse sand.

The SWRC parameters were in agreement with one-another except for the Modified Kovacs method. The Van Genuchten (1980) n shape parameter showed a value that was similar for three of the methods with the Modified Kovacs estimate being significantly higher. The a parameter saw significantly more variation between each of the methods with no distinct pattern. The hydraulic properties of the soil from the laboratory experiments is the average of all the laboratory values collected (Modified Kovacs inclusive). The average porosity will not include the modeled results of C2.

6.2.1.3 Comparison of Model to Laboratory Estimates

The best fit parameters for C1 and C2 are compared to the laboratory measured values in Table 6.8 and Figure 6.13.

Table 6.8 – Comparison of SWRC parameters and K_{sat} between laboratory experiments and optimized water transport models.

Parameter	Laboratory Estimates	Optimized C1 Model	Optimized C2 Model
a (kPa)	2.4	2.2	2.4
n (unitless)	3.3	4.1	4.3
Porosity (m^3/m^3)	0.40	0.35	0.345
θ_{res} (m^3/m^3)	0.057	0.070	0.075
K_{sat} (m/s)	1.4E-4	2.5E-5	2.0E-5

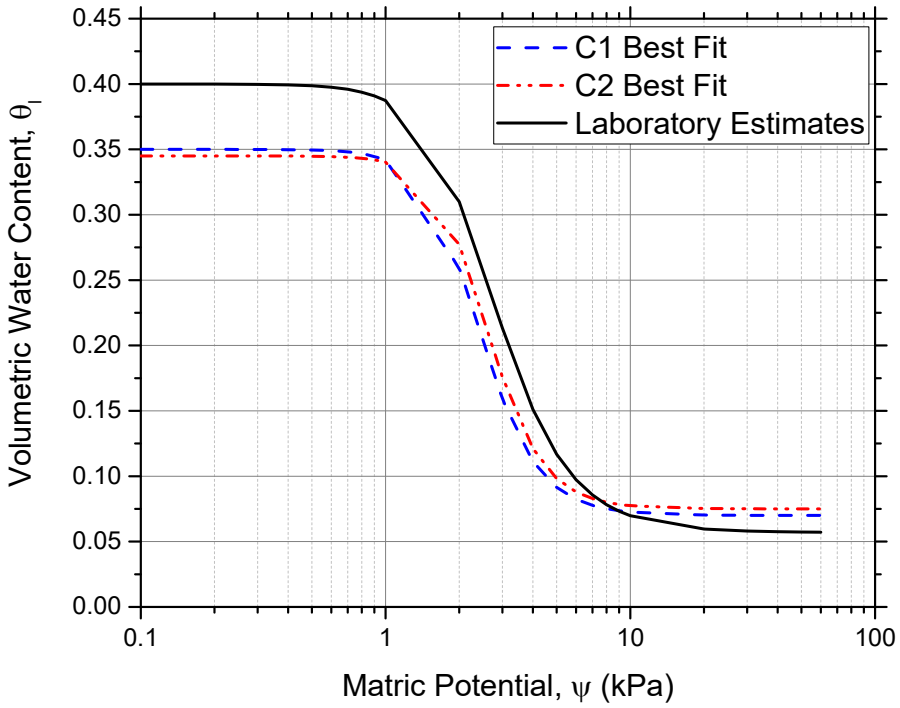

Figure 6.13 - Best fit and initial water transport parameters for the experimental columns C1 and C2.

It is apparent from Table 6.8 and Figure 6.13 that the shape of the SWRC between the two column experiments is similar. The similarity in the shapes gives an indication that the packing method and sand mixture used was consistent between the two columns. The main difference between the initial parameters and the best fit was the soil porosity, n and K_{sat}. The soil porosity, while different from the estimate, is as expected due to the densification of the soil by saturation and draining.

The n parameter for the best fit indicates a steeper drainage characteristic, compared to the initial parameters, and the hydraulic conductivity is approximately one order of magnitude lower than expected. The hydraulic conductivity value that was observed in the columns, matched closely to the falling head hydraulic conductivity experiment.

The reduction in porosity compared to the lab experiments should have increased the air entry value (AEV) of the soil (loosely related to the Van Genuchten (1980) a parameter), but the AEV remained the same. With an increased density, θ_{res} should have increased, but remained as initially estimated.

Another consideration regarding the θ_l profiles is the less dense top layer that was present. Modeling of a less dense top layer, approximately 0.2 m thick, would not improve the fit of the models. A high volume of water is stored in the top portions of the column in the early times. If the density was decreased, the amount of water stored should be lower, as there is less matric potential to hold water in the pore space. The increased volume stored at the top of the profiles during early times, is most likely present due to hysteresis.

6.2.2 Peclet Profiles

The water flux (q_l) and θ_l profiles from the numerical models were used to calculate the Peclet (Pe) number for C1 and C2 over the column height and over the duration of the experiment. The Pe number is calculated as,

$$Pe = \frac{vd}{D} \quad \text{.....(6.2)}$$

where v is the soil water velocity (m/s), d is the plume length (m), and D is the molecular diffusion rate (m^2/s).

Fetter (1999) presented a plot indicating how Pe numbers are related to the dispersive and diffusive spreading values. The plot, shown here in Figure 6.14, highlights Pe number ranges and identifies what transport processes are dominant in each. The traditional plot only shows three regions, low Pe numbers, where molecular diffusion is dominant (red), mid Pe numbers where both transport mechanisms are active, and high Pe numbers where mechanical dispersion is dominant (blue). For this work, the mid-range is divided into two sections; one lower Pe number range where both

transport mechanisms are active but diffusion has a greater influence on transport (yellow) and a higher Pe number range where mechanical dispersion has a larger influence on transport (green). These four ranges presented will be used to identify where and when in the column experiments each of the transport mechanisms are dominant.

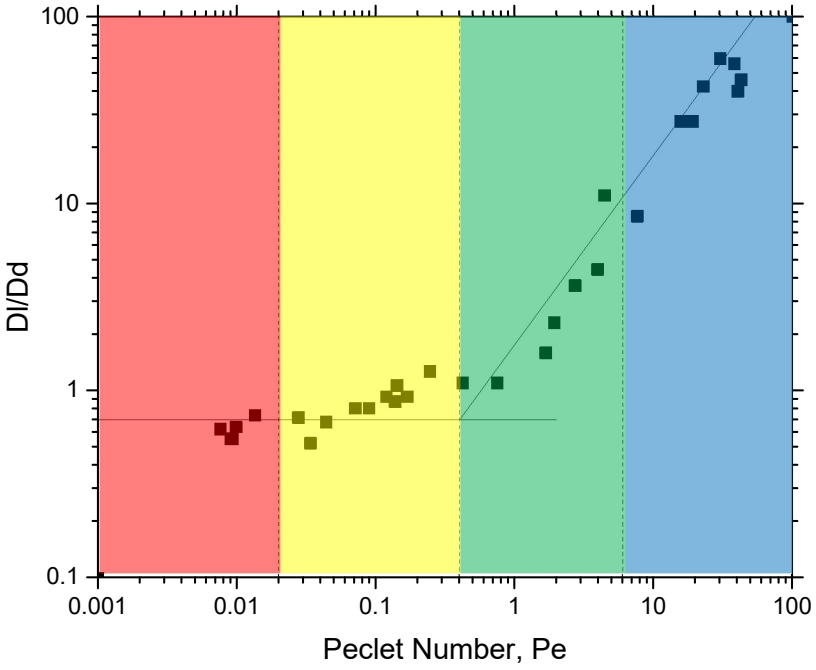

Figure 6.14 – Spreading control plot. Colored areas showing the different regions to be outlined in the column modeling data. Red – diffusion dominated, yellow – diffusion mechanical dispersion dominated, green – mechanical dispersion diffusion dominated, and blue – mechanical dispersion dominated. (after Fetter, 1999)

The value of v is calculated from the model outputs (q_l/θ_l), and the D value is calculated from the D_{com} functional relationship (Section 6.1.2) at each θ_l. The value of D_{com} for use in Equation 6.2 is divided by θ_l to make the form of the diffusion value consistent with the form of Fick's First Law used for the Pe calculation (Fetter, 1999). The plume length (d) was defined from top of the column to 10% C/C_0 at each sample time. The plume lengths for C1 and C2 at all sample times are found in Table 6.9.

Table 6.9 – Plume length in C1 and C2 at each sample time. Plume length is where the normalized concentration is at 10%. Plume lengths are depth into the column from the surface elevation of 1.45m.

Column	S1 Plume Length (m)	S2 Plume Length (m)	S3 Plume Length (m)	S4 Plume Length (m)
C1	0.350	0.525	0.900	0.900
C2	0.200	0.225	0.450	0.500

The Pe number was calculated and contoured for each node location and time step from the numerical model, for C1 and C2 (Figure 6.15 and Figure 6.16). The plume length for each sample time was the plume length at the end of that sample time (start to S1 the plume length is that of S1, S1 to S2 the plume length is that of S2, etc.).

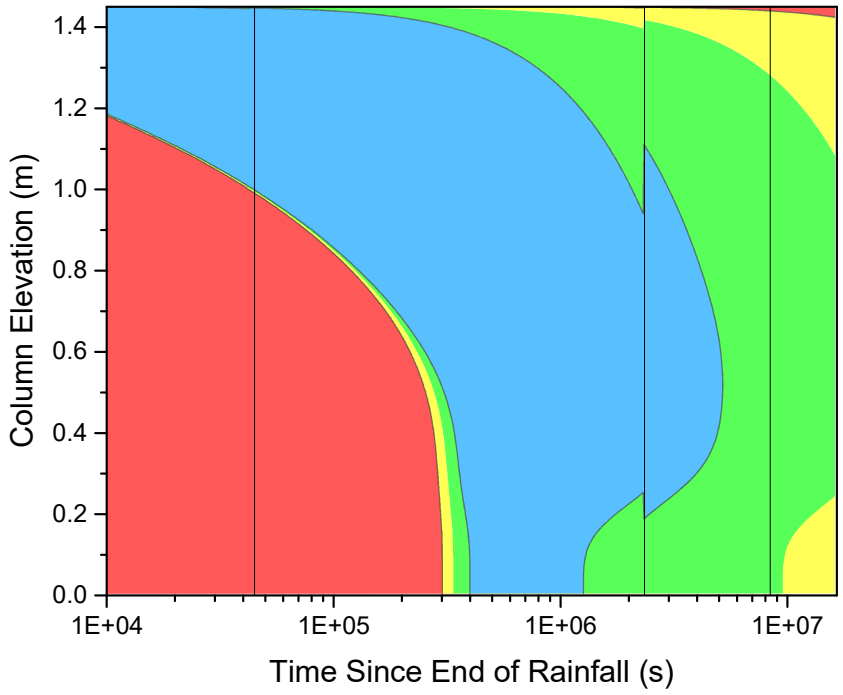

Figure 6.15 – Pe profile for C1. The colors on the plot correspond to the dominant transport mechanism presented in Figure 6.14. The black vertical lines show S1, S2, and S3, while the right hand side of the plot is S4 when the experiment was terminated.

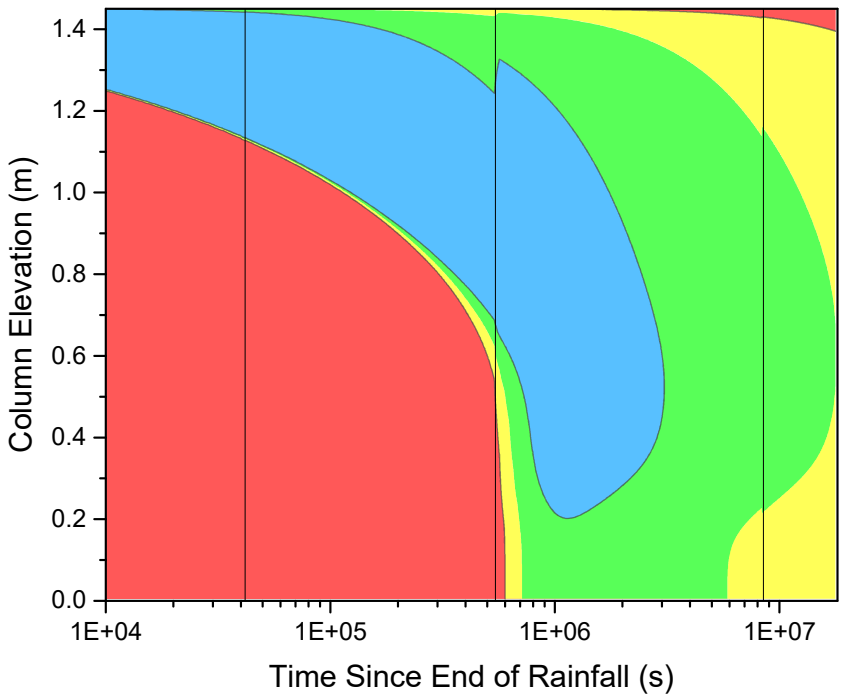

Figure 6.16 – Pe profile for C2. The colors on the plot correspond to the dominant transport mechanism presented in Figure 6.14. The black vertical lines show S1, S2, and S3, while the right hand side of the plot is S4 when the experiment was terminated.

The pattern of evolution of the Pe number is similar for both columns. All spreading up to S1 is dominated by mechanical dispersion. Up to S2 the role of mechanical dispersion starts to diminish. Between S2 and S3, the diffusive transport begins to become dominant in upper portions of the column where the increased isotope values are located. Between S3 and S4 diffusion appears to be the dominant mechanism of hydrodynamic dispersion.

Based on the Pe number profiles the transport modeling for the columns will be done in two parts. First, the diffusive spreading that is captured in samples S3 and S4 will be modeled using diffusion only. The concentration profiles collected at S2 will be used as initial conditions. The second part will use the best fit diffusion function from the S3 and S4 models along with different Λ functions to model the initial spreading to S2. Dispersive effects between S2 and S4 are not considered in Part 1. The two modeling parts are summarized in Table 6.10.

Table 6.10 – Breakdown of two model parts for column transport analysis. This will be applied to columns C1 and C2.

Model Part	Initial conditions	Sample times being modelled	Diffusion Models used	Mechanical Dispersion Models used
1	Measured data for S2	S3 and S4	Dual-phase, Constant, Lim et al. (1998)	None
2	C = 0	S1 and S2	Best fit from part 1	Constant, Sato et al. (2003), Bell Shaped

6.2.3 Diffusive Transport Analysis

For the diffusive analysis, the measured S2 data for each of the columns was used as the initial conditions for modeling (Figure 6.17).

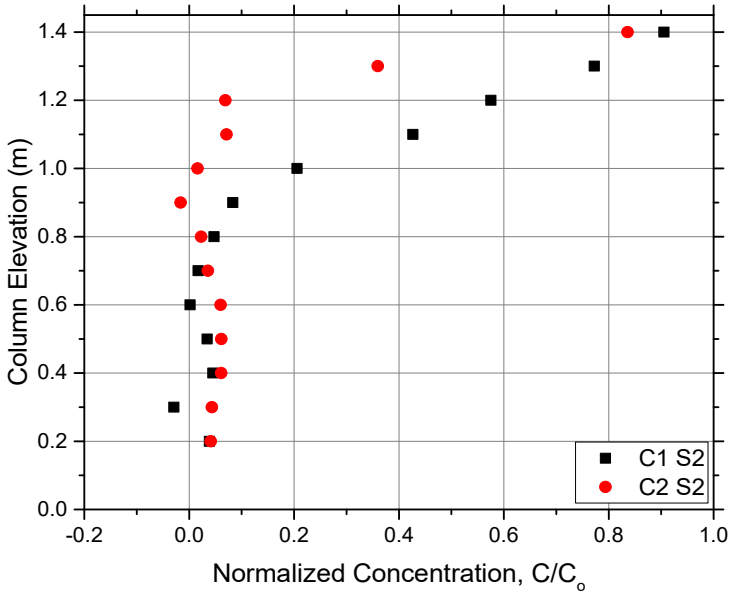

Figure 6.17 – Model part 1 initial conditions as measured.

In the lower portions of the column where no change in concentration should have been observed, the normalized concentration was set to zero (Figure 6.18).

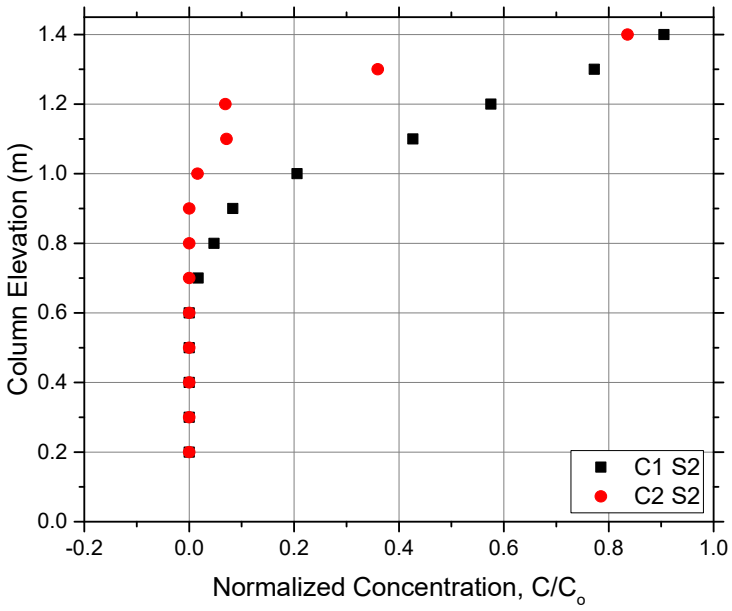

Figure 6.18 - Model part 1 initial conditions with lower portion adjusted to zero where no elevated isotope concentrations should be present.

The aqueous phase diffusion models used in the diffusion simulation were the dual-phase model (PN – PD4) from the diffusion cell analysis, a constant coefficient of diffusion, and a linear model representing a linear decrease in D_{com} with decreasing θ_l. The linear model is used in place of the Lim et al. (1998) model, as it will be easier to input into the numerical models (Figure 6.19). The constant value and linear models are anchored at saturation to the same value as the dual-phase model. A description of the transport numerical model can be found in Appendix E.

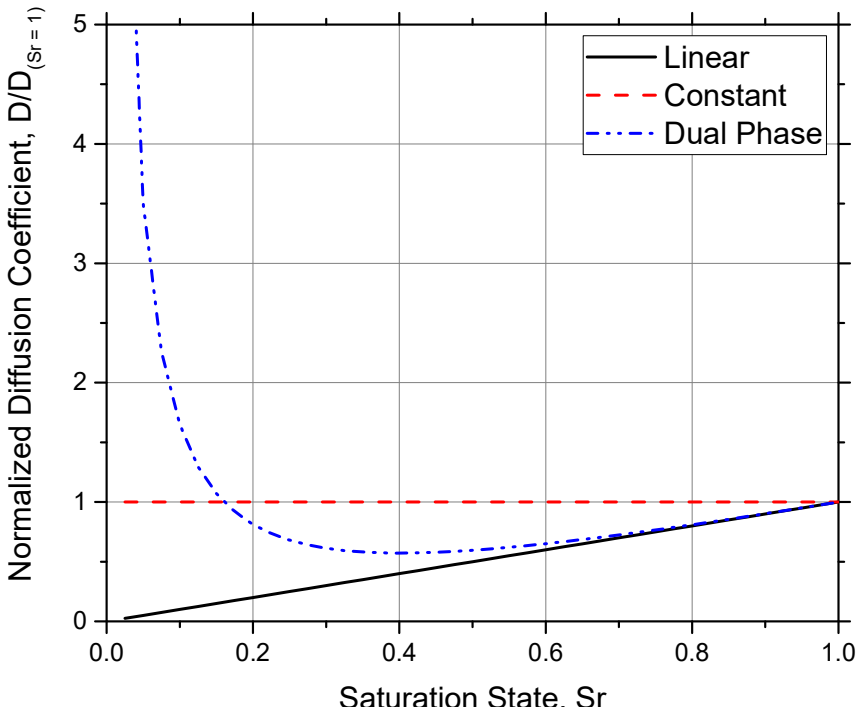

Figure 6.19 – Normalized diffusion models used for comparison to observed isotope data. The models do not go to a saturation state of zero because the dual pahse model becomes undefined at that point. Leaving the models close to zero will not effect analysis as the residual saturation state is higher than that value (residual saturation ~ 20%). This plot is similar to that presented earlier but note the larger scale for the normalized D value. Here actual values are used for the dual-phase model and the diffusion values at S ~ 0 are much higher than the assumed values presented in Chapter 3. Here $D = D_{com}/\theta_{com}$.

The model was run with the previous inputs and the results of the diffusion analysis are plotted below in Figure 6.20 and Figure 6.21. The plots are broken down into S3 and S4 for C1 and C2.

For C1 S3, the best fits to the measured data are the dual-phase and constant models in the lower portion of the column, while the best fit near the surface is the linear model. The same observation can be made for S4.

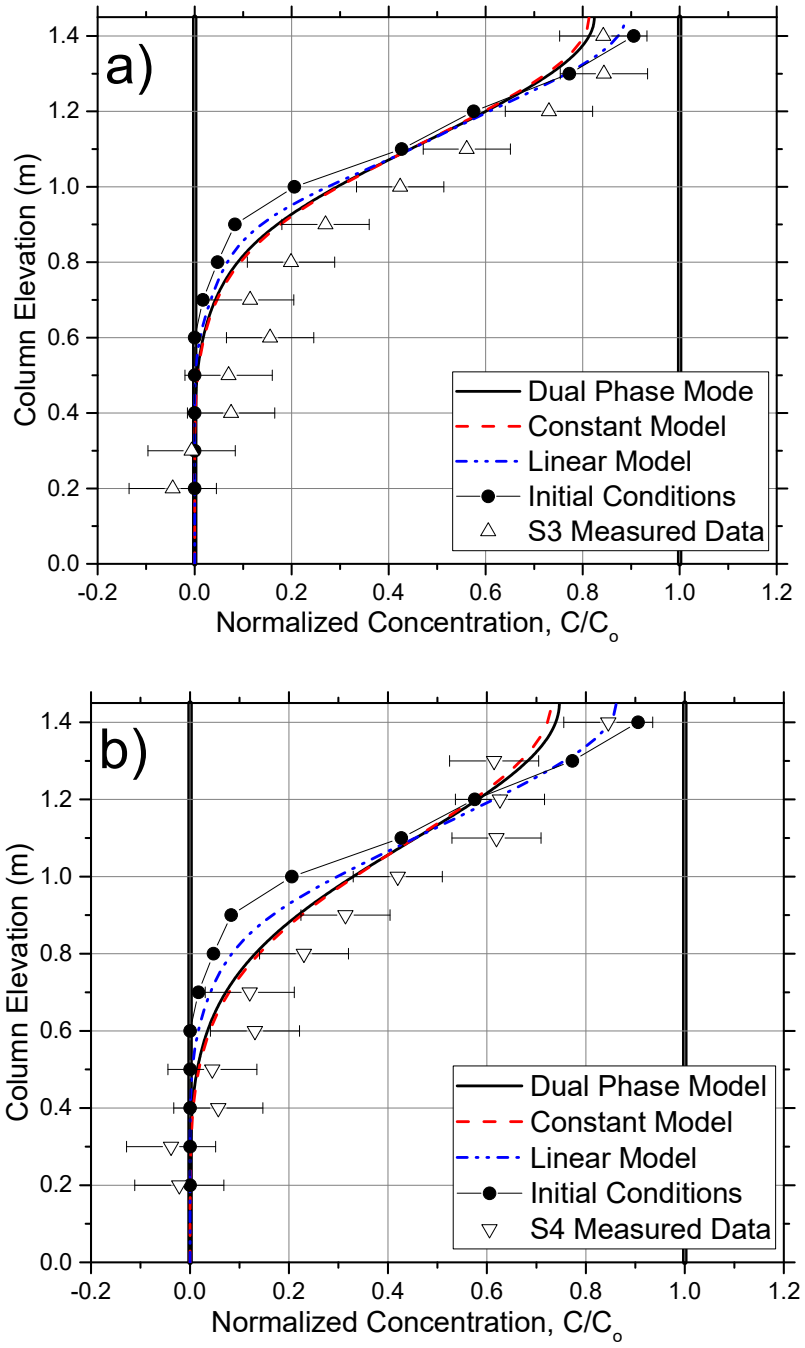

Figure 6.20 – Diffusion models for C1 compared to a) the S3 measured data and b) the S4 measured data. Also showing the measured data for S2 as initial conditions. The initial conditions are presented as a line to represent the linear interpolation used in the modeling software.

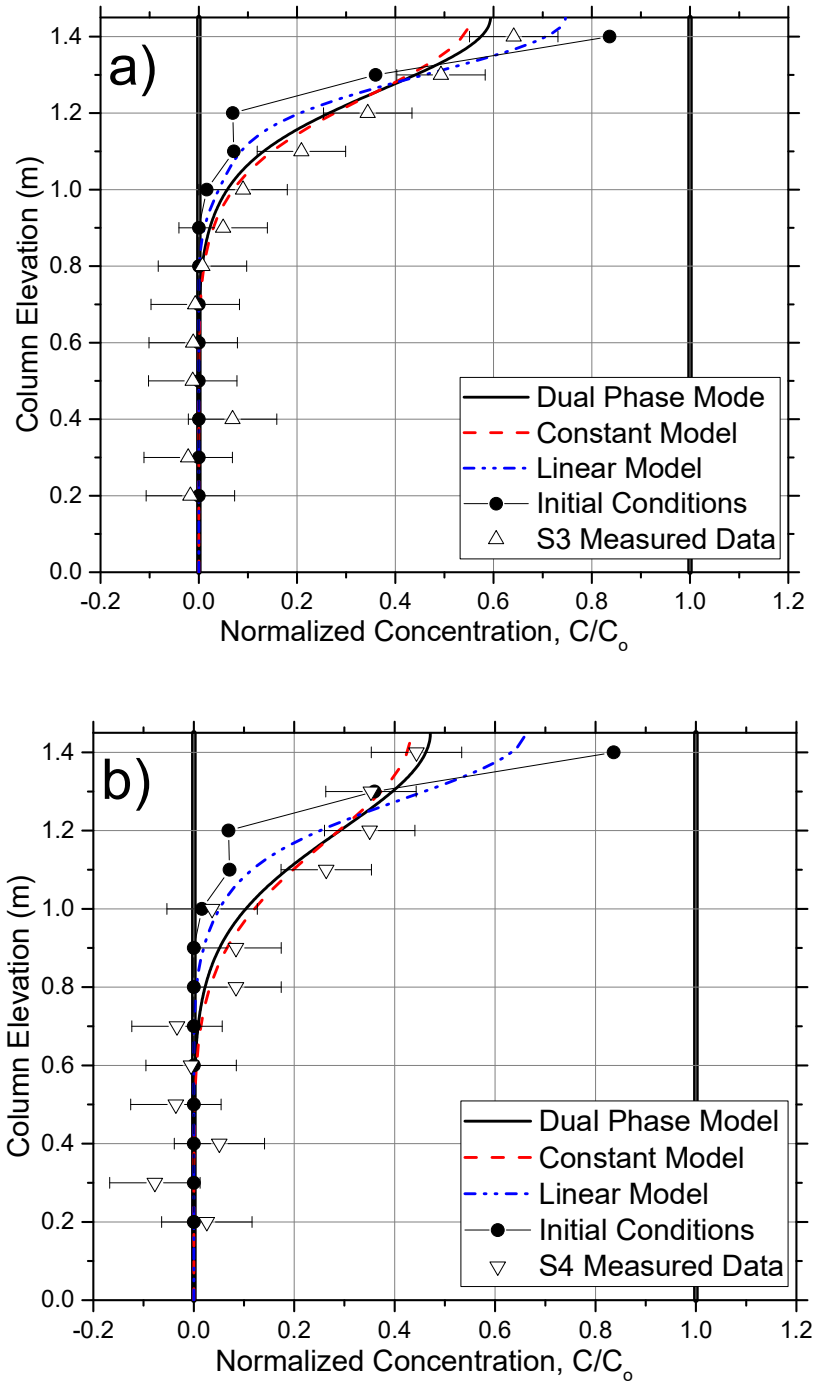

Figure 6.21 – Diffusion models for C2 compared to a) the S3 measured data and b) the S4 measured data. Also showing the measured data for S2 as initial conditions. The initial conditions are presented as a line to represent the linear interpolation used in the modeling software.

The same observations for C1 are also applicable to C2. At the bottom of the column, the dual-phase and constant models are the best fit, and at the top the linear model is the best fit.

The previously noted difficulties with the mass balance (Chapter 5) appear to influence the comparison of the measured data to the simulation results. The modeled profiles are mass conservative and consequently if the observed data is not mass conservative differences should be apparent. The mostly likely source of errors in the observed concentrations would be due to evaporative water losses. Evaporative enrichment will result in an increase in the measured isotope values. In the lower portions of the column, evaporation could occur through the sampling ports, the TDR probe ports, or through the acrylic itself. At the surface, in additional evaporation could occur through the rain cap. The impact of water loss would be more pronounced near the top of the column because of the lower θ_l present. The evaporative enrichment may be high enough to cause changes in the measured concentrations but still be within measurement error when plotted on the mixing line. As noted in Section 5.2.3.1, the isotope mixing line does not indicate significant enrichment. Specific points plotted do indicate evaporation, but those are likely due to leaking from a sample port.

The dual-phase and constant models, at this time, are deemed to be the best fit as they best capture the shape of the observed data in the lower portion of the columns. The bottom of the columns is where effect of evaporative enrichment should be the lowest and the observed values should be closest to correct.

The potential impact of evaporative enrichment was evaluated by assuming that a known mass of water (0.010 kg) had been lost from each of the column segments. Knowing the fraction of water lost from each segment allows the fractionation of the resident water to be calculated assuming that the system acts as a closed system in equilibrium undergoing a loss in water vapour.

To adjust the observed isotope values, the following procedure was used:

- First measured θ_l were converted into a mass of water stored in each segment using the representative volume presented earlier.
- The amount of water lost between the two sampling times was added to the mass of water stored at the end of each time frame to get the amount of water that should have been present before evaporation. The two masses were used to calculate the fraction of water remaining.
- Third, the normalized isotope data was changed into the δ values.

- Using Rayleigh distillation from Clark and Fritz (1997) the initial isotope concentration was found using the equilibrium fractionation factor, and then re-normalized.

The resulting isotope profiles are shown in Figure 6.22 and Figure 6.23.

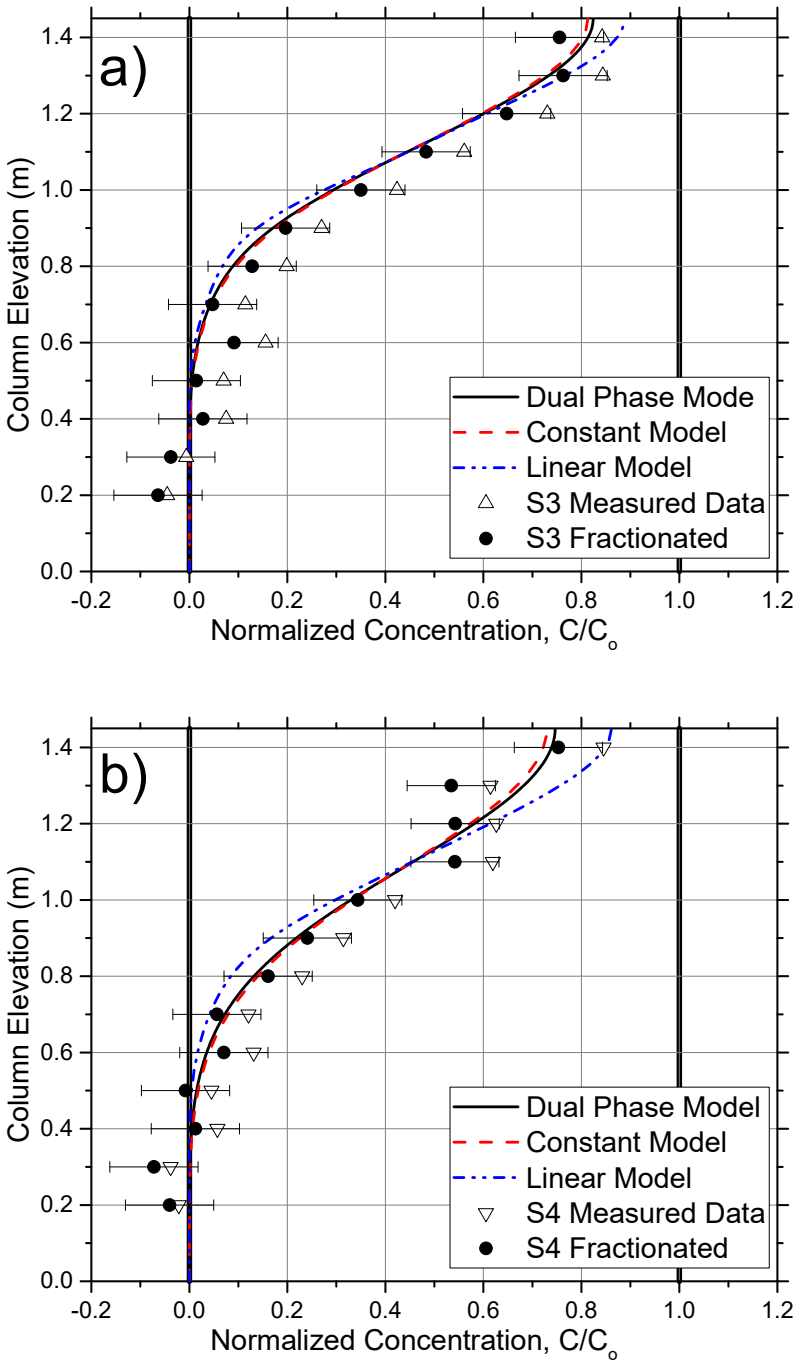

Figure 6.22 – Diffusion models for C1 compared to a) the S3 measured and fractionated data and b) the S4 measured and fractionated data.

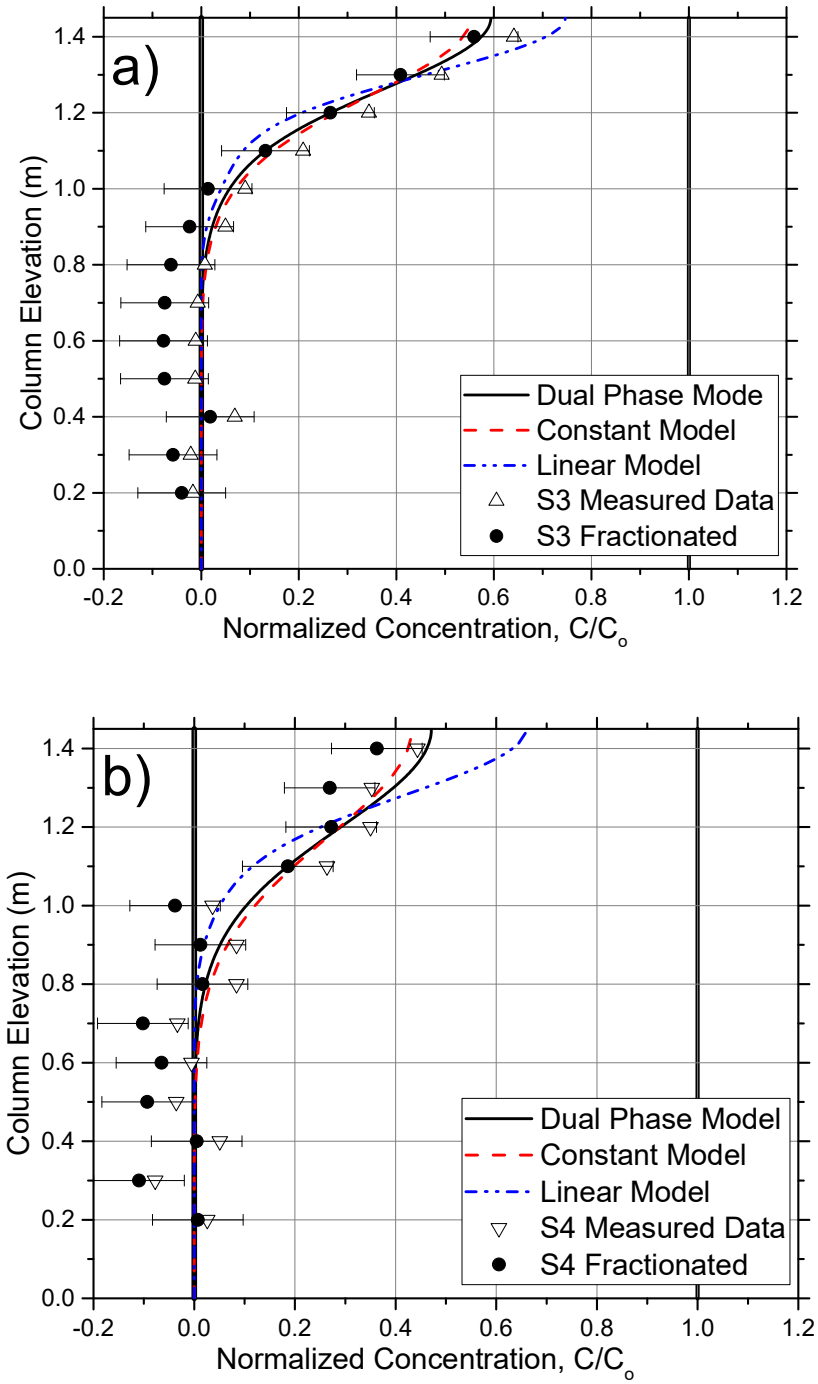

Figure 6.23 – Diffusion models for C1 compared to a) the S3 measured and fractionated data and b) the S4 measured and fractionated data.

For C1 S3 the addition of evaporative fractionation causes the data points to fit the dual-phase and constant models over most of the elevation range. However, considering the error in the measurements the fractionated data points could fit all of the diffusion models. C1 S4, after

fractionation, shows a best fit to the dual phase and constant models, with the exception of 1.1 m to 1.3 m. Again considering the error in the fractionated values, any of the diffusion models could be deemed appropriate.

C2 S3 shows a better fit to the diffusion models before fractionation is applied to the observed data. From 1.1 m and up, the fractionated data shows the best fit to the dual phase and constant diffusion models. Below 1.1 m, the fractionated data shifts below the background concentration and does not have a best fit model. For this sample time the error covers all of the models used, with the exception of 1.4 m. C2 S4 with its erratic data, again shows a best fit to the dual phase and constant models after fractionation.

The total water loss from each column segment is estimated in Appendix F. The total mass that was estimated to be lost from the column is very small, on the order of 1E-5 kg (0.01 ml) of water. From the previous analysis, evaporative enrichment of the top portions of the column creates a better fit between the observed data and modeled data but a source for this water loss could not be identified.

The results from the column experiment are in agreement with the observations made for the diffusion cells. The columns stayed above the θ_{res} and the dual phase and constant models showed similar results.

6.2.4 Advective Transport Analysis

The advective transport in the columns will be analyzed using three formulations for the soil Λ. They will be a constant value, a value that increases with de-saturation (Sato et al., 2003 model), and a bell-shaped function in which Λ initial increases but then decreases with de-saturation. The Λ models used are presented in Section 3.5 (derivation in Appendix A).

The Λ models are added to the dual-phase diffusion coefficient and a hydrodynamic dispersion coefficient is given to the software instead of a pure molecular diffusion coefficient. (Appendix E). The numerical model was executed from the time the rain is started to S2, with initial concentration set to zero. The results for the C1 models are presented in Figure 6.24, analyzed, with the results and analysis for C2 to follow.

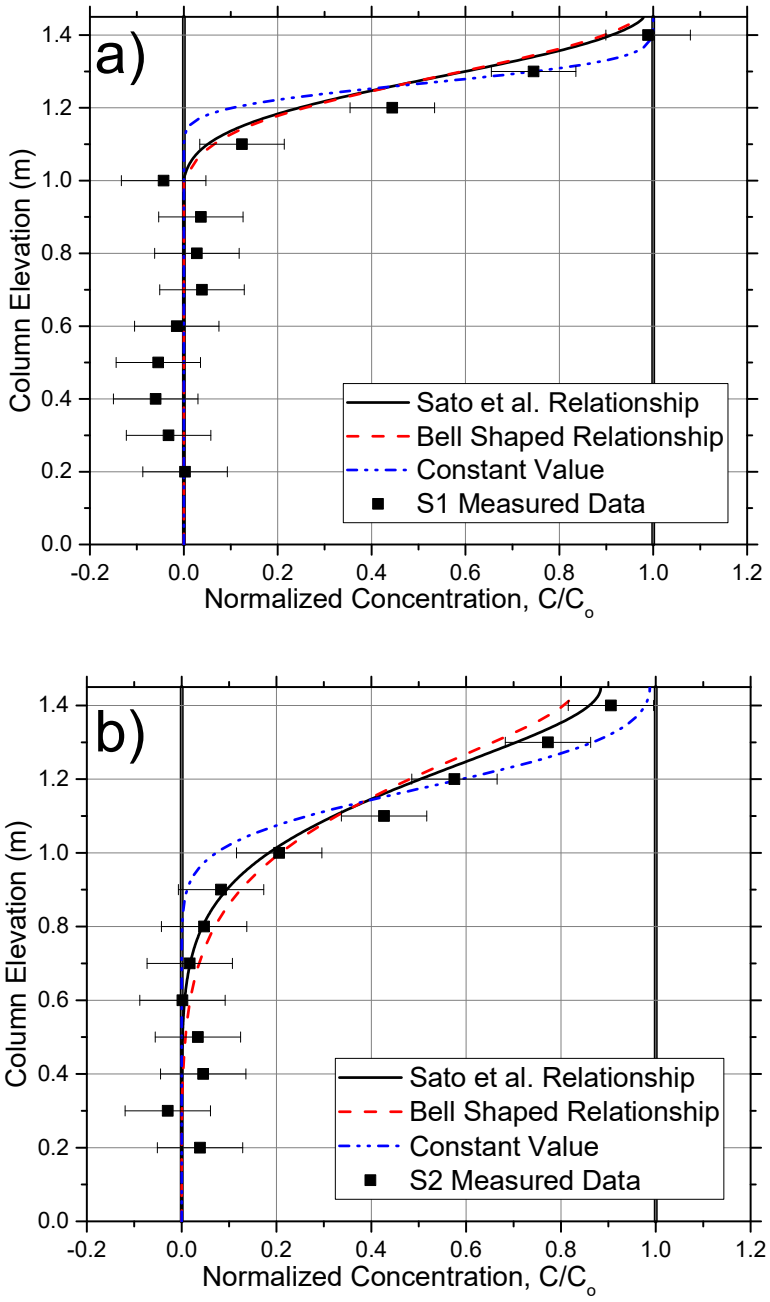

Figure 6.24 –C1 Λ models plotted at a) S1 and b) S2.

For C1 at S1, the bell shaped and the Sato et al. (2003) models show the same shape while the constant value shows much less spread. The two similar models show the same shape as the observed data, but have not infiltrated deep enough into the column. The constant value model shows a fit to the top two data points but does not capture any of the shape deeper than 1.3 m. At

S2, from 1.1 m up, the Sato et al. (2003) model shows the best fit to the observed data, and below the two similar models show the best fit.

The difference between the measured data and models is most likely due to variations in the θ_{res}. Evaporative enrichment was deemed insignificant at early times as the time between the rain and S1 was very short (12 hours). The results from adjusting the θ_{res} from 0.07 to 0.05 can be seen in Figure 6.25.

After adjusting the θ_{res}, S1 shows a good fit with all three of the models. At S2 the two similar models start to diverge. Above 1.1 m, the best fit model is the bell shaped profile. Below 1.1 m, the constant value shows the best fit.

The excessive spreading of all the models in the lower portion of the column and the reasonable fit at the top suggests that the lower density soil at the surface (hence lower θ_{res}) caused faster infiltration at the surface at early experiment times. A decreased θ_{res} for the entire column did not help fit the model to the S2 data. This suggests that the originally selected θ_{res} was the best fit and reinforces the presence of the less dense top layer.

The mechanical dispersion models compared to the collected data for C2 are presented in Figure 6.26.

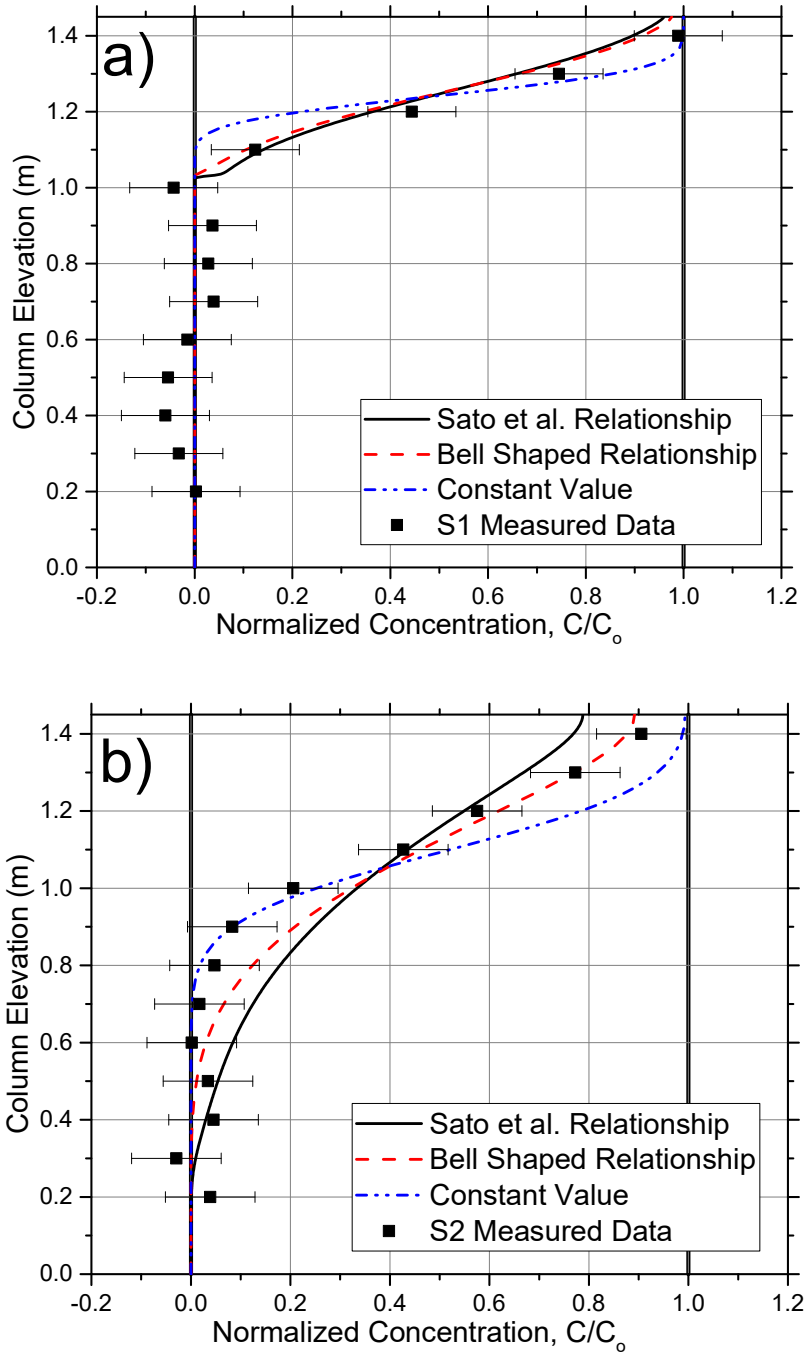

Figure 6.25 – Modeled Λ profiles for C1 after adjusting the θ_{res} to 0.05 for a) S1 and b) S2.

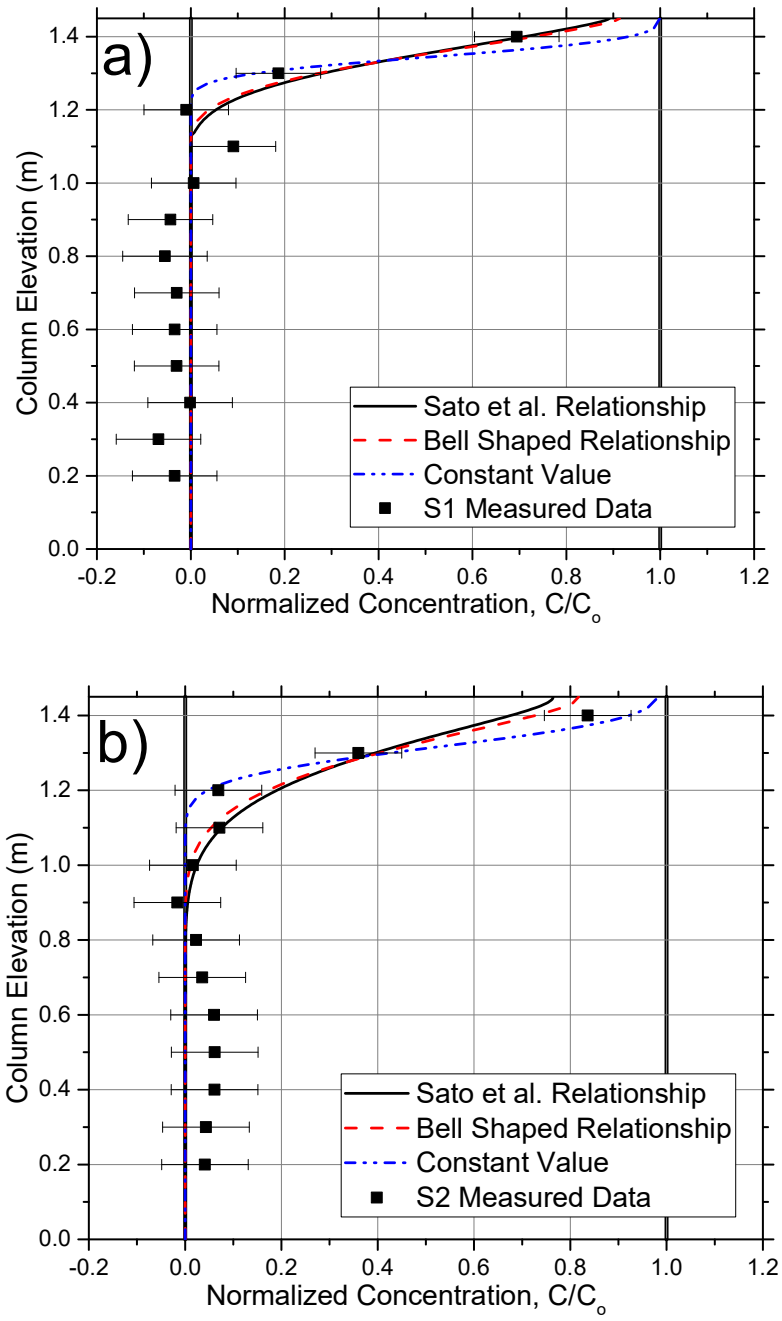

Figure 6.26 – C2 Λ models plotted at a) S1 and b) S2. The data point at 1.1 m for S1 appears to have a leaking port, as the isotope value is significantly more enriched than expected.

For C2 S1 the spreading is well captured by the bell shaped and Sato et al. (2003) models, except at 1.3 m elevation, where the observed data is lower than modeled. The constant model captures the data point at 1.3 m elevation, but greatly overestimates the observed data at 1.4 m. Proceeding to S2, the two similar shaped models noted above overestimate the spreading observed, while the

constant model fits the observed data well. At this time it is not clear which of the models shows the best fit to the data. Figure 6.27 highlights the effects of increasing the θ_{res} from 0.075 to 0.085 to reduce the depth at which the water has penetrated the soil.

After θ_{res} is increased the two similar models intersect the observed data at S1 but show too much spread at S2. The constant model, at S1, shows not enough spread, but at S2 captures the observed data perfectly.

For both of the columns the differences between the bell shaped and Sato et al. (2003) models was not significant and each of the models could be deemed appropriate for the results gathered. The constant value model show fits to the data at some points but not others. The dispersive transport regimes within the column were not over large enough time scales or did not have a large enough soil water velocity to produce significantly different results between the different mechanical dispersion-saturation relationships. Characterization of the functional form for the Λ was not the primary focus of this study.

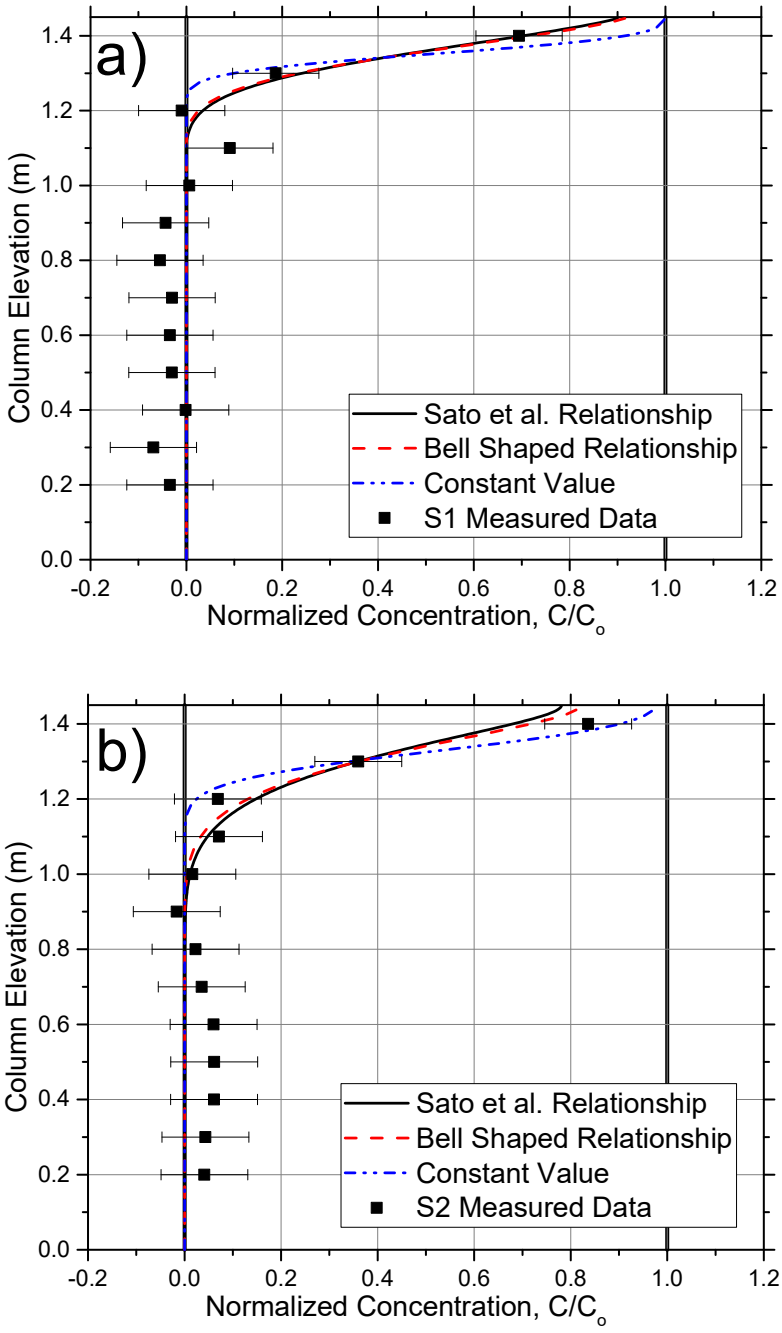

Figure 6.27 – C2 Λ results after increasing the θ_{res} from 0.075 to 0.085 for a) S1 and b) S2.

6.3 Summary

The results from the experimental analysis were as expected. The analysis of the diffusion cells compared many different τ models to measured diffusion data. A best fit model was selected for the three different porosity ranges used in the experiments. The 0.4 porosity cell diffusion data had

the most data points available so the resulting PN – PD1 diffusion model was used in the column study.

The analysis of the column study presented several difficulties with possible water losses and variations in soil structure, resulting in additional analysis needed to explain the observed data. The analysis of the column θ_l did not present significant challenges aside from the water balance, which could not be successfully closed.

The analysis of the diffusion part of the columns compared three presented diffusion - θ_l relationships. The diffusion model that best represented the observed data shape in the lower parts of the column were the dual-phase model, presented and refined in the diffusion cell analysis and the constant model. The top most portion of the columns was best represented by the linear model. After evaporation was considered the results remained the same, and no further analysis of enrichment was done, as no source for water loss could be found. The linear model was deemed less appropriate when the potential of water loss and isotopic enrichment in the upper portions of the column was considered. In the middle to lower portions have a low θ_l where the models start to diverge, the effects of evaporation should be negligible.

The final part of the analysis was looking at the early time dispersive processes. Three models were selected for comparison. However, the short time scale for mechanical dispersion and the low advection velocities yielded little dispersive spread over the early time experiments and did not allow for a clear definition of a preferred Λ model.

Chapter 7 - Conclusions and Recommendations

The goal of this research was to define the best transport parameters for the stable isotopes of water within unsaturated soil, with the goal of extracting more information from the high resolution isotope profiles that are routinely collected at field sites. A better understanding of transport parameters of the isotopes that are collected will allow for better calculation of recharge rates and amounts, and help model migration of seasonal water signatures present at most field locations.

7.1 Specific Conclusions

In order to refine the transport parameters for the stable isotopes of water, the following objectives were outlined:

1. Measure the relationship between the combined coefficient of molecular diffusion and compare it to a theoretical relationship based on dual-phase diffusion,
2. Develop a set of observations of stable isotope of water transport at a bench scale through the use of column testing, and
3. Characterize the advective, dispersive and diffusive processes of stable isotopes of water in unsaturated soils.

The first objective was met by measuring the coefficient of diffusion for δD over a range of θ_l from residual saturation to near fully saturated. These measured diffusion values were compared to theoretical relationships for dual-phase diffusion and a best fit model was selected. The half-cell method used for the diffusion testing was fraught with a number of limitations. The construction procedure that was used required several iterations to overcome the shortcomings of the experimental design. Overall the quality of the data was deemed sufficient to conclude that a dual-phase diffusion model is able to capture the diffusive transport of δD in unsaturated sand. This finding was further reinforced by analysis of the data collected for Objective 2.

The collection of isotope transport data from an unsaturated column had fewer limitations. The main issues that were faced when doing QA/QC analysis on the observed data were closing mass balances within the columns for both water and isotopes. After further analysis it was determined that the issues with the water balance was due to measurement errors, soil structure, preferential pathways, and hysteresis. The errors in isotope mass balance were attributed to the limited number

of measurements made on the background isotope concentrations and potential occurrence of evaporative enrichment.

The final objective was to model the water infiltration and δD transport within the columns. The θ_l profile modeling proved to be relatively straightforward although some trial and error was needed for the models to accurately represent the observed data, despite the mass balance issues. Further interpretation of the observed isotope profiles was required to enable the simulation results to more fully match the observed results. The separation of the transport into diffusion and advection/dispersion dominated phases was shown to be useful in isolating the dominant mechanisms. Three different models for mechanical dispersion as a function of saturation were evaluated. Any of the models provided a reasonable fit to the observations as long as the average mechanical dispersion over the range of θ_l present within the column was elevated relative to the expected value under saturated conditions.

The diffusion analysis compared two traditional models, to the dual-phase model presented in this work. After analysis was complete the model that best captured the shape of the observed data in the lower portion of the column were the dual-phase and constant models but the upper parts were best fit by a linear diffusion model. In specific conditions, such as a soil with a very low θ_{res}, the dual phase model will be the better model for diffusive analysis. If the soil does not have a low θ_{res} and the soil is not expected to dry past field capacity, a constant diffusion value over a θ_l range would be a better estimate of diffusion than a traditional aqueous only phase tracer.

7.2 Specific Recommendations

After the analysis was complete, several recommendations are suggested to increase the confidence in the observed data that the laboratory experiments produced. For the diffusion cells, a more reliable method for packing and saturating is needed for creating consistent density and ω profiles. An additional method to reliable create and measure the background conditions is needed. Application of a different testing procedure (single reservoir or a dual reservoir) may aid in the collection of reliable data. More testing needs to be done on the extreme saturation states of the soil (S = 1 and S = 0) to anchor the observed data to theoretical values at these points. Finally some method of diffusion testing below residual θ_l needs to be sought after.

For the column experiment better control on the water loss from the column, and a tighter control on the isotope mass balance are needed to further refine the estimates made by this study. Simulation of vapour transport due to thermal fluctuation should be investigated to see if condensation in the column or headspace is adding to the uncertainty in the collected data. The findings of this experiment should also be applied to larger scale (time and space) profiles of isotopic composition under field conditions to evaluate if the theoretical refinements have applied to the interpretation of the field profiles, such as those shown in Barbour et al. (2016).

Chapter 8 - References

Aachib, M., M. Mbonimpa and M. Aubertin (2004). "Measurement and prediction of the oxygen diffusion coefficient in unsaturated media, with applications to soil covers." Water, air, and soil pollution **156**(1): 163-193.

Adomako, D., P. Maloszewski, C. Stumpp, S. Osae and T. T. Akiti (2010). "Estimating groundwater recharge from water isotope (δ2H, δ18O) depth profiles in the Densu River basin, Ghana." Hydrological Sciences Journal **55**(8): 1405-1416.

Allison, G. and C. Barnes (1985). "Estimation of evaporation from the normally "dry" Lake Frome in South Australia." Journal of Hydrology **78**(3-4): 229-242.

Allison, G., C. Barnes and M. Hughes (1983). "The distribution of deuterium and 18 O in dry soils 2. Experimental." Journal of Hydrology **64**(1): 377-397.

Asano, Y., T. Uchida and N. Ohte (2002). "Residence times and flow paths of water in steep unchannelled catchments, Tanakami, Japan." Journal of Hydrology **261**(1): 173-192.

Aubertin, M., M. Aachib and K. Authier (2000). "Evaluation of diffusive gas flux through covers with a GCL." Geotextiles and Geomembranes **18**(2): 215-233.

Aubertin, M., M. Mbonimpa, B. Bussière and R. P. Chapuis (2003). "A model to predict the water retention curve from basic geotechnical properties." Canadian Geotechnical Journal **40**(6): 1104-1122.

Baertschi, P. (1976). "Absolute ^{18}O content of standard mean ocean water." Earth and Planetary Science Letters **31**(3): 341-344.

Barbour, S., L, P. C. Lim and D. G. Fredlund (1996). "A new technique for diffusion testing of unsaturated soil."

Barbour, S. L., M. J. Hendry and S. K. Carey (2016). "High-resolution profiling of the stable isotopes of water in unsaturated coal waste rock." Journal of Hydrology **534**: 616-629.

Barnes, C. and G. Allison (1983). "The distribution of deuterium and 18O in dry soils: 1. Theory." Journal of Hydrology **60**(1): 141-156.

Bath, A., W. Darling and A. Brunsdon (1982). "The stable isotopic composition of infiltration moisture in the unsaturated zone of the English Chalk." Stable Isotopes: 161-166.

Braud, I., T. Bariac, P. Biron and M. Vauclin (2009b). "Isotopic composition of bare soil evaporated water vapor. Part II: Modeling of RUBIC IV experimental results." Journal of Hydrology **369**(1–2): 17-29.

Braud, I., T. Bariac, J. P. Gaudet and M. Vauclin (2005a). "SiSPAT-Isotope, a coupled heat, water and stable isotope (HDO and $H_2{}^{18}O$) transport model for bare soil. Part I. Model description and first verifications." Journal of Hydrology **309**(1): 277-300.

Braud, I., T. Bariac, M. Vauclin, Z. Boujamlaoui, J. P. Gaudet, P. Biron and P. Richard (2005b). "SiSPAT-Isotope, a coupled heat, water and stable isotope (HDO and $H_2{}^{18}O$) transport model for bare soil. Part II. Evaluation and sensitivity tests using two laboratory data sets." Journal of Hydrology **309**(1–4): 301-320.

Braud, I., P. Biron, T. Bariac, P. Richard, L. Canale, J. P. Gaudet and M. Vauclin (2009a). "Isotopic composition of bare soil evaporated water vapor. Part I: RUBIC IV experimental setup and results." Journal of Hydrology **369**(1–2): 1-16.

Brooks, R. and T. Corey (1964). "Hydraulic Properties of Porous Media."

Bruch, P. G. (1993). Laboratory study of evaporative fluxes in homogeneous and layered soils. Masters of Science, University of Saskatchewan.

Cane, G. and I. D. Clark (1999). "Tracing ground water recharge in an agricultural watershed with isotopes." Groundwater **37**(1): 133-139.

Carrier III, W. D. (2003). "Goodbye, Hazen; Hello, Kozeny-Carman." Journal of geotechnical and geoenvironmental engineering **129**(11): 1054-1056.

Carslaw, H. and J. Jaeger (1959). Heat in solids, Clarendon Press, Oxford.

Cheng, L., W. Liu, Z. Li and J. Chen (2014). "Study of soil water movement and groundwater recharge for the Loess Tableland using environmental tracers." TRANSACTIONS OF THE ASABE **57**(1): 23-30.

Clark, I. D. and P. Fritz (1997). Environmental Isotopes in Hydrogeology, CRC press.

Cook, P., W. Edmunds and C. Gaye (1992). "Estimating paleorecharge and paleoclimate from unsaturated zone profiles." Water Resources Research **28**(10): 2721-2731.

Craig, H. (1961). "Isotopic variations in meteoric waters." Science **133**(3465): 1702-1703.

Criss, R. E. (1999). Principles of Stable Isotope Distribution. New York, New York, Oxford University press.

DePaolo, D. J., M. E. Conrad, K. Maher and G. W. Gee (2004). "Evaporation effects on oxygen and hydrogen isotopes in deep vadose zone pore fluids at Hanford, Washington." Vadose Zone Journal **3**(1): 220-232.

Dincer, T., A. Al-Mugrin and U. Zimmermann (1974). "Study of the infiltration and recharge through the sand dunes in arid zones with special reference to the stable isotopes and thermonuclear tritium." Journal of Hydrology **23**(1): 79-109.

Dusek, J., T. Vogel and M. Sanda (2012). "Hillslope hydrograph analysis using synthetic and natural oxygen-18 signatures." Journal of Hydrology **475**(0): 415-427.

Fetter, C. W. (1999). Contaminant hydrogeology, Prentice hall New Jersey.

Flint, A. L., L. E. Flint, E. M. Kwicklis, J. T. Fabryka-Martin and G. S. Bodvarsson (2002). "Estimating recharge at Yucca Mountain, Nevada, USA: comparison of methods." Hydrogeology Journal **10**(1): 180-204.

Fredlund, D., A. Xing and S. Huang (1994). "Predicting the permeability function for unsaturated soils using the soil-water characteristic curve." Canadian Geotechnical Journal **31**(4): 533-546.

Garvelmann, J., C. Külls and M. Weiler (2012). "A porewater-based stable isotope approach for the investigation of subsurface hydrological processes." Hydrology and Earth System Sciences **16**(2): 631-640.

Gaye, C. and W. Edmunds (1996). "Groundwater recharge estimation using chloride, stable isotopes and tritium profiles in the sands of northwestern Senegal." Environmental Geology **27**(3): 246-251.

Gazis, C. and X. Feng (2004). "A stable isotope study of soil water: evidence for mixing and preferential flow paths." Geoderma **119**(1): 97-111.

Gelhar, L. W., C. Welty and K. R. Rehfeldt (1992). "A critical review of data on field-scale dispersion in aquifers." Water resources research **28**(7): 1955-1974.

Gillham, R., M. Robin, D. Dytynyshyn and H. Johnston (1984). "Diffusion of nonreactive and reactive solutes through fine-grained barrier materials." Canadian Geotechnical Journal **21**(3): 541-550.

Hagemann, R., G. Nief and E. Roth (1970). "Absolute isotopic scale for deuterium analysis of natural waters. Absolute D/H ratio for SMOW1." Tellus **22**(6): 712-715.

Hamamoto, S., M. S. A. Perera, A. Resurreccion, K. Kawamoto, S. Hasegawa, T. Komatsu and P. Moldrup (2009). "The Solute Diffusion Coefficient in Variably Compacted, Unsaturated Volcanic Ash Soils." Vadose Zone Journal **8**(4): 942-952.

Hoefs, J. (2009). Stable Isotope Geochemistry, U.S. Government Printing Office.

Hutchison, J., J. Seaman, S. Aburime and D. Radcliffe (2003). "Chromate transport and retention in variably saturated soil columns." Vadose Zone Journal **2**(4): 702-714.

Kamp, G. v. d., L. Luba, J. Cherry and H. Maathuis (1994). "Field study of a long and very narrow contaminant plume." Ground Water **32**(6): 1008-1016.

Klaus, J., E. Zehe, M. Elsner, C. Külls and J. McDonnell (2013). "Macropore flow of old water revisited: experimental insights from a tile-drained hillslope." Hydrology and Earth System Sciences **17**(1): 103-118.

Lewis, J. and J. Sjöstrom (2010). "Optimizing the experimental design of soil columns in saturated and unsaturated transport experiments." Journal of Contaminant Hydrology **115**(1–4): 1-13.

Lim, P., S. Barbour and D. Fredlund (1998). "The influence of degree of saturation on the coefficient of aqueous diffusion." Canadian geotechnical journal **35**(5): 811-827.

Majoube, M. (1971). "Fractionnement en oxyge`ne-18 et en deute´rium entre l'eau et sa vapeur." Journal de Chimie Physique et de Physico-Chimie Biologique **68**(July-Dec).

Mathieu, R. and T. Bariac (1996a). "A numerical model for the simulation of stable isotope profiles in drying soils." Journal of Geophysical Research: Atmospheres (1984–2012) **101**(D7): 12685-12696.

Maxwell, J. C. (1881). A treatise on electricity and magnetism, Clarendon press.

Mbonimpa, M., M. Aubertin, M. Aachib and B. Bussière (2003). "Diffusion and consumption of oxygen in unsaturated cover materials." Canadian Geotechnical Journal **40**(5): 916-932.

Melayah, A., L. Bruckler and T. Bariac (1996a). "Modeling the Transport of Water Stable Isotopes in Unsaturated Soils Under Natural Conditions: 1. Theory." Water Resources Research **32**(7): 2047-2054.

Melayah, A., L. Bruckler and T. Bariac (1996b). "Modeling the transport of water stable isotopes in unsaturated soils under natural conditions: 2. Comparison with field experiments." Water Resources Research **32**(7): 2055-2065.

Merlivat, L. (1978). "Molecular diffusivities of $H_2{}^{16}O$, $HD^{16}O$, and $H_2{}^{18}O$ in gases." The Journal of Chemical Physics **69**(6): 2864-2871.

Mueller, M. H., A. Alaoui, C. Kuells, H. Leistert, K. Meusburger, C. Stumpp, M. Weiler and C. Alewell (2014). "Tracking water pathways in steep hillslopes by δ18O depth profiles of soil water." Journal of Hydrology **519, Part A**(0): 340-352.

Ogata, A. and R. B. Banks (1961). "A solution of the differential equation of longitudinal dispersion in porous media."

Oliviera, I., A. Demond and A. Salehzadeh (1996). "Packing of sands for the production of homogeneous porous media." Soil Science Society of America Journal **60**(1): 49-53.

Padilla, I. Y., T. C. J. Yeh and M. H. Conklin (1999). "The effect of water content on solute transport in unsaturated porous media." Water Resources Research **35**(11): 3303-3313.

Patil, A., K. King and M. Miller (1963). "Self-diffusion of rubidium as influenced by soil moisture tension." Canadian Journal of Soil Science **43**(1): 44-51.

Penman, H. (1940). "Gas and vapour movements in the soil: I. The diffusion of vapours through porous solids." The Journal of Agricultural Science **30**(03): 437-462.

Price, W. A. (2009). "Prediction manual for drainage chemistry from sulphidic geologic materials." MEND report **1**(1): 579.

Sato, T., H. Tanahashi and H. A. Loáiciga (2003). "Solute dispersion in a variably saturated sand." Water resources research **39**(6).

Sato, T., H. TANAHASHI, T. Uno and A. YUASA (1995). Adsorption and Dispersion Characteristics Within the Unsaturated Zone. Proceedings of the First International Conference on Unsaturated Soils, Paris, France.

Scanlon, B. R., R. W. Healy and P. G. Cook (2002). "Choosing appropriate techniques for quantifying groundwater recharge." Hydrogeology Journal **10**(1): 18-39.

Shackelford, C. D. (1991). "Laboratory diffusion testing for waste disposal—A review." Journal of Contaminant Hydrology **7**(3): 177-217.

Shackelford, C. D. and D. E. Daniel (1991). "Diffusion in saturated soil. I: Background." Journal of Geotechnical Engineering **117**(3): 467-484.

Shurbaji, A.-R. M. and F. M. Phillips (1995). "A numerical model for the movement of H_2O, $H_2{}^{18}O$, and ^2HHO in the unsaturated zone." Journal of Hydrology **171**(1): 125-142.

Šimůnek, J. and D. L. Suarez (1993). "Modeling of carbon dioxide transport and production in soil 1. model development."

Sreedeep, S. and D. Singh (2008). "A novel technique for studying diffusion of contaminants in fine-grained soils." Geomechanics and Geoengineering: An International Journal **3**(3): 199-209.

Thoma, G., N. Esser, C. Sonntag, W. Weiss, J. Rudolph and P. Leveque (1978). New Technique of in-situ Soil-moisture Sampling for Environmental Isotope Analysis Applied at Pilat Sand Dune

Near Bordeaux. Proc. Int. Symp. Isotope Hydrology. Neuherberg, International Atomic Energy Agency, Vienna. **2**.

Toride, N., M. Inoue and F. J. Leij (2003). "Hydrodynamic dispersion in an unsaturated dune sand." Soil Science Society of America Journal **67**(3): 703-712.

Torkzaban, S., S. Hassanizadeh, J. Schijven, H. de Bruin and A. de Roda Husman (2006). "Virus transport in saturated and unsaturated sand columns." Vadose Zone Journal **5**(3): 877-885.

Van Genuchten, M. T. (1980). "A closed-form equation for predicting the hydraulic conductivity of unsaturated soils." Soil Science Society of America Journal **44**(5): 892-898.

Van Rees, K. C., E. A. Sudicky, P. S. C. Rao and K. R. Reddy (1991). "Evaluation of laboratory techniques for measuring diffusion coefficients in sediments." Environmental science & technology **25**(9): 1605-1611.

Wassenaar, L. I., M. J. Hendry, V. L. Chostner and G. P. Lis (2008). "High Resolution Pore Water δ2H and δ18O Measurements by H2O(liquid)−H2O(vapor) Equilibration Laser Spectroscopy." Environmental Science & Technology **42**(24): 9262-9267.

Zimmermann, U., D. Ehhalt and K. Münnich (1967b). Soil-water movement and evapotranspiration: changes in the isotopic composition of the water. Isotopes in hydrology. Proceedings of a symposium.

Zimmermann, U., K. Münnich and W. Roether (1967a). "Downward movement of soil moisture traced by means of hydrogen isotopes." Isotope techniques in the hydrologic cycle: 28-36.

APPENDIX TABLE OF CONTENTS

APPENDIX LIST OF TABLES

APPENDIX LIST OF FIGURES

Appendix A

This Appendix outlines the literature based properties that are used for analysis and modeling in the thesis such as the well-defined properties for calculating D_{com}, the many available tortuosity models that are present in the literature and a presentation of the few dispersion water content relationships available..

A.1 Well Defined Isotope Properties

These properties are used in calculating D_{com} but there is little variation in the literature on what theses parameters are, and therefore, no investigation on the best parameters needs to be done.

A.1.1 Equilibrium Fractionation

The most common form of the equilibrium fractionation factor as a function of temperature comes from comes from Majoube, 1971 and is shown below (Clark and Fritz, 1997),

$$10^3 \ln(\alpha_i^*) = 10^6 A T^{-2} + 10^3 B T^{-1} + C \quad \text{.....(A.1)}$$

Where α_i^* is the equilibrium fractionation factor of δD or $\delta^{18}O$ between aqueous and vapour phases (unitless), T is the temperature (K), and A, B, and C are fitting constants presented in Table A.1.

Table A.1 – Fitting parameters for equilibrium fractionation factor for stable isotopes of water.

Isotope	A (K^2)	B (K)	C (unitless)
δD	24.844	-76.248	52.612
$\delta^{18}O$	1.137	-0.4156	-2.0667

A.1.2 Henry's Law Constant for Isotopes

The property used in this work that is equivalent to Henry's Law was derived from Braud et al. (2005a). It is calculated as,

$$H = \frac{1}{\alpha_i^*} \frac{\rho_v}{\rho_w} \quad \text{.....(A.2)}$$

Where H is the Henry's Law (unitless), α_i^* is the equilibrium fractionation factor of δD or $\delta^{18}O$ between aqueous and vapour phases (unitless), ρ_v is the density of water vapour in air (kg/m^3), and ρ_w is the density of liquid water (kg/m^3). The fractionation factor was defined previously. The vapour density is defined as a function of temperature in Equation A.3 (Nave,).

$$\rho_v = \frac{(a + bT + cT^2 + dT^3)}{1000} \qquad \text{.....(A.3)}$$

Where T is the temperature in (°C), and a, b, c, and d are fitting parameters (Table A.2).

Table A.2 – Fitting parameters for the density of water vapour in air.

	a (g/m^3)	b (g/m^3/T)	c (g/m^3/T^2)	d (g/m^3/T^3)
Value	5.018	0.32321	8.1847E-3	3.1243E-4

The water density is defined as a function of temperature in Equation A.4 (Becerra and Centeno, 2006).

$$\rho_w = \left(e\left(1 - \frac{(T + a)^2(T + b)}{c(T + d)}\right) + C_{ad}\right)F_c \qquad \text{.....(A.4)}$$

Where T is the temperature (°C), C_{ad} is a correction for dissolved gas (kg/m^3), F_c is a correction for atmospheric pressure (Pa), and a, b, c, d, and e are fitting parameters found in Table A.3. For this work the water was assumed to be degassed (C_{ad} = 0) and the atmospheric pressure was at standard pressure (101,325 Pa) so F_c = 1.

Table A.3 – Fitting parameters for the density of liquid water.

	a (°C)	b (°C)	c (°C^2)	d (°C)	e (kg/m^3)
Value	-3.983035	301.797	522 528.9	69.34881	999.97140

A.1.3 Free Solution Diffusion coefficients for Isotopes in the Aqueous Phase

The free solution diffusion coefficients for δD and $\delta^{18}O$ as a function of temperature are presented by Easteal et al. (1984) using a polynomial relationship in Equation A.5.

$$\ln\left(10^9 D_l^{i0}\right) = a + b\left(\frac{1000}{T}\right) + c\left(\frac{1000}{T}\right)^2 \quad \text{.....(A.5)}$$

Where D_l^{i0} is the free solution diffusion coefficient of the isotope in H_2O (m^2/s), T is the temperature (K), and a, b, and c are fitting parameters (Table A.4).

Table A.4 – Fitting parameters for free solution diffusion coefficient of isotopes in liquid water.

Isotope	a	b	c
δD	1.624449 65	1.72986727	-0.587098179
$\delta^{18}O$	1.67662250	1.68167989	-0.577341011

A.1.4 Free Solution Diffusion coefficients for Isotopes in the Vapour Phase

The free solution diffusion coefficients are presented differently for the vapour phase compared to the aqueous phase. From Braud et al. (2005a) the free solution diffusion coefficient for isotopes in the vapour phase is,

$$D_v^{i0} = D_v\left(\frac{D_i^v}{D_v}\right)^{n_D} \quad \text{.....(A.6)}$$

Where D_v^{i0} is the free solution diffusion coefficient for isotopes in moist air (m^2/s), D_v is the free solution diffusion coefficient of regular water in air (m^2/s), (D_i^v/D_v) is the diffusivity ratio of isotopes to normal water (unitless) and n_D is an exponent relating to the flow nature of the air transport is occurring in. From Kimball et al. (1976) the D_v as a function of temperature is,

$$D_v = \frac{0.229\left(\frac{T+273}{273}\right)^{1.75}}{100^2} \quad \text{.....(A.7)}$$

Where T is the temperature (°C). n_D for molecular diffusion has a value of 1, and the diffusivity ratios as found by Merlivat (1978) are presented in Table A.5.

Table A.5 – diffisivity ratios for isotopes and regular water in air.

Isotope	Value
δD	0.9755
$\delta^{18}O$	0.9723

A.1.5 Temperature Dependent Parameters at Laboratory Temperature

The following table highlights all parameters used for analysis at the average laboratory temperature of 22.5 °C.

Table A.6 – Free solution diffusion coefficients and Henry's law for δD. No parameters for $\delta^{18}O$ were calculated as no transport analysis was done for it.

Parameter for δD	Value at 22.5 °C
D_l^{i0} (m^2/s)	2.13E-9
D_v^{i0} (m^2/s)	2.57E-5
H(unitless)	1.85E-5

A.2 Soil Tortuosity Models

Many tortuosity models are available in the literature. This section presents the most popular aqueous phase, vapour phase, and dual phase models that will be applied to the diffusion cell analysis.

A.2.1 Aqueous Phase Models

The soil τ models that will be investigated in this work are discussed following. The τ of aqueous phase solutes has been well studied. One of the simplest models to extend a saturated aqueous phase τ value to unsaturated soils, is to use a linear scaling as done by Padilla et al. (1999).

$$\tau_l = \tau_{sat}\left(\frac{\theta_l - \theta_{res}}{n - \theta_{res}}\right) \quad \text{.....(A.8)}$$

where θ_{res} is the residual water content of the soil (m^3/m^3) but here it will be assumed to be zero. The main parameter of interest in this equation is the saturated τ value, τ_{sat}. Many saturated models have been presented over the years. A collection of models has been presented by Boudreau (1996) and a selected few, that do not use fitting parameters, will be presented here (Table A.7) for use in the previous equation.

Table A.7 - τ_{sat} models from Boudreau (1996), with no adjustable parameter, where n is the soil porosity. The PD model number shows which PD model each of the τ_{sat} models creates.

Model	Equation	PD Model	Equation Number
Maxwell (1881)	$\left(\frac{3-n}{2}\right)^{-1}$	PD1	A.9
Rayleigh (1892)	$(2-n)^{-1}$	PD2	A.10
Bruggemann (1935)	$\left(n^{-1/2}\right)^{-1}$	PD3	A.11
Millington (1959)	$\left(n^{-1/3}\right)^{-1}$	PD4	A.12
Weissberg (1963)	$(1-0.5ln(n))^{-1}$	PD5	A.13
Tsai and Strieder (1986)	$(1-ln(n))^{-1}$	PD6	A.14
Beeckman (1990)	$\left(\frac{n}{1-(1-n)^{1/3}}\right)^{-1}$	PD7	A.15
Mackie and Meares (1955)	$\left(\left(\frac{2-n}{n}\right)^2\right)^{-1}$	PD8	A.16

Another model that has been successfully applied to gas phase diffusion and adapted to unsaturated aqueous phase studies is the Millington and Quirk (1961) model. It has been shown to have a good fit to sand diffusion data (Moldrup et al., 2003). The model is,

$$\tau_l = \frac{\theta_l^{\frac{7}{3}}}{n^2} \quad \text{.....(A.17)}$$

A final, widely used aqueous phase model is the Kemper and Van Schaik (1966) model. This model was designed for use with clayey soils, with a suction range from field capacity (~33 kPa) to wilting point (~1500 kPa, Olsen and Kemper, 1968). As a result the models is not appropriate for medium to coarse textured soils such as those tested in this study.

A.2.2 Vapour Phase Models

Many more studies have been completed on unsaturated soil gas phase τ's compared to the aqueous phase (Buckingham, 1904, Penman, 1940, Marshall, 1959, Millington, 1959, Millington and Quirk, 1961, Collin and Rasmuson, 1988, Moldrup et al., 2000b). The best fit models to observed data, determined by Moldrup et al. (2000a) are the Penman (1940) and Millington (1959) models. The accuracy of these two models was extended by Moldrup et al. (2000a) by adding a linear scaling term (θ_v/n). The linearly reduced form of the Penman (1940) and Millington (1959) are found below,

$$\tau_v = 0.66\left(\frac{\theta_v}{n}\right) \quad \text{.....(A.18)}$$

$$\tau_v = \theta_v^{\frac{1}{3}}\left(\frac{\theta_v}{n}\right) \quad \text{.....(A.19)}$$

A.2.3 Dual Phase Models

In addition to the single-phase models, dual-phase τ's models have been applied to transport dissolvable or volatile species. Two separate dual-phase models have been successfully applied to dissolved gas in cover designs. Aachib et al. (2004) applies the dual phase approach to oxygen gas diffusion in unsaturated cover soils. The model used (Equations A.20 and A.21) is a modified Millington and Shearer model (Collin and Rasmuson, 1987 and Collin and Rasmuson, 1988).

$$\tau_v = \frac{{\theta_v}^{2x+1}}{n^2} \quad \text{.....(A.20)}$$

$$\tau_l = \frac{{\theta_l}^{2y+1}}{n^2} \quad \text{.....(A.21)}$$

Where x and y are calculated by solving Equations A.22 and A.23 for the desired water content.

$${\theta_v}^{2x} + (1-\theta_v)^x = 1 \quad \text{.....(A.22)}$$

$${\theta_l}^{2y} + (1-\theta_l)^y = 1 \quad \text{.....(A.23)}$$

The second dual-phase model was developed by Moldrup et al. (2003) (Equations A.24 and A.25), where the τ for each phase is described with fitting exponents.

$$\tau_v = \theta_v{}^{T-1}\left(\frac{\theta_v}{n}\right)^W \quad \text{.....(A.24)}$$

$$\tau_l = \theta_l{}^{T-1}\left(\frac{\theta_l}{n}\right)^W \quad \text{.....(A.25)}$$

where T and W are fitting parameters based on soil conditions (Moldrup et al., 2003) and the values for each are presented in Table A.8.

Table A.8 –Tortuosity fitting parameters for the Moldrup et al. (2003) dual phase model

Fitting Parameter	Aqueous Phase	Vapour Phase
T	2	1.5
W	1/3	1

By removing the linear scaling factor, $\left(\frac{\theta_v}{n}\right)^W$, the remaining portion of the equations with the recommended T parameter show a form that is the same as classic tortuosity models. The vapour phase is the same as Marshall (1959) and the aqueous phase is the same as the Buckingham (1904) model. All of the single and dual-phase models presented are summarized in Table A.9, along with an abbreviated name used to denote each model in subsequent figures.

A.2.4 Model Names and Fits to Observed Data

Table A.9 – Overview of tortuosity models presented with a shorthand description for easy representation of models. The PD model has eight variations, depending on which of the τ_{sat} models is used.

Model	Shorthand	Eqn #	Phase
Padilla et al., 1999	PD1	A.8 and A.9	Aqueous
Padilla et al., 1999	PD2	A.8 and A.10	Aqueous
Padilla et al., 1999	PD3	A.8 and A.11	Aqueous
Padilla et al., 1999	PD4	A.8 and A.12	Aqueous
Padilla et al., 1999	PD5	A.8 and A.13	Aqueous
Padilla et al., 1999	PD6	A.8 and A.14	Aqueous
Padilla et al., 1999	PD7	A.8 and A.15	Aqueous
Padilla et al., 1999	PD8	A.8 and A.16	Aqueous
Millington and Quirk, 1961	MQ	A.17	Aqueous
Aachib et al., 2004	AC	A.21	Aqueous
Moldrup et al., 2003	ML	A.25	Aqueous
Penman, 1940	PN	A.18	Vapour
Millington, 1959	MI	A.19	Vapour
Aachib et al., 2004	AC	A.20	Vapour
Moldrup et al., 2003	ML	A.24	Vapour

These models were all combined with the D_{com} formula and compared to the observed diffusion data. 11 aqueous phase models and 4 vapour phase models were combined to create 44 total models that were compared. The fit of each combination is shown in Table A.10. The models are named by the vapour phase tortuosity model then the aqueous phase.

Table A.10 – All 44 D_{com} models and their fit to the observed data at the three porosities used to analyze diffusion cell data.

Model	RMSE of 0.30 Porosity	RMSE of 0.35 Porosity	RMSE of 0.40 Porosity
'PN - MQ'	2.33E-10	1.42E-10	1.27E-10
'PN - AC'	2.2E-10	1.41E-10	1.22E-10
'PN - ML'	2.79E-10	1.95E-10	1.54E-10
'PN - PD-1'	1.47E-10	1.38E-10	8.56E-11

'PN - PD-2'	1.86E-10	1.09E-10	9.28E-11
'PN - PD-3'	1.97E-10	1.09E-10	9.18E-11
'PN - PD-4'	1.65E-10	1.22E-10	8.48E-11
'PN - PD-5'	1.76E-10	1.12E-10	8.65E-11
'PN - PD-6'	2.24E-10	1.31E-10	1.12E-10
'PN - PD-7'	2.47E-10	1.74E-10	1.45E-10
'PN - PD-8'	3.53E-10	3.52E-10	2.45E-10
'MI - MQ'	2.42E-10	1.48E-10	1.33E-10
'MI - AC'	2.3E-10	1.46E-10	1.28E-10
'MI - ML'	2.88E-10	1.99E-10	1.6E-10
'MI - PD-1'	1.57E-10	1.41E-10	8.68E-11
'MI - PD-2'	1.95E-10	1.14E-10	9.69E-11
'MI - PD-3'	2.06E-10	1.15E-10	9.58E-11
'MI - PD-4'	1.74E-10	1.26E-10	8.67E-11
'MI - PD-5'	1.86E-10	1.17E-10	8.95E-11
'MI - PD-6'	2.33E-10	1.36E-10	1.17E-10
'MI - PD-7'	2.56E-10	1.78E-10	1.51E-10
'MI - PD-8'	3.61E-10	3.55E-10	2.51E-10
'AC - MQ'	2.55E-10	1.63E-10	1.53E-10
'AC - AC'	2.43E-10	1.62E-10	1.48E-10
'AC - ML'	3.01E-10	2.11E-10	1.77E-10
'AC - PD-1'	1.71E-10	1.53E-10	9.16E-11
'AC - PD-2'	2.09E-10	1.31E-10	1.09E-10
'AC - PD-3'	2.2E-10	1.31E-10	1.08E-10
'AC - PD-4'	1.88E-10	1.4E-10	9.35E-11
'AC - PD-5'	1.99E-10	1.32E-10	9.9E-11
'AC - PD-6'	2.46E-10	1.51E-10	1.32E-10
'AC - PD-7'	2.69E-10	1.91E-10	1.67E-10
'AC - PD-8'	3.73E-10	3.63E-10	2.68E-10
'ML - MQ'	2.5E-10	1.58E-10	1.44E-10
'ML - AC'	2.38E-10	1.57E-10	1.38E-10

'ML - ML'	2.96E-10	2.07E-10	1.69E-10
'ML - PD-1'	1.65E-10	1.49E-10	8.7E-11
'ML - PD-2'	2.04E-10	1.25E-10	1.02E-10
'ML - PD-3'	2.15E-10	1.26E-10	1E-10
'ML - PD-4'	1.83E-10	1.36E-10	8.82E-11
'ML - PD-5'	1.94E-10	1.27E-10	9.26E-11
'ML - PD-6'	2.41E-10	1.47E-10	1.24E-10
'ML - PD-7'	2.64E-10	1.87E-10	1.58E-10
'ML - PD-8'	3.69E-10	3.6E-10	2.59E-10

A.3 Soil Dispersion Models

This section outlines some dispersion water content data that has been collected by other authors and presents several dispersion models to represent this data and a constant model that is most commonly used.

A.3.1 Sato Dispersion Model

Sato et al. (1995) and Sato et al. (2003) proposed a relationship between the saturation state of a soil and the soil dispersivity, Λ. This relationship follows a power function described below.

$$\Lambda = aS_r^{-b} \quad \text{.....(A.26)}$$

Where Λ is the soil dispersivity (m), S_r is the saturation state (unitless, as a decimal), and a and b are fitting parameters. Several consistency issues were noted in the works so the fitting parameters will not be carried forward to use in this work. For this work Equation A.26 will be redefined as,

$$\frac{\Lambda}{L} = AS_r^{-B} \quad \text{.....(A.27)}$$

Where Λ/L is the dispersivity normalized to the problem scale (unitless), and S_r is the saturation state (unitless, as a decimal), specifically defined as

$$S_r = \frac{\theta_l}{Porosity} \quad \text{.....(A.28)}$$

Defining the dispersivity in this manner will allow for fitting parameters to be determined from data collected from other authors and applied to this work. Dispersion vs saturation data was collected from Toride et al. (2003) and Padilla et al. (1999) and plotted with normalized dispersion in Figure A.1.

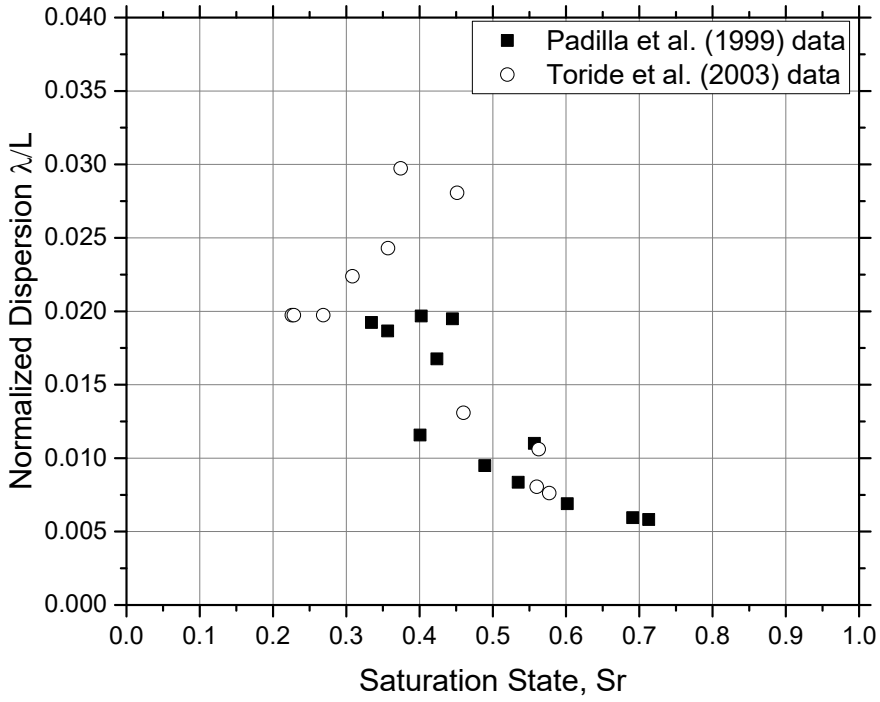

Figure A.1 – Collected dispersion saturation data from literature

As the data approaches a saturation state of 0.3 to 0.4 the data points start to show high variability. Typically a power relationship would be fit through the average of the data, as done in Sato et al., 2003. Here the power function will be fit to the right hand side of the data as it is proposed that a bell shaped relationship with saturation would explain the drop in normalized dispersivity below S_r = 0.4. Figure A.2 shows the power relationship fit to the collected data (A = 0.0025 and B = 2.4).

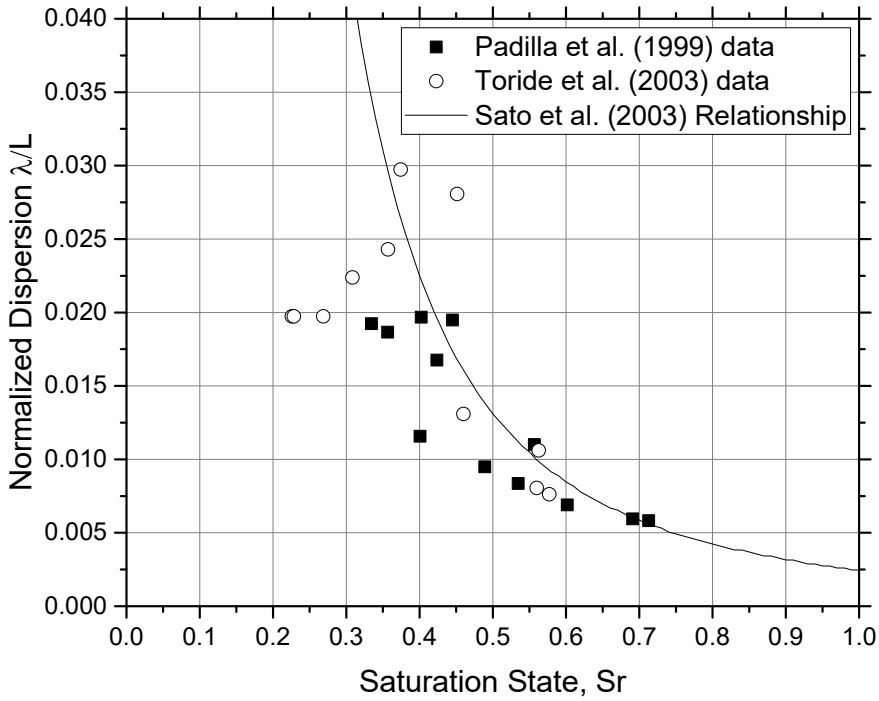

Figure A.2 - Collected dispersion saturation data from literature with Sato et al. (2003) power relationship fit.

A.3.2 Bell Shaped Model

From the previous section a bell shaped relationship is proposed to capture the reduction in measured dispersivity past a saturation of 0.4. A bell shaped profile was found by applying a tortuosity concept to the power relationship presented by Sato et al. (2003) (Equation A.29)

$$\left(\frac{\Lambda}{L}\right)_{bell} = \tau \frac{\Lambda}{L} \quad \text{.....(A.29)}$$

Where τ was determined by checking different functions to get the desired shape. The best relationship for τ was found to be,

$$\tau = 1 - \left(1 + (aS_r)^n\right)^{-m} \quad \text{.....(A.30)}$$

Where S_r is the saturation state (unitless, as a decimal), and a, n, and m are fitting parameters. The second part of the τ function is the same as the Van Genuchten (1980) SWCC relationship.

Here m was treated as a free parameter. With the best fit parameters selected (a = 4, n = 6, and m = 0.5) the bell shaped relationship can be compared to the collected data and power relationship (Figure A.3).

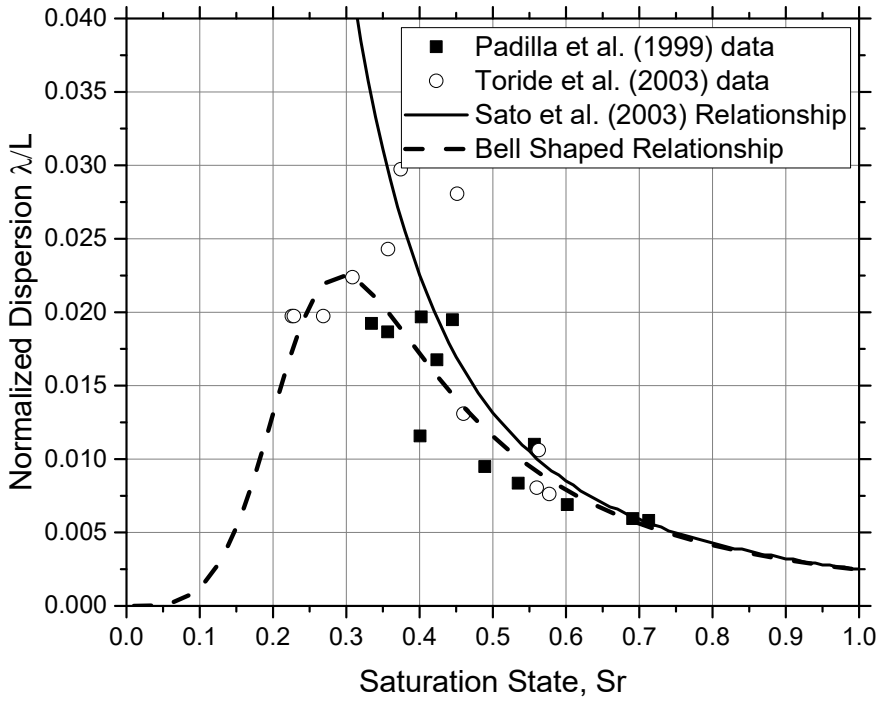

Figure A.3 - Collected dispersion saturation data from literature with Sato et al. (2003) power relationship and Bell relationship fit.

A bell shaped relationship captures the accepted increase in dispersivity as the soil starts to desaturate, where the flow paths are made smaller, thus increasing the soil water velocity and increasing the spreading due to dispersion. However, as the soil approached residual saturation, typically S_r of approximately .25 to 0.40 the water channels break down and the water phase connectivity disappears. When this happens the transported specie is moving faster, but has a much more tortuous pathway to take along fluid films, thus reducing the amount of spreading seen.

A.3.3 Constant values

Another classical dispersivity - saturation relationship that is used is a constant value over the saturation range. Here a value that meets the Sato et al. (2003) and bell shaped functions at

saturation will be used. This constant value plotted with the rest of the dispersion relationships can be found in Figure A.4.

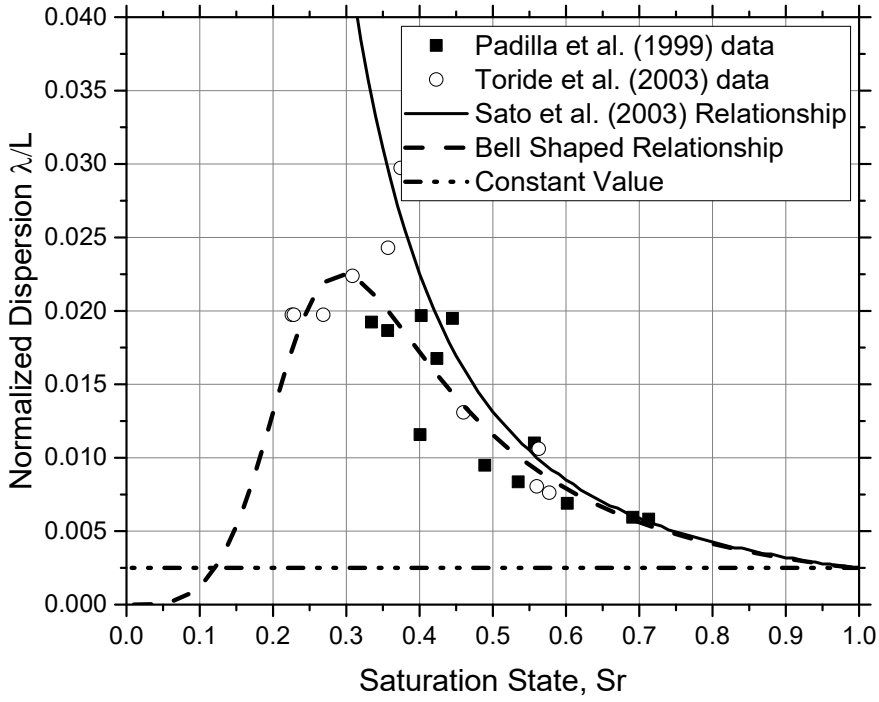

Figure A.4 - Collected dispersion saturation data from literature with Sato et al., 2003 power relationship, Bell relationship, and constant relationship fit.

A.4 Use of δ as a Concentration in Governing Equations

Two equations and a data set from the column experiment will used to justify the use of isotope del values (i.e. δ) in place of concentration. Barnes and Allison (1983) showed that the isotope ratio (R) can be related to a concentration by using the density of the water in a phase. For example in water the concentration of isotopes is,

$$C_i = R\rho_{water} \quad \text{.....(A.31)}$$

where C_i is the concentration of isotopes in liquid water (kg/m^3), R is the isotope ratio (unitless), and ρ_{water} is the density of liquid water (kg/m^3). The other equation is from Clark and Fritz (1997), which presented in the body of the thesis (Equation 2.2). Two parameters are needed. First

is ρ_{water} and it is assumed to be 1 000 kg/m^3. Second is the VSMOW ratio for δD (R_{std} = 1.5575E-4).

The isotope δ data for the first column at sample time 1 and the top and bottom isotope boundaries are presented in Table A.11. The δ data is converted to R using Equation 2.2. The R values are then converted to concentration using Equation A.31. The δ and concentration data are then normalized (using Equation 6.1) and the results compared with a simple difference.

Table A.11 – Comparison of normalized concentration from isotope δ values and isotope concentrations.

Sample	δD (‰)	R (unitless)	Concentration (kg/m^3)	C/C0 δ	C/C0 C	diff
1.4 m	-86.2825	1.42E-04	1.42E-01	0.9889453	0.9889453	0.0000000
1.3 m	-97.526	1.41E-04	1.41E-01	0.7451422	0.7451422	0.0000000
1.2 m	-111.401	1.38E-04	1.38E-01	0.4442778	0.4442778	0.0000000
1.1 m	-126.171	1.36E-04	1.36E-01	0.1240099	0.1240099	0.0000000
1.0 m	-133.87	1.35E-04	1.35E-01	-0.0429306	-0.0429306	0.0000000
0.9 m	-130.213	1.35E-04	1.35E-01	0.0363667	0.0363667	0.0000000
0.8 m	-130.604	1.35E-04	1.35E-01	0.0278799	0.0278799	0.0000000
0.7 m	-130.104	1.35E-04	1.35E-01	0.0387245	0.0387245	0.0000000
0.6 m	-132.582	1.35E-04	1.35E-01	-0.0150129	-0.0150129	0.0000000
0.5 m	-134.394	1.35E-04	1.35E-01	-0.0542916	-0.0542916	0.0000000
0.4 m	-134.652	1.35E-04	1.35E-01	-0.0598884	-0.0598884	0.0000000
0.3 m	-133.387	1.35E-04	1.35E-01	-0.0324705	-0.0324705	0.0000000

0.2 m	-131.766	1.35E-04	1.35E-01	0.0026769	0.0026769	0.0000000
Top Boundary	-85.7727	1.42E-04	1.42E-01			
Bottom Boundary	-131.89	1.35E-04	1.35E-01			

There is no difference between the two different normalized concentrations, so normalization based on isotope δ values is acceptable for this study.

A.5 References

Aachib, M., M. Mbonimpa and M. Aubertin (2004). "Measurement and prediction of the oxygen diffusion coefficient in unsaturated media, with applications to soil covers." Water, air, and soil pollution **156**(1): 163-193.

Barnes, C. and G. Allison (1983). "The distribution of deuterium and 18O in dry soils: 1. Theory." Journal of Hydrology **60**(1): 141-156.

Becerra, L. O. and L. M. Centeno (2006). Density determination of the water produced at CENAM by the use of solid density standards. XVIII IMEKO World Congress Metrology for a Sustainable Development, Rio de Janeiro, Brazil.

Boudreau, B. P. (1996). "The diffusive tortuosity of fine-grained unlithified sediments." Geochimica et Cosmochimica Acta **60**(16): 3139-3142.

Braud, I., T. Bariac, J. P. Gaudet and M. Vauclin (2005a). "SiSPAT-Isotope, a coupled heat, water and stable isotope (HDO and $H_2{}^{18}O$) transport model for bare soil. Part I. Model description and first verifications." Journal of Hydrology **309**(1): 277-300.

Buckingham, E. (1904). "Contributions to our knowledge of the aeration of soils."

Clark, I. D. and P. Fritz (1997). Environmental Isotopes in Hydrogeology, CRC press.

Collin, M. and A. Rasmuson (1987). "Mathematical modeling of water and oxygen transport in layered soil covers for deposits of pyritic mine tailings." Licenciate Treatise. Royal Institute of Technology. Department of Chemical Engineering. S-10044 Stockholm, Sweden.

Collin, M. and A. Rasmuson (1988). "A comparison of gas diffusivity models for unsaturated porous media." Soil Science Society of America Journal **52**(6): 1559-1565.

Easteal, A. J., A. V. J. Edge and L. A. Woolf (1984). "Isotope effects in water. Tracer diffusion coefficients for water (oxygen-18)($H_2{}^{18}O$) in ordinary water." The Journal of Physical Chemistry **88**(24): 6060-6063.

Kemper, W. and J. Van Schaik (1966). "Diffusion of salts in clay-water systems." Soil Science Society of America Journal **30**(5): 534-540.

Kimball, B. A., R. Jackson, R. Reginato, F. Nakayama and S. Idso (1976). "Comparison of field-measured and calculated soil-heat fluxes." Soil Science Society of America Journal **40**(1): 18-25.

Majoube, M. (1971). "Fractionnement en oxyge`ne-18 et en deute´rium entre l'eau et sa vapeur." Journal de Chimie Physique et de Physico-Chimie Biologique **68**(July-Dec).

Marshall, T. (1959). "The diffusion of gases through porous media." Journal of Soil Science **10**(1): 79-82.

Merlivat, L. (1978). "Molecular diffusivities of $H_2{}^{16}O$, $HD^{16}O$, and $H_2{}^{18}O$ in gases." The Journal of Chemical Physics **69**(6): 2864-2871.

Millington, R. (1959). "Gas diffusion in porous media." Science **130**(3367): 100-102.

Millington, R. and J. Quirk (1961). "Permeability of porous solids." Transactions of the Faraday Society **57**: 1200-1207.

Millington, R. J. (1959). "Gas Diffusion in Porous Media." Science **130**(3367): 100-102.

Moldrup, P., T. Olesen, J. Gamst, P. Schjønning, T. Yamaguchi and D. Rolston (2000a). "Predicting the gas diffusion coefficient in repacked soil water-induced linear reduction model." Soil Science Society of America Journal **64**(5): 1588-1594.

Moldrup, P., T. Olesen, T. Komatsu, S. Yoshikawa, P. Schjønning and D. Rolston (2003). "Modeling diffusion and reaction in soils: X. A unifying model for solute and gas diffusivity in unsaturated soil." Soil Science **168**(5): 321-337.

Moldrup, P., T. Olesen, P. Schjønning, T. Yamaguchi and D. Rolston (2000b). "Predicting the gas diffusion coefficient in undisturbed soil from soil water characteristics." Soil Science Society of America Journal **64**(1): 94-100.

Nave, R. "Empirical fit of saturated vapor density versus Celsius Temperature." Retrieved April 5, 2017, from http://hyperphysics.phy-astr.gsu.edu/hbase/kinetic/relhum.html#c3.

Olsen, S. and W. Kemper (1968). "Movement of nutrients to plant roots." Adv. Agron **20**: 91-151.

Padilla, I. Y., T. C. J. Yeh and M. H. Conklin (1999). "The effect of water content on solute transport in unsaturated porous media." Water Resources Research **35**(11): 3303-3313.

Penman, H. (1940). "Gas and vapour movements in the soil: I. The diffusion of vapours through porous solids." The Journal of Agricultural Science **30**(03): 437-462.

Sato, T., H. Tanahashi and H. A. Loáiciga (2003). "Solute dispersion in a variably saturated sand." Water resources research **39**(6).

Sato, T., H. TANAHASHI, T. Uno and A. YUASA (1995). Adsorption and Dispersion Characteristics Within the Unsaturated Zone. Proceedings of the First International Conference on Unsaturated Soils, Paris, France.

Toride, N., M. Inoue and F. J. Leij (2003). "Hydrodynamic dispersion in an unsaturated dune sand." Soil Science Society of America Journal **67**(3): 703-712.

Van Genuchten, M. T. (1980). "A closed-form equation for predicting the hydraulic conductivity of unsaturated soils." Soil Science Society of America Journal **44**(5): 892-898.

Appendix B

This appendix presents all the collected data for the diffusion cell laboratory experiment.

B.1 Cell Raw Water Content Data

The raw cell slice gravimetric water content (ω) data is presented in Table B.1 to Table B.7. The tables also include the average gravimetric water content and the target set out for the cell, if applicable.

Table B.1 – Cell raw gravimetric water content data.

Cell	R1-1	Cell	R1-2	Cell	R1-3
Target ω (%)	7.5	Target ω (%)	10.0	Target ω (%)	12.5
Average (%)	7.3	Average (%)	9.8	Average (%)	12.4
Position (cm)	GWC (%)	Position (cm)	GWC (%)	Position (cm)	GWC (%)
18.0	7.8	17.0	10.6	17.0	12.7
15.0	7.5	13.0	10.7	13.0	12.5
13.0	7.2	11.0	7.0	11.0	12.2
11.0	7.1	9.0	9.2	9.0	12.3
9.0	6.9	7.0	9.3	7.0	13.0
7.0	7.0	5.0	9.1	5.0	12.6
5.0	6.8	3.0	8.8	3.0	12.6
3.0	6.8	1.0	9.6	1.0	12.0
1.0	6.9	-1.0	9.6	-1.0	11.7
-1.0	7.4	-3.0	9.9	-3.0	12.3
-3.0	7.4	-5.0	10.1	-5.0	12.8
-5.0	7.0	-7.0	10.0	-7.0	12.4
-7.0	7.4	-9.0	10.0	-9.0	12.3
-9.0	6.8	-11.0	12.5	-11.0	12.3
-11.0	8.1	-13.0	10.2	-13.0	12.3
-13.0	7.1	-17.0	10.4	-17.0	12.5
-15.0	8.1				
-18.0	7.6				

Table B.2 – Cell raw gravimetric water content data.

Cell	R1-4	Cell	R1-5	Cell	R2-1
Target ω (%)	15.0	Target ω (%)	17.5	Target ω (%)	6.0
Average (%)	14.9	Average (%)	17.4	Average (%)	7.4
Position (cm)	GWC (%)	Position (cm)	GWC (%)	Position (cm)	GWC (%)
18.0	14.7	17.0	15.9	17.0	7.5
15.0	15.8	13.0	15.6	15.0	7.5
13.0	14.9	11.0	15.5	13.0	7.6
11.0	14.6	9.0	16.0	11.0	7.4
9.0	15.7	7.0	16.3	9.0	7.3
7.0	14.8	5.0	17.4	7.0	7.4
5.0	16.3	3.0	20.9	5.0	7.4
3.0	15.7	1.0	21.6	3.0	7.3
1.0	14.8	-1.0	20.7	1.0	7.0
-1.0	14.5	-3.0	18.5	-1.0	7.5
-3.0	14.9	-5.0	17.3	-3.0	7.5
-5.0	15.0	-7.0	16.6	-5.0	7.4
-7.0	14.6	-9.0	16.1	-7.0	7.1
-9.0	14.5	-11.0	16.8	-9.0	7.0
-11.0	14.7	-13.0	17.1	-11.0	7.5
-13.0	14.5	-17.0	15.9	-13.0	7.6
-17.0	14.4			-16.0	7.2

Table B.3 – Cell raw gravimetric water content data.

Cell	R2-2	Cell	R2-3	Cell	R2-4
Target ω (%)	9.0	Target ω (%)	13.0	Target ω (%)	20.0
Average (%)	10.6	Average (%)	15.4	Average (%)	21.6
Position (cm)	GWC (%)	Position (cm)	GWC (%)	Position (cm)	GWC (%)
17.0	10.8	17.0	15.7	19.0	23.0
13.0	10.9	13.0	15.5	15.0	22.1
11.0	10.7	11.0	15.2	13.0	22.6
9.0	10.7	9.0	15.5	11.0	22.0
7.0	10.5	7.0	15.7	9.0	23.4
5.0	11.2	5.0	15.6	7.0	22.8
3.0	11.1	3.0	15.7	5.0	23.6
1.0	11.5	1.0	15.3	3.0	21.3
-1.0	10.4	-1.0	15.1	1.0	22.1
-3.0	10.5	-3.0	16.7	-1.0	20.7
-5.0	10.8	-5.0	15.4	-3.0	21.4
-7.0	10.3	-7.0	14.9	-5.0	20.4
-9.0	10.1	-9.0	14.8	-7.0	20.2
-11.0	9.9	-11.0	14.9	-9.0	19.9
-13.0	10.2	-13.0	15.5	-11.0	20.5
-17.0	10.1	-17.0	14.6	-13.0	20.9
				-15.0	20.9
				-19.0	21.6

Table B.4 – Cell raw gravimetric water content data.

Cell	R2-5	Cell	R3-2	Cell	R3-3
Target ω (%)	16.0	Target ω (%)	23.3	Target ω (%)	17.6
Average (%)	18.4	Average (%)	20.8	Average (%)	20.5
Position (cm)	GWC (%)	Position (cm)	GWC (%)	Position (cm)	GWC (%)
17.0	18.3	17.0	22.1	17.0	21.7
13.0	18.0	13.0	20.9	13.0	20.7
11.0	18.1	11.0	20.8	11.0	20.6
9.0	17.7	9.0	20.4	9.0	20.3
7.0	16.9	7.0	20.2	7.0	20.0
5.0	17.8	5.0	19.9	5.0	19.7
3.0	18.5	3.0	19.2	3.0	19.3
1.0	20.2	1.0	20.4	1.0	20.3
-1.0	19.6	-1.0	20.1	-1.0	20.6
-3.0	19.8	-3.0	20.1	-3.0	20.0
-5.0	17.2	-5.0	20.6	-5.0	20.0
-7.0	17.6	-7.0	21.0	-7.0	20.3
-9.0	19.3	-9.0	21.4	-9.0	20.6
-11.0	19.0	-11.0	21.3	-11.0	20.8
-13.0	18.3	-13.0	21.5	-13.0	20.9
-17.0	18.6	-17.0	22.4	-17.0	22.1

Table B.5 – Cell raw gravimetric water content data.

Cell	R3-4	Cell	R3-5	Cell	R4-1
Target ω (%)	11.3	Target ω (%)	6.9	Target ω (%)	
Average (%)	18.6	Average (%)	19.1	Average (%)	13.5
Position (cm)	GWC (%)	Position (cm)	GWC (%)	Position (cm)	GWC (%)
17.0	20.3	17.0	20.0	26.0	14.9
13.0	19.8	13.0	19.3	19.5	14.6
11.0	19.6	11.0	19.2	16.5	14.6
9.0	19.2	9.0	18.6	13.5	14.5
7.0	19.2	7.0	18.7	10.5	14.4
5.0	19.0	5.0	18.5	7.5	13.3
3.0	18.9	3.0	18.0	4.5	11.9
1.0	19.4	1.0	18.5	1.5	9.8
-1.0	19.8	-1.0	19.1	-1.5	11.9
-3.0	19.1	-3.0	18.4	-4.5	12.7
-5.0	19.0	-5.0	18.7	-7.5	13.8
-7.0	19.4	-7.0	19.0	-10.5	13.9
-9.0	15.0	-9.0	19.2	-13.5	14.2
-11.0	8.7	-11.0	19.5	-16.5	13.8
-13.0	20.3	-13.0	19.8	-19.5	14.1
-17.0	21.2	-17.0	20.6	-26.0	14.2

Table B.6 – Cell raw gravimetric water content data.

Cell	R4-2	Cell	R4-3	Cell	R4-4
Target ω (%)		Target ω (%)		Target ω (%)	
Average (%)	11.1	Average (%)	8.8	Average (%)	8.2
Position (cm)	GWC (%)	Position (cm)	GWC (%)	Position (cm)	GWC (%)
26.0	10.9	26.0	7.7	26.0	9.0
19.5	11.0	19.5	8.3	19.5	8.5
16.5	11.9	16.5	8.6	16.5	8.2
13.5	12.1	13.5	8.4	13.5	8.3
10.5	11.6	10.5	8.5	10.5	8.1
7.5	11.7	7.5	8.5	7.5	8.2
4.5	10.9	4.5	8.4	4.5	7.7
1.5	9.7	1.5	7.5	1.5	7.2
-1.5	9.9	-1.5	7.4	-1.5	8.0
-4.5	10.0	-4.5	8.2	-4.5	8.3
-7.5	11.2	-7.5	9.1	-7.5	8.3
-10.5	11.1	-10.5	9.2	-10.5	8.9
-13.5	11.7	-13.5	10.1	-13.5	8.8
-16.5	12.0	-16.5	10.4	-16.5	9.0
-19.5	11.7	-19.5	10.9	-19.5	8.4
-26.0	10.8	-26.0	9.1	-26.0	7.2

Table B.7 – Cell raw gravimetric water content data.

Cell	R4-5
Target ω (%)	
Average (%)	7.1
Position (cm)	GWC (%)
26.0	6.7
19.5	7.4
16.5	7.5
13.5	7.4
10.5	7.4
7.5	6.9
4.5	6.7
1.5	6.4
-1.5	6.3
-4.5	6.6
-7.5	7.3
-10.5	7.5
-13.5	7.5
-16.5	7.3
-19.5	7.5
-26.0	7.1

B.2 Cell Isotope Data

The isotope data that was collected for different cells was done on several pieces of equipment (Table B.8).

Table B.8 - Equipment used for isotope analysis for each cell.

Cell	Equipment Manufacturer	Model
R1-1	Picarro	2120
R1-2	Picarro	2120
R1-3	Picarro	2120
R1-4	Picarro	2120
R1-5	Picarro	2120
R2-1	Picarro	2120
R2-2	Picarro	2120
R2-3	Picarro	2120
R2-4	Picarro	2120
R2-5	Picarro	2120
R3-1	N/A	N/A
R3-2	Picarro	1102i
R3-3	Picarro	1102i
R3-4	Picarro	1102i
R3-5	Picarro	2120
R4-1	Los Gatos Research (LGR)	WV1A - 45 - EP
R4-2	Los Gatos Research (LGR)	WV1A - 45 - EP
R4-3	Los Gatos Research (LGR)	WV1A - 45 - EP
R4-4	Los Gatos Research (LGR)	WV1A - 45 - EP
R4-5	Los Gatos Research (LGR)	WV1A - 45 - EP

The raw (corrected from instrument) isotope data for δD and $\delta^{18}O$ is presented in Table B.9 to Table B.18.

Table B.9 – δD and $\delta^{18}O$ results for each cell.

Cell	R1-1	R1-1	Cell	R1-2	R1-2
Position (cm)	δD (‰)	δ18O (‰)	Position (cm)	δD (‰)	δ18O (‰)
18.0	-74.6	-15.1	17.0	-128.1	-15.3
15.0	-84.6	-15.6	13.0	-127.1	-16.0
13.0	-82.9	-15.3	11.0	-125.9	-16.0
11.0	-85.5	-15.4	9.0	-123.3	-15.8
9.0	-71.5	-13.6	7.0	-118.1	-15.8
7.0	-78.2	-14.0	5.0	-118.2	-16.0
5.0	-81.6	-13.6	3.0	-113.0	-15.9
3.0	-88.2	-14.0	1.0	-103.0	-14.6
1.0	-104.9	-14.7	-1.0	-98.0	-15.0
-1.0	-111.2	-14.9	-3.0	-92.5	-15.5
-3.0	-114.8	-15.0	-5.0	-87.5	-15.6
-5.0	-121.9	-15.1	-7.0	-83.7	-15.6
-7.0	-116.7	-13.7	-9.0	-75.3	-15.6
-9.0	-123.9	-14.3	-11.0	-81.0	-16.0
-11.0	-124.9	-14.1	-13.0	-73.6	-15.5
-13.0	-129.2	-15.5	-17.0	-73.2	-15.3
-15.0	-127.5	-14.4			
-18.0	-126.7	-14.6			

Table B.10 – δD and $\delta^{18}O$ results for each cell.

Cell	R1-3	R1-3	Cell	R1-4	R1-4
Position (cm)	δD (‰)	δ18O (‰)	Position (cm)	δD (‰)	δ18O (‰)
17.0	-60.1	-16.3	18.0	-55.5	-15.9
13.0	-65.2	-16.2	15.0	-58.8	-16.6
11.0	-65.5	-16.4	13.0	-64.1	-16.4
9.0	-70.9	-16.4	11.0	-73.3	-16.5
7.0	-72.1	-16.1	9.0	-76.4	-16.7
5.0	-78.6	-16.6	7.0	-78.9	-16.8
3.0	-82.5	-16.4	5.0	-82.7	-16.2
1.0	-92.6	-16.4	3.0	-91.7	-16.3
-1.0	-96.1	-16.0	1.0	-97.9	-16.3
-3.0	-101.7	-15.9	-1.0	-103.9	-16.4
-5.0	-114.3	-16.2	-3.0	-105.5	-16.1
-7.0	-121.5	-16.6	-5.0	-117.1	-16.6
-9.0	-125.6	-16.8	-7.0	-118.4	-16.3
-11.0	-127.0	-16.3	-9.0	-123.7	-16.4
-13.0	-128.8	-16.5	-11.0	-125.0	-16.0
-17.0	-130.4	-16.0	-13.0	-128.5	-16.0
			-17.0	-130.4	-15.9

Table B.11 – δD and $\delta^{18}O$ results for each cell.

Cell	R1-5	R1-5	Cell	R2-1	R2-1
Position (cm)	δD (‰)	δ18O (‰)	Position (cm)	δD (‰)	δ18O (‰)
17.0	-52.7	-15.8	17.0	-35.1	-16.1
13.0	-59.5	-16.1	15.0	-53.8	-16.1
11.0	-61.9	-16.4	13.0	-35.9	-15.7
9.0	-65.0	-15.9	11.0	-40.7	-15.7
7.0	-68.9	-16.1	9.0	-44.0	-15.7
5.0	-74.8	-16.3	7.0	-51.7	-15.4
3.0	-81.8	-16.1	5.0	-67.7	-16.3
1.0	-89.1	-15.9	3.0	-72.5	-15.1
-1.0	-96.7	-15.6	1.0	-86.5	-15.0
-3.0	-102.5	-15.9	-1.0	-105.1	-15.8
-5.0	-112.1	-15.8	-3.0	-110.4	-15.7
-7.0	-117.6	-15.9	-5.0	-116.5	-15.8
-9.0	-121.9	-16.1	-7.0	-125.7	-16.1
-11.0	-125.0	-15.9	-9.0	-126.8	-16.1
-13.0	-127.6	-15.7	-11.0	-125.5	-16.1
-17.0	-130.6	-15.6	-13.0	-126.2	-15.8
			-16.0	-126.0	-15.6

Table B.12 – δD and $\delta^{18}O$ results for each cell.

Cell	R2-2	R2-2	Cell	R2-3	R2-3
Position (cm)	δD (‰)	δ18O (‰)	Position (cm)	δD (‰)	δ18O (‰)
17.0	-34.1	-16.7	17.0	-31.1	-16.6
13.0	-40.7	-15.8	13.0	-36.1	-16.8
11.0	-48.5	-16.7	11.0	-39.4	-16.6
9.0	-48.4	-16.1	9.0	-44.0	-16.8
7.0	-55.3	-16.7	7.0	-48.3	-17.1
5.0	-56.2	-15.5	5.0	-57.3	-16.6
3.0	-71.3	-16.7	3.0	-65.0	-16.9
1.0	-78.8	-15.7	1.0	-76.0	-16.9
-1.0	-87.6	-16.2	-1.0	-88.7	-16.9
-3.0	-97.2	-15.9	-3.0	-104.0	-17.1
-5.0	-108.3	-16.1	-5.0	-114.3	-17.0
-7.0	-115.2	-16.0	-7.0	-118.4	-16.6
-9.0	-120.9	-16.2	-9.0	-126.5	-16.8
-11.0	-124.3	-16.0	-11.0	-130.1	-16.6
-13.0	-130.7	-16.4	-13.0	-131.7	-17.2
-17.0	-130.9	-16.1	-17.0	-134.7	-16.8

Table B.13 – δD and $\delta^{18}O$ results for each cell.

Cell	R2-4	R2-4	Cell	R2-5	R2-5
Position (cm)	δD (‰)	δ18O (‰)	Position (cm)	δD (‰)	δ18O (‰)
19.0	-44.7	-17.4	17.0	-52.3	-17.3
15.0	-33.1	-16.9	13.0	-51.7	-17.5
13.0	-28.5	-17.6	11.0	-43.3	-17.3
11.0	-30.7	-17.6	9.0	-42.1	-17.0
9.0	-43.4	-17.3	7.0	-51.7	-17.5
7.0	-41.7	-17.6	5.0	-57.0	-16.5
5.0	-64.8	-17.5	3.0	-66.9	-17.1
3.0	-69.0	-16.6	1.0	-86.3	-16.9
1.0	-82.5	-17.1	-1.0	-89.8	-16.3
-1.0	-95.9	-17.0	-3.0	-101.0	-17.4
-3.0	-107.5	-17.2	-5.0	-109.1	-16.9
-5.0	-118.3	-17.1	-7.0	-118.8	-17.1
-7.0	-123.0	-17.5	-9.0	-120.5	-16.5
-9.0	-127.8	-17.1	-11.0	-129.6	-16.7
-11.0	-130.6	-17.6	-13.0	-133.7	-17.4
-13.0	-134.9	-17.3	-17.0	-134.3	-17.1
-15.0	-134.8	-17.0			
-19.0	-137.6	-17.3			

Table B.14 – δD and $\delta^{18}O$ results for each cell.

Cell	R3-2	R3-2	Cell	R3-3	R3-3
Position (cm)	δD (‰)	δ18O (‰)	Position (cm)	δD (‰)	δ18O (‰)
17.0	-127.6	-16.2	17.0	-126.1	-16.6
13.0	-130.4	-16.4	13.0	-121.4	-16.7
11.0	-125.9	-16.6	11.0	-126.8	-16.3
9.0	-125.1	-16.2	9.0	-121.6	-16.2
7.0	-112.5	-16.4	7.0	-116.2	-16.0
5.0	-106.0	-16.0	5.0	-105.2	-17.2
3.0	-95.9	-16.0	3.0	-97.6	-15.7
1.0	-85.7	-16.0	1.0	-83.1	-16.3
-1.0	-82.9	-16.7	-1.0	-82.0	-16.2
-3.0	-71.8	-16.0	-3.0	-68.2	-17.0
-5.0	-66.8	-16.4	-5.0	-67.4	-16.5
-7.0	-55.4	-16.3	-7.0	-60.6	-16.6
-9.0	-54.8	-16.0	-9.0	-40.2	-16.5
-11.0	-47.0	-16.7	-11.0	-37.3	-17.0
-13.0	-43.3	-16.1	-13.0	-45.2	-16.2
-17.0	-42.4	-15.3	-17.0	-40.6	-16.1

Table B.15 – δD and $\delta^{18}O$ results for each cell.

Cell	R3-4	R3-4	Cell	R3-5	R3-5
Position (cm)	δD (‰)	δ18O (‰)	Position (cm)	δD (‰)	δ18O (‰)
17.0	-129.2	-15.6	17.0	-136.0	-16.4
13.0	-129.8	-16.8	13.0	-128.4	-15.2
11.0	-120.3	-16.4	11.0	-124.5	-16.4
9.0	-118.4	-16.0	9.0	-123.6	-16.6
7.0	-111.0	-16.3	7.0	-115.6	-16.1
5.0	-103.8	-15.7	5.0	-113.8	-16.7
3.0	-95.5	-15.8	3.0	-97.0	-16.6
1.0	-86.9	-15.8	1.0	-90.0	-15.7
-1.0	-83.5	-16.7	-1.0	-83.2	-15.3
-3.0	-69.6	-15.7	-3.0	-69.4	-16.2
-5.0	-60.2	-16.2	-5.0	-64.6	-15.4
-7.0	-56.3	-15.9	-7.0	-57.4	-16.1
-9.0	-50.7	-16.1	-9.0	-51.8	-15.7
-11.0	-45.9	-16.5	-11.0	-48.1	-16.0
-13.0	-39.4	-15.6	-13.0	-46.7	-16.7
-17.0	-37.8	-16.2	-17.0	-38.9	-15.6

Table B.16 – δD and $\delta^{18}O$ results for each cell.

Cell	R4-1	R4-1	Cell	R4-2	R4-2
Position (cm)	δD (‰)	δ18O (‰)	Position (cm)	δD (‰)	δ18O (‰)
26.0	-71.4	-16.7	26.0	-68.7	-14.5
19.5	-72.2		19.5	-70.5	-15.5
16.5	-67.0	-16.0	16.5	-66.7	-15.5
13.5	-70.4	-16.1	13.5	-70.4	-15.1
10.5	-72.6	-17.0	10.5	-71.9	-14.5
7.5	-75.1	-14.7	7.5	-78.4	-14.4
4.5	-86.9	-13.1	4.5	-85.4	-14.9
1.5	-100.9	-13.3	1.5	-94.7	-14.6
-1.5	-112.3	-14.2	-1.5	-105.8	-13.0
-4.5	-118.4	-13.0	-4.5	-120.2	-13.5
-7.5	-127.1	-15.0	-7.5	-128.7	-14.1
-10.5	-123.7	-15.3	-10.5	-130.2	-15.0
-13.5	-130.8	-15.9	-13.5	-129.5	-15.4
-16.5	-126.8	-16.3	-16.5	-131.2	-15.1
-19.5	-127.9	-15.6	-19.5	-131.6	-15.1
-26.0	-123.2	-14.1	-26.0	-130.8	-14.6

Table B.17 – δD and $\delta^{18}O$ results for each cell.

Cell	R4-3	R4-3	Cell	R4-4	R4-4
Position (cm)	δD (‰)	δ18O (‰)	Position (cm)	δD (‰)	δ18O (‰)
26.0	-69.2	-14.1	26.0	-69.2	-14.0
19.5	-69.8	-14.9	19.5	-74.7	-16.3
16.5	-69.6	-14.8	16.5	-69.4	-13.6
13.5	-74.4	-13.1	13.5	-67.3	-14.3
10.5	-73.1	-13.5	10.5	-74.7	-12.5
7.5	-77.8	-12.1	7.5	-76.5	-18.5
4.5	-85.0	-11.0	4.5	-89.6	-12.2
1.5	-99.1	-12.2	1.5	-104.8	-18.7
-1.5	-105.7	-11.1	-1.5	-106.6	-13.4
-4.5	-112.9	-9.9	-4.5	-120.4	-15.7
-7.5	-122.6	-10.9	-7.5	-120.5	-12.7
-10.5	-132.6	-12.8	-10.5	-130.7	-15.5
-13.5	-136.5	-13.9	-13.5	-130.1	-16.0
-16.5	-136.3	-13.8	-16.5	-131.0	-15.0
-19.5	-133.1	-14.9	-19.5	-130.7	-14.5
-26.0	-130.8	-14.6	-26.0	-123.2	-13.0

Table B.18 – δD and $\delta^{18}O$ results for each cell.

Cell	R4-5	R4-5
Position (cm)	δD (‰)	δ18O (‰)
26.0	-64.6	-14.4
19.5	-72.8	-15.6
16.5	-72.7	-14.1
13.5	-75.1	-15.1
10.5	-75.1	-14.9
7.5	-76.8	-15.3
4.5	-84.5	-13.9

1.5	-99.7	-14.5
-1.5	-110.9	-13.9
-4.5	-117.1	-14.3
-7.5	-126.6	-15.6
-10.5	-132.9	-15.7
-13.5	-132.1	-15.9
-16.5	-134.5	-16.7
-19.5	-131.9	-15.0
-26.0	-130.5	-16.0

B.3 Cell Initial Conditions

The initial spiked and non-spiked conditions, measured at different times in the construction process are shown in Table B.19 and Table B.20.

Table B.19 – initial isotope measurements for the spiked half-cells.

Spiked Water							
R	Cell	Isotopes of Water prepared		Isotopes of mixed sand prepared		Isotopes of drained water	
		Delta O (‰)	Delta D (‰)	Delta O (‰)	Delta D (‰)	Delta O (‰)	Delta D (‰)
1	1	-16.38	-63.98				
1	2	-15.71	-50.34	-14.98	-61.53		
1	3	-16.03	-44.53	-14.90	-42.34		
1	4	-16.31	-42.30	-15.04	-36.74		
1	5	-16.11	-47.38	-15.11	-38.26		
2	1	-17.31	-31.46	-16.80	-67.44		
2	2	-17.52	-34.95	-17.15	-45.65		
2	3	-18.31	-41.35	-17.07	-51.53		
2	4	-19.31	-57.62	-16.84	-61.71		
2	5	-18.25	-31.83	-16.67	-26.91		
3	2	-17.08	-34.50				
3	3	-17.08	-34.50				
3	4	-16.86	-33.22				
3	5	-16.64	-30.43				
4	1	-16.41	-65.57	-17.24	-71.68	-15.71	-72.14
4	2	-16.41	-65.57	-17.24	-71.68	-15.40	-73.78
4	3	-16.41	-65.57	-17.24	-71.68	-16.66	-68.54
4	4	-16.41	-65.57	-17.24	-71.68	-15.74	-71.13
4	5	-16.41	-65.57	-17.24	-71.68	-16.85	-73.63

Table B.20 – initial isotope measurements for the spiked half-cells.

Non-Spiked Water							
R	Cell	Isotopes of Water prepared		Isotopes of mixed sand prepared		Isotopes of drained water	
		Delta O (‰)	Delta D (‰)	Delta O (‰)	Delta D (‰)	Delta O (‰)	Delta D (‰)
1	1	-16.02	-128.31				
1	2	-16.29	-128.97	-14.09	-121.96		
1	3	-16.39	-129.23	-14.96	-125.68		
1	4	-16.49	-130.56	-14.81	-124.59		
1	5	-16.15	-128.97	-14.39	-122.04		
2	1	-18.20	-138.62	-16.59	-125.80		
2	2	-18.20	-138.62	-16.95	-127.60		
2	3	-18.20	-138.62	-16.76	-132.08		
2	4	-18.20	-138.62	-17.38	-140.47		
2	5	-18.20	-138.62	-17.64	-144.23		
3	2	-17.29	-135.00				
3	3	-16.97	-133.94				
3	4	-17.58	-136.19				
3	5	-17.21	-132.61				
4	1	-17.82	-132.14			-15.82	-130.89
4	2	-17.82	-132.14			-16.80	-133.71
4	3	-17.82	-132.14			-16.86	-130.16
4	4	-17.82	-132.14			-15.81	-130.92
4	5	-17.82	-132.14			-15.96	-135.18

B.4 Cell Slice Thickness Measurements

The average thickness of each slice used to calculate the slice density is presented in Table B.21 to Table B.27.

Table B.21 – Average thickness of each slice of each diffusion cell.

Cell	R1-1	Cell	R1-2	Cell	R1-3
Position (cm)	Thickness (cm)	Position (cm)	Thickness (cm)	Position (cm)	Thickness (cm)
18.0	Not Measured	17.0	Not Measured	17.0	Not Measured
15.0	Not Measured	13.0	Not Measured	13.0	Not Measured
13.0	Not Measured	11.0	Not Measured	11.0	Not Measured
11.0	Not Measured	9.0	Not Measured	9.0	Not Measured
9.0	Not Measured	7.0	Not Measured	7.0	Not Measured
7.0	Not Measured	5.0	Not Measured	5.0	Not Measured
5.0	Not Measured	3.0	Not Measured	3.0	Not Measured
3.0	Not Measured	1.0	Not Measured	1.0	Not Measured
1.0	Not Measured	-1.0	Not Measured	-1.0	Not Measured
-1.0	Not Measured	-3.0	Not Measured	-3.0	Not Measured
-3.0	Not Measured	-5.0	Not Measured	-5.0	Not Measured
-5.0	Not Measured	-7.0	Not Measured	-7.0	Not Measured
-7.0	Not Measured	-9.0	Not Measured	-9.0	Not Measured
-9.0	Not Measured	-11.0	Not Measured	-11.0	Not Measured
-11.0	Not Measured	-13.0	Not Measured	-13.0	Not Measured
-13.0	Not Measured	-17.0	Not Measured	-17.0	Not Measured

-15.0	Not Measured				
-18.0	Not Measured				

Table B.22 – Average thickness of each slice of each diffusion cell.

Cell	R1-4	Cell	R1-5	Cell	R2-1
Position (cm)	Thickness (cm)	Position (cm)	Thickness (cm)	Position (cm)	Thickness (cm)
18.0	Not Measured	17.0	Not Measured	17.0	Not Measured
15.0	Not Measured	13.0	Not Measured	15.0	Not Measured
13.0	Not Measured	11.0	Not Measured	13.0	Not Measured
11.0	Not Measured	9.0	Not Measured	11.0	Not Measured
9.0	Not Measured	7.0	Not Measured	9.0	Not Measured
7.0	Not Measured	5.0	Not Measured	7.0	Not Measured
5.0	Not Measured	3.0	Not Measured	5.0	Not Measured
3.0	Not Measured	1.0	Not Measured	3.0	Not Measured
1.0	Not Measured	-1.0	Not Measured	1.0	Not Measured
-1.0	Not Measured	-3.0	Not Measured	-1.0	Not Measured
-3.0	Not Measured	-5.0	Not Measured	-3.0	Not Measured
-5.0	Not Measured	-7.0	Not Measured	-5.0	Not Measured
-7.0	Not Measured	-9.0	Not Measured	-7.0	Not Measured

-9.0	Not Measured	-11.0	Not Measured	-9.0	Not Measured
-11.0	Not Measured	-13.0	Not Measured	-11.0	Not Measured
-13.0	Not Measured	-17.0	Not Measured	-13.0	Not Measured
-17.0	Not Measured			-16.0	Not Measured

Table B.23 – Average thickness of each slice of each diffusion cell.

Cell	R2-2	Cell	R2-3	Cell	R2-4
Position (cm)	Thickness (cm)	Position (cm)	Thickness (cm)	Position (cm)	Thickness (cm)
17.0	6.72	17.0	7.55	19.0	6.77
13.0	1.99	13.0	1.72	15.0	1.60
11.0	1.90	11.0	2.10	13.0	2.20
9.0	1.68	9.0	1.87	11.0	1.73
7.0	1.92	7.0	1.96	9.0	2.03
5.0	2.11	5.0	1.78	7.0	1.76
3.0	1.71	3.0	2.10	5.0	2.13
1.0	1.68	1.0	1.40	3.0	1.90
-1.0	2.10	-1.0	2.07	1.0	1.55
-3.0	2.04	-3.0	1.99	-1.0	2.14
-5.0	1.52	-5.0	1.97	-3.0	1.78
-7.0	1.65	-7.0	2.02	-5.0	1.97
-9.0	2.36	-9.0	1.83	-7.0	1.91
-11.0	1.74	-11.0	1.89	-9.0	1.90
-13.0	2.06	-13.0	1.65	-11.0	1.84
-17.0	6.16	-17.0	6.19	-13.0	1.85
				-15.0	2.00
				-19.0	5.93

Table B.24 – Average thickness of each slice of each diffusion cell.

Cell	R2-5	Cell	R3-2	Cell	R3-3
Position (cm)	Thickness (cm)	Position (cm)	Thickness (cm)	Position (cm)	Thickness (cm)
17.0	6.67	17.0	4.83	17.0	4.61
13.0	1.70	13.0	1.95	13.0	2.03
11.0	1.72	11.0	1.71	11.0	1.35
9.0	2.29	9.0	1.92	9.0	1.99
7.0	1.74	7.0	1.85	7.0	1.86
5.0	1.90	5.0	2.04	5.0	2.12
3.0	1.77	3.0	1.93	3.0	1.84
1.0	1.71	1.0	1.68	1.0	1.53
-1.0	1.96	-1.0	2.03	-1.0	2.09
-3.0	2.40	-3.0	1.82	-3.0	1.82
-5.0	1.62	-5.0	1.86	-5.0	1.73
-7.0	1.81	-7.0	1.98	-7.0	1.89
-9.0	1.88	-9.0	1.92	-9.0	1.87
-11.0	1.91	-11.0	1.48	-11.0	1.21
-13.0	1.68	-13.0	2.04	-13.0	2.14
-17.0	6.20	-17.0	4.81	-17.0	4.13

Table B.25 – Average thickness of each slice of each diffusion cell.

Cell	R3-4	Cell	R3-5	Cell	R4-1
Position (cm)	Thickness (cm)	Position (cm)	Thickness (cm)	Position (cm)	Thickness (cm)
17.0	4.32	17.0	5.50	26.0	7.05
13.0	1.81	13.0	1.82	19.5	2.59
11.0	1.74	11.0	1.59	16.5	3.08
9.0	2.08	9.0	2.18	13.5	3.15
7.0	1.88	7.0	1.67	10.5	2.79
5.0	1.74	5.0	1.98	7.5	2.33
3.0	1.95	3.0	2.02	4.5	3.20
1.0	1.74	1.0	1.56	1.5	2.54
-1.0	1.79	-1.0	2.09	-1.5	2.78
-3.0	1.82	-3.0	1.90	-4.5	2.94
-5.0	2.02	-5.0	1.65	-7.5	2.80
-7.0	1.64	-7.0	1.64	-10.5	2.87
-9.0	2.05	-9.0	1.97	-13.5	2.78
-11.0	1.90	-11.0	1.53	-16.5	3.08
-13.0	1.60	-13.0	2.42	-19.5	2.66
-17.0	4.05	-17.0	5.27	-26.0	6.75

Table B.26 – Average thickness of each slice of each diffusion cell.

Cell	R4-2	Cell	R4-3	Cell	R4-4
Position (cm)	Thickness (cm)	Position (cm)	Thickness (cm)	Position (cm)	Thickness (cm)
26.0	8.41	26.0	8.00	26.0	7.63
19.5	3.08	19.5	2.81	19.5	2.96
16.5	2.78	16.5	2.99	16.5	2.71
13.5	3.16	13.5	3.04	13.5	2.74
10.5	2.37	10.5	2.56	10.5	2.83
7.5	2.74	7.5	2.68	7.5	2.76
4.5	2.82	4.5	3.02	4.5	3.12
1.5	2.96	1.5	2.71	1.5	3.06
-1.5	3.09	-1.5	2.79	-1.5	3.00
-4.5	2.49	-4.5	2.88	-4.5	2.94
-7.5	2.82	-7.5	2.52	-7.5	2.72
-10.5	2.11	-10.5	2.94	-10.5	2.71
-13.5	2.72	-13.5	3.00	-13.5	2.99
-16.5	3.28	-16.5	2.77	-16.5	2.73
-19.5	2.97	-19.5	2.94	-19.5	2.84
-26.0	7.92	-26.0	8.08	-26.0	7.07

Table B.27 – Average thickness of each slice of each diffusion cell.

Cell	R4-5
Position (cm)	Thickness (cm)
26.0	8.01
19.5	3.02
16.5	2.78
13.5	2.80
10.5	3.02
7.5	3.15
4.5	2.95
1.5	2.89
-1.5	3.08
-4.5	2.94
-7.5	3.33
-10.5	2.84
-13.5	3.28
-16.5	2.98
-19.5	3.20
-26.0	7.58

B.5 Cell Chloride Raw Data

The raw chloride data as received from the commercial lab is presented in Table B.28.

Table B.28 - Raw chloride data.

	Chloride Concentration (mg/L)				
Position (cm)	R4-1	R4-2	R4-3	R4-4	R4-5
26	29.64831	30.06062	21.3240	21.3315	
19.5	29.50371	30.49465	23.0667	21.9437	24.4709
16.5	30.8189	29.93814	20.7739	21.9669	24.1888
13.5	29.32268	30.09192	22.7386	22.9284	23.9191
10.5	30.06129	33.81632	20.0612	21.5597	
7.5	29.60834	32.08841	20.9248	22.0598	23.1732
4.5	22.8311	33.08386	21.0444	21.0671	22.4884
1.5	19.36741		19.9697	19.8857	
-1.5	9.208216		6.9077	7.8027	9.2936
-4.5	6.794029	8.190229	5.8773	6.3074	7.9129
-7.5	6.434945	6.212196	5.4103	5.4236	6.1827
-10.5	6.165191	6.751218	5.2314	5.3842	5.1045
-13.5	5.946921	6.177661	0.3615	5.4170	5.2809
-16.5	5.913974	5.794529	0.1647	5.2380	6.5245
-19.5		6.06414	0.3070	5.3736	6.7560
-26	6.515796	6.413086	0.1909	5.1646	6.5855

Appendix C

This appendix presents all the collected data for column laboratory experiment.

C.1 Column Water Content Data

The water content data will be presented with the oven dried measurements first followed by the TDR measurements.

C.1.1 Measured Gravimetric Water Content

The measured gravimetric water content (GWC) for Column 1 is presented in Table C.1 and the data for Column 2 in Table C.2.

Table C.1 – Gravimetric water content data measured for Column 1

Column Elevation	S1 GWC	S2 GWC	S3 GWC	S4 GWC
1.4	0.077	0.040	0.037	0.035
1.3	0.096	0.046	0.040	0.040
1.2	0.085	0.043	0.039	0.038
1.1	0.078	0.045	0.041	0.042
1.0	0.055	0.048	0.043	0.042
0.9	0.051	0.049	0.043	0.043
0.8	0.053	0.049	0.045	0.045
0.7	0.055	0.048	0.047	0.049
0.6	0.052	0.049	0.049	0.052
0.5	0.043	0.043	0.056	0.059
0.4	0.067	0.056	0.066	0.070
0.3	0.083	0.073	0.101	0.092
0.2	0.123	0.139	0.171	0.167

Table C.2 – Gravimetric water content data measured for Column 2

Column Elevation	S1 GWC	S2 GWC	S3 GWC	S4 GWC
1.4	0.084	0.063	0.039	0.039
1.3	0.076	0.060	0.037	0.037
1.2	0.065	0.061	0.039	0.040
1.1	0.053	0.056	0.040	0.040
1.0	0.053	0.055	0.040	0.041
0.9	0.055	0.054	0.042	0.043
0.8	0.056	0.056	0.044	0.045
0.7	0.057	0.058	0.045	0.044
0.6	0.054	0.055	0.046	0.052
0.5	0.061	0.056	0.048	0.053
0.4	0.079	0.065	0.061	0.067
0.3	0.103	0.092	0.085	0.095
0.2	0.171	0.131	0.134	0.168

C.1.2 TDR Volumetric Water Content

The recorded TDR volumetric water content (VWC) data at the sample times for Column 1 and 2 in Table C.3 and Table C.4 respectively.

Table C.3 – Volumetric water content recorded by TDR for Column 1

Column Elevation	S1 VWC	S2 VWC	S3 VWC	S4 VWC
1.35	0.112	0.059	0.047	Not Collected
1.25	0.086	0.037	0.028	Not Collected
1.15	0.095	0.052	0.040	Not Collected
1.05	Not Collected	Not Collected	Not Collected	Not Collected
0.95	0.051	0.052	0.041	Not Collected
0.85	0.101	0.105	0.086	Not Collected
0.75	Not Collected	Not Collected	Not Collected	Not Collected
0.65	0.052	0.055	0.050	Not Collected
0.55	0.091	0.093	0.090	Not Collected
0.45	0.101	0.103	0.103	Not Collected
0.35	0.124	0.121	0.126	Not Collected
0.25	0.107	Not Collected	Not Collected	Not Collected
0.15	0.342	0.336	0.342	Not Collected

Table C.4 – Volumetric water content recorded by TDR for Column 1

Column Elevation	S1 VWC	S2 VWC	S3 VWC	S4 VWC
1.35	0.112	0.072	0.056	Not Collected
1.25	0.117	0.104	0.080	Not Collected
1.15	0.080	0.091	0.073	Not Collected
1.05	0.071	0.077	0.060	Not Collected
0.95	0.074	0.084	0.066	Not Collected
0.85	0.092	0.096	0.084	Not Collected
0.75	0.092	0.096	0.078	Not Collected
0.65	0.080	0.081	0.071	Not Collected
0.55	0.104	0.105	0.099	Not Collected
0.45	0.117	0.116	0.116	Not Collected
0.35	0.122	0.124	0.122	Not Collected
0.25	0.196	0.191	0.186	Not Collected
0.15	0.319	0.313	0.314	Not Collected

C.2 Column Soil Mass Collected

The mass of soil collected at each sample time for Column 1 and 2 is presented in Table C.5 and Table C.6 respectively.

Table C.5 – Mass collected at each sample time in the Shelby Tube for Column 1

Column Elevation	S1 (g)	S2 (g)	S3 (g)	S4 (g)	Total Mass Collected S1 to S3 (g)
1.4	55.74	62.00	51.43	Not Measured	169.17
1.3	65.51	76.76	76.10	Not Measured	218.37
1.2	64.35	77.82	75.14	Not Measured	217.31
1.1	61.79	80.98	76.84	Not Measured	219.61
1.0	68.19	79.89	73.95	Not Measured	222.03
0.9	66.27	77.83	78.11	Not Measured	222.21
0.8	65.94	76.64	77.02	Not Measured	219.60
0.7	59.26	72.30	75.97	Not Measured	207.53
0.6	69.02	76.39	77.05	Not Measured	222.46
0.5	64.60	83.62	74.31	Not Measured	222.53
0.4	59.50	79.86	76.20	Not Measured	215.56
0.3	68.89	77.54	75.84	Not Measured	222.27
0.2	68.21	80.06	76.32	Not Measured	224.59

Table C.6 – Mass collected at each sample time in the Shelby Tube for Column 2

Column Elevation	S1 (g)	S2 (g)	S3 (g)	S4 (g)	Total Mass Collected S1 to S3 (g)
1.4	79.51	45.10	72.58	Not Measured	197.19
1.3	78.62	58.04	64.81	Not Measured	201.47
1.2	63.46	72.67	79.30	Not Measured	215.43
1.1	67.16	70.47	78.79	Not Measured	216.42
1.0	70.52	76.93	77.51	Not Measured	224.96
0.9	68.07	78.76	74.49	Not Measured	221.32
0.8	70.17	73.72	78.39	Not Measured	222.28
0.7	68.42	76.54	80.11	Not Measured	225.07
0.6	72.44	71.47	78.98	Not Measured	222.89
0.5	69.37	71.91	78.99	Not Measured	220.27
0.4	66.32	74.17	77.60	Not Measured	218.09
0.3	64.57	75.08	79.64	Not Measured	219.29
0.2	70.71	75.15	78.42	Not Measured	224.28

C.3 Column Sample Isotope Analysis

The raw non-normalized isotope data, corrected from instruments is presented in Table C.7 and Table C.8 for Column 1 and 2 respectively. The equipment used to analyze the sample rounds is presented in Table C.9.

Table C.7 – Raw isotope data for Column 1

Column Elevation	S1		S2		S3		S4	
	δD (‰)	δ18O (‰)	δD (‰)	δ18O (‰)	δD (‰)	δ18O (‰)	δD (‰)	δ18O (‰)
1.4	-86.3	-11.8	-90.1	-12.9	-93.0	-12.3	-92.9	-12.4
1.3	-97.5	-12.9	-96.3	-13.7	-93.0	-12.6	-103.6	-13.7
1.2	-111.4	-13.9	-105.4	-14.1	-98.2	-13.0	-103.0	-13.8
1.1	-126.2	-15.2	-112.2	-14.2	-106.0	-13.3	-103.3	-13.3
1.0	-133.9	-16.8	-122.4	-15.0	-112.4	-13.5	-112.5	-13.3
0.9	-130.2	-15.8	-128.1	-15.9	-119.4	-15.1	-117.4	-14.4
0.8	-130.6	-16.1	-129.7	-16.0	-122.7	-14.5	-121.3	-15.0
0.7	-130.1	-15.9	-131.1	-16.3	-126.6	-14.9	-126.3	-15.1
0.6	-132.6	-16.3	-131.8	-16.5	-124.7	-15.1	-125.8	-15.4
0.5	-134.4	-16.7	-130.3	-16.3	-128.7	-14.9	-129.8	-16.0
0.4	-134.7	-16.9	-129.8	-16.9	-128.4	-14.9	-129.3	-15.5
0.3	-133.4	-16.4	-133.2	-16.6	-132.2	-16.2	-133.7	-15.8
0.2	-131.8	-16.2	-130.1	-16.1	-134.0	-16.4	-132.9	-16.7

Table C.8 – Raw isotope data for Column 2

Column Elevation	S1		S2		S3		S4	
	δD (‰)	δ18O (‰)	δD (‰)	δ18O (‰)	δD (‰)	δ18O (‰)	δD (‰)	δ18O (‰)
1.4	-100.0	-13.4	-93.4	-12.3	-102.5	-13.3	-111.6	-14.9
1.3	-123.6	-15.4	-115.5	-14.5	-109.4	-13.4	-115.9	-14.6
1.2	-132.7	-16.3	-129.1	-15.2	-116.3	-14.6	-116.0	-14.9
1.1	-128.1	-15.9	-129.0	-15.1	-122.6	-15.3	-120.0	-13.9
1.0	-132.0	-16.3	-131.5	-15.5	-128.1	-15.8	-130.6	-15.7
0.9	-134.3	-16.6	-133.0	-16.6	-130.0	-15.9	-128.4	-16.0
0.8	-134.8	-16.4	-131.2	-15.8	-131.9	-16.4	-128.4	-15.4
0.7	-133.7	-16.5	-130.6	-15.9	-132.6	-16.1	-133.8	-16.3
0.6	-133.9	-16.8	-129.5	-16.1	-132.8	-16.5	-132.5	-15.3
0.5	-133.7	-16.8	-129.4	-15.5	-132.8	-15.9	-133.9	-16.9
0.4	-132.4	-16.5	-129.4	-15.4	-129.1	-16.2	-129.9	-16.4
0.3	-135.5	-16.7	-130.3	-15.8	-133.3	-16.3	-135.9	-17.0
0.2	-133.9	-16.6	-130.4	-15.3	-133.1	-16.2	-131.1	-15.8

Table C.9 - Column isotope analysis equipment

Column	Sample	Equipment Manufacturer	Model
C1	S1	Picarro	2130
	S2	Picarro	2120
	S3	Los Gatos Research (LGR)	WV1A - 45 - EP
	S4	Los Gatos Research (LGR)	WV1A - 45 - EP

C2	S1	Picarro	1102i
	S2	Picarro	2120
	S3	Los Gatos Research (LGR)	WV1A - 45 - EP
	S4	Los Gatos Research (LGR)	WV1A - 45 - EP

C.4 Column Infiltrated Water Isotope Analysis

The isotope content of the infiltrating Aquafina® water was average from three isotope measurements (Table C.10)

Table C.10 – Analysis of Aquafina® water for infiltration

Measurement	δD (‰)	δ18O (‰)
1	-11.8	-87.3
2	-11.5	-84.9
3	-12.2	-85.1
Average	-11.8	-85.8

Appendix D

This appendix derives the mixing plot to justify the change in measured isotope content after water is mixed with the air dried soil. The reasoning is there is a small mass of high isotope content left in the soil and this residual water, when mixed with the added water, can change what is measured. The basis for this plot is the following mixing equation for isotopes (Clark and Fritz, 1997),

$$\delta_{mixed} = \chi\delta_{added} + (1-\chi)\delta_{residual} \quad \text{.....(D.1)}$$

Where δ_{mixed} is the isotope content of the mixed water (‰), χ is the proportion of water of each part in the mixture (unitless), $\delta_{residual}$ is the isotope content of the residual water in the dried soil (‰), and δ_{added} is the isotope content of the water added to the soil (‰).

This analysis assumes 100 g of soil has been dried from a gravimetric water content of 0.25 to 0.007. The initial isotope concentration of the water dried from the sand was similar to Saskatoon tap water (-135 ‰), which was used to wash the sands before analysis. After the sand was dried at 25 °C the final isotope concentration of the remaining water ($\delta_{residual}$), due to Rayleigh type distillation, was -101.8 ‰.

D.1 Spiked Cells

For the spiked cells, the added water was spiked to approximately -50 ‰. The mass of residual water in the sand was 0.7 g. The proportion of water added to the soil (χ) was calculated by dividing the M_{added} by the M_{total}. Normalization was found by $\delta_{added}/\delta_{mixed}$.

The normalized isotope concentration at various gravimetric water contents is presented in Table D.1.

Table D.1 - Normalized concentration of water mixed with soil for a spiked cell.

GWC	M_{added}	M_{total}	χ	1 - χ	δ_{mixed}	normalized
0.25	25	25.7	0.973	0.027	-51.41	0.97
0.24	24	24.7	0.972	0.028	-51.47	0.97
0.23	23	23.7	0.970	0.030	-51.53	0.97
0.22	22	22.7	0.969	0.031	-51.60	0.97

0.21	21	21.7	0.968	0.032	-51.67	0.97
0.2	20	20.7	0.966	0.034	-51.75	0.97
0.19	19	19.7	0.964	0.036	-51.84	0.96
0.18	18	18.7	0.963	0.037	-51.94	0.96
0.17	17	17.7	0.960	0.040	-52.05	0.96
0.16	16	16.7	0.958	0.042	-52.17	0.96
0.15	15	15.7	0.955	0.045	-52.31	0.96
0.14	14	14.7	0.952	0.048	-52.47	0.95
0.13	13	13.7	0.949	0.051	-52.65	0.95
0.12	12	12.7	0.945	0.055	-52.85	0.95
0.11	11	11.7	0.940	0.060	-53.10	0.94
0.1	10	10.7	0.935	0.065	-53.39	0.94
0.09	9	9.7	0.928	0.072	-53.74	0.93
0.08	8	8.7	0.920	0.080	-54.17	0.92
0.07	7	7.7	0.909	0.091	-54.71	0.91
0.06	6	6.7	0.896	0.104	-55.41	0.90
0.05	5	5.7	0.877	0.123	-56.36	0.89
0.04	4	4.7	0.851	0.149	-57.71	0.87
0.03	3	3.7	0.811	0.189	-59.80	0.84
0.02	2	2.7	0.741	0.259	-63.43	0.79
0.01	1	1.7	0.588	0.412	-71.33	0.70
0.009	0.9	1.6	0.563	0.438	-72.66	0.69
0.008	0.8	1.5	0.533	0.467	-74.17	0.67
0.007	0.7	1.4	0.500	0.500	-75.90	0.66
0.006	0.6	1.3	0.462	0.538	-77.89	0.64
0.005	0.5	1.2	0.417	0.583	-80.21	0.62
0.004	0.4	1.1	0.364	0.636	-82.96	0.60
0.003	0.3	1	0.300	0.700	-86.26	0.58
0.002	0.2	0.9	0.222	0.778	-90.28	0.55
0.001	0.1	0.8	0.125	0.875	-95.32	0.52

D.2 Non-Spiked Cells

For the non - spiked cells, the added water was spiked to approximately -135 ‰. The mass of residual water in the sand was 0.7 g. The proportion of water added to the soil (χ) was calculated by dividing the M_{added} by the M_{total}. Normalization was found by δ_{added} /δ_{mixed}.

The normalized isotope concentration at various gravimetric water contents is presented in Table D.2.

Table D.2 - Normalized concentration of water mixed with soil for a non-spiked cell.

GWC	M_{added}	M_{total}	χ	1 - χ	δ_{mixed}	normalized
0.25	25	25.7	0.973	0.027	-134.10	1.01
0.24	24	24.7	0.972	0.028	-134.06	1.01
0.23	23	23.7	0.970	0.030	-134.02	1.01
0.22	22	22.7	0.969	0.031	-133.98	1.01
0.21	21	21.7	0.968	0.032	-133.93	1.01
0.2	20	20.7	0.966	0.034	-133.88	1.01
0.19	19	19.7	0.964	0.036	-133.82	1.01
0.18	18	18.7	0.963	0.037	-133.76	1.01
0.17	17	17.7	0.960	0.040	-133.69	1.01
0.16	16	16.7	0.958	0.042	-133.61	1.01
0.15	15	15.7	0.955	0.045	-133.52	1.01
0.14	14	14.7	0.952	0.048	-133.42	1.01
0.13	13	13.7	0.949	0.051	-133.30	1.01
0.12	12	12.7	0.945	0.055	-133.17	1.01
0.11	11	11.7	0.940	0.060	-133.01	1.01
0.1	10	10.7	0.935	0.065	-132.83	1.02
0.09	9	9.7	0.928	0.072	-132.60	1.02
0.08	8	8.7	0.920	0.080	-132.33	1.02
0.07	7	7.7	0.909	0.091	-131.98	1.02
0.06	6	6.7	0.896	0.104	-131.53	1.03
0.05	5	5.7	0.877	0.123	-130.92	1.03
0.04	4	4.7	0.851	0.149	-130.05	1.04

0.03	3	3.7	0.811	0.189	-128.72	1.05
0.02	2	2.7	0.741	0.259	-126.39	1.07
0.01	1	1.7	0.588	0.412	-121.33	1.11
0.009	0.9	1.6	0.563	0.438	-120.47	1.12
0.008	0.8	1.5	0.533	0.467	-119.50	1.13
0.007	0.7	1.4	0.500	0.500	-118.40	1.14
0.006	0.6	1.3	0.462	0.538	-117.12	1.15
0.005	0.5	1.2	0.417	0.583	-115.63	1.17
0.004	0.4	1.1	0.364	0.636	-113.87	1.19
0.003	0.3	1	0.300	0.700	-111.76	1.21
0.002	0.2	0.9	0.222	0.778	-109.17	1.24
0.001	0.1	0.8	0.125	0.875	-105.94	1.27

D.3 Final Plot

The final plot presented in the body of the thesis is found by plotting the normalized isotope mixture at the gravimetric water content for both cells and is found here in Figure A.1.

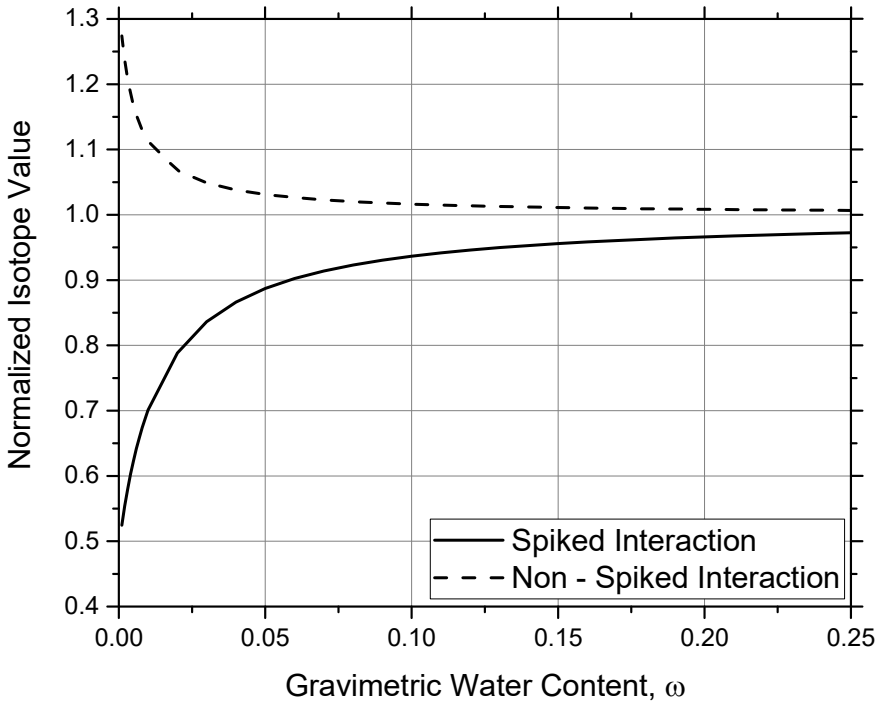

Figure D.1 – Normalized mixed concentration of spiked and non-spiked water added to air dried soil

D.4 References

Clark, I. D. and P. Fritz (1997). Environmental Isotopes in Hydrogeology, CRC press.

Appendix E

This appendix describes the Geo-Slope GeoStudio 2012 (version 8.15.5.11777) models that were used to model the water and isotope transport in this study. The water transport was simulated in SEEP/W and the isotope transport was simulated in CTRAN/W.

E.1 Model Geometry

The geometry for the water transport, isotope transport and for Columns 1 and 2 were the same. The column was modeled as 1.45 m high, and 0.18 m in width. The width was taken as the same as the column diameters. To ensure the masses added to the columns was the same as added in the laboratory a depth of each element was set to 0.1429 m so the cross sectional area of the model and the columns was the same. The general column geometry is found in Figure E.1.

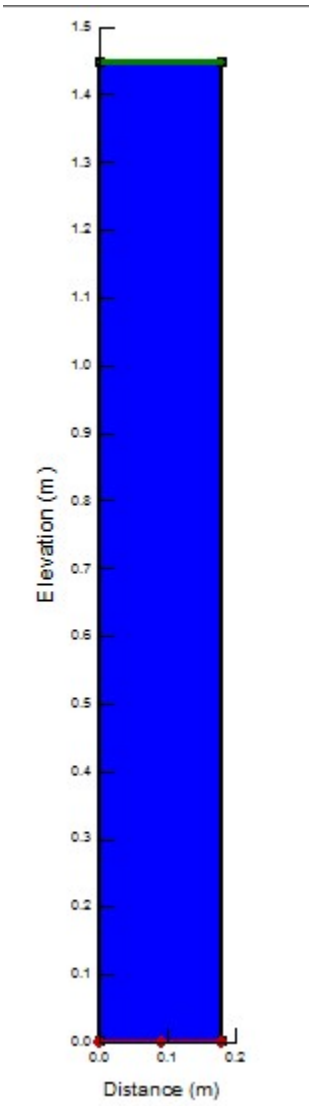

Figure E.1 – Geometry for all column modeling

For each of the analysis as finite element mesh of 0.003 m was used. This small mesh value was designed for the isotope transport to keep the model from becoming unstable due to Peclet and Courant criteria.

Specific details for each of the model types can be found in the following sections.

E.2 Water Content Models

The model for each column is broken down into 4 separate analysis. The first starts with a fully saturated column that is allowed to drain to steady state. Following is the rainfall portion of the

experiment. The third analysis covers the advective movement of the water and covers transport occurring at sample times 1 and 2. The final analysis covers the long term water movement after significant water distribution has ceased, covering the transport that occurs for sample times 3 and 4. The details for each of the columns for the water content models can be found below in Table E.1 and Table E.2 for Column 1 and 2 respectively.

Table E.1 – Numerical model details for Column 1 water transport model

	Analysis 1	Analysis 2	Analysis 3	Analysis 4
Top Boundary Condition	None	Rainfall as a unit flux q = 6.31E-6 m/sec	unit flux q 0 m/sec	None - carries over from previous analysis
Bottom Boundary Condition	Pressure head = 0 m	Pressure head = 0 m	Pressure head = 0 m	Pressure head = 0 m
Initial Pore Water Pressure Conditions	Activation porewater pressure of 0 kPa	Porewater pressure profile from Analysis 1 final time step	Porewater pressure profile from Analysis 2 final time step	Porewater pressure profile from Analysis 2 final time step
Time start (s)	Steady State	0	3600	2 347 289
Time end (s)	Steady State	3600	2 347 289	16 508 260
Sample times covered	None	None	S1 and S2	S3 and S4
Time Step Scale	None	linear	Exponential	Linear
Initial Δt (s)	None	60	100	23 601.618
Number of Time Steps	None	60	300	600
SWCC model	Van Genuchten, 1980	Van Genuchten, 1980	Van Genuchten, 1980	Van Genuchten, 1980
K_{sat} model	Van Genuchten, 1980	Van Genuchten, 1980	Van Genuchten, 1980	Van Genuchten, 1980

Table E.2 – Numerical model details for Column 2 water transport model

	Analysis 1	Analysis 2	Analysis 3	Analysis 4
Top Boundary Condition	None	Rainfall as a unit flux q = 7.0832e-006 m/sec	unit flux q 0 m/sec	None - carries over from previous analysis
Bottom Boundary Condition	Pressure head = 0 m	Pressure head = 0 m	Pressure head = 0 m	Pressure head = 0 m
Initial Pore Water Pressure Conditions	Activation porewater pressure of 0 kPa	Porewater pressure profile from Analysis 1 final time step	Porewater pressure profile from Analysis 2 final time step	Porewater pressure profile from Analysis 2 final time step
Time start (s)	Steady State	0	1800	543 960
Time end (s)	Steady State	1800	543 960	18 151 860
Sample times covered	None	None	S1 and S2	S3 and S4
Time Step Scale	None	linear	Exponential	Linear
Initial Δt (s)	None	30	100	29 346.5
Number of Time Steps	None	60	200	600
SWCC model	Van Genuchten, 1980	Van Genuchten, 1980	Van Genuchten, 1980	Van Genuchten, 1980
K_{sat} model	Van Genuchten, 1980	Van Genuchten, 1980	Van Genuchten, 1980	Van Genuchten, 1980

E.3 Isotope Transport Models

The transport models for each column is broken down into 3 separate analysis. The first is the initial application of the infiltrated isotopically enhanced water and covers the initial dispersive spreading. The second covers the rest of the dispersive spreading and the transition into diffusive spreading. The final part covers the long term diffusive redistribution of isotopes concentrations within the column. The details for each of the columns for the isotope transport models can be found below in Table E.3 and Table E.4 for Column 1 and 2 respectively.

Table E.3 – Numerical model details for Column 1 isotope transport model

	Analysis 1	Analysis 2	Analysis 3
Top Boundary Condition	Rainfall as a Source Concentration (q * C) C = 1	None	None
Bottom Boundary Condition	Mass flux (q) = 0 and Qd > 0	Mass flux (q) = 0 and Qd > 0	Mass flux (q) = 0 and Qd > 0
Initial Isotope Conditions	0	Concentration profile from Analysis 2 final time step	Concentration profile from Analysis 3 final time step
Time start (s)	0	3600	2 347 289
Time end (s)	3600	2 347 289	16 508 260
Sample times covered	None	S1 and S2	S3 and S4
Time Step Scale	linear	Exponential	Linear
Initial Δt (s)	60	100	23 601.618
Number of Time Steps	60	300	600
Longitudinal and Transverse Dispersivity	1E-300	1E-300	1E-300
Diffusion Model	$D_e = \Lambda\|v\| + \frac{D_{com}}{\theta_l}$	$D_e = \Lambda\|v\| + \frac{D_{com}}{\theta_l}$	$D_e = \frac{D_{com}}{\theta_l}$
SWCC model	Van Genuchten, 1980	Van Genuchten, 1980	Van Genuchten, 1980
K_{sat} model	Van Genuchten, 1980	Van Genuchten, 1980	Van Genuchten, 1980

Table E.4 – Numerical model details for Column 2 isotope transport model

	Analysis 1	Analysis 2	Analysis 3
Top Boundary Condition	Rainfall as a Source Concentration (q * C) C = 1	None	None
Bottom Boundary Condition	Mass flux (q) = 0 and Qd > 0	Mass flux (q) = 0 and Qd > 0	Mass flux (q) = 0 and Qd > 0
Initial Isotope Conditions	0	Concentration profile from Analysis 2 final time step	Concentration profile from Analysis 3 final time step
Time start (s)	0	1800	543 960
Time end (s)	1800	543 960	18 151 860
Sample times covered	None	S1 and S2	S3 and S4
Time Step Scale	linear	Exponential	Linear
Initial Δt (s)	30	100	29 346.5
Number of Time Steps	60	200	600
Longitudinal and Transverse Dispersivity	1E-300	1E-300	1E-300
Diffusion Model	$D_e = \Lambda\|v\| + \frac{D_{com}}{\theta_l}$	$D_e = \Lambda\|v\| + \frac{D_{com}}{\theta_l}$	$D_e = \frac{D_{com}}{\theta_l}$
SWCC model	Van Genuchten, 1980	Van Genuchten, 1980	Van Genuchten, 1980
K_{sat} model	Van Genuchten, 1980	Van Genuchten, 1980	Van Genuchten, 1980

E.6 Column Outflow Water Fit to Model Outputs

The column modeling laboratory experiment was anchored by matching measured outflow volumes to the output of the numerical models to select initial best fit parameters for Column 1 and 2 in Figure E.2 and Figure E.3.

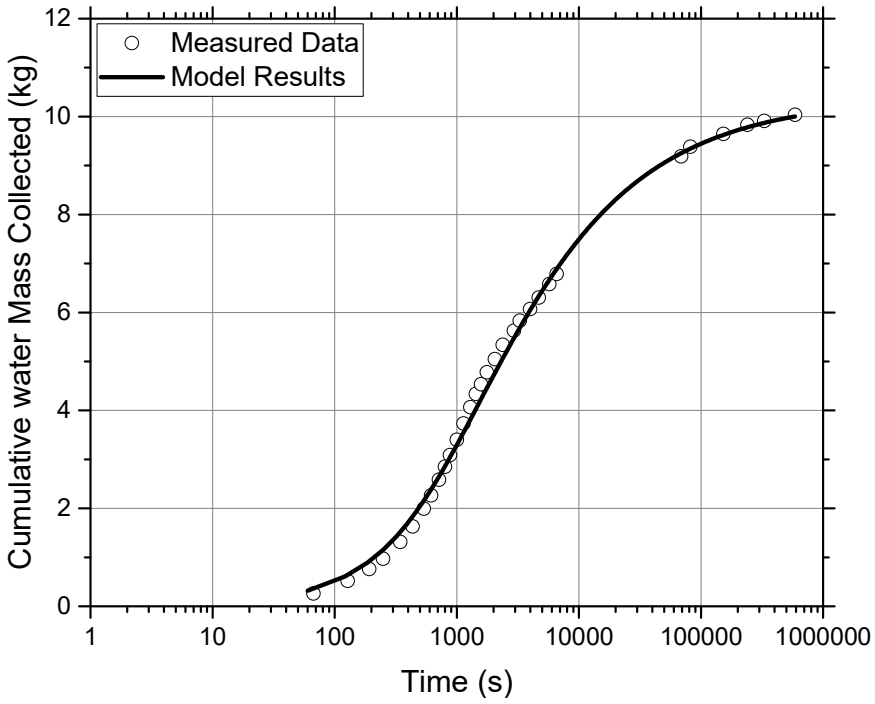

Figure E.2 – Model outflow compared to measured outflow for Column 1.

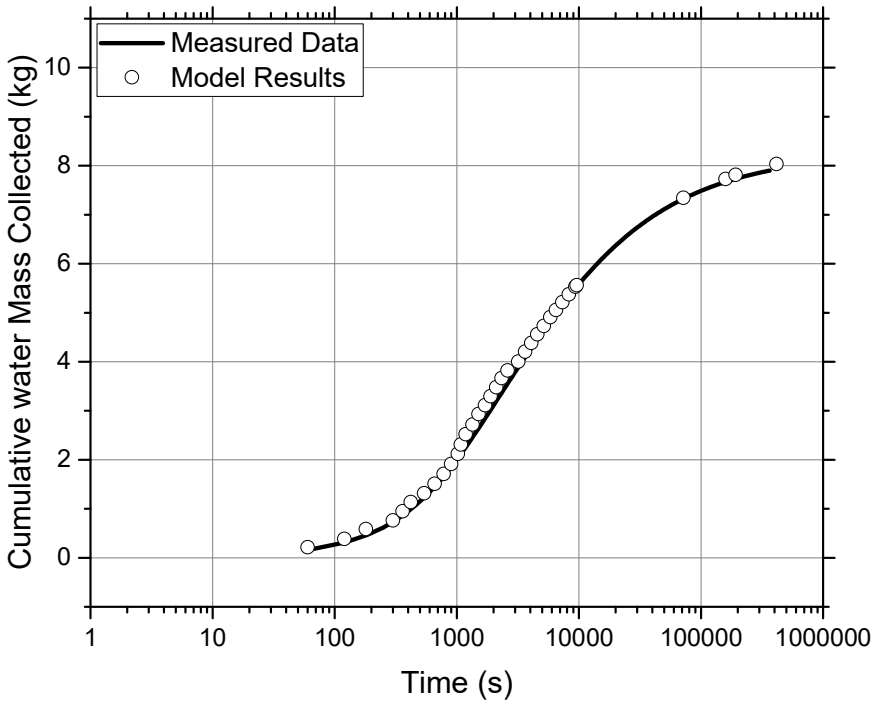

Figure E.3 – Model outflow compared to measured outflow for Column 2.

E.5 References

Van Genuchten, M. T. (1980). "A closed-form equation for predicting the hydraulic conductivity of unsaturated soils." Soil Science Society of America Journal **44**(5): 892-898.

Appendix F

The estimates of water loss from the column are presented here for various sources of water lost. Vapour loss from the column is calculated as,

$$J = \tau D \frac{\Delta \rho}{\Delta x} \quad \text{.....(F.1)}$$

Where J is the rate of mass loss (g/m^2/s), τ is the tortuosity (unitless), D is the diffusion coefficient of the medium of water loss (m^2/s), and $\Delta\rho/\Delta x$ is the vapour pressure gradient that drives water movement. For the diffusion models a vapour pressure gradient over the acrylic, PVC, or opening is assumed to be unity ($\Delta\rho/\Delta x$ = 1) and no tortuosity value is used (τ = 1).

F.1 Acrylic Column

The D for acrylic is 1.9E-12 m^2/s and based on Equation F.1 is equal to J. The surface area of the inside of the 0.182 m diameter column, over a 0.10 m elevation is 0.05718 m^2. Table A.1 shows water lost between S2 and S4 for both columns.

Table F.1 – Water lost from column through acrylic.

Column	J (g/m^2/s)	Area (m^2)	Time (s)	Mass lost (g)
C1	1.9E-12	0.05718	14 160 971	1.54E-6
C2	1.9E-12	0.05718	17 607 900	1.91E-6

The water losses from the acrylic are deemed insignificant.

F.2 PVC

The water loss through the PVC rainfall simulator or sample caps could be calculated, however, the diffusion value for water vapour through PVC was difficult to find. Assuming a D value similar to acrylic, based on the hydrophobic nature of the PVC Doyon et al., 1991, and the smaller area for transport the loss of water through PVC is estimated to be equivalent or less that through the acrylic, again being negligible.

F.3 Air Gaps

F.3.1 Sample Port O-rings

Assuming the O-rings have poor contact (0.001 m gap between the O-ring and acrylic) an amount of water loss can be found for each sample port. Giving each 0-ring a diameter of 0.045 m (assumed, not measured) the area over which water could be lost is 0.0001414 m^2. At laboratory temperature (22.5 °C) the D for water vapour is 2.6E-5. Assuming these parameters, the water lost for each column can be found in Table F.2.

Table F.2 – Water lost from columns due to gap between O-rings and acrylic.

Column	J ($g/m^2/s$)	Area (m^2)	Time (s)	Mass lost (g)
C1	2.6E-5	0.0001414	14 160 971	5.21E-02
C2	2.6E-5	0.0001414	17 607 900	6.47E-02

Again, the loss around the sample ports is negligible assuming a large gap that should not have existed in the laboratory.

F.3.2 TDR Probes

The loss from around the TDR probes has the same conditions as the sample ports, with the exception of a different area over which water is lost. The probes are 0.0032 m in diameter in a hole approximately 0.004 m in diameter. The hole diameter is assumed to be similar to the size of the probes as the probes fit in the holes with very little room to move. The open area around 2 probes is 9.048E-06 m^2. This is much smaller than the area around the sample ports. The probes were then siliconed into place to further reduce the amount of area available for water loss. From these calculations water loss from around the TDR probes is also insignificant.

F.4 References

Doyon, G., J. Gagnon, C. Toupin and F. Castaigne (1991). "Gas transmission properties of polyvinyl chloride (PVC) films studied under subambient and ambient conditions for modified atmosphere packaging applications." Packaging Technology and Science **4**(3): 157-165.